Modifications de nanocapsules lipidiques par des procédés post-formulation. Elaboration de vecteurs multifonctionnels de médicaments.

Thomas Perrier,

Université d'Angers

Année 2009
N° d'ordre 1022

Modifications de nanocapsules lipidiques par des procédés post-formulation. Elaboration de vecteurs multifonctionnels de médicaments.

Thèse de doctorat

Spécialité : Neurosciences

Ecole Doctorale Nantes-Angers-Le Mans

Présentée et soutenue publiquement
Le 27 novembre 2009
A la Faculté de Pharmacie d'Angers

Par Thomas PERRIER

Devant le jury ci-dessous :

François BERGER	Rapporteur	Professeur des Universités, Grenoble
Philippe BARTHELEMY	Rapporteur	Professeur des Universités, Bordeaux
Jean-Luc PUEL	Examinateur	Professeur des Universités, Montpellier
Patrick SAULNIER	Examinateur	Professeur des Universités, Angers
Jean-Pierre BENOIT	Examinateur	Professeur des Universités, Angers

Directeur de thèse : **Patrick Saulnier**

Laboratoire : INSERM U646, Ingénierie de la Vectorisation Particulaire
10, rue André Boquel
49100 Angers

Je voudrais tout d'abord remercier le Professeur Jean-Pierre Benoît pour m'avoir offert l'opportunité d'effectuer cette thèse de doctorat au sein de son unité. Je le remercie aussi pour sa disponibilité tout au long de ces trois années de travail.

Je remercie vivement mon directeur de thèse, le Professeur Patrick Saulnier, pour m'avoir encadré et accordé beaucoup de temps. Je n'oublierai jamais ces années ou nous avons travaillé ensemble, que ce soit à l'échelle de l'unité ou bien au sein du consortium NanoEar. Son expérience, partagée chaleureusement tout au long de ce doctorat, m'aura appris beaucoup de choses, tant du point de vue personnel que professionnel.

Je tiens à remercier vivement les docteurs Guillaume Bastiat et Pascal Gayet pour m'avoir aidé et guidé durant cette thèse. Votre assistance et nos discussions ont été source de réflexions importantes pour l'élaboration de ce travail. Je tiens à remercier Sandy Vrignaud, doctorante, qui a eu le courage de subir de nombreux tours de l'étang Saint-Nicolas.

J'exprime mes plus sincères remerciements à Nolwenn Lautram et Floriant Fouchet pour m'avoir donné beaucoup de leur temps dans la réalisation des nombreuses expériences que nous avons conduites ensemble.

Je tiens à témoigner ma gratitude au docteur Emmanuel Garcion, au professeur Claudia Monterro-Meneï ainsi qu'à Erika Bourseau pour m'avoir permis de réaliser les tests sur culture cellulaire humaine.

Je tiens à remercier l'ensemble des personnels de l'unité 646 pour ces trois années agréables de travail passées ensemble.

Enfin, je remercie vivement les membres du jury de m'accorder leur vision sur ce travail de thèse et de m'apporter un point de vue externe au laboratoire sur le travail présenté.

Sommaire

Chapitre V : Discussion générale. Conclusion générale et perspectives

---

Introduction générale

Le développement d'objets nanométriques tient une place très importante dans bien des domaines scientifiques. De nombreux travaux se consacrent au développement de nano-objets et des procédés de formulation qui permettent leur fabrication. Ces dernières années, les moyens d'analyses ont connu un développement non négligeable et permettent d'établir la carte d'identité physico-chimique de chaque nano-objet produit. En bref, les nano-objets, que l'on dénomme vecteurs dans le monde pharmaceutique, ont évolué avec la connaissance de leur structure intime. C'est dans ce cadre que le laboratoire a développé un système colloïdal nanométrique basé sur une formulation de nano-émulsions, elle-même basée sur la méthode des inversions thermiques de phase émulsionnées. Ce système a été appelé nanocapsule lipidique (LNC) du fait de la taille nanométriques des objets produits (entre 20 et 100 nm) d'une part, et d'autres part du fait que les constituants organiques de la formulation sont en majorité de nature lipidique(triglycérides et phospholipides). Ce système est idéal pour l'encapsulation de molécules hydrophobes avec des propriétés physico-chimiques interéssantes (taille maîtrisée avec une distribution assez étroite, bonne stabilité colloïdale) ainsi qu'une très bonne compatibilité envers les systèmes biologiques (faible activation du système immunitaire, bonnes pénétration cellulaire, temps de demi-vie plasmatique intéressant et ajustables). En effet, les divers excipients de la formulation sont biocompatibles et biodégradables. Le problème principal est que les LNCs sont inadaptées pour l'encapsulation et la délivrance des molécules hydrophiles (comme les siRNA) et que leur surface furtive ne permet pas un ciblage actif d'une population cellulaire donnée et/ou ne permet pas la fixation et le transport d'actifs hydrophiles.

De nos jours, en parallèle des procédés de formulation, une nouvelle approche a émergé : elle consiste en l'utilisation des nano-objets comme plateformes pré-établies

permettant une modification à façon des propriétés interfaciales avec le milieu extérieur. Cette approche a été rendue possible par la mise au point de nano-objets de plus en plus stables et le développement de procédés assez doux qui ne perturbent pas leur structure et leur stabilité. Parmi ces procédés on peut citer la post-insertion, initialement développée sur les liposomes. On peut citer aussi des méthodes chimiques comme la click chemistry ou celles développées sur la base de réactions de métathèse. Nombres de ces procédés utilisent des systèmes catalytiques qui permettent la fonctionnalisation de l'interface des nano-objets en un temps relativement court compris entre quelques minutes et quelques heures. Le facteur temps est très important car d'une part, plus le temps de fonctionnalisation est long, plus les propriétés colloïdales de l'objet risquent d'être altérées. D'autre part la fonctionnalisation s'inscrit dans une suite d'étapes qui vont de la formulation initiale jusqu'à l'obtention de l'objet final. Ces étapes sont entrecoupées de procédés de purification (dialyses, chromatographies, centrifugation) qui doivent se faire dans un laps de temps raisonnable pour permettre une production et une analyse rapide des nano-objets.

Dans ce contexte, l'objectif de ma thèse de doctorat a été tout d'abord l'étude de la structure intime des nanocapsules lipidiques. Par la suite, nous avons étudié et développé deux procédés de modification de l'interface des nanocapsules lipidiques en respectant le cahier des charges suivant : les procédés doivent se réaliser à partir de la formulation initiale des LNCs ; ils ne doivent pas détériorer les propriétés physico-chimiques initiales des LNCs ; les produits utilisés doivent être biocompatibles, bioresorbables et ne pas amoindrir le caractère biomimétiques des LNCs ; ces procédés doivent apporter une plus value par rapport aux propriétés des LNCs initiales. Enfin, ces procédés doivent être faciles de mise en œuvre et doivent pouvoir s'adapter au cahier des charges de chaque utilisation des LNCs modifiées. La présentation des stratégies et résultats expérimentaux sera effectuée après une revue des différents types de nanovecteurs existant. On proposera une analyse des procédés récents les

plus prometteurs s'appuyant sur une modification post-formulation. Le manuscrit est composé de cinq chapitres :

Le chapitre I *Présentation, évolution des systèmes nano-particulaires et méthodes pour leur modification post-formulation* est une étude bibliographique qui sert de référence pour le travail développé dans cette thèse. Ce chapitre comporte un article de revue qui sera présenté dans *Biomaterials*.

Le chapitre II *Caractérisation physique des nanocapsules lipidiques* présente d'une part une étude de stabilité des LNCs puis d'autre part les résultats de l'analyse des LNCs par diffusion des neutrons aux petits angles. Ce chapitre comporte un article qui sera soumis à *Nanoletters*.

Le chapitre III *Modifications post-formulation des LNCs* expose les travaux effectués sur les LNCs selon deux axes principaux : le premier est l'étude du procédé de post-insertion d'abord d'une façon descriptive puis nous discuterons des possibles mécanismes pour tenter d'expliquer ce phénomène. Le deuxième point est la mise au point d'un procédé original de fonctionnalisation, le procédé de transacylation des LNCs. Nous montrerons que ce procédé satisfait pleinement aux exigences décrites précédemment, et qu'il en résulte des propriétés intéressantes pour les LNCs. Nous illustrerons ce propos en démontrant qu'il est possible avec un objet lipophile transacylé de délivrer des siRNA hydrophiles au sein de cellules humaines cancéreuses et d'avoir un effet sur le taux d'ARNm d'intérêt *in vitro*. Ce chapitre comporte deux articles : le premier en soumission dans *Journal of Physical Chemsitry B*, le second attend la parution du brevet pour être soumis.

Le chapitre IV *Etude in vitro et in vivo des LNCs modifiées à travers le modèle de l'oreille interne* présentera quelques résultats obtenus *in vitro* et *in vivo* avec des partenaires membres du consortium NanoEar. Nous discuterons aussi de l'importance du mode d'administration des LNCs vis-à-vis de l'effet biologique recherché. Ce chapitre comporte deux articles élaborés et publiés en partenariat avec d'autres équipes du projet NanoEar dans *Journal of Biomedical Materials Research Part B : Applied Biomaterials* et dans *Nanomedicine*.

Le chapitre V est une discussion générale du travail effectué au cours de ces trois années de thèse de doctorat. Il sera suivi d'une conclusion générale et d'une discussion des perspectives qui se dégagent suite à cette thèse de doctorat.

Chapitre I

Présentation, évolution des systèmes nano-particulaires et méthodes pour leur modification post-formulation

Introduction

Depuis de nombreuses années, la connaissance des pathologies humaines ne cesse d'augmenter. Cela a été rendu possible, entre autre, par le séquençage du génome humain et par une compréhension à l'échelle moléculaire de l'origine des pathologies. Ces avancées multidisciplinaires ont su tirer profit d'une nouvelle famille de sciences : les nanotechnologies. Il apparaît clairement que les pathologies comme le cancer ou les maladies génétiques requièrent un traitement à l'échelle moléculaire (voir Figure I.1) et cela au sein d'un organisme vivant composé d'une multitude de cellules de différents types. Or, les systèmes dévéloppés dans le champ des nano-technologies se prêtent à ces stratégies thérapeutiques. Pour mener à bien ces traitements, les scientifiques ont conçu des assemblages moléculaires appelés vecteurs. Ces vecteurs sont des assemblages moléculaires organisés qui ont pour but de délivrer le principe actif au sein d'une cellule cible.

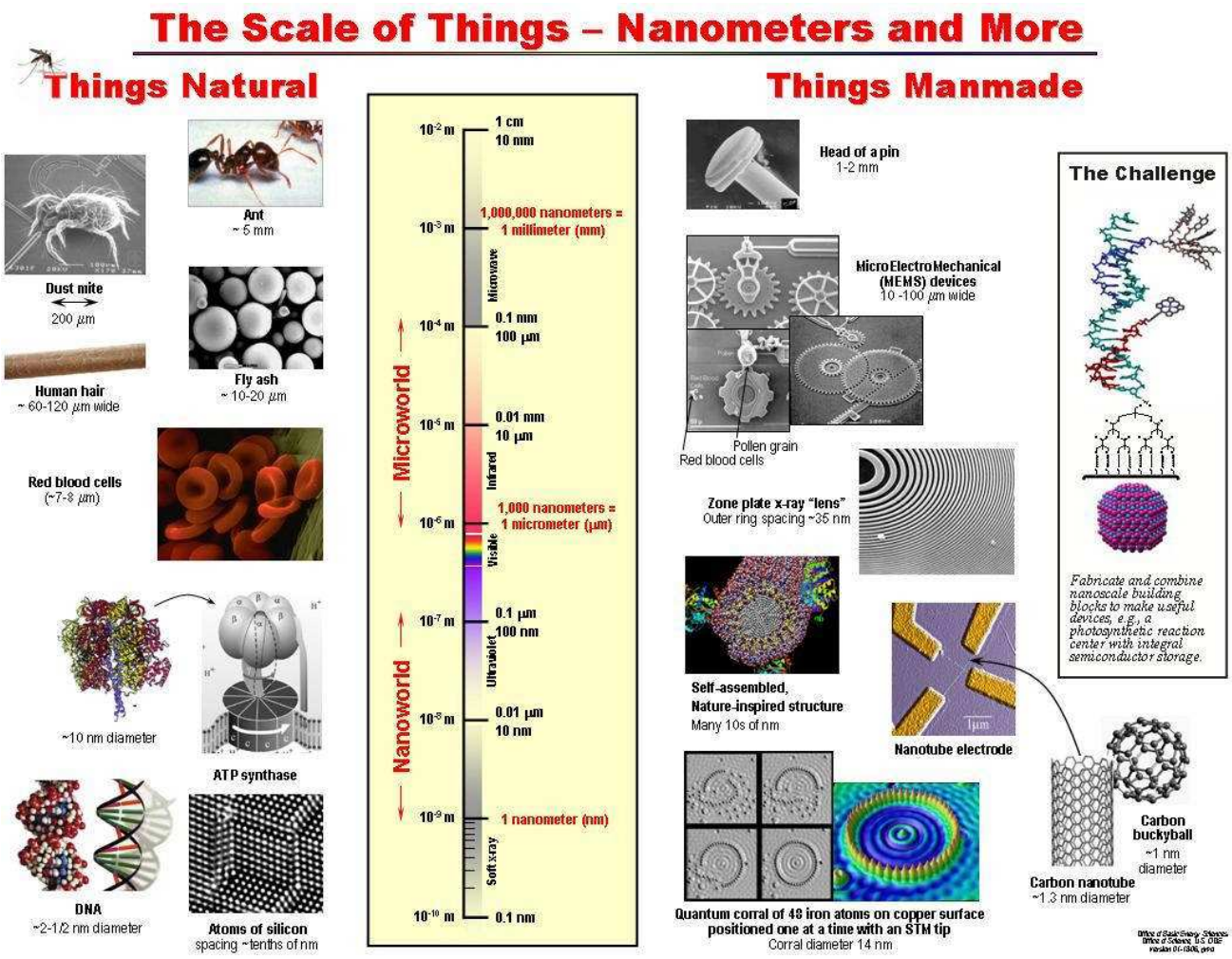

Figure I.1 : Echelle de taille d'objets naturels ou synthétiques (source : US Department of Energy).

Il existe aujourd'hui de nombreux types de vecteurs, cependant ils ont tous en commun certaine caractéristiques : en effet, ils disposent d'une partie interne, que l'on appelle généralement cœur ; et d'une partie extérieure que l'on dénomme généralement sous le terme de membrane, paroi ou coque.

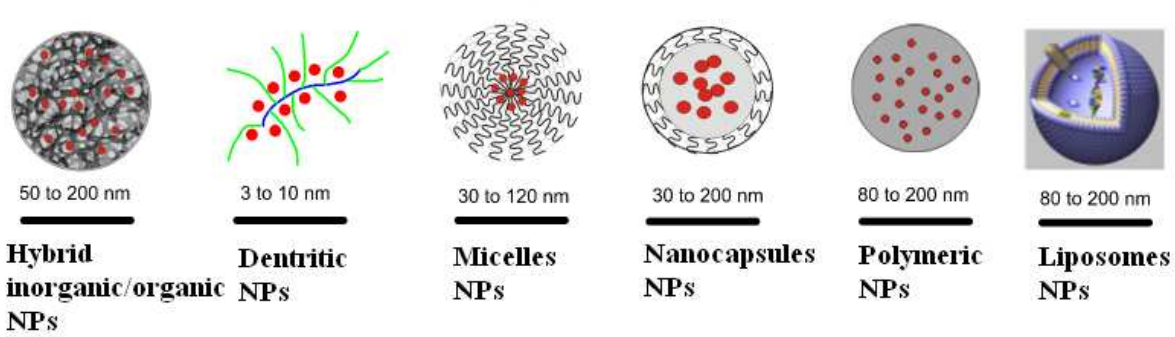

Figure I.2 : Présentation schématique des différents types de nanoparticules disponibles au sein du consortium NanoEar.

I) Présentation des différents types de nanovecteurs existants

I.1) Liposomes

Les liposomes sont des particules dont la structure est fermée et constituée d'une ou plusieurs bicouches de phospholipides concentriques avec une phase aqueuse au cœur et entre les couches phospholipidiques s'il y en a plusieurs[1,2]. Les liposomes peuvent être classés en quatre catégories selon leur taille et leur structure[3] : les liposomes multi-lamellaires, dont la taille varie de 500 à 5000 nm, et qui sont formés de plusieurs bicouches concentriques ; les liposomes unilamelaires de grande taille comprise entre 200 et 800 nm ; les liposomes unilamellaires de petite taille proche de 100 nm ; les liposomes géants dont la taille est supérieure à 1000 nm.

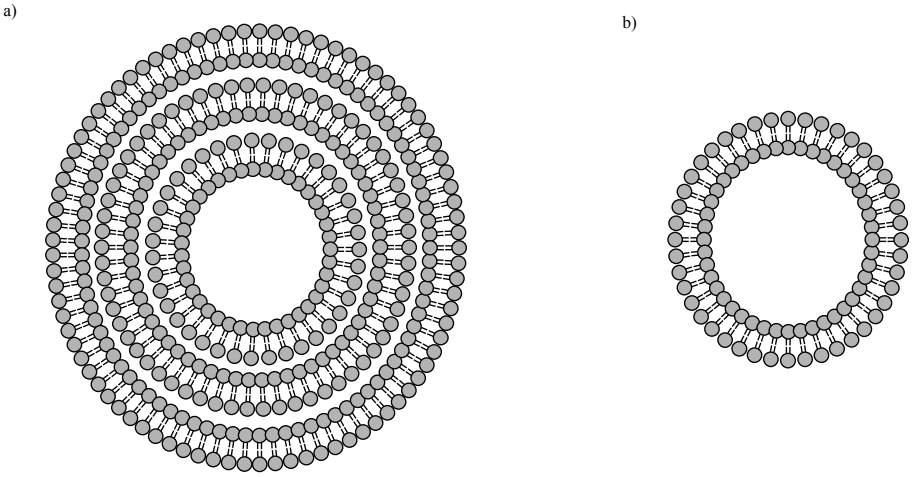

Figure I.3 : Représentation schématique d'un liposome multilamellaire a) et d'un liposome unilamellaire b).

[1]Malmsten, m.
Surfactants and polymers in drug delivery, Marcel Dekker, new York, 2002.
[2] Samad, A., Sultana, Y., Aqil, M.
Liposomal drug delivery systems: An update review
(2007) Current Drug Delivery, 4 (4), pp. 297-305.
[3] Sharma, A., Sharma, U.S.
Liposomes in drug delivery: Progress and limitations
(1997) International Journal of Pharmaceutics, 154 (2), pp. 123-140.

I.2) Vésicules[4]

Hormis les liposomes, il existe d'autres types de systèmes vésiculaires comme les nanocapusles, les polymérosomes, les niosomes ou les vésicules de type catanionique.

I.2.a) Les nanocapsules et les polymerosomes[5] sont des systèmes « réservoir » constitués d'un cœur liquide entouré d'une enveloppe dont l'épaisseur ne dépasse pas quelques nanomètres (jusqu'à 20nm). Une des différences principales entre ces deux systèmes est la structure de l'enveloppe. Dans le cas des nanocapsules, la membrane est formée par une monocouche de tensio-actifs, par un homopolymère ou un copolymère à blocs. Le cœur des nanocapsules peut-être soit huileux, soit aqueux.

Les polymèrosomes[6] ont une membrane formée par un copolymère à blocs organisés en bicouche, à l'instar des liposomes. La bicouche phospholipidique est remplacée par une couche de copolymères amphiphiles construits à partir de substances naturelles, comme des dérivés de polyoses, ou synthétiques comme le poly(butadiène)-co-poly(acide glutamique), le poly (éthylene glycol)-co-poly(éthyléthylène) , le poly(éthylène glycol)-co-poly(acide lactique) ou le poly(lysine)-co-poly(leucine).

I.2.b) Dans la famille des vésicules, on peut également citer les niosomes[7] qui ont une structure identique à celle des liposomes. La différence réside dans le fait que les phospholipides sont remplacés par des tensio-actifs non ioniques. Les niosomes ont une taille assez grande, de l'ordre du micron. Cependant, leur taille peut-être diminuée par sonication,

[4] Biju, S., Talegaonkar, S., Mishra, P., Khar, R.
Vesicular systems: An overview
(2006) Indian Journal of Pharmaceutical Sciences, 68 (2), pp. 141-153.
[5] Meng, F., Engbers, G.H.M., Feijen, J.
Biodegradable polymersomes as a basis for artificial cells: Encapsulation, release and targeting
(2005) Journal of Controlled Release, 101 (1-3 SPEC. ISS.), pp. 187-198.
[6] Rijcken, C.J.F., Soga, O., Hennink, W.E., Nostrum, C.F.v.
Triggered destabilisation of polymeric micelles and vesicles by changing polymers polarity: An attractive tool for drug delivery
(2007) Journal of Controlled Release, 120 (3), pp. 131-148.
[7] Uchegbu, I.F., Vyas, S.P.
Non-ionic surfactant based vesicles (niosomes) in drug delivery
(1998) International Journal of Pharmaceutics, 172 (1-2), pp. 33-70.

microfluidisation ou par homogénisation à haute pression pour atteindre des tailles de l'ordre de 300 nm. Pour stabiliser les niosomes, des molécules de type cholestérol doivent être ajoutées aux tensio-actifs non ioniques.

I.2.c) Les vésicules catanioniques sont formées par mélange dans l'eau de tensio-actifs ioniques portant des charges opposées[8,9,10]. Pour éviter la précipitation des tensio-actifs lorsqu'ils sont mélangés, on utilise le plus souvent un excès de l'un des tensio-actifs utilisés. Ces vésicules ont démontré leur aptitude à encapsuler des médicaments[11,12,13,14]. Ci-dessous, différents types de tensio-actifs ioniques, employés dans la formulation de vésicules catanioniques, sont présentés par la Figure 1.4. Ce sont souvent des tensio-actifs à base d'oses modifiés. Ici, nous présentons des adduits d'oses et d'amines aliphatiques. Dans le dernier cas, l'amine aliphatique est remplacée par un dérivé de l'indomethacine..

[8] Kaler, E.W., Murthy, A.K., Rodriguez, B.E., Zasadzinski, J.A.
Spontaneous vesicle formation in aqueous mixtures of single-tailed surfactants
(1989) Science, 245 (4924), pp. 1371-1374.
[9] Kondo, Y., Uchiyama, H., Yoshino, N., Nishiyama, K., Abe, M.
Spontaneous vesicle formation from aqueous solutions of didodecyldimethylammonium bromide and Sodium Dodecyl Sulfate mixtures
(1995) Langmuir, 11 (7), pp. 2380-2384.
[10] Bhattacharya, S., De Soma, Subramanian, M.
Synthesis and vesicle formation from hybrid bolaphile/ amphiphile ion-pairs. Evidence of membrane property modulation by molecular design
(1998) Journal of Organic Chemistry, 63 (22), pp. 7640-7651.
[11] Bramer, T., Dew, N., Edsman, K.
Pharmaceutical applications for catanionic mixtures
(2007) Journal of Pharmacy and Pharmacology, 59 (10), pp. 1319-1334.
[12] Fischer, A., Hebrant, M., Tondre, C.
Glucose encapsulation in catanionic vesicles and kinetic study of the entrapment/release processes in the sodium dodecyl benzene sulfonate/cetyltrimethylammonium tosylate/water system
(2002) Journal of Colloid and Interface Science, 248 (1), pp. 163-168.
[13] Rosa, M., del Carmen Morán, M., da Graça Miguel, M., Lindman, B.
The association of DNA and stable catanionic amino acid-based vesicles
(2007) Colloids and Surfaces A: Physicochemical and Engineering Aspects, 301 (1-3), pp. 361-375.
[14] Bramer, T., Dew, N., Edsman, K.
Catanionic mixtures involving a drug: A rather general concept that can be utilized for prolonged drug release from gels
(2006) Journal of Pharmaceutical Sciences, 95 (4), pp. 769-780.

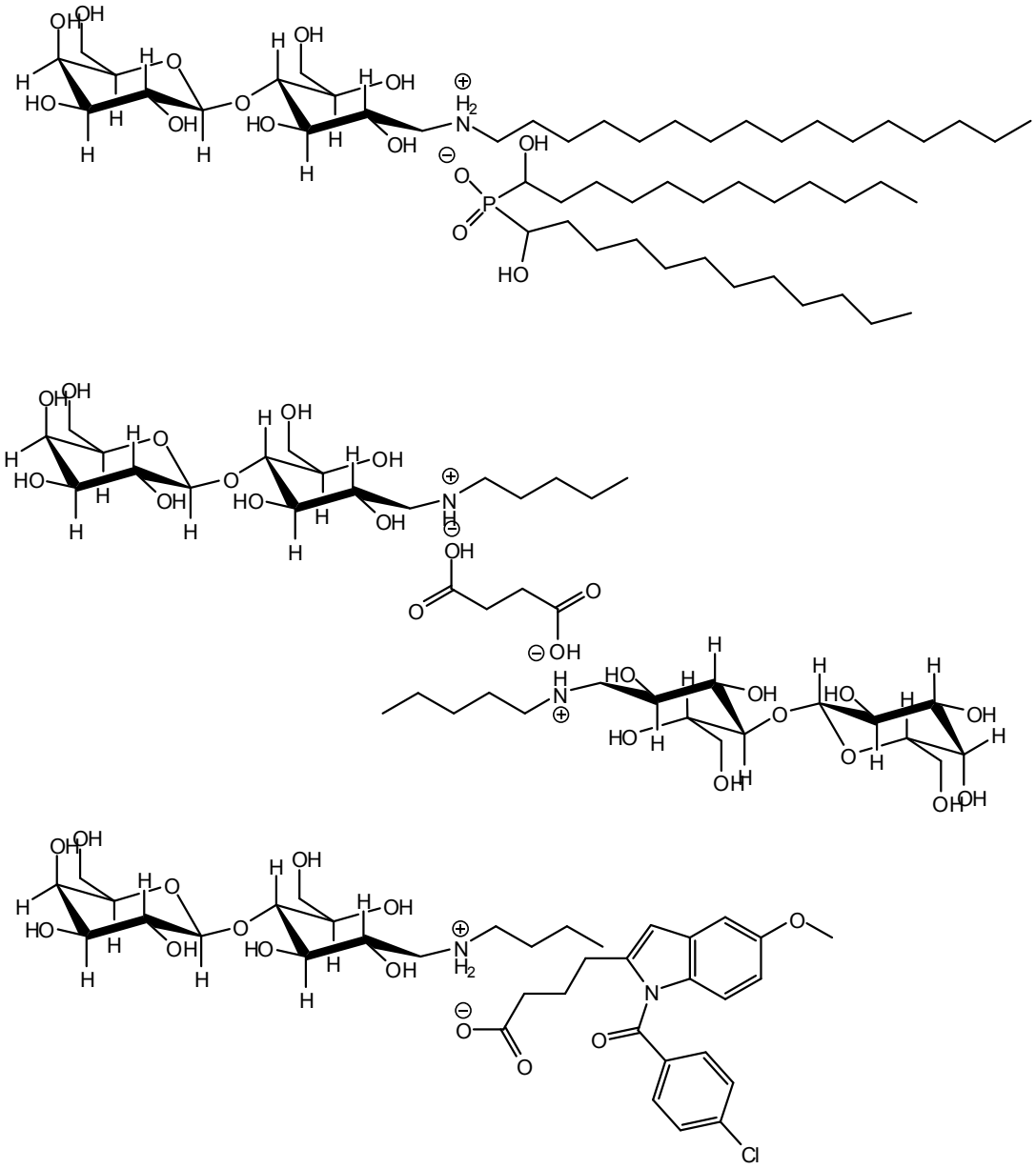

Figure I.4 : Formules chimiques de tensio-actifs utilisés pour la formation de vésicules catanioniques.

I.3) Nanoparticules polymériques

Les nanoparticules polymériques sont formées par un cœur solide de type polymérique (cas des nanosphères) ou de type solide cristallin (cas des nanoparticules lipidiques solides ou SLN).

I.3.a) Les nanosphères[15] ont des diamètres compris entre 100 et 200 nm. Des polymères naturels ou synthétiques peuvent être utilisés pour leur préparation. Leur méthode de fabrication dépend de la nature du polymère. La nature solide du cœur leur confère une grande stabilité. Cependant, leur utilisation à l'échelle industrielle est limitée car leur fabrication requiert l'utilisation de solvants organiques et/ou de monomères toxiques difficiles à éliminer.

I.3.b) Les SLN[16,17,18] ont un cœur composé de glycérides à point de fusion adapté et dont le degré de cristallinité peut-être contrôlé, en fonction de la méthode utilisée pour leur préparation. Le polymorphisme cristallin est un paramètre important pour l'utilisation des SLNs, car il est directement lié à la stabilité de ces nanoparticules.

I.4) Micelles

Les micelles sont des nano-assemblages composés de molécules amphiphiles, solubles dans le solvant utilisé, qui s'auto-organisent à partir d'une concentration donnée appelée concentration micellaire critique (CMC)[19,20]. Cette CMC dépend de la nature de la molécule amphiphile et des conditions expérimentales. On obtient des nano-objets dont la forme et le nombre dépendent de la nature de l'amphiphile utilisé[21,22,23]. Globalement, il existe deux types

[15] Vauthier, C., Bouchemal, K.
Methods for the Preparation and Manufacture of Polymeric Nanoparticles
(2009) Pharmaceutical Research, 26 (5), pp. 1025-1058.
[16] Gasco, M.R., Trotta, M.
Nanoparticles from microemulsions
(1986) International Journal of Pharmaceutics, 29 (2-3), pp. 267-268.
[17] Müller, R.H., Mäder, K., Gohla, S.
Solid lipid nanoparticles (SLN) for controlled drug delivery - A review of the state of the art
(2000) European Journal of Pharmaceutics and Biopharmaceutics, 50 (1), pp. 161-177.
[18] Gasco, M.R.
Solid lipid nanoparticles for drug delivery
(2001) Pharmaceutical Technology Europe, 13 (2), pp. 32+34+36-38+40+42.
[19] Kataoka, Kazunori
Design of nanoscopic vehicles for drug targeting based on micellization of amphiphilic block copolymers
(1994) Journal of Macromolecular Science - Pure and Applied Chemistry, A31 (11), pp. 1759-1769.
[20] Kwon, G.S., Kataoka, K.
Block copolymer micelles as long-circulating drug vehicles
(1995) Advanced Drug Delivery Reviews, 16 (2-3), pp. 295-309.
[21]Kataoka, K., Harada, A., Nagasaki, Y.
Block copolymer micelles for drug delivery: Design, characterization and biological significance

de micelles : les micelles à cœur hydrophobe dispersibles dans un solvant aqueux et les micelles à cœur hydrophile dispersible dans un solvant apolaire.

Il y a quelques années, le segment hydrophobe des amphiphiles utilisés était le plus souvent composé d'une ou plusieurs chaînes alkyl ou acyl et le segment hydrophile était le plus souvent du poly(oxyde d'éthylene) de part son excellente biocompatibilité, sa solubilité dans l'eau et son effet de protection stérique des molécules biologiquement actives.

De nos jours, le segment hydrophobe peut-être de nature polymérique tel le poly(oxyde de propylène) ou la poly(ε-caprolactone). La partie hydrophile peut-être de la poly(N-vinylpyrrolidone), du poly(alcool vinylique) ou du poly(N-isopropylacrylamide).

I.5) Dendrimères

Un dendrimère est une molécule composée de monomères (ou dendrons) qui sont reliés les uns aux autres formant une structure arborescente autour d'un cœur[24]. Les dendrimères sont des macromolécules qui peuvent être divisées en trois parties : le cœur, une partie intermédiaire composée de couches répétitives et une partie externe[25]. Ils sont synthétisés par voie chimique de manières convergente ou divergente.

La famille des dendrimères comporte quatre grands sous-groupes différents de part leur architecture[26] : les dendrimeres, les polymères hyperbranchés, les polymères supportant

(2001) Advanced Drug Delivery Reviews, 47 (1), pp. 113-131.
[22]Francis, M.F., Cristea, M., Winnik, F.M.
Polymeric micelles for oral drug delivery: Why and how
(2004) Pure and Applied Chemistry, 76 (7-8), pp. 1321-1335.
[23] Zeng, Y., Pitt, W.G.
A polymeric micelle system with a hydrolysable segment for drug delivery
(2006) Journal of Biomaterials Science, Polymer Edition, 17 (5), pp. 591-604.
[24] Tomalia, D.A., Baker, H., Dewald, J., Hall, M., Kallos, G., Martin, S., Roeck, J., Ryder, J., Smith, P.
New class of polymers: starburst-dendritic macromolecules.
(1984) Polymer Journal, 17 (1), pp. 117-132.
[25] Hawker, C.J., Fréchet, J.M.J.
Preparation of polymers with controlled molecular architecture. A new convergent approach to dendritic macromolecules
(1990) Journal of the American Chemical Society, 112 (21), pp. 7638-7647.
[26] Carlmark, A., Hawker, C., Hult, A., Malkoch, M.
New methodologies in the construction of dendritic materials
(2009) Chemical Society Reviews, 38 (2), pp. 352-362.

des dendrimeres (dendronized polymers) et les polymères à structure arborescente (dendrigrafts).

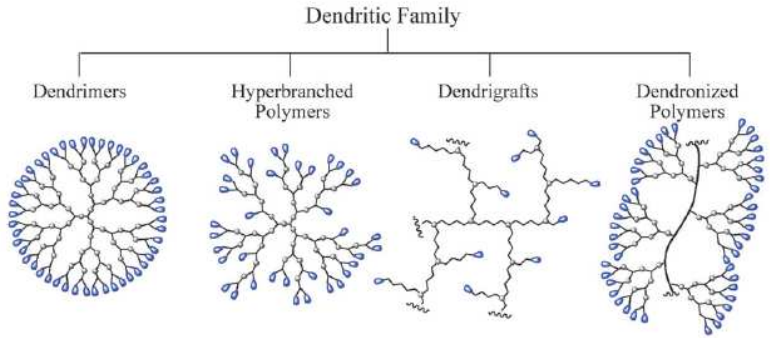

Figure I.5 : Représentation schématique des différents types de dendrimères (issu de la référence 27).

La Figure I.6 montre des exemples de dendrimères obtenus à partir de divers dendrons.

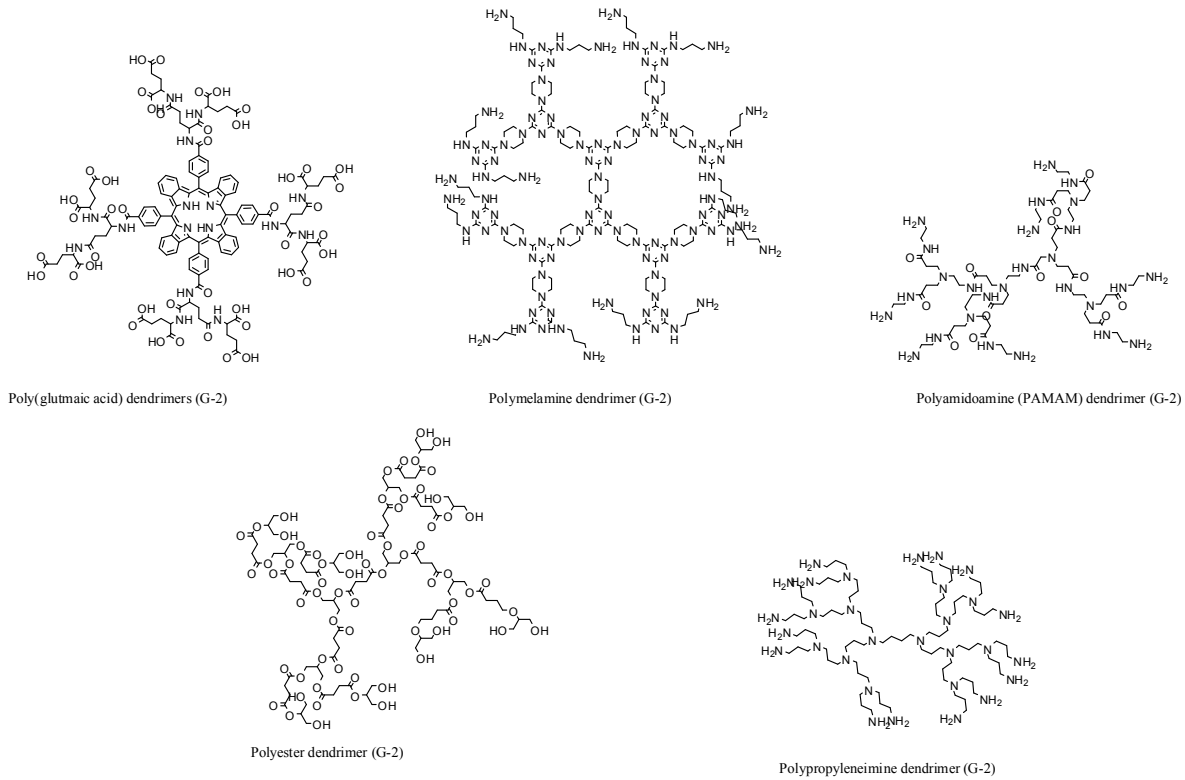

Figure I.6 : Structure moléculaire de dendrimères réalisés à partir de dendrons différents.

Des applications de dendrimères sont indiquées ci-après selon le type de dendron utilisé[27].

[27] Lee, C.C., MacKay, J.A., Fréchet, J.M.J., Szoka, F.C.
Designing dendrimers for biological applications
(2005) Nature Biotechnology, 23 (12), pp. 1517-1526.

Application	Types de dendrimers	Références
Imagerie	PAMAM, polypeptide	28,29,30,31,32
Thérapie anticancéreuse	PAMAM, polyether, polyester, polypeptide	33,34,35,36,37,38,39,40
Délivrance de drogues, vaccins	Polypeptide, PAMAM	41,42
Transport de matériels génétiques	PAMAM, polypropylène imine	43,44,45
Réparation tissulaire	Polypeptide, polyester	46,47

[28] Wiener, E.C., Brechbiel, M.W., Brothers, H., Magin, R.L., Gansow, O.A., Tomalia, D.A., Lauterbur, P.C.
Dendrimer-based metal chelates: A new class of magnetic resonance imaging contrast agents
(1994) Magnetic Resonance in Medicine, 31 (1), pp. 1-8.
[29]Margerum, Lawrence D., Campion, Brian K., Koo, Mike, Shargill, Narinder, Lai, Jan-Ji, Marumoto, Alan, Sontum, Per Christian
Gadolinium(III) DO3A macrocycles and polyethylene glycol coupled to dendrimers. Effect of molecular weight on physical and biological properties of macromolecular magnetic resonance imaging contrast agents
(1997) Journal of Alloys and Compounds, 249 (1 -2 pt 1), pp. 185-190.
[30] Dunphy, I., Vinogradov, S.A., Wilson, D.F.
Oxyphor R2 and G2: Phosphors for measuring oxygen by oxygen-dependent quenching of phosphorescence
(2002) Analytical Biochemistry, 310 (2), pp. 191-198.
[31] Rozhkov, V., Wilson, D., Vinogradov, S.
Phosphorescent Pd porphyrin-dendrimers: Tuning core accessibility by varying the hydrophobicity of the dendritic matrix [3]
(2002) Macromolecules, 35 (6), pp. 1991-1993.
[32] Ziemer, L.S., Lee, W.M.F., Vinogradov, S.A., Sehgal, C., Wilson, D.F.
Oxygen distribution in murine tumors: Characterization using oxygen-dependent quenching of phosphorescence
(2005) Journal of Applied Physiology, 98 (4), pp. 1503-1510.
[33] Kojima, C., Kono, K., Maruyama, K., Takagishi, T.
Synthesis of polyamidoamine dendrimers having poly(ethylene glycol) grafts and their ability to encapsulate anticancer drugs
(2000) Bioconjugate Chemistry, 11 (6), pp. 910-917.
[34] Liu, M., Kono, K., Fréchet, J.M.J.
Water-soluble dendritic unimolecular micelles: Their potential as drug delivery agents
(2000) Journal of Controlled Release, 65 (1-2), pp. 121-131.
[35] King, H.D., Dubowchik, G.M., Mastalerz, H., Willner, D., Hofstead, S.J., Firestone, R.A., Lasch, S.J., Trail, P.A.
Monoclonal antibody conjugates of doxorubicin prepared with branched peptide linkers: Inhibition of aggregation by methoxytriethyleneglycol chains
(2002) Journal of Medicinal Chemistry, 45 (19), pp. 4336-4343.
[36] Choe, Y.H., Conover, C.D., Wu, D., Royzen, M., Gervacio, Y., Borowski, V., Mehlig, M., Greenwald, R.B.
Anticancer drug delivery systems: Multi-loaded N4-acyl poly(ethylene glycol) prodrugs of ara-C. II. Efficacy in ascites and solid tumors
(2002) Journal of Controlled Release, 79 (1-3), pp. 55-70.
[37] Morgan, M.T., Carnahan, M.A., Immoos, C.E., Ribeiro, A.A., Finkelstein, S., Lee, S.J., Grinstaff, M.W.
Dendritic Molecular Capsules for Hydrophobic Compounds
(2003) Journal of the American Chemical Society, 125 (50), pp. 15485-15489.
[38] De Groot, F.M.H., Albrecht, C., Koekkoek, R., Beusker, P.H., Scheeren, H.W.
"Cascade-release dendrimers" liberate all end groups upon a single triggering event in the dendritic core
(2003) Angewandte Chemie - International Edition, 42 (37), pp. 4490-4494.
[39] Pasut, G., Scaramuzza, S., Schiavon, O., Mendichi, R., Veronese, F.M.
PEG-epirubicin conjugates with high drug loading
(2005) Journal of Bioactive and Compatible Polymers, 20 (3), pp. 213-230.
[40] Haba, K., Popkov, M., Shamis, M., Lerner, R.A., Barbas III, C.F., Shabat, D.
Single-triggered trimeric prodrugs
(2005) Angewandte Chemie - International Edition, 44 (5), pp. 716-720.
[41] Defoort, J.-P., Nardelli, B., Huang, W., Ho, D.D., Tam, J.P.
Macromolecular assemblage in the design of a synthetic AIDS vaccine
(1992) Proceedings of the National Academy of Sciences of the United States of America, 89 (9), pp. 3879-3883.
[42] Bourne, N., Stanberry, L.R., Kern, E.R., Holan, G., Matthews, B., Bernstein, D.I.
Dendrimers, a new class of candidate topical microbicides with activity against herpes simplex virus infection
(2000) Antimicrobial Agents and Chemotherapy, 44 (9), pp. 2471-2474.
[43] Haensler, J., Szoka Jr., F.C.
Polyamidoamine cascade polymers mediate efficient transfection of cells in culture
(1993) Bioconjugate Chemistry, 4 (5), pp. 372-379.
[44] Tang, M.X., Redemann, C.T., Szoka Jr., F.C.
In vitro gene delivery by degraded polyamidoamine dendrimers
(1996) Bioconjugate Chemistry, 7 (6), pp. 703-714.
[45] Vincent, L., Varet, J., Pille, J.-Y., Bompais, H., Opolon, P., Maksimenko, A., Malvy, C., Mirshahi, M., Lu, H., Vannier, J.-P., Soria, C., Li, H.
Efficacy of dendrimer-mediated angiostatin and TIMP-2 gene delivery on inhibition of tumor growth and angiogenesis: In vitro and in vivo studies
(2003) International Journal of Cancer, 105 (3), pp. 419-429.
[46] Wathier, M., Jung, P.J., Carnahan, M.A., Kim, T., Grinstaff, M.W.
Dendritic macromers as in situ polymerizing biomaterials for securing cataract incisions
(2004) Journal of the American Chemical Society, 126 (40), pp. 12744-12745.

I.6) Nanoparticules hybrides organiques/inorganiques

Ce sont le plus souvent des particules ayant un cœur métallique recouvert par une couche de molécules qui peuvent être de nature hydrophile ou hydrophobe. Ces molécules sont des agents de recouvrement qui permettent de contrôler le caractère hydrophile ou lipophile des objets finaux. Ces agents de recouvrement peuvent être de nature tensio-active ou non.

I.6.a) Nanoparticules magnétiques

Elles sont composées de différentes susbstances comme des oxydes de fer[48,49] (Fe_3O_4, γ-Fe_2O_3), des métaux purs[50,51] (Fe, Co), des oxydes de fer dopés[52,53] ($MgFe_2O_4$, $MnFe_2O_4$, $CoFe_2O_4$) ou bien des alliages[54,55,56] ($CoPt_3$, FePt).

Les procédés de synthèse sont aujourd'hui nombreux et peuvent-être classés en quatre catégories : co-précipitation[57,58,59,60], décomposition thermique[61,62,63,64], microémulsion[65,66,67] et synthèse en milieu aqueux[68,69].

[47] Velazquez, A.J., Carnahan, M.A., Kristinsson, J., Stinnett, S., Grinstaff, M.W., Kim, T.
New dendritic adhesives for sutureless ophthalmic surgical procedures: In vitro studies of corneal laceration repair
(2004) Archives of Ophthalmology, 122 (6), pp. 867-870.
[48] Weissleder, R., Lee, A.S., Fischman, A.J., Reimer, P., Shen, T., Wilkinson, R., Callahan, R.J., Brady, T.J.
Polyclonal human immunoglobulin G labeled with polymeric iron oxide: Antibody MR imaging
(1991) Radiology, 181 (1), pp. 245-249.
[49] Bulte, J.W.M., Kraitchman, D.L.
Iron oxide MR contrast agents for molecular and cellular imaging
(2004) NMR in Biomedicine, 17 (7), pp. 484-499.
[50] Park, S.-J., Kim, S., Lee, S., Khim, Z.G., Char, K., Hyeon, T.
Synthesis and magnetic studies of uniform iron nanorods and nanospheres [12]
(2000) Journal of the American Chemical Society, 122 (35), pp. 8581-8582.
[51] Puntes, V.F., Krishnan, K.M., Alivisatos, A.P.
Colloidal nanocrystal shape and size control: The case of cobalt
(2001) Science, 291 (5511), pp. 2115-2117.
[52] Lee, J.-H., Huh, Y.-M., Jun, Y.-W., Seo, J.-W., Jang, J.-T., Song, H.-T., Kim, S., Cho, E.-J., Yoon, H.-G., Suh, J.-S., Cheon, J.
Artificially engineered magnetic nanoparticles for ultra-sensitive molecular imaging
(2007) Nature Medicine, 13 (1), pp. 95-99.
[53] Lu, A.-H., Salabas, E.L., Schüth, F.
Magnetic nanoparticles: Synthesis, protection, functionalization, and application
(2007) Angewandte Chemie - International Edition, 46 (8), pp. 1222-1244.
[54] Park, J.-I., Cheon, J.
Synthesis of "solid solution" and "core-shell" type cobalt-platinum magnetic nanoparticles via transmetalation reactions
(2001) Journal of the American Chemical Society, 123 (24), pp. 5743-5746.
[55] Shevchenko, E.V., Talapin, D.V., Rogach, A.L., Kornowski, A., Haase, M., Weller, H.
Colloidal synthesis and self-assembly of CoPt3 nanocrystals
(2002) Journal of the American Chemical Society, 124 (38), pp. 11480-11485.
[56] Sun, S.
Recent advances in chemical synthesis, self-assembly, and applications of FePt nanoparticles
(2006) Advanced Materials, 18 (4), pp. 393-403.

Elles présentent des intérêts multiples dans le domaine des biotechnologies et des biomédecines. On peut citer notamment les techniques de séparation magnétique, qui permettent d'isoler des protéines ou des acides nucléiques présents à des concentrations très faibles (femtomoles) à partir d'un échantillon biologique. On peut aussi citer le traitement du cancer par hyperthermie locale ou l'imagerie RMN. Dans une démarche analogue à celle développée pour les autres types de nanoparticules, les nanoparticules magnétiques doivent être recouvertes par des agents stabilisants dans le but d'assurer leur solubilité et leur stabilité dans différents milieux en fonction de leur utilisation.

[57] Kandori, K., Kawashima, Y., Ishikawa, T.
Effects of citrate ions on the formation of monodispersed cubic hematite particles
(1992) Journal of Colloid And Interface Science, 152 (1), pp. 284-288.
[58] Lee, J., Isobe, T., Senna, M.
Magnetic properties of ultrafine magnetite particles and their slurries prepared via in-situ precipitation
(1996) Colloids and Surfaces A: Physicochemical and Engineering Aspects, 109, pp. 121-127.
[59] Cushing, B.L., Kolesnichenko, V.L., O'Connor, C.J.
Recent advances in the liquid-phase syntheses of inorganic nanoparticles
(2004) Chemical Reviews, 104 (9), pp. 3893-3946.
[60] Willis, A.L., Turro, N.J., O'Brien, S.
Spectroscopic characterization of the surface of iron oxide nanocrystals
(2005) Chemistry of Materials, 17 (24), pp. 5970-5975.
[61] Park, J., An, K., Hwang, Y., Park, J.E.-G., Noh, H.-J., Kim, J.-Y., Park, J.-H., Hwang, N.-M., Hyeon, T.
Ultra-large-scale syntheses of monodisperse nanocrystals
(2004) Nature Materials, 3 (12), pp. 891-895.
[62] Redl, F.X., Black, C.T., Papaefthymiou, G.C., Sandstrom, R.L., Yin, M., Zeng, H., Murray, C.B., O'Brien, S.P.
Magnetic, electronic, and structural characterization of nonstoichiometric iron oxides at the nanoscale
(2004) Journal of the American Chemical Society, 126 (44), pp. 14583-14599.
[63] Jana, N.R., Chen, Y., Peng, X.
Size- and shape-controlled magnetic (Cr, Mn, Fe, Co, Ni) oxide nanocrystals via a simple and general approach
(2004) Chemistry of Materials, 16 (20), pp. 3931-3935.
[64] Sun, S., Zeng, H., Robinson, D.B., Raoux, S., Rice, P.M., Wang, S.X., Li, G.
Monodisperse MFe2O4 (M = Fe, Co, Mn) Nanoparticles
(2004) Journal of the American Chemical Society, 126 (1), pp. 273-279.
[65] Moumen, N., Pileni, M.P.
Control of the size of cobalt ferrite magnetic fluid
(1996) Journal of Physical Chemistry, 100 (5), pp. 1867-1873.
[66] Carpenter, E.E., Seip, C.T., O'Connor, C.J.
Magnetism of nanophase metal and metal alloy particles formed in ordered phases
(1999) Journal of Applied Physics, 85 (8 II A), pp. 5184-5186.
[67] Woo, K., Lee, H.J., Ahn, J.-P., Park, Y.S.
Sol-Gel Mediated Synthesis of Fe2O3 Nanorods
(2003) Advanced Materials, 15 (20), pp. 1761-1764.
[68] Wang, X., Zhuang, J., Peng, Q., Li, Y.
A general strategy for nanocrystal synthesis
(2005) Nature, 437 (7055), pp. 121-124.
[69] Deng, H., Li, X., Peng, Q., Wang, X., Chen, J., Li, Y.
Monodisperse magnetic single-crystal ferrite microspheres
(2005) Angewandte Chemie - International Edition, 44 (18), pp. 2782-2785.

I.6.b) Nanoparticules d'or

Depuis leur découverte par Faraday[70] au 19ème siècle, l'or colloïdal a connu nombre d'applications. Elles sont obtenues le plus souvent par réduction[71,72] de $HAuCl_4$ par divers agents réducteurs comme le citrate de sodium. Cette méthode a connu plusieurs modifications qui ont permis d'améliorer les distributions de taille ainsi que d'améliorer les tailles moyennes, désormais comprises entre 9 et 120 nm[73]. Elles peuvent être recouvertes par de nombreux ligands notamment des thiols[74]. La méthode de Shiffrin-Brust permet la synthèse de nanoparticules d'or et l'introduction de thiols fonctionnels simultanément[75,76].

I.6.c) Quantum dots[77]

Les quantum dots sont des semi-conducteurs[78,79,80] dont les excitons sont confinés dans les trois dimensions de l'espace. Ils ont des propriétés particulières, comprises entre celles des semiconducteurs classiques et celles des molécules discrètes. Dans un semi-

[70] Faraday, M. Philos. Trans. R. Soc. London, 1857, 147, 145-181.
[71] Turkevich, J., Stevenson, P.C., Hillier, J.
A study of the nucleation and growth processes in the synthesis of colloidal gold
(1951) Discussions of the Faraday Society, 11, pp. 55-75.
[72] Tréguer-Delapierre, M., Majimel, J., Mornet, S., Duguet, E., Ravaine, S.
Synthesis of non-spherical gold nanoparticles
(2008) Gold Bulletin, 41 (2), pp. 195-207.
[73] Kimling, J., Maier, M., Okenve, B., Kotaidis, V., Ballot, H., Plech, A.
Turkevich method for gold nanoparticle synthesis revisited
(2006) Journal of Physical Chemistry B, 110 (32), pp. 15700-15707.
[74] Templeton, A.C., Wuelfing, W.P., Murray, R.W.
Monolayer-protected cluster molecules
(2000) Accounts of Chemical Research, 33 (1), pp. 27-36.
[75] Brust, M., Walker, M., Bethell, D., Schiffrin, D.J., Whyman, R.
Synthesis of thiol-derivatised gold nanoparticles in a two-phase liquid-liquid system
(1994) Journal of the Chemical Society, Chemical Communications, (7), pp. 801-802.
[76] Daniel, M.-C., Astruc, D.
Gold Nanoparticles: Assembly, Supramolecular Chemistry, Quantum-Size-Related Properties, and Applications Toward Biology, Catalysis, and Nanotechnology
(2004) Chemical Reviews, 104 (1), pp. 293-346.
[77] Reiss, P., Protière, M., Li, L.
Core/shell semiconductor nanocrystals
(2009) Small, 5 (2), pp. 154-168.
[78] Hines, M.A., Guyot-Sionnest, P.
Synthesis and characterization of strongly luminescing ZnS-capped CdSe nanocrystals
(1996) Journal of Physical Chemistry, 100 (2), pp. 468-471.
[79] Peng, X., Schlamp, M.C., Kadavanich, A.V., Alivisatos, A.P.
Epitaxial growth of highly luminescent CdSe/CdS core/shell nanocrystals with photostability and electronic accessibility
(1997) Journal of the American Chemical Society, 119 (30), pp. 7019-7029.
[80] Dabbousi, B.O., Rodriguez-Viejo, J., Mikulec, F.V., Heine, J.R., Mattoussi, H., Ober, R., Jensen, K.F., Bawendi, M.G.
(CdSe)ZnS core-shell quantum dots: Synthesis and characterization of a size series of highly luminescent nanocrystallites
(1997) Journal of Physical Chemistry B, 101 (46), pp. 9463-9475.

conducteur classique, la paire électron-trou est séparée d'une distance que l'on appelle le rayon de Bohr de l'exciton. Si l'électron et le trou sont confinés ensemble, les propriétés du semi-conducteur changent. Les quantum dots sont composés de quelques centaines à quelques milliers d'atomes, avec une taille comprise entre 2 et 10 nm.

Ils sont fabriqués à partir de cadmium, de sélénium, de tellure, d'indium, d'arsenic et de soufre.

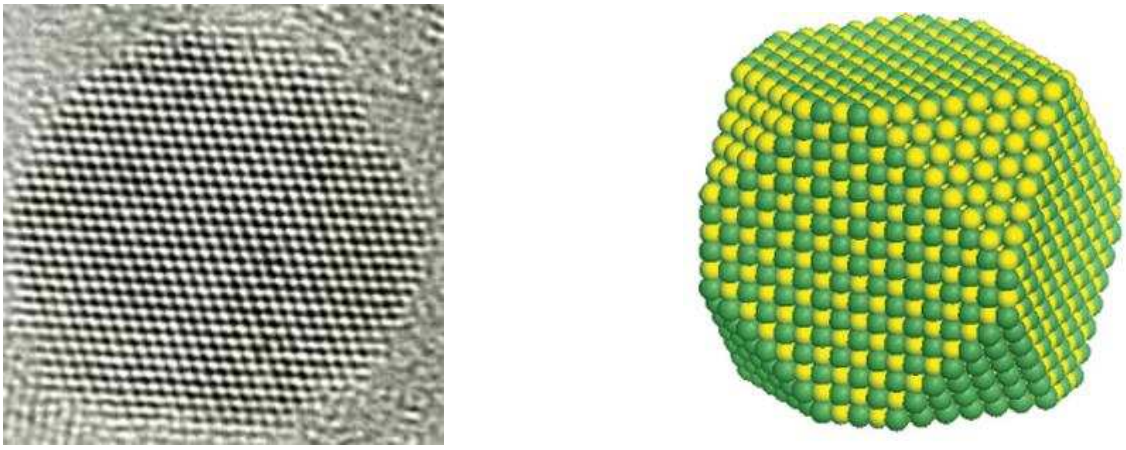

Figure I.7 : Structure d'un quantum dots par microscopir éléctronique à haute résolution (à gauche) et modèle simulé (à droite).

Ils contiennent au moins deux éléments semi-conducteurs dans une structure de type oignon. Leur cœur est porteur des propriétés optiques comme la longueur d'onde de fluorescence, le rendement quantique ou la durée de vie de fluorescence. La partie externe est une barrière physique entre le cœur optiquement actif et l'environnement extérieur. Cela permet de diminuer les effets de l'environnement sur les propriétés optiques des quantum dots[81].

Il existe différents types de quantum dots ayant une structure cœur-couronne[82,83]. Ces systèmes peuvent être classés en fonction de la position de la bande de conduction et de la

[81] Scholes, G.D.
Controlling the optical properties of inorganic nanoparticles
(2008) Advanced Functional Materials, 18 (8), pp. 1157-1172.
[82] Van Embden, J., Jasieniak, J., Gómez, D.E., Mulvaney, P., Giersig, M.
Review of the synthetic chemistry involved in the production of core/shell semiconductor nanocrystals
(2007) Australian Journal of Chemistry, 60 (7), pp. 457-471.

bande de valence du cœur et de la couronne respectivement. On peut schématiser cela par la Figure suivante :

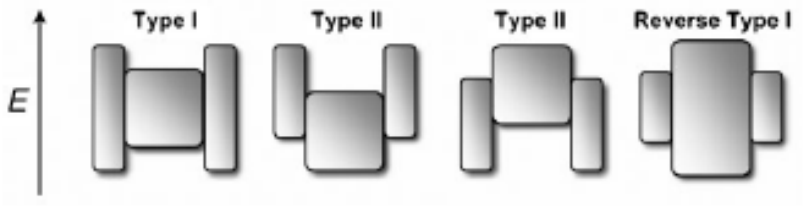

Figure I.8 : Position relative des bandgaps du cœur et de la courronne pour les différents types de quantum dots.

Pour les particules de type I, le bandgap de la couronne est plus large que celui du cœur, les couples trou-électron étant confinés dans le cœur. A contrario, pour les particules de type I inversé, le bandgap de la couronne est plus étroit que celui du cœur. En fonction de l'épaisseur de la couronne, les trous et les électrons sont partiellement ou complètement confinés à l'intérieur de celle-ci. Pour les particules de type II, la bande de valence ou la bande de conduction de la couronne est localisée dans le bandgap du cœur.

Pour les particules de type I, la couronne sert à isoler le cœur du milieu extérieur. Dans les particules de type I inversé, les transporteurs de charge (trous et éléctrons) sont déplacés vers la couronne.

Dans les particules de type II, la croissance de la couronne entraîne un déplacement des longueurs d'onde d'émission vers le rouge. L'intérêt de tous ces systèmes réside dans le fait que la couleur d'émission peut-être réglée en jouant sur l'épaisseur de la couronne.

[83] Dorfs, D., Eychmüller, A.
Multishell semiconductor nanocrystals
(2006) Zeitschrift fur Physikalische Chemie, 220 (12), pp. 1539-1552.

II) Evolution des nanovecteurs au cours du temps

II.1) Nanovecteurs de première génération

Les nanovecteurs de première génération sont des particules nanométriques qui ont une structure cœur/interface et dont cette dernière est peu ou pas travaillée. Elle est constituée de molécules tensioactives qui n'apportent pas de propriétés de ciblage et/ou de furtivité vis-à-vis de l'hôte. Ces nanoparticules présentent des temps de circulation sanguine très faible. Une famille de protéines plasmatiques, les opsonines, présentent la propriété de se lier à la surface de ces particules. Le « complexe » ainsi formé est reconnu par les macrophages qui les internalisent par endocytose. Cela se traduit au niveau de l'organisme par une accumulation des constituants de ces nanovecteurs au niveau du foie, de la rate ou de la moelle. De ce fait, ces nanovecteurs ont un intérêt thérapeutique uniquement si le foie ou la rate sont les organes cibles.

II.2) Nanovecteurs de deuxième génération

Dans le but de réduire les interactions nanovecteur-opsonines, l'interface des nanovecteurs doit comporter des groupements chimiques qui limitent la fixation des opsonines. Ceci est réalisé en utilisant des polymères non naturels comme les poly éthylène glycols ou les poly éthylène-poly propylène glycols ; ou des polymères naturels comme des polysaccharides. On dit alors que les nanovecteurs de deuxième génération sont furtifs vis-à-vis des systèmes de reconnaissance de l'hôte. Le temps de circulation plasmatique est augmenté de façon significative. Le caractère immunogène des nanovecteurs peut être déterminé, entre autre, quantitativement par mesure de l'activation du complément. De plus,

la présence de poly oxyde d'éthylène semble améliorer la biocompatibilité des nanovecteurs. L'ensemble de ces facteurs aboutissent à un relargage plus long du principe actif.

II.3) Nanovecteurs de troisième génération

Une partie de l'interface des nanovecteurs de deuxième génération peut comporter des ligands spécifiques d'un organe, d'une population cellulaire ou d'un organite donné. On parle alors de ciblage actif. Plusieurs stratégies ont été utilisées avec succès :

- greffage d'un anticorps spécifique d'une cible donnée (récepteurs cellulaires, par exemple) par voie covalente (réversible ou non réversible). On parle alors d'immunonanoparticules[84].
- greffage de séquence peptidique visant des récepteurs particuliers[85] :

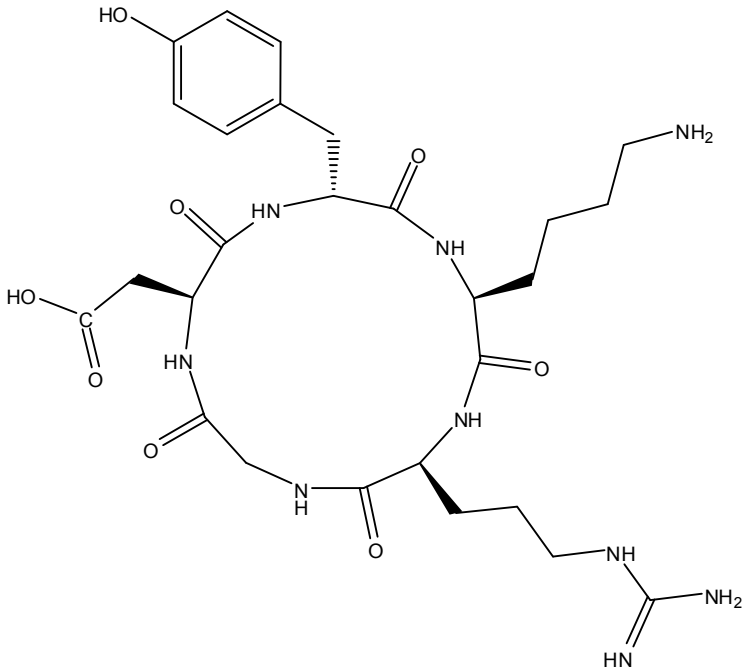

Figure I.9 : Peptide RGD (arginine-glycine-acide aspartique) reconnaissant les intégrines $\alpha_5\beta_3$.

[84] Obermajer, N., Kocbek, P., Repnik, U., Kužnik, A., Cegnar, M., Kristl, J., Kos, J.
Immunonanoparticles - An effective tool to impair harmful proteolysis in invasive breast tumor cells
(2007) FEBS Journal, 274 (17), pp. 4416-4427.
[85] Dunehoo, A.L., Anderson, M., Majumdar, S., Kobayashi, N., Berkland, C., Siahaan, T.J.
Cell adhesion molecules for targeted drug delivery
(2006) Journal of Pharmaceutical Sciences, 95 (9), pp. 1856-1872.

- reffage d'oses pour le ciblage de cellules ayant des récepteurs de sucre spécifiques comme les cellules hépatiques[86] ou certaines cellules cancéreuses[87]

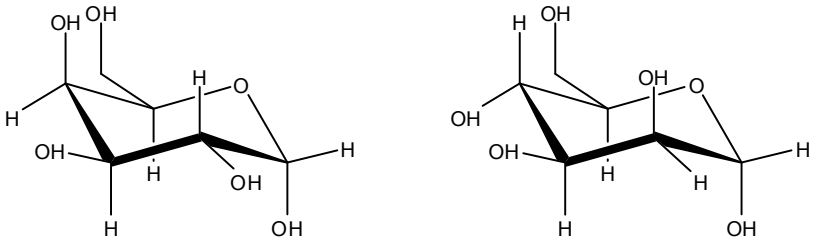

Figure I.10 : Structure chimique du galactose (à gauche) et du maltose (à droite).

- greffage d'acide folique pour le ciblage des cellules surexprimant le récepteur à l'acide folique[88,89]

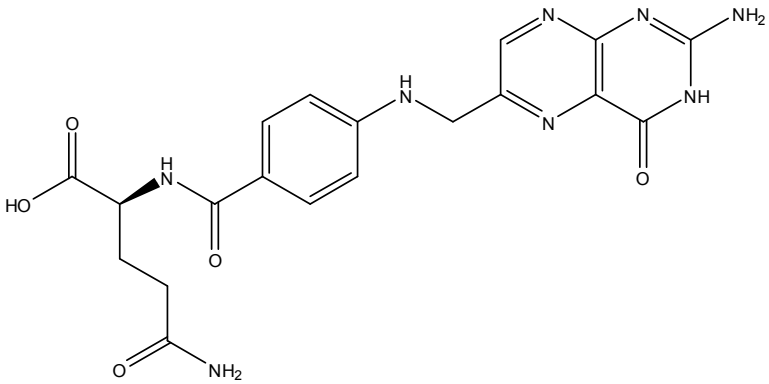

Figure I.11 : Structure de l'acide folique utilisé pour cibler les cellules surexprimant son récépteur.

Il est important de souligner que la façon dont le ligand est présenté influe sur l'activité biologique des nanoparticules. En effet, la densité de ligand à la surface a un rôle important sur la reconnaissance et la fixation sur le récepteur. De plus, cela détermine les paramètres physico-chimiques des nanovecteurs.

Les nanovecteurs de troisième génération représentent ainsi un début de solutions thérapeutiques.

[86] Kasuya, T., Kuroda, S.
Nanoparticles for human liver-specific drug and gene delivery systems: In vitro and in vivo advances
(2009) Expert Opinion on Drug Delivery, 6 (1), pp. 39-52.
[87] Irache, J.M., Salman, H.H., Gamazo, C., Espuelas, S.
Mannose-targeted systems for the delivery of therapeutics
(2008) Expert Opinion on Drug Delivery, 5 (6), pp. 703-724.
[88] Sudimack, J., Lee, R.J.
Targeted drug delivery via the folate receptor
(2000) Advanced Drug Delivery Reviews, 41 (2), pp. 147-162.
[89] Zhao, X.B., Lee, R.J.
Tumor-selective targeted delivery of genes and antisense oligodeoxyribonucleotides via the folate receptor
(2004) Advanced Drug Delivery Reviews, 56 (8), pp. 1193-1204.

II.4) Nanovecteurs de génération ultérieure

Dans cette présentation de l'évolution des systèmes nanovectoriels, l'accent a été mis sur la partie interfaciale des nanovecteurs et les propriétés qu'elle leur confère. Cependant, il apparaît important de souligner que les nanovecteurs doivent pouvoir assurer plusieurs fonctions et ce, simultanément. En effet, on ne peut dissocier les aspects thérapeutiques des aspects diagnostiques et/ou de traçage des nanovecteurs. Autrement dit, les nanovecteurs doivent pouvoir transporter l'actif pharmaceutique vers une cible précise mais on doit pouvoir aussi suivre le cheminement de ces vecteurs à l'intérieur de l'hôte. Les nanovecteurs doivent comporter des systèmes de traçage qui peuvent être optiques (fluorescence), radioactifs ou physiques (agent de contraste pour l'IRM). On construit alors des nanovecteurs multifonctionnels. Cependant, l'analyse fine de leur comportement vis-à-vis de l'hôte est rendue plus complexe et plus coûteuse à cause du nombre important de paramètres mis en jeu.

La partie externe du vecteur, quelle que soit sa nature, a deux rôles majeurs :
-assurer la protection de la partie interne du vecteur vis-à-vis des agressions extérieures ;
-elle est le support des fonctions de reconnaissance et d'adressage du vecteur.

Depuis les origines des nanovecteurs, il apparaît clairement que ceux-ci sont de plus en plus organisés et polarisés et que la partie interfaciale est le support d'une ou plusieurs fonctions du vecteur. Les nanovecteurs sont devenus des nano-objets multifonctionnels et multipotents.

III) Méthodes pour la modification post-formulation des nanovecteurs

Methods to functionalize organic nanoparticles, new insights and perspectives : a review

Thomas Perrier, Jean-Pierre Benoît and Patrick Saulnier*

Inserm U646, Ingénierie de la vectorisation particulaire, Université d'Angers, 49100 Angers, France

*To whom correspondence should be addressed. E-mail address : patrick.saulnier@univ-angers.fr

Abstract

In the field of nanometric drug delivery systems, a wide range of colloidal systems has been formulated in the last decades. All the systems have a similar global structure, that is to say an inner part and an external surface/interface. In several applications, the external interface is the support for desired properties and the base of future developments. By the way, the engineering of the particle's surface is an emerging step in the design of systems at the nanometric scale. This review presents and summarizes the available techniques with a particular attention to recent advances. It is also a base for future works in this expanding area of research.

Keywords: Nanoparticles; Post-insertion; Layer-by-layer; Metathesis; Click chemistry, Diels-Alder, Multifunctional Nanoparticles.

Introduction

Nowadays, drug delivery systems[90,91,92,93] are the center of interest in many fields from chemistry to medicine[94]. Some of them, called organic nanoparticles take advantage of particular molecular associations leading to colloidal objects elaborated upon a lot of formulation protocols. However, few organic nanoparticles can be formulated directly with the final properties, that is to say satisfying the followings goals: correct assembly at the molecular level, loaded with drug and/or reporter, interface mastered and engineered. Indeed, modifications of the formulation protocols are difficult and can dramatically change the properties of nanoparticles and/or lead to an incapability to form them. So, production processes are relevant in narrow formulation windows, called feasibility domains. For example, formulations based on PIT methods[95,96] are strongly affected by parameters as simple as the salt concentration: that is to say, starting from the same amount of materials, feasibility zone can be set at a temperature ranging from 45°C to almost 90°C. The

[90] Torchilin, V.P.
Multifunctional nanocarriers
(2006) Advanced Drug Delivery Reviews, 58 (14), pp. 1532-1555.
[91] Torchilin, V.
Multifunctional and stimuli-sensitive pharmaceutical nanocarriers
(2009) European Journal of Pharmaceutics and Biopharmaceutics, 71 (3), pp. 431-444.
[92] Rico-Lattes, I., Blanzat, M., Franceschi-Messant, S., Perez, É., Lattes, A.
Catanionic sugar derived surfactants, polymers and dendrimers: From molecules to targeted self-organized systems
(2005) Comptes Rendus Chimie, 8 (5), pp. 807-814.
[93] Soussan, E., Cassel, S., Blanzat, M., Rico-Lattes, I.
Drug delivery by soft matter: Matrix and vesicular carriers
(2009) Angewandte Chemie - International Edition, 48 (2), pp. 274-288.
[94] Suh, W.H., Suh, Y.-H., Stucky, G.D.
Multifunctional nanosystems at the interface of physical and life sciences
(2009) Nano Today, 4 (1), pp. 27-36.
[95] Shinoda, K., Saito, H.
The Stability of O/W type emulsions as functions of temperature and the HLB of emulsifiers: The emulsification by PIT-method
(1969) Journal of Colloid And Interface Science, 30 (2), pp. 258-263.
[96] Anton, N., Benoit, J.-P., Saulnier, P.
Design and production of nanoparticles formulated from nano-emulsion templates-A review
(2008) Journal of Controlled Release, 128 (3), pp. 185-199.

importance of such variations is emphasized when nanoparticles have to be loaded with thermosensible anti-cancer drugs. Another example is the formulation of pegylated liposomes: from a protocol designed from the production of first generation liposomes, the introduction of pegylated amphiphiles requires to re-build completely the feasibility window. Furthermore, these difficulties explain why few commercial liposomes are available to the market even if they are developed since many decades. An important number of nanoparticles are designed for the vectorization of hydrophobic substances and should be composed by a hydrophobic phase such as triglycerides. Modifications of the triglycerides chain lengths can destroy the established protocols and work should be re-done from then beginning, with evident additional financial costs.

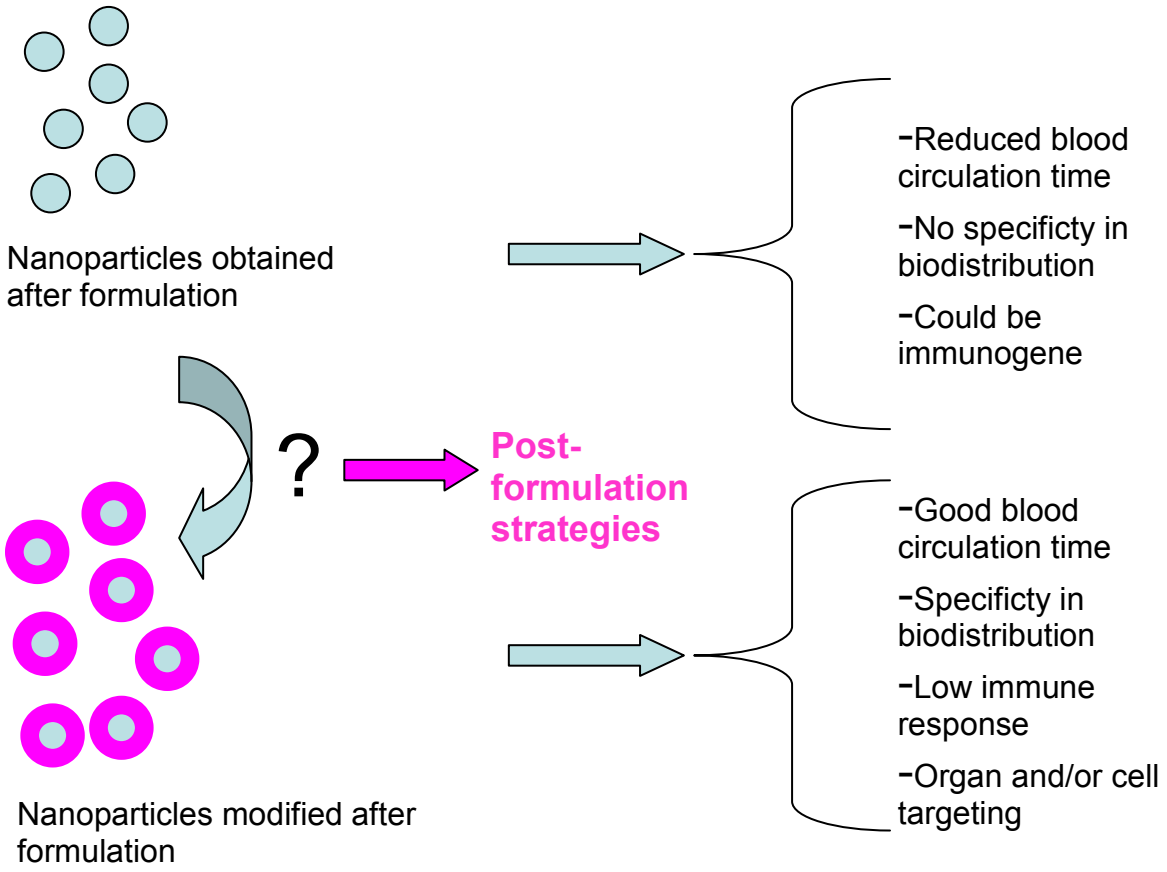

Figure I.12: Characteristics of nanoparticles before and after modifications.

Figure I.12 illustrates the use of nanoparticles in the nanomedecine field. If particles are used directly after formulation, their parameters (size, presence of electric charges at the

surface, zeta potential) can dramatically decrease their potentialities[97,98]. Limited blood time circulation and distribution of active drugs in the whole body bring more problems than solutions. On the other hand, if particles are modified trough post-formulation strategies, problems can be solved without the need to set up the formulation process.

By the way, a new approach has emerged: instead of working to modify manufacturing process in a hard way, nanoparticles could be considered as nanometric platforms on which one can performs modifications in a rational and a controlled way. Thus, besides manufacturing processes, strategies for nanoparticle post-modification have arisen. Herein, we present rational methods, based on molecular physic and chemistry, which are the main ways to functionalize soft organic nanoparticles.

III.1) Molecular physical methods

III.1.a) Post-insertion

Generally speaking, post-insertion is the transfer of amphipathic molecules from micellar assemblies to a preformed nanoparticles. This process leads to the incorporation of a molar fraction of amphipathic molecules (or all of them) into the external layer of the receiver. This technique was developed initially on the liposomes[99,100] and has been adapted for nanoparticles of other types, in particular LipidicNanoCapsules (LNCs)[101,102]. Globally,

[97] Vonarbourg, A., Passirani, C., Saulnier, P., Simard, P., Leroux, J.C., Benoit, J.P.
Evaluation of pegylated lipid nanocapsules versus complement system activation and macrophage uptake
(2006) Journal of Biomedical Materials Research - Part A, 78 (3), pp. 620-628.
[98] Vonarbourg, A., Passirani, C., Saulnier, P., Benoit, J.-P.
Parameters influencing the stealthiness of colloidal drug delivery systems
(2006) Biomaterials, 27 (24), pp. 4356-4373.
[99] Moreira, J.N., Ishida, T., Gaspar, R., Allen, T.M.
Use of the post-insertion technique to insert peptide ligands into pre-formed stealth liposomes with retention of binding activity and cytotoxicity
(2002) Pharmaceutical Research, 19 (3), pp. 265-269.
[100] Perouzel, E., Jorgensen, M.R., Keller, M., Miller, A.D.
Synthesis and formulation of neoglycolipids for the functionalization of liposomes and lipoplexes
(2003) Bioconjugate Chemistry, 14 (5), pp. 884-898.
[101] Heurtault, B., Saulnier, P., Pech, B., Proust, J.-E., Benoit, J.-P.
A novel phase inversion-based process for the preparation of lipid nanocarriers
(2002) Pharmaceutical Research, 19 (6), pp. 875-880.
[102] Hoarau, D., Delmas, P., David, S., Roux, E., Leroux, J.-C.

the post-insertion is used in order to insert amphiphilic chemicals of high interest after thermal incubation of functionalized micelles with the nanoparticles. Subsequently, it leads directly to functionalize nanoparticles bearing a tuneable amount of specific amphiphilic chemicals. Post-insertion can be used to introduce a specific anchor ligand which can react afterwards with a wide range of chemicals, depending on the nature of the ligand in a classical chemical approach. In the literature, the amphiphile comes very often from the family of pegylated phospholipids or from the family of pegylated sterols[103,104,105]. No attention has been paid to the length of the hydrocarbon part or if one or more aliphatic chains are required. Finally, we do not know if the hydrophilic part could be different from ethylene glycol polymers.

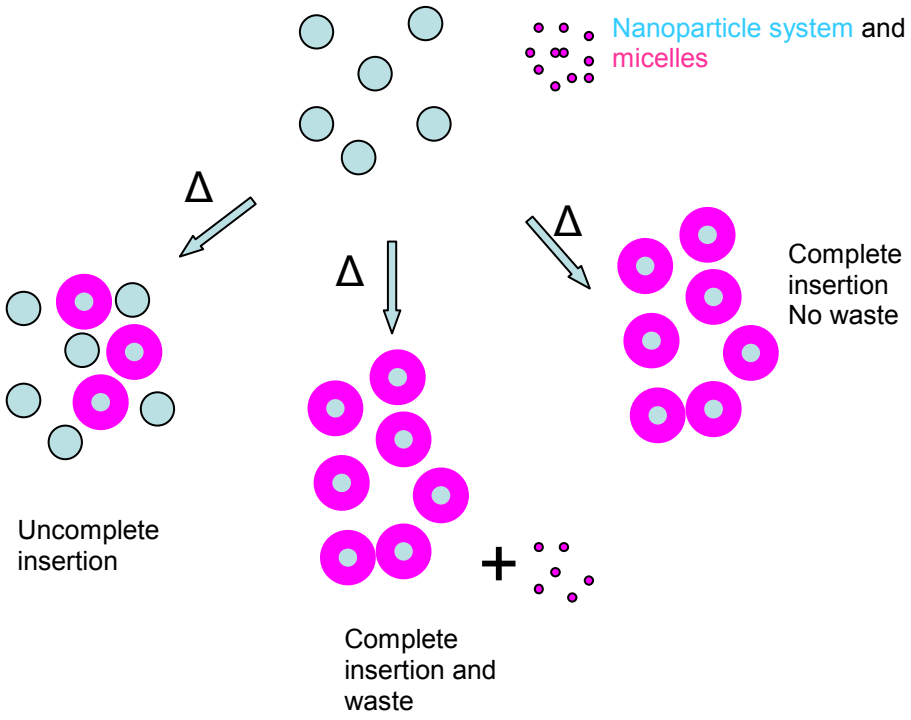

Figure I.13: The possible results of post-insertion.

Novel long-circulating lipid nanocapsules
(2004) Pharmaceutical Research, 21 (10), pp. 1783-1789.
[103] Steenpaß, T., Lung, A., Schubert, R.
Tresylated PEG-sterols for coupling of proteins to preformed plain or PEGylated liposomes
(2006) Biochimica et Biophysica Acta - Biomembranes, 1758 (1), pp. 20-28.
[104] Zhao, X.B., Muthusamy, N., Byrd, J.C., Lee, R.J.
Cholesterol as a bilayer anchor for PEGylation and targeting ligand in folate-receptor-targeted liposomes
(2007) Journal of Pharmaceutical Sciences, 96 (9), pp. 2424-2435.
[105] Pan, X., Wu, G., Yang, W., Barth, R.F., Tjarks, W., Lee, R.J.
Synthesis of cetuximab-immunoliposomes via a cholesterol-based membrane anchor for targeting of EGFR
(2007) Bioconjugate Chemistry, 18 (1), pp. 101-108.

As shown in Figure I.13, post-insertion can lead to different nanoparticle systems. Three cases are possible, depending on experimental conditions: first, uncomplete insertion can be obtain if the amount of amphiphile is not adapted in regards with the number and the nature of the receiver; complete insertion can be reach if the ratio amount of amphiphile/amount of nanoparticles is correct, with or without excess of materials.

Nevertheless, few studies are available for the quantitative assessment of the amount of transferred materials considering that the yield of post-insertion technique is difficult to evaluate. Indeed, as shown in Figure I.13, one should be able to separate obtained nanoparticles from micelles and wastes; after what the yield could be evaluate by means of additional experiments such as spectrophotometric/fluorometric quantifications. In the same general concern, the chemical nature of the amphiphile required for the post-insertion has not been fully investigated. To put it in a nutshell, the post-insertion process leads to the manufacturing of functionalized nanoparticles suspensions without the use of a complete formulation process[106,107,108]. In addition, the avoidance of the use of organic solvents is a strong argument towards pharmaceuticals regulations and allows the development of nanodevices in an ecological friendly way.

III.1.b) Layer-by-layer (LBL)

From a historical point of view, the deposition of polymer bearing groups of opposite charges into nano-assemblies has been developed for plane macroscopic surfaces[109]. This approach consists in the sequential soaking of a solid support into different polyelectrolyte

[106] Zhu, J., Xue, J., Guo, Z., Zhang, L., Marchant, R.E.
Biomimetic glycoliposomes as nanocarriers for targeting P-selectin on activated platelets
(2007) Bioconjugate Chemistry, 18 (5), pp. 1366-1369.
[107] Béduneau, A., Saulnier, P., Hindré, F., Clavreul, A., Leroux, J.-C., Benoit, J.-P.
Design of targeted lipid nanocapsules by conjugation of whole antibodies and antibody Fab' fragments
(2007) Biomaterials, 28 (33), pp. 4978-4990.
[108] Thompson, B., Mignet, N., Hofland, H., Lamons, D., Seguin, J., Nicolazzi, C., De La Figuera, N., Kuen, R.L., Meng, X.Y., Scherman, D., Bessodes, M.
Neutral postgrafted colloidal particles for gene delivery
(2005) Bioconjugate Chemistry, 16 (3), pp. 608-614.
[109] Decher, G.
Fuzzy nanoassemblies: Toward layered polymeric multicomposites
(1997) Science, 277 (5330), pp. 1232-1237.

solutions with washing steps in order to remove excess of materials. Since many years, this technology has been transferred to the design of colloidal systems functionalized by polyelectrolyte brushes[110]. As described in Figure I.14, polymer with opposite charges is added to nanoparticles with a given charged surface. Electrostatic attraction leads to particles covered by an additional layer. Purification is needed and consists in centrifugation and supernatant exchange or in dyialysis. The principal aims are the chemical modification of the particle's surface conferring in the same time new properties[111,112,113]. The LBL strategy follows two mains goals: the first one is the covering of nanoparticles in order to modify the colloidal stability[114] and/or the kinetics of drug release[115]. In a complementary way, the LBL is used to bind and trap drugs (charged or uncharged) into polyelectrolyte layers. Moreover, these layers could be the base for the chemical grafting[116] of signalling molecules setting up an advance base for the development of multifunctional nanocarriers. The used polymers can be naturals like homopolypeptides, polyoses; or fully synthetic substances. It allows the scientist to play with the degradation properties of the nanoparticle. Furthermore, this strategy puts forward an alternative way to the use of cationic lipids in the encapsulation of naturals or synthetics nucleic acids[117].

[110] Sukhorukov, G.B., Donath, E., Davis, S., Lichtenfeld, H., Caruso, F., Popov, V.I., Möhwald, H.
Stepwise polyelectrolyte assembly on particle surfaces: A novel approach to colloid design
(1998) Polymers for Advanced Technologies, 9 (10-11), pp. 759-767.
[111] Angelatos, A.S., Katagiri, K., Caruso, F.
Bioinspired colloidal systems via layer-by-layer assembly
(2006) Soft Matter, 2 (1), pp. 18-23.
[112] Fujimoto, K., Toyoda, T., Fukui, Y.
Preparation of bionanocapsules by the layer-by-layer deposition of polypeptides onto a liposome
(2007) Macromolecules, 40 (14), pp. 5122-5128.
[113] Biggs, S., Sakai, K., Addison, T., Schmid, A., Armes, S.P., Vamvakaki, M., Bütün, V., Webber, G.
Layer-by-layer formation of smart particle coatings using oppositely charged block copolymer micelles
(2007) Advanced Materials, 19 (2), pp. 247-250.
[114] Ciobanu, M., Heurtault, B., Schultz, P., Ruhlmann, C., Muller, C.D., Frisch, B.
Layersome: Development and optimization of stable liposomes as drug delivery system
(2007) International Journal of Pharmaceutics, 344 (1-2), pp. 154-157.
[115] De Geest, B.G., Sanders, N.N., Sukhorukov, G.B., Demeester, J., De Smedt, S.C.
Release mechanisms for polyelectrolyte capsules
(2007) Chemical Society Reviews, 36 (4), pp. 636-649.
[116] Germain, M., Grube, S., Carriere, V., Richard-Foy, H., Winterhalter, M., Fournier, D.
Composite nanocapsules: Lipid vesicles covered with several layers of crosslinked polyelectrolytes
(2006) Advanced Materials, 18 (21), pp. 2868-2871.
[117] Elbakry, A., Zaky, A., Liebl, R., Rachel, R., Goepferich, A., Breunig, M.
Layer-by-layer assembled gold nanoparticles for sirna delivery
(2009) Nano Letters, 9 (5), pp. 2059-2064.

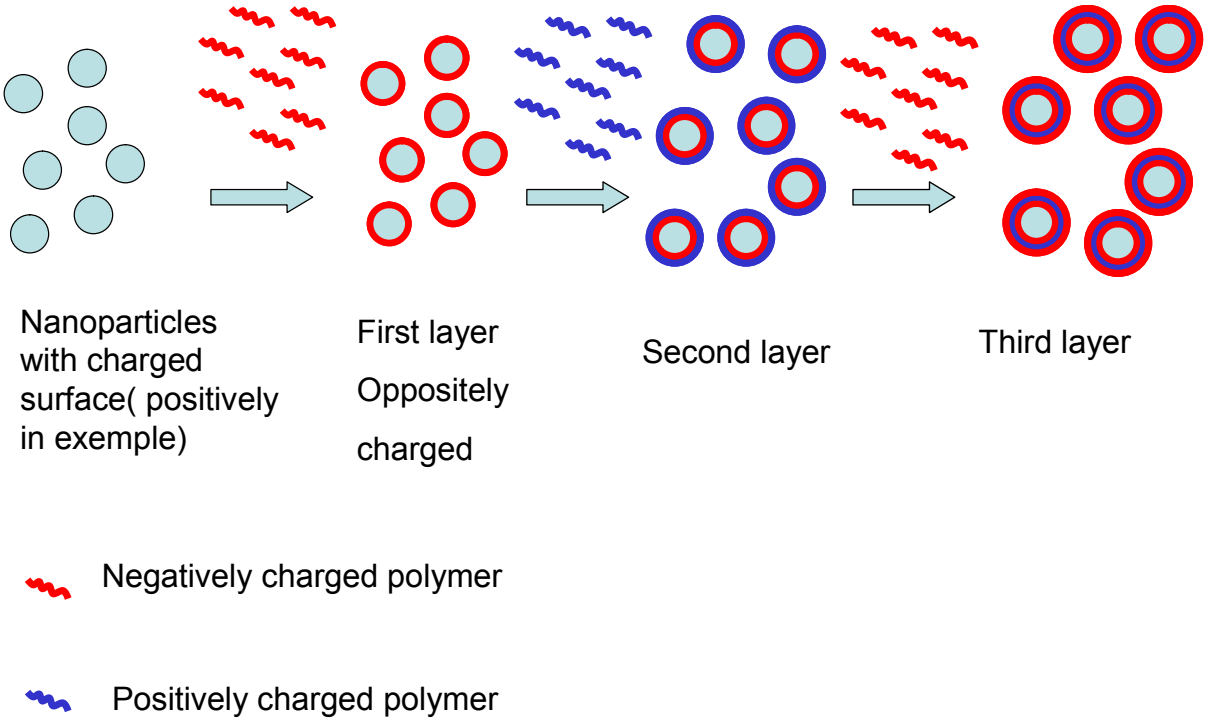

Figure I.14: Sequential deposition of polymers onto nanoparticles by LBL. Blue arrows include purification steps.

In a larger point of view, the LBL approach promotes the development of nanoparticles in other areas, different from the intensively investigated nanomedicine systems. Another point must be underlined: LBL can produce polyelectrolyte capsules starting from nanoparticles coated with alternate layers of polymers, after that the core of the nanoparticles is decomposed. The result consists in hollow polyelectrolyte capsules with a defined number of layers and with controlled sizes.

III.2) Chemical methods

Chemistry could be the source of interesting helps towards the engineering of nanoparticle interfaces. But chemical reactions should be performed at room temperature, in mild conditions as nanoparticles stability and lifetime could be dramatically affected under stronger conditions. Thus, among the known chemical reactions, few of them can satisfy such

experimental conditions. As a reminder, most of nanoparticles are produced in water medium or tend to be used in water containing media. In other words, water should be the solvent for the chemical modification of nanoparticles. Here, we report reactions that could be carried in these conditions.

III.2.a) Classical coupling methods

Before presenting novel and attractive methods for the modification of nanoparticles, classical methods based on chemistry are illustrated. In the past decades, a lot of work has been done in the synthesis of valuable molecules. First examples are the synthesis of phospholipidic derivatives, which are further incorporated into formulations keeping in mind that important amount of work was spent on setting up feasible formulations, as explained in the introduction. In this way, pegylated phospholipids are coupled to sialyl Lewis x with a 60% yield[118]. Authors demonstrate that inhibition of cell adhesion increases when sialyl Lewis x liposomes are used. In the same extent, pegylated phospholipids have also been coupled to anti-cancer drugs like doxorubicin using the carbodiimide chemistry[119]. The doxorubicin adduct is incorporated into liposome formulations and the resulting liposomes are shown to be able to bring doxorubicin into cells and inhibit tumor growth. These systems are summarized into Figure I.15: the first molecule is a phospholipid conjugated to Sialyl Lewis x (carbohydrates moiety), the two parts are connected by a spacer; the second molecule is a doxorubicin adduct.

[118] DeFrees, S.A., Phillips, L., Guo, L., Zalipsky, S.
Sialyl Lewis x liposomes as a multivalent ligand and inhibitor of E-selectin mediated cellular adhesion
(1996) Journal of the American Chemical Society, 118 (26), pp. 6101-6104.
[119] Hwang, T., Han, H.D., Song, C.K., Seong, H., Kim, J.H., Chen, X., Shin, B.C.
Anticancer drug-phospholipid conjugate for enhancement of intracellular drug delivery
(2007) Macromolecular Symposia, 249-250, pp. 109-115.

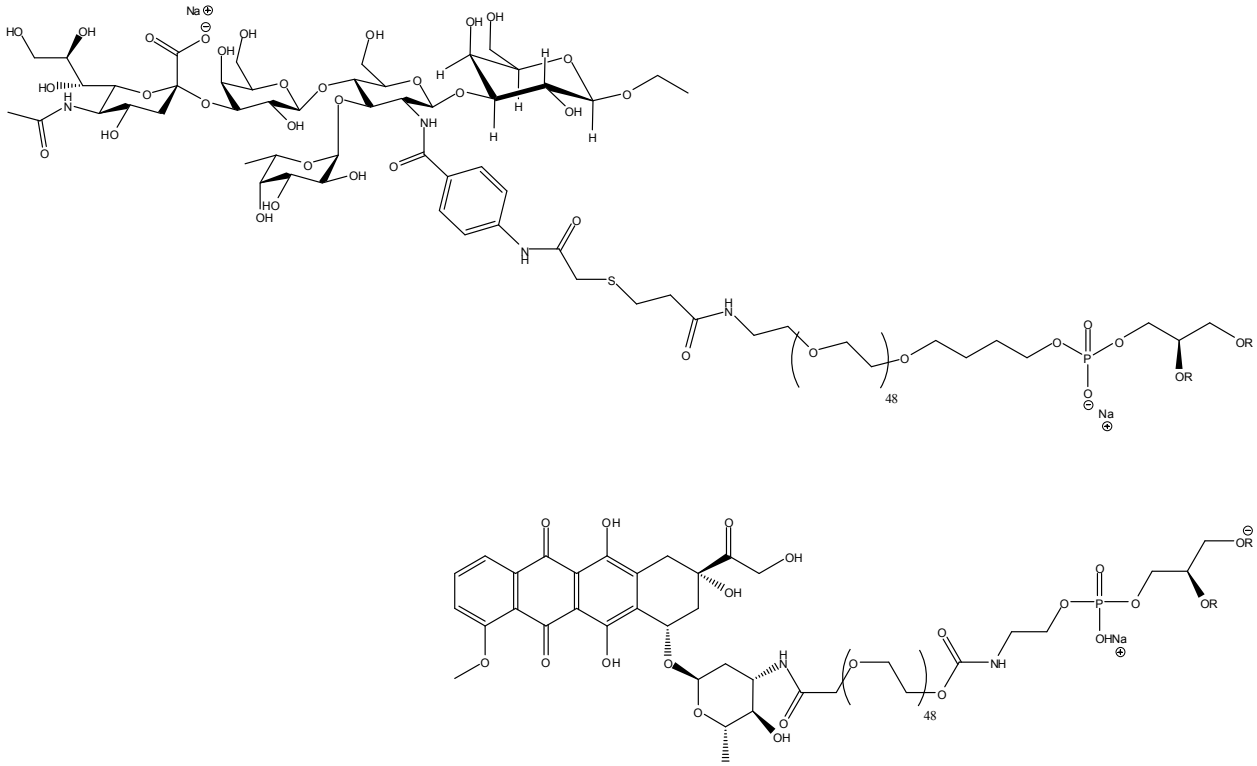

Figure I.15: Chemical structures of amphiphilic phospholipids conjugates (Sialyl Lewis X, upper exemple; Doxorubicin, lower exemple).

Alternatives to the use of carbodiimide chemistry exist and allow the introduction of peptides[120] (as TAT peptide) on phospholipids. One more time, the modified liposomes show new properties like good intracellular delivery even in unusual conditions.

Another well established approach consists in the use of valuable molecules containing thiols, designed to be grafted onto gold surface. For example, gold nanoparticles have been covered with sugar derivatives and peptides (both modified to contain thiol) to produce multifunctional glyconanoparticles as platform for potential carbohydrate-based anticancer vaccines[121].

Today, conjugation between nanoparticles and molecules tends to be done after the formulation step. For example, GFP (Green Fluorescent Protein) derivatives have been inserted onto the outer layer of liposomes. This reaction has been made possible by the use of

[120] Torchilin, V.P., Rammohan, R., Weissig, V., Levchenko, T.S.
TAT peptide on the surface of liposomes affords their efficient intracellular delivery even at low temperature and in the presence of metabolic inhibitors
(2001) Proceedings of the National Academy of Sciences of the United States of America, 98 (15), pp. 8786-8791.
[121] Ojeda, R., de Paz, J.L., Barrientos, A.G., Martín-Lomas, M., Penadés, S.
Preparation of multifunctional glyconanoparticles as a platform for potential carbohydrate-based anticancer vaccines
(2007) Carbohydrate Research, 342 (3-4), pp. 448-459.

both activated liposomes and GFP derivatives. Other reactions, like addition of thiols on carbon double bond, have been intensively investigated and permit the fixation of various substrates as antibodies and peptides[122]. Thiols are interesting groups as they are naturally present in proteins via the cysteine amino acids.

Some reactions, like transacylation, have been exploited to modify microparticles, bringing new interesting properties. In general, transacylation is the exchange of acyl chains. If acyl chains are immobilized into a particule shell (through ester bonds, for example) transacylation leads to the fixation of reactants onto the particule shell. Thus, transacylation between alginate microparticles and model protein as Bovine Serun Albumin (BSA) produced capsule-like structures[123] (see Figure I.16). The capsule around the microparticles modifies initial properties and shows promising results[124,125,126,127]. But, to date, even if a lot of surfactants bear ester groups, transacylation has not been used onto nanoparticles.

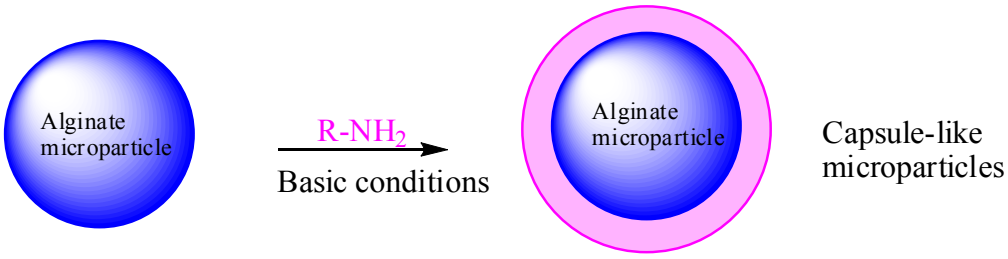

Figure I.16: Modifications of microparticles by transacylation.

[122] Reulen, S.W.A., Brusselaars, W.W.T., Langereis, S., Mulder, W.J.M., Breurken, M., Merkx, M.
Protein-liposome conjugates using cysteine-lipids and native chemical ligation
(2007) Bioconjugate Chemistry, 18 (2), pp. 590-596.
[123] Levy, M.-C., Edwards-Levy, F.
Coating alginate beads with cross-linked biopolymers: A novel method based on a transacylation reaction
(1996) Journal of Microencapsulation, 13 (2), pp. 169-183.
[124] Levy, M.-C., Edwards-Levy, F.
Novel encapsulation methods based on a transacylation reaction
(1998) Artificial Cells, Blood Substitutes, and Immobilization Biotechnology, 26 (1), p. 96.
[125] Hurteaux, R., Edwards-Lévy, F., Laurent-Maquin, D., Lévy, M.-C.
Coating alginate microspheres with a serum albumin-alginate membrane: Application to the encapsulation of a peptide
(2005) European Journal of Pharmaceutical Sciences, 24 (2-3), pp. 187-197.
[126] Carin, M., Barthès-Biesel, D., Edwards-Lévy, F., Postel, C., Andrei, D.C.
Compression of biocompatible liquid-filled HSA-alginate capsules: Determination of the membrane mechanical properties
(2003) Biotechnology and Bioengineering, 82 (2), pp. 207-212.
[127] Callewaert, M., Millot, J.-M., Lesage, J., Laurent-Maquin, D., Edwards-Lévy, F.
Serum albumin-alginate coated microspheres: Role of the inner gel in binding and release of the KRFK peptide
(2009) International Journal of Pharmaceutics, 366 (1-2), pp. 103-110.

III.2.b) Olefins metathesis

The olefin metathesis[128] allows the exchange of substituent between different olefins according to the following equation, where [cat] is catalytic specie:

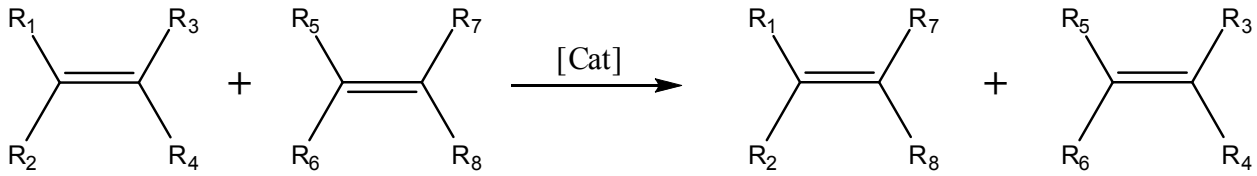

Figure I.17: General scope of metathesis with two different alkenes. R_1, R_2, R_3, R_4, R_5, R_6, R_7 and R_8 are H atoms or organic radicals.

Metathesis is catalyzed by organometallic compounds based on transition metals[129]. As shown in Figure I.18, the metathesis catalysts are metallocarbene species, and metathesis starts when olefin reacts with the metallocarbene to form metallacyclobutane (step 1). Thus intermediate metallocarbene reacts further (step 2), forming the product and a new metallocarbene, which can be recycled closing by the way the catalytic cycle. As an illustration, the catalytic cycle could be written, in a very general case, as depicted in Figure I.18 (here the driven force is a continual removal of ethylene):

[128] Grubbs, R.H.
Olefin metathesis
(2004) Tetrahedron, 60 (34), pp. 7117-7140.
[129] Grubbs, R.H.
Olefin-metathesis catalysts for the preparation of molecules and materials (Nobel lecture)
(2006) Angewandte Chemie - International Edition, 45 (23), pp. 3760-3765.

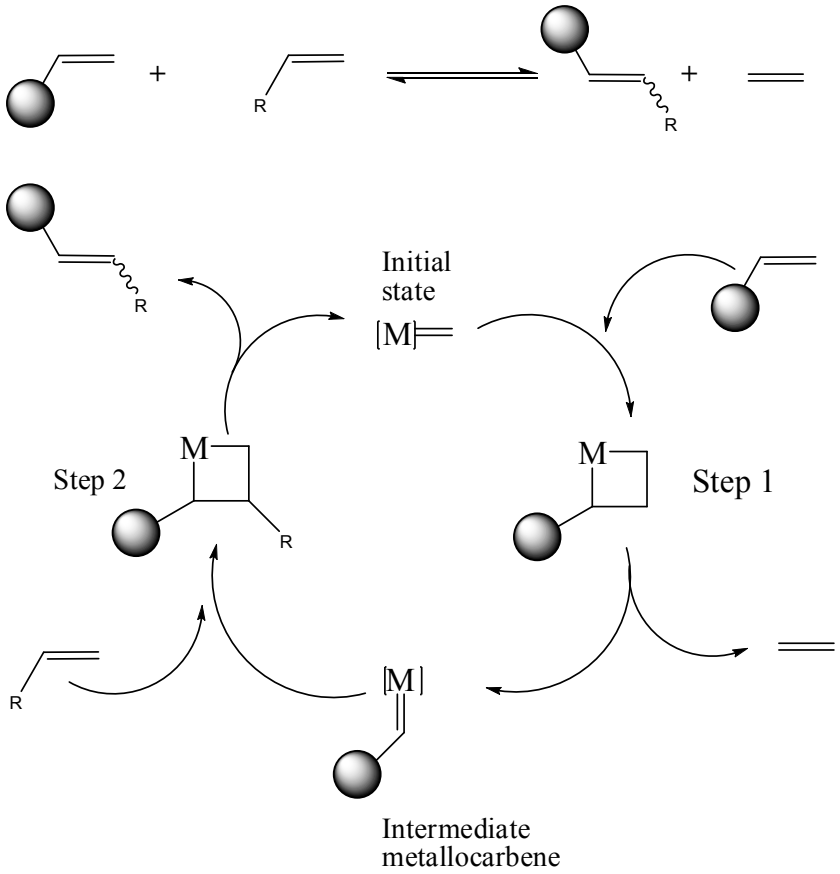

Figure I.18: Metathesis catalytic cycle. [M] represents organometallic catalyst with its ligands. The shaded sphere is the schematic representation of a nanoparticle.

The high potential of this reaction relies in the fact that it could be realised according to several ways. Indeed, intramolecular or intermolecular reactions can be carried out with cyclic or acyclic olefins. Here, we summarize the different approaches through five examples (Figure I.19):

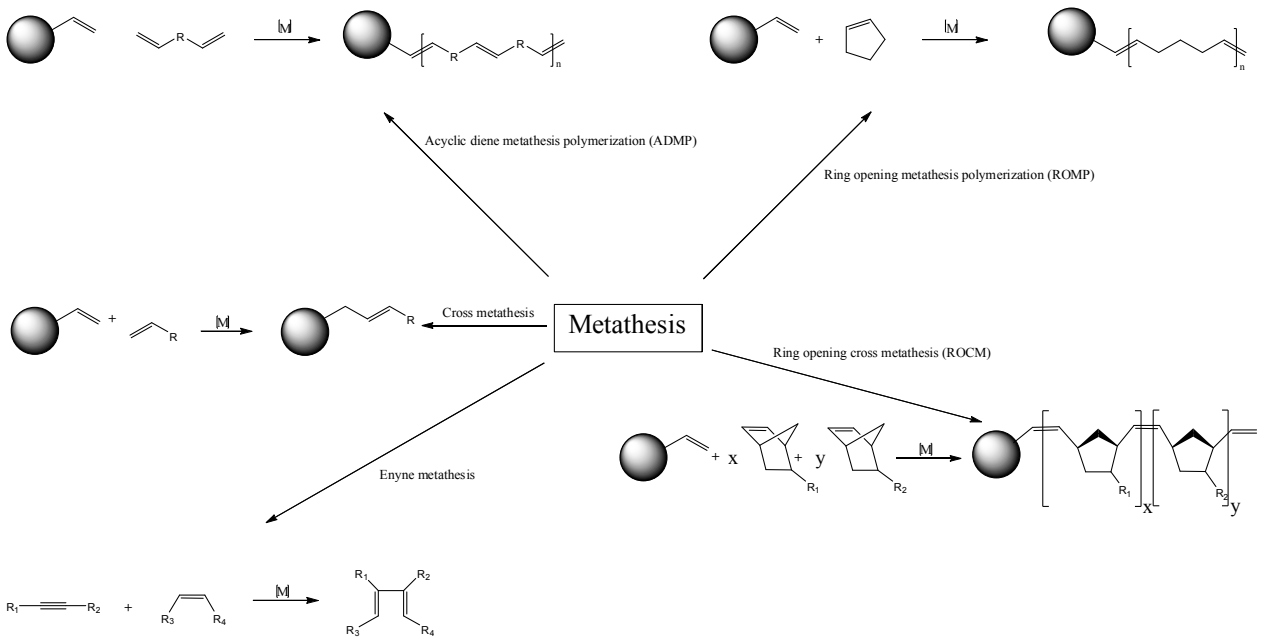

Figure I.19: The versatile possibilities of metathesis.

As shown in Figure I.19, polymerization reactions can be carried out both by cross methatesis (ADMP) and by ring opening metathesis (ROMP and ROCM). To date enyne metathesis has not been exploited onto nanoparticles.

Concerning the use of these different reactions towards the functionalization of nanoparticles, Ring Opening Metathesis (ROM), ROMP and ROCM have been used with success. Furthermore starting from the first catalysts, many generations have been developed. The actual catalysts are more stable towards experimental conditions (less sensitive to air and moisture) and more active (higher turn-over number)[130,131].

[130] Vougioukalakis, G.C., Grubbs, R.H.
Ruthenium-based olefin metathesis catalysts coordinated with unsymmetrical N-heterocyclic carbene ligands: Synthesis, structure, and catalytic activity
(2008) Chemistry - A European Journal, 14 (25), pp. 7545-7556.
[131] Vougioukalakis, G.C., Grubbs, R.H.
Synthesis and activity of ruthenium olefin metathesis catalysts coordinated with thiazol-2-ylidene ligands
(2008) Journal of the American Chemical Society, 130 (7), pp. 2234-2245.

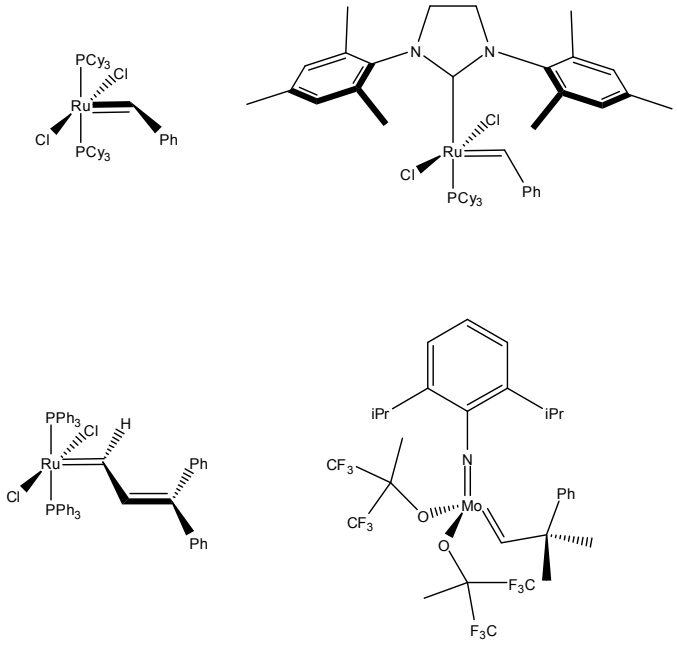

Figure I.20: Examples of metathesis catalysts.

A major breakthrough is the development of hydrosoluble catalysts, offering unexpected potentiabilities for the chemistry on nanoparticles in water[132,133,134]. Indeed, as most of drug delivery systems are used in water and biological molecules such as proteins or nucleic acids are soluble into water, it is very important to have hydro-soluble catalysts to perform these reactions into this medium (see Figure I.20).

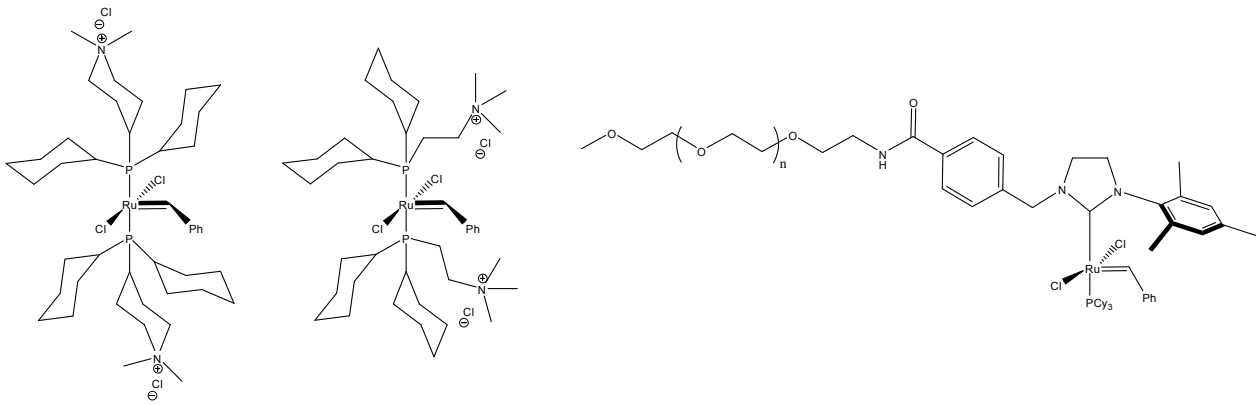

Figure I.21: Water soluble metathesis catalysts.

[132] Hong, S.H., Grubbs, R.H.
Highly active water-soluble olefin metathesis catalyst
(2006) Journal of the American Chemical Society, 128 (11), pp. 3508-3509.
[133] Gallivan, J.P., Jordan, J.P., Grubbs, R.H.
A neutral, water-soluble olefin metathesis catalyst based on an N-heterocyclic carbene ligand
(2005) Tetrahedron Letters, 46 (15), pp. 2577-2580.
[134] Jordan, J.P., Grubbs, R.H.
Small-molecule N-heterocyclic-carbene-containing olefin-metathesis catalysts for use in water
(2007) Angewandte Chemie - International Edition, 46 (27), pp. 5152-5155.

As shown in Figure I.21, water soluble metathesis catalysts can be synthetized by introducing electric charges or water-soluble polymer, here polyethylene oxide chains.

The use of olefin metathesis on nanostructures[135] can be performed according to two main methods depending on the shape of the particle, the nature of the metathesis substrate(s) and the nature of the catalytic species. Metathesis can be performed laterally at the surface of the particles producing core-shell structure or in a radial approach suited for the chemical modification of nanoparticles as shown in Figure I.22.

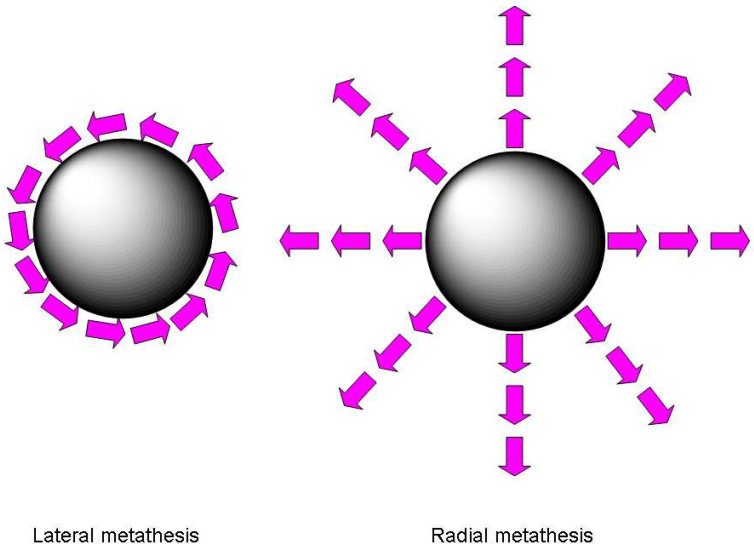

Figure I.22: Approaches for the use of metathesis on nanostructures. Shaded spheres represent nanoparticules and violet arrows mimic the direction of metathesis reaction.

- Lateral metathesis

Lateral metathesis can be run in the ring closure or in the ring opening polymerization. In the case of ring closure metathesis, the particles are covered with multi-alkene substrates which can react by two processes: internal cross linking if alkenes groups are from the same molecule or cross linking between alkenes from different molecules[136]. In both cases, the

[135] Liu, X., Basu, A.
Olefin metathesis on nanostructures
(2006) Journal of Organometallic Chemistry, 691 (24-25), pp. 5148-5154.
[136] Balasubramanian, R., Kwon, Y.-G., Wei, A.
Encapsulation and functionalization of nanoparticles in crosslinked resorcinarene shells
(2007) Journal of Materials Chemistry, 17 (1), pp. 105-112.

reaction leads to a cross linked polymer shell around the particles. This reaction has been carried out on gold nanoparticles covered by different alkyl dendrimers[137]. RCM on these particles (Figure I.23) enhances kinetic stability both to chemical processes (such as cyanide etching) and thermal processes (thermal ripening).

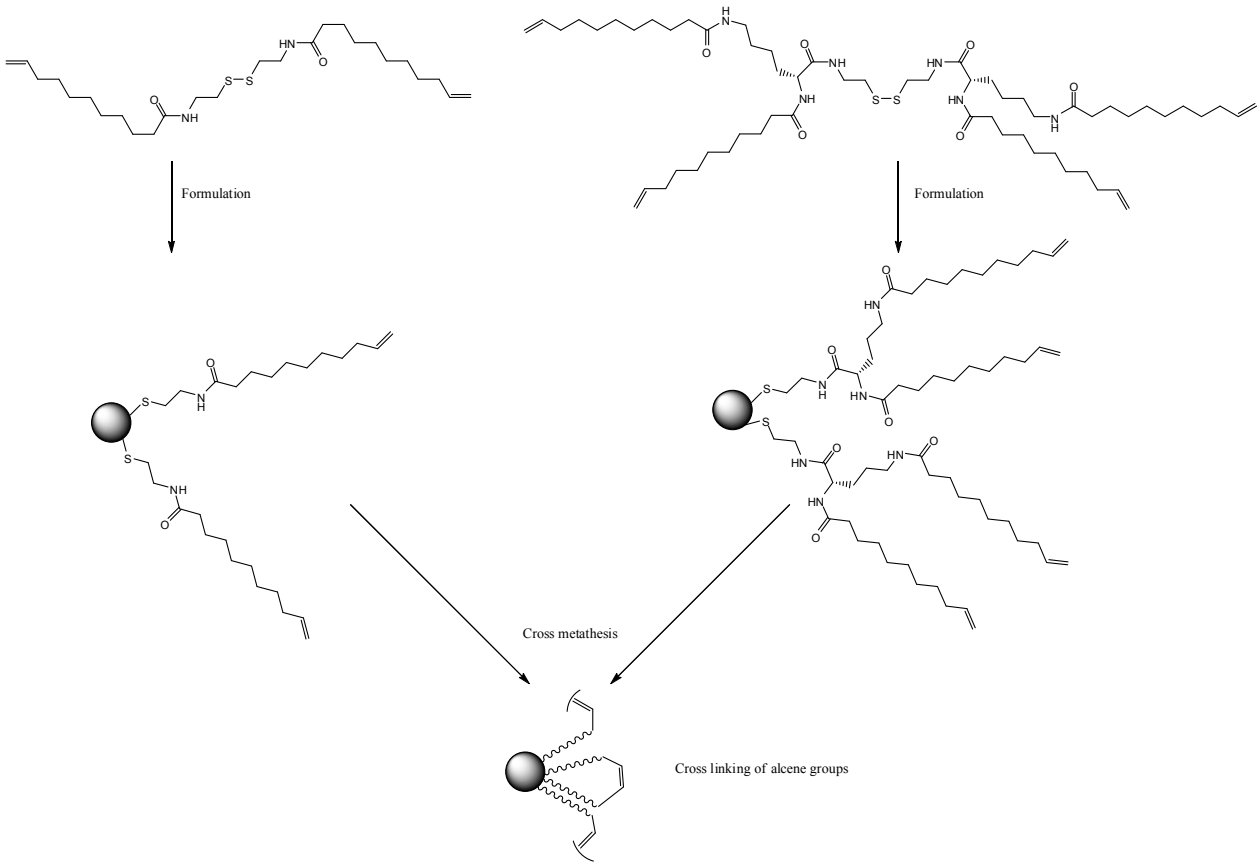

Figure I.23: RCM on gold nanoparticles according to reference 138.

In a similar way, cross-linked glycerol based dendrimers[138] have been produced. Starting from glycerol dendrimers, these latter have been allylated and then treated with RCM catalysts to produce cross-linked structures. The obtained carbon double bond can be further hydrogenated using Adams catalyst or dihydroxylated by osmium tetroxide. This latter reaction leads to water soluble dendrimers, starting from initial hydrophobic architectures.

[137] Love, C.S., Ashworth, I., Brennan, C., Chechik, V., Smith, D.K.
Dendritic nanoparticles - the impact of ligand cross-linking on nanocore stability
(2007) Langmuir, 23 (10), pp. 5787-5794.
[138] Zimmerman, S.C., Quinn, J.R., Burakowska, E., Haag, R.
Cross-linked glycerol dendrimers and hyperbranched polymers as ionophoric, organic nanoparticles soluble in water and organic solvents
(2007) Angewandte Chemie - International Edition, 46 (43), pp. 8164-8167.

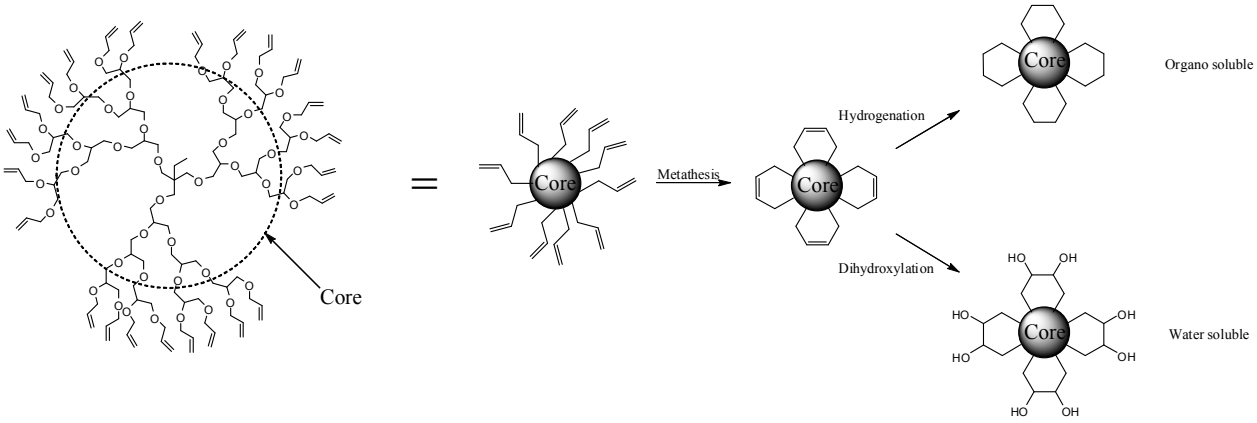

Figure I.24: RCM on glycerol dendrimers which are further modified leading to nanoparticles with opposite solubility.

- Radial metathesis

In a similar way, radial metathesis is the orthogonal modification of the outer layer of the particles using one of the available metathesis catalysts. A first example is the modification of the external part of gold nanoparticles by ROCM as shown in Figure I.25. Different norbornene derivatives bearing ferrocenyl groups are polymerized from the particles surface to the external medium. The reaction is stopped by the addition of ethyl vinyl ether, a known ROCM termination agent. The sequential addition of the norbornene derivatives and the efficacy of the reaction lead to particles with a layered structure.

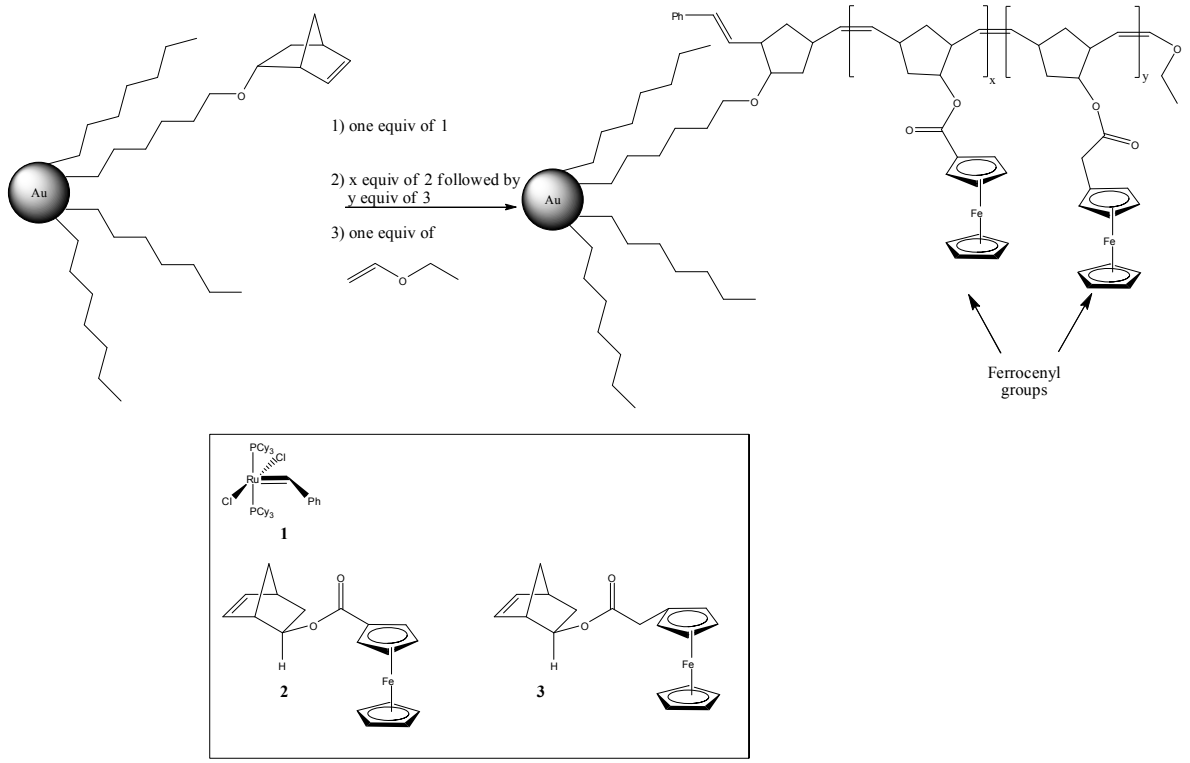

Figure I.25: Radial metathesis on gold nanoparticles. Layered particles are obtained.

A similar strategy is used to prepare cadmium selenide-polyolefin composites. Starting from CdSe quantum dots covered with trioctylphosphine (TOPO), ligand exchange is performed by thermal treatment of quantum dots with p-vinylbenzyl-dioctylphosphine (p-vinylbenzyl-DOPO). Hence, metathesis catalyst (Ruthenium based catalyst, RuL_n in Figure I.26) is inserted on the particles, producing activated quantum dots. Finally, cyclooctene is added and ROCM takes place. As described above, reaction is terminated by addition of ethyl vinyl ether. In addition, these quantum dots are organized at the interface between water droplets and toluene. Polymerization at the interface, by means of an amphiphilic catalyst, produces water droplets coated with quantum dots, at the micrometer scale.

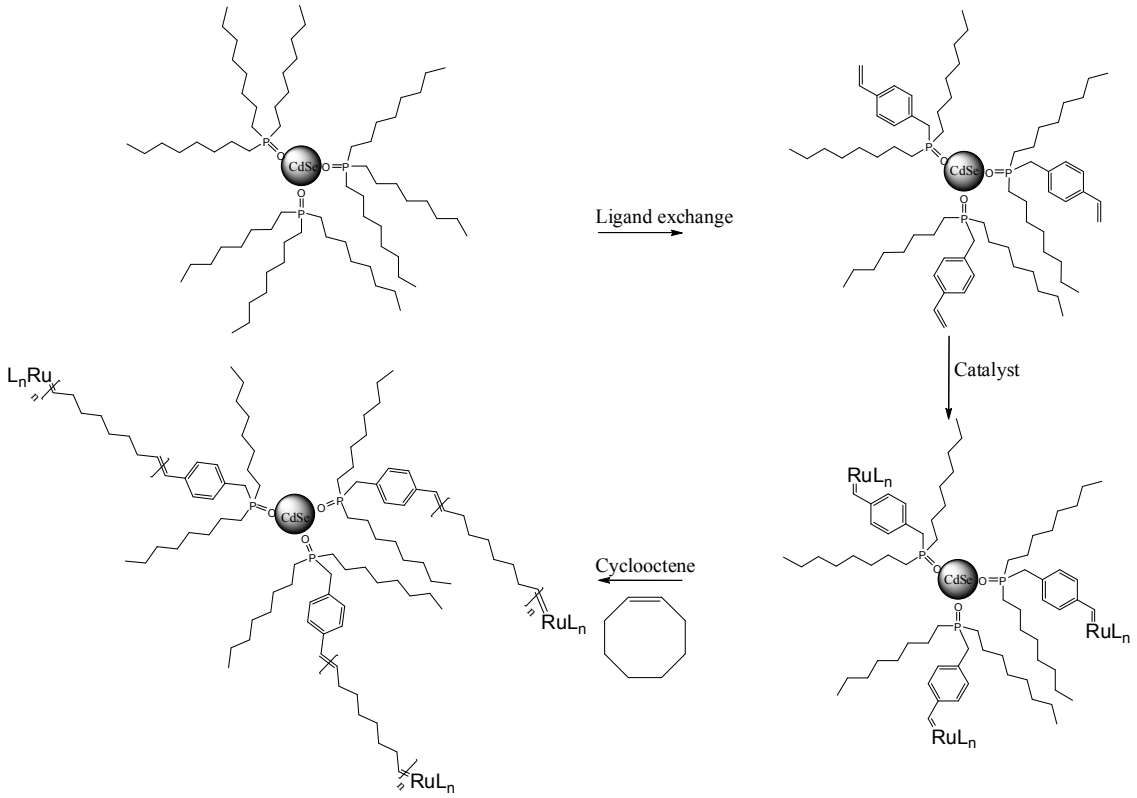

Figure I.26: ROMP on quantum dots.

In the simplest way, radial metathesis can be used to introduce functional groups on the nanoparticles[139].

III.2.c) CuAAC (Copper(I)-catalyzed Azide-Alkyne Cycloaddition) and click chemistry

- CuAAC

The Azide-Alkyne Huisgen Cycloaddition is a 1,3-dipolar cycloaddition between an azide and a terminal or an internal alkyne to give a 1,2,3-triazole. Rolf Huisgen was the first to understand the scope of this organic reaction. This reaction was improved, independtly, by the groups of K. Barry Sharpless and Morten Meldal to give the well known click chemistry

[139] Ornelas, C., Méry, D., Cloutet, E., Aranzaes, J.R., Astruc, D.
Cross olefin metathesis for the selective functionalization, ferrocenylation, and solubilization in water of olefin-terminated dendrimers, polymers, and gold nanoparticles and for a divergent dendrimer construction
(2008) Journal of the American Chemical Society, 130 (4), pp. 1495-1506.

azide-alkyne coupling[140,141]. This strategy comports advantages like the use of water as a non-toxic solvents. The large favorable thermodynamic effect of the reaction is also interesting. The use of copper sulfate and sodium ascorabte produces a nice way to functionnalize soft nanoparticles under mild conditions. As shown in Figure I.27, uncatalyzed reaction requires heating (Δ) and produces a mix of 1,2,3 and 1,2,4 triazoles. Copper catalyzed reaction takes place at room temperature and produces only 1,2,3-triazoles.

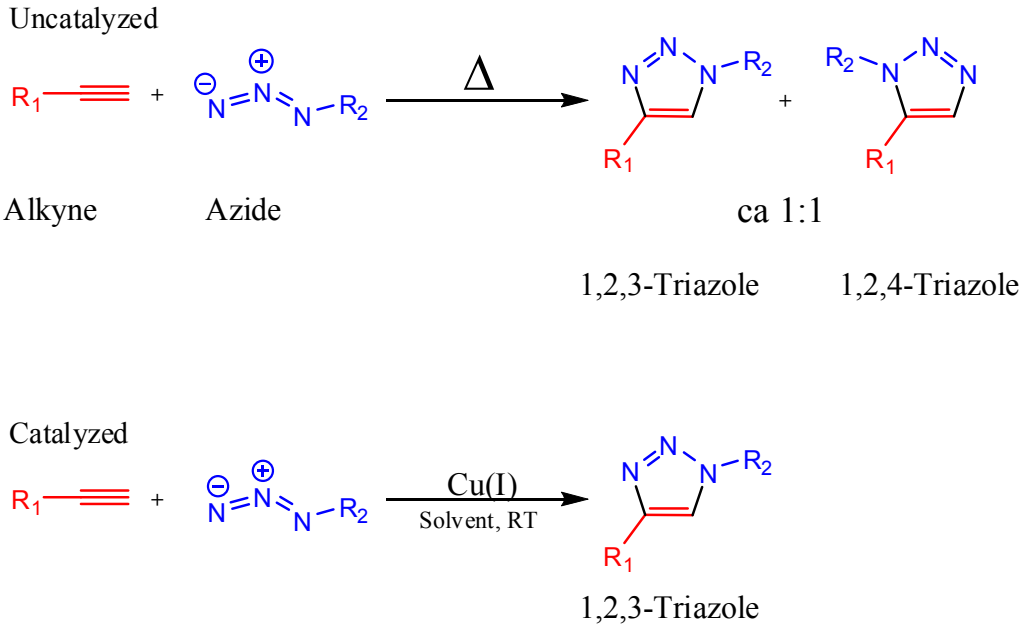

Figure I.27: Uncatalyzed and catalyzed Huisgen's reaction.

One example of the use of CuAAC towards functionalization of nanoparticles is the introduction of mannose ligands on liposomes[142]. A synthetic lipid, presenting a terminal alkyne group, is introduced into liposomes formulation. The formulation process is based on the hydratation of a lipid layer, producing monodisperse liposomes. Coupling with mannosyl moiety, having a spacer with a reactive azido group, is achieved in Hepes buffer under the catalysis by $CuSO_4$/sodium L-ascorbate. Catalytic specie (Cu(I) complexe) is stabilized by

[140] Tornøe, C.W., Christensen, C., Meldal, M.
Peptidotriazoles on solid phase: [1,2,3]-Triazoles by regiospecific copper(I)-catalyzed 1,3-dipolar cycloadditions of terminal alkynes to azides
(2002) Journal of Organic Chemistry, 67 (9), pp. 3057-3064.
[141] Evans, R.A.
The rise of azide-alkyne 1,3-Dipolar 'click' cycloaddition and its application to polymer science and surface modification
(2007) Australian Journal of Chemistry, 60 (6), pp. 384-395.
[142] Hassane, F.S., Frisch, B., Schuber, F.
Targeted liposomes: Convenient coupling of ligands to preformed vesicles using "click chemistry"
(2006) Bioconjugate Chemistry, 17 (3), pp. 849-854.

chelation with a water soluble bathophenanthroline derivative. Under these conditions, the coupling yield is almost quantitative. Furthermore, as a model study, introduced mannosyl moities areaccessible to Concanavalin A; demonstrating the ability of liposomes to interact with other ligand. This experiment is the proof of concept for targeting tumor with cells expressing receptors to sugar, especially mannose.

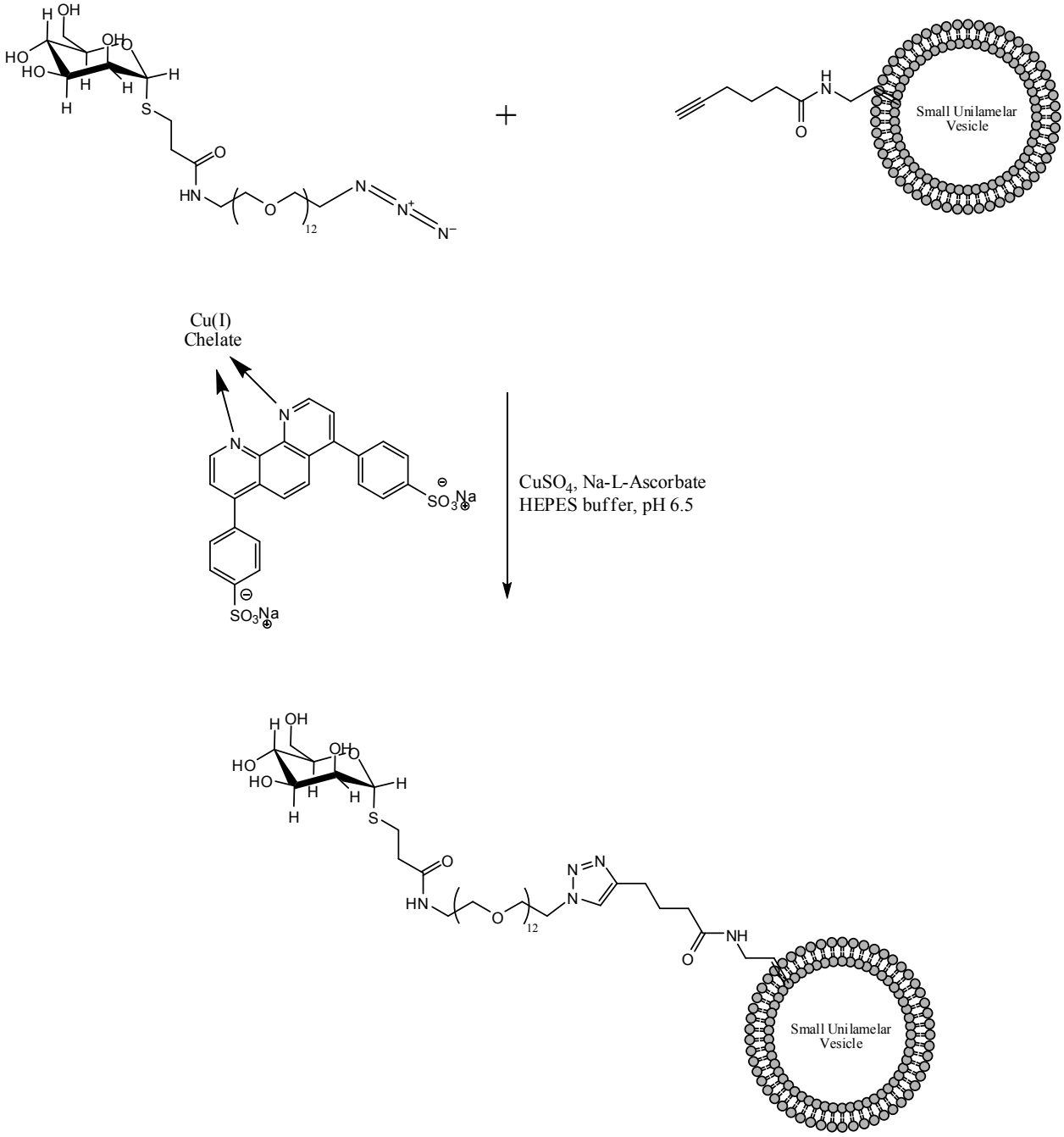

Figure I.28: Reaction between alkyne-liposomes and azido-mannose.

Another example is the reaction of poly(alkylcyanoacrylate) nanoparticles[143], made from modified cyanoacrylate polymers, with alkyne substrates like alkyne-dansyl or alkyne-PEG. Same methodology can be applied on hybrid organic/inorganic particles for the introduction of bio-linkers (biotin), fluorescent markers (indocyanin, fluorescein), steroïd moieties (oestrogen) and drugs (paclitaxel), as alkyne or azide groups can easily be introduced into these kinds of molecules. In a same way, tumor targeting inorganic nanoparticles have been covered with cyclic peptides and show an extended blood circulation time as well as binding to a specific targets within the tumors, here p-32 expressing cells[144].

- Other click chemistry approaches

"Click chemistry"[145,146,147] is a chemical philosophy introduced by K. Barry Sharpless in 2001 and describes chemistry tailored to generate substances quickly and reliably by joining small units together. This is inspired by the fact that Nature also generates substances in a similar way. This philosophy is extended to the production of tailored nanoparticles using favorable reactions like the addition of isocyanates or isothiocyanates to amine functionnalized nanoparticles via urea or thiourea bonds. The last reaction has been used since the 1960s to produce macromolecules labeled with the well known FITC (FluoresceinIsoThioCyanate). This reaction is usual to produce engineered nanoparticles, starting with nanoparticles bearing amino groups. One of the disadvantages of this approach is the lack of catalysts leading to classical chemistry yields.

[143] Nicolas, J., Bensaid, F., Desmaële, D., Grogna, M., Detrembleur, C., Andrieux, K., Couvreur, P.
Synthesis of highly functionalized poly(alkyl cyanoacrylate) nanoparticles by means of click chemistry
(2008) Macromolecules, 41 (22), pp. 8418-8428.
[144] Von Maltzahn, G., Ren, Y., Park, J.-H., Min, D.-H., Kotamraju, V.R., Jayakumar, J., Fogal, V., Sailor, M.J., Ruoslahti, E., Bhatia, S.N.
In vivo tumor cell targeting with "click" nanoparticles
(2008) Bioconjugate Chemistry, 19 (8), pp. 1570-1578.
[145] Kolb, H.C., Finn, M.G., Sharpless, K.B.
Click Chemistry: Diverse Chemical Function from a Few Good Reactions
(2001) Angewandte Chemie - International Edition, 40 (11), pp. 2005-2021.
[146] Finn, M.G., Kolb, H.C., Fokin, V.V., Sharpless, K.B.
Click chemistry - Definition and aims
(2008) Progress in Chemistry, 20 (1), pp. 1-4.
[147] Meldal, M., Tomøe, C.W.
Cu-catalyzed azide - Alkyne cycloaddition
(2008) Chemical Reviews, 108 (8), pp. 2952-3015.

III.2.d) Reaction of Diels-Alder

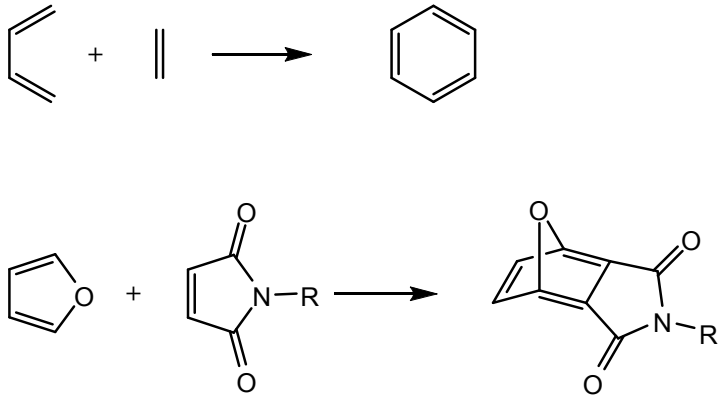

Figure I.29: Diels-Alder reactions. First equation is the production of benzene from butadiene (diene) and ethylene (dienophile). Second example is the reaction between furan and maleimide moieties.

The reaction of Diels-Alder, as shown in Figure I.29, has been little investigated towards the functionalization of nanoparticles. Nevertheless, it could represent an interesting way to produce engineered nanoparticles. One interesting things is the fact that this reaction could be carried out in water[148] if the diene and the dienophile have been correctly chosen; even more the reaction could be accelerated in water with or without Lewis acid catalysis[149,150]. Furthermore, Diels-Alder reactions can be catalyzed by Copper species[151]. An important point is the reversibility of this reaction leading to degradable assemblies. This last point must be underlined because degradation capacity of multifunctional nanocarriers is a challenging issue in many fields like nanomedicine. Diels-Alder reaction represents a tuning way to produce reversible assemblies on nanoparticles or between nanoparticles. To date, maleimide and furan are the most employed dienophiles and dienes.

[148] Meijer, A., Otto, S., Engberts, J.B.F.N.
Effects of the hydrophobicity of the reactants on Dieis-Alder reactions in water
(1998) Journal of Organic Chemistry, 63 (24), pp. 8989-8994.
[149] Engberts, J.B.F.N., Feringa, B.L., Keller, E., Otto, S.
Lewis-acid catalysis of carbon carbon bond forming reactions in water
(1996) Recueil des Travaux Chimiques des Pays-Bas-Journal of the Royal Netherlands, 115 (11-12), pp. 457-464.
[150] Otto, S., Engberts, J.B.F.N., Kwak, J.C.T.
Million-fold acceleration of a Diels-Alder reaction due to combined Lewis acid and micellar catalysis in water
(1998) Journal of the American Chemical Society, 120 (37), pp. 9517-9525.
[151] Reymond, S., Cossy, J.
Copper-catalyzed diels - Alder reactions
(2008) Chemical Reviews, 108 (12), pp. 5359-5406.

To date little investigated reaction like Diels-Alder cycloaddition must find outstanding applications in material sciences to create new hydrid organic/inorganic assemblies[152,153]. One example is the conjugation of gold nanoparticles to polymers (see Figure I.30) which allows to achieve uniform composites, the basement of efficient electronic interfacial interactions between the constituents.

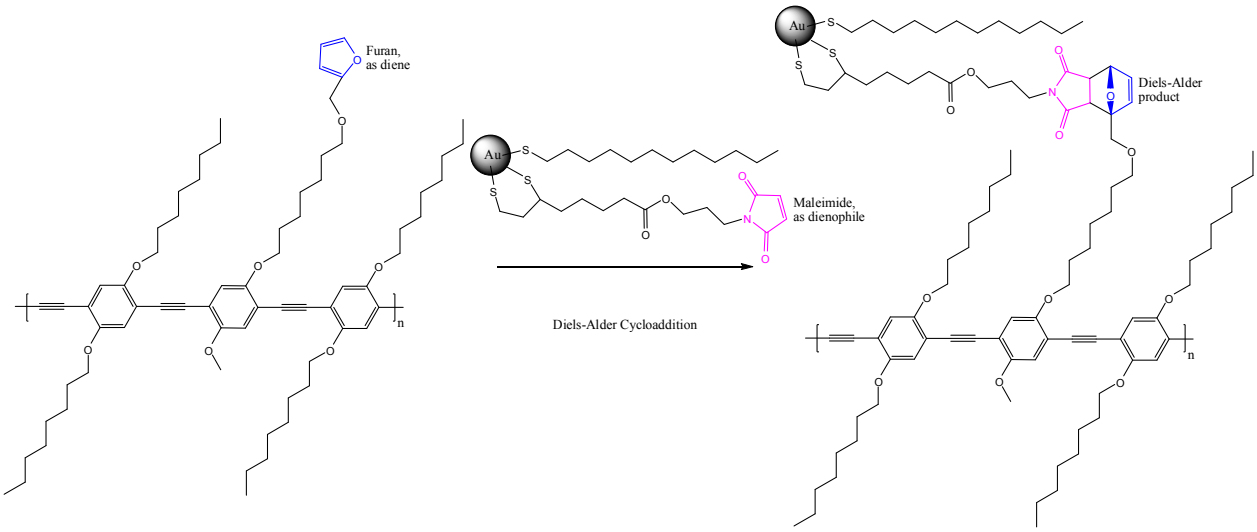

Figure I.30: Grafting of gold nanoparticles on polymer by the mean of Diels-Alder reaction.

III.3) Selected examples

As post-insertion has been developed on liposomes, many of the applications are relevant in the medical field. In these cases, post-insertion could provide a help to introduce targeting ligands on the surface of liposomes. Many examples could illustrate this fact; post-insertion allows the fast development of multifunctional carriers[154] in combination of reliable encapsulation technique. LBL has been used with success to create siRNA delivery systems as gold nanoparticles coated with polyethylene imine (PEI)/siRNA mixed layers[118]. It demonstrates the feasability of creating advanced nanoparticles in only few steps. This

[152] McElhanon, J.R., Zifer, T., Kline, S.R., Wheeler, D.R., Loy, D.A., Jamison, G.M., Long, T.M., Rahimian, K., Simmons, B.A.
Thermally cleavable surfactants based on furan-maleimide diels-alder adducts
(2005) Langmuir, 21 (8), pp. 3259-3266.
[153] Liu, X., Zhu, M., Chen, S., Yuan, M., Guo, Y., Song, Y., Liu, H., Li, Y.
Organic-inorganic nanohybrids via directly grafting gold nanoparticles onto conjugated copolymers through the Diels-Alder reaction
(2008) Langmuir, 24 (20), pp. 11967-11974.
[154] Gantert, M., Lewrick, F., Adrian, J.E., Rössler, J., Steenpaß, T., Schubert, R., Peschka-Süss, R.
Receptor-specific targeting with liposomes in vitro based on sterol-PEG1300 anchors
(2009) Pharmaceutical Research, 26 (3), pp. 529-538.

example also establishes that siRNA assembled into layers on the surface of nanoparticles are more effective in gene silencing than PEI/siRNA random conjugates.

LBL is also a very promising technique towards the use of nanoparticles in other fields than nanomedecine. One important field of research is the development of devices based on LBL and nanoparticles. Such devices are developed for photovoltaic cells composed of fullerenes functionalized with the help of Bingel reaction[155]. Another example is the building of layered systems where enzymes are embedded, providing multi-enzyme reactor at the nanometric scale[156]. Development of hydrid organic/inorganic nanoparticles could also be done, creating nano-hybrid catalyst for example[157].

ROMP is employed for the production of nanoassemblies with defined properties. For example, starting from substituted norbornenes (with PEG for compound 2 or cinnamoyl groups for compound 1, as shown in Figure I.31), ROMP is carried out to produce amphiphilic polymers.

[155] Mwaura, J.K., Pinto, M.R., Witker, D., Ananthakrishnan, N., Schanze, K.S., Reynolds, J.R.
Photovoltaic cells based on sequentially adsorbed multilayers of conjugated poly(p-phenylene ethynylene)s and a water-soluble fullerene derivative
(2005) Langmuir, 21 (22), pp. 10119-10126.
[156] Onda, M., Lvov, Y., Ariga, K., Kunitake, T.
Sequential reaction and product separation on molecular films of glucoamylase and glucose oxidase assembled on an ultrafilter
(1996) Journal of Fermentation and Bioengineering, 82 (5), pp. 502-506.
[157] Dotzauer, D.M., Dai, J., Sun, L., Bruening, M.L.
Catalytic membranes prepared using layer-by-layer adsorption of polyelectrolyte/metal nanoparticle films in porous supports
(2006) Nano Letters, 6 (10), pp. 2268-2272.

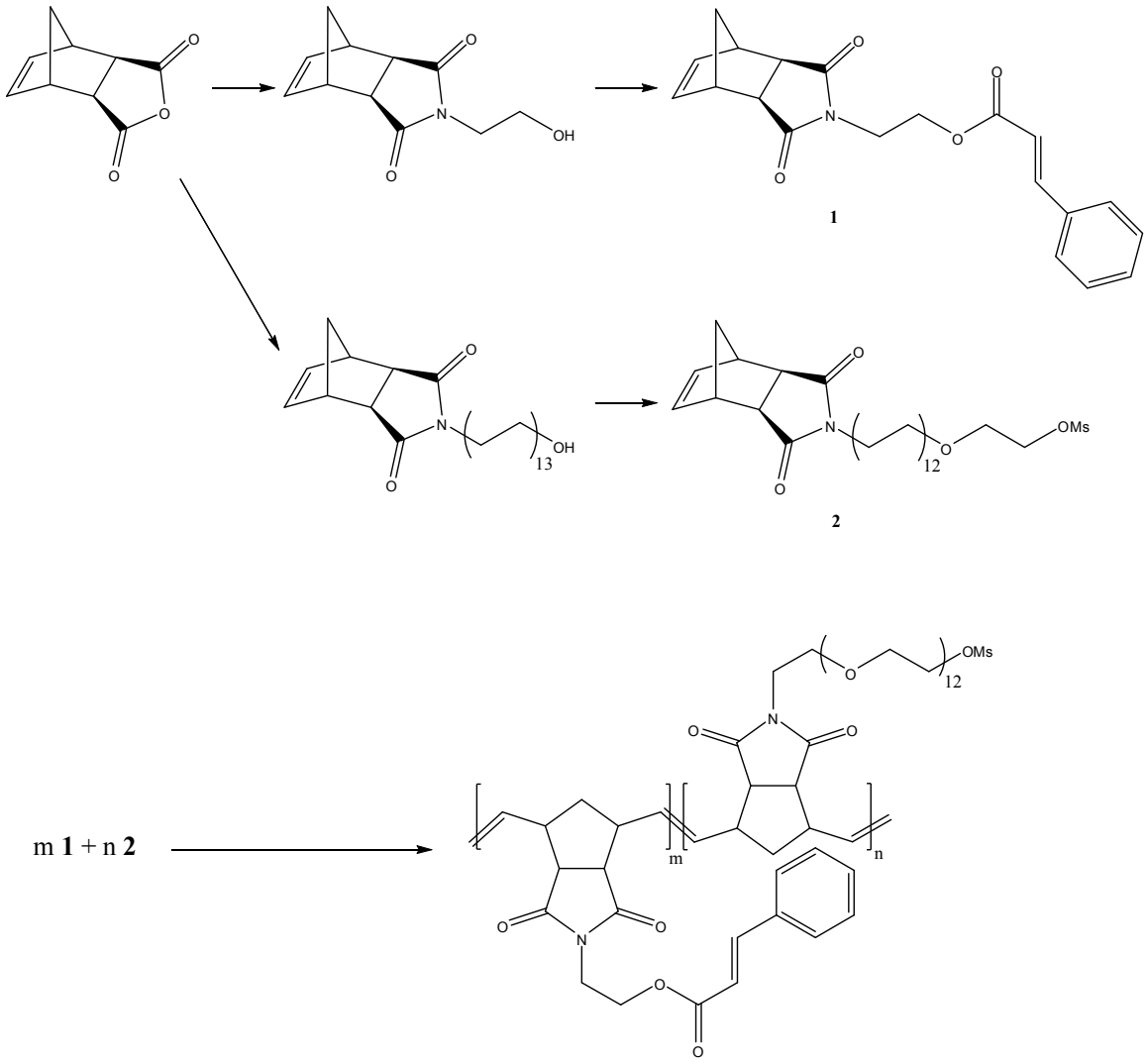

Figure I.31: Synthesis of amphiphilic polymers by ROMP starting from substituted norbornenes.

Self-assembly of these polymers leads to micelles, which were further cross-linked by UV light irradiation and radiolabeled with ^{18}F according to classical radiolabeling methods[158]. Thus ROMP produces well defined polymers bearing several reacting groups. Micelles with high specific activity are produced through only three steps.

The production of engineered polymers by ROMP has been also employed to coat fluorescent nanocrystals in water[159]. In this case, norbornene derivative is conjugated with PEGs and phospholipids to produce amphiphilic monomers. Subsequent oligomerization by

[158] Matson, J.B., Grubbs, R.H.
Synthesis of fluorine-18 functionalized nanoparticles for use as in vivo molecular imaging agents
(2008) Journal of the American Chemical Society, 130 (21), pp. 6731-6733.
[159] Travert-Branger, N., Dubois, F., Carion, O., Carrot, G., Mahler, B., Dubertret, B., Doris, E., Mioskowski, C.
Oligomeric PEG-phospholipids for solubilization and stabilization of fluorescent nanocrystals in water
(2008) Langmuir, 24 (7), pp. 3016-3019.

Grubbs II catalyst produces biocompatible structures (figurated as blue and pink rectangles, Figure I.32) able to solubilise quantum dots into water without modifying fluorescence.

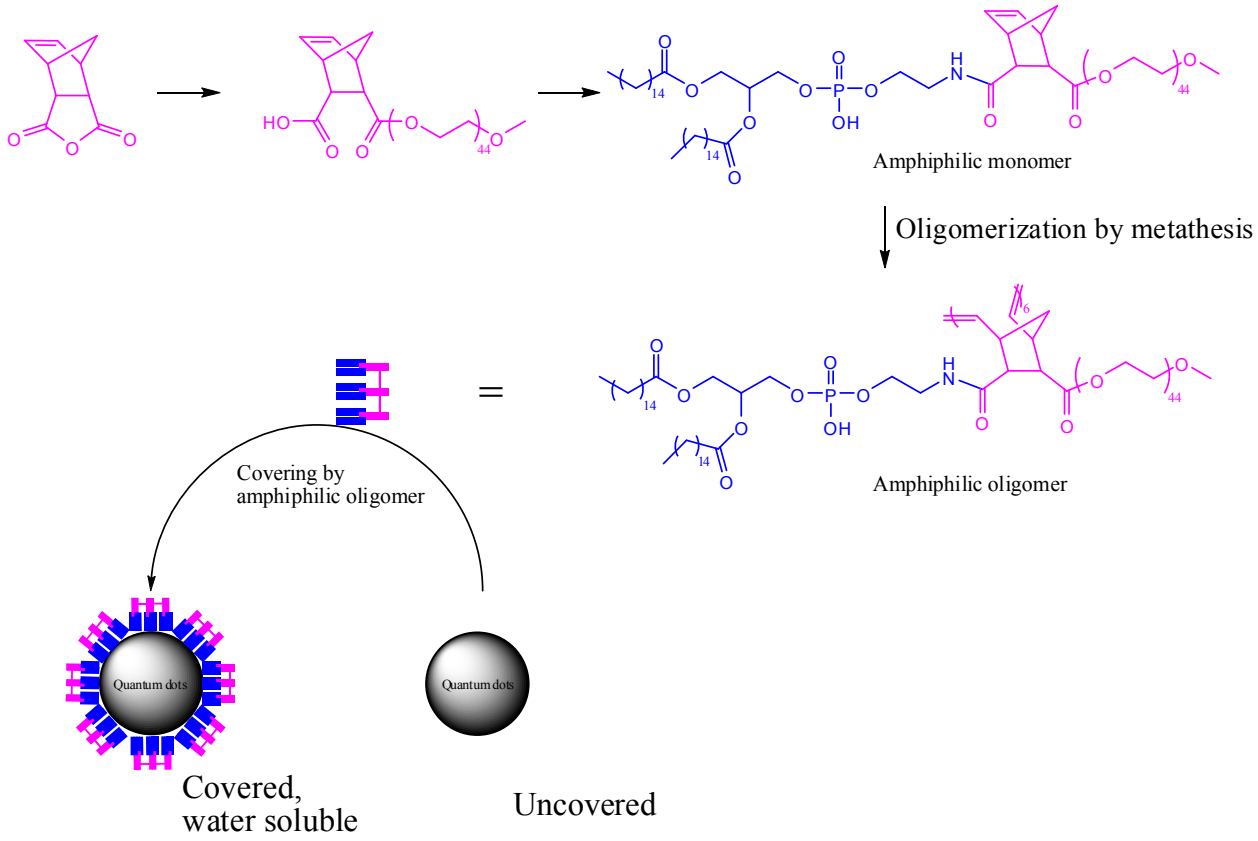

Figure I.32: Covering of quantum dots by nanostructures formed by ROMP.

Similar approach was used to yield multifunctional polymeric nanoparticles bearing both anti HER-2 antibodies, Bcl-2 antisense oligonucleotide and anticancer drug (indomethacin) in a straight way[160]. Synergistic actions were demonstrated and make this approach very unique and promising[161].

[160] Bertin, P.A., Smith, D., Nguyen, S.T.
High-density doxorubicin-conjugated polymeric nanoparticles via ring-opening metathesis polymerization
(2005) Chemical Communications, (30), pp. 3793-3795.
[161] Bertin, P.A., Gibbs, J.M., Shen, C.K.-F., Thaxton, C.S., Russin, W.A., Mirkin, C.A., Nguyen, S.T.
Multifunctional polymeric nanoparticles from diverse bioactive agents
(2006) Journal of the American Chemical Society, 128 (13), pp. 4168-4169.

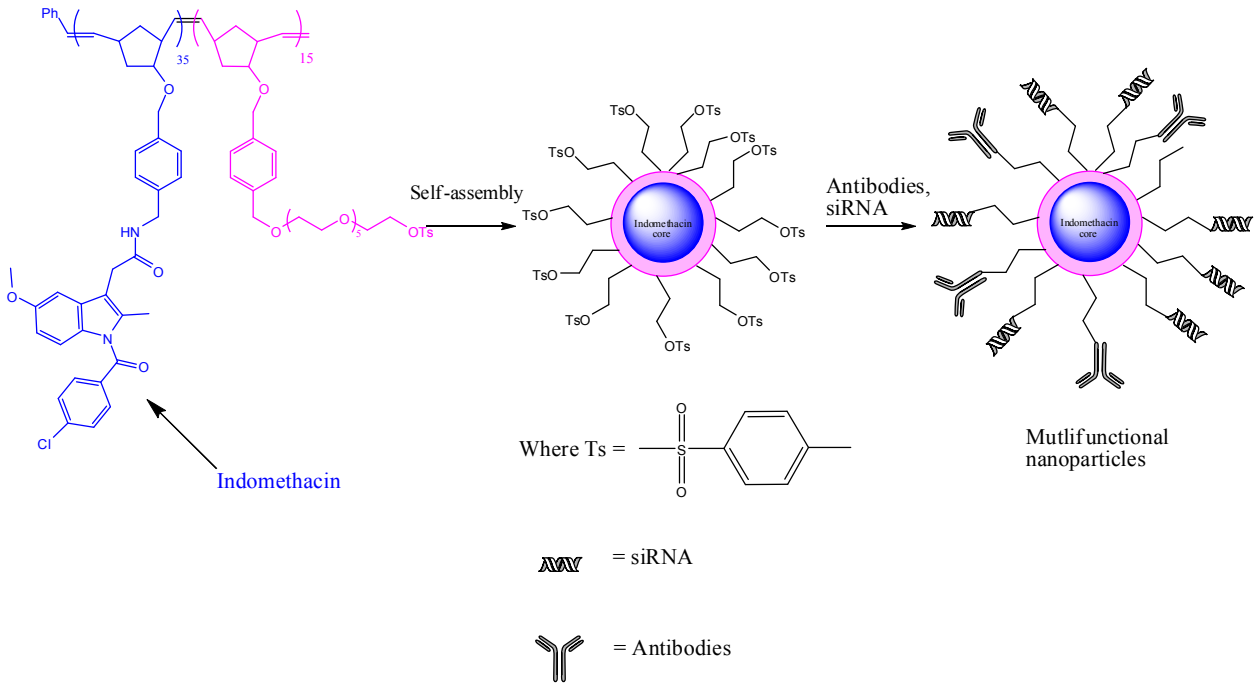

Figure I.33: Synthesis of polymers by sequential ROMP and functionalization of nanoparticles. Multifunctionnal carriers are created.

It appears that combination of several techniques (formulation and post-modification) can create advanced colloidal systems. In this way, CuAAC performed on nanoparticles can bring out essential properties such as responsibility to external stimuli. For example, layered micelles have been created by association of chemical cross-linking and coverage by dendrimers bearing azido groups[162]. The cross-linked core is pH responsive and dendrimers are thermo-responsive. The enhanced colloid stabilities at important temperatures, as well as the pH-responsive behaviour, make these layered micelles, potential carriers for advanced drug delivery. In addition, nanoparticles with alkyne or azido groups can be assembled together by the combination of emulsification process and interfacial click reaction[163]. Authors have produced stable magnetic colloïdosomes by a convenient approach.

Furthermore, authors underline the fact that the properties of these assemblies can be

[162] Jiang, X., Zhang, G., Narain, R., Liu, S.
Covalently stabilized temperature and pH responsive four-layer nanoparticles fabricated from surface 'clickable' shell cross-linked micelles
(2009) Soft Matter, 5 (7), pp. 1530-1538.
[163] Samanta, B., Patra, D., Subramani, C., Ofir, Y., Yesilbag, G., Sanyal, A., Rotello, V.M.
Stable magnetic colloidosomes via click-mediated crosslinking of nanoparticles at water-oil interfaces
(2009) Small, 5 (6), pp. 685-688.

tuned by the choice of the nature of starting nanoparticles, providing access to versatile applications.

In general, CuAAC allows the convenient synthesis of nanohybryde systems such MultiWallcarbonNanoTubes (MWNT) covered click magnetic nanoparticles[164]. Furthermore, as CuAAC can be realized between distinct particles, synthesis of supramolecular assemblies such as hydrogel[165] can be achieved.

III.4) Conclusion

The creation of high value nanoparticles should be done by combination of both formulation and post-formulation methods. Strategies are available and are under constant improvements. Integration of the presented strategies into production processes should lead to the discovery of nanoparticles, pushing the actual limits forward. The choice of the strategy depends on the nature of nanoparticles and on other factors such as the cost of the reactants and purification issues. We should also keep in mind that this breakthrough should be possible only if biodegradability/biocompatibility is imprinted into nanoparticles at an early stage.

[164] He, H., Zhang, Y., Gao, C., Wu, J.
'Clicked' magnetic nanohybrids with a soft polymer interlayer
(2009) Chemical Communications, (13), pp. 1655-1657.
[165] Crescenzi, V., Cornelio, L., Di Meo, C., Nardecchia, S., Lamanna, R.
Novel hydrogels via click chemistry: Synthesis and potential biomedical applications
(2007) Biomacromolecules, 8 (6), pp. 1844-1850.

Chapitre II

Caractérisations physiques des nanocapsules lipidiques

Introduction

Les nanocapsules de départ sont produites selon le procédé initié au laboratoire dans le travail de thèse de Béatrice Heurtault. Après pesée des constituants, ces derniers sont mélangés par agitation et chauffage à 90°C. On laisse ensuite refroidir le système jusqu'à la température de 35°C. On reproduit le cycle chauffage-refroidissement trois fois ; plusieurs constatations expérimentales peuvent alors être soulignées (Figure II.2):

- l'aspect macroscopique du mélange passe d'une solution incolore et peu visqueuse à une solution blanche de viscosité plus importante lors du chauffage,
- lors des refroidissements, il apparaît à une certaine température que le mélange semble homogène macroscopiquement et totalement translucide,
- la température à laquelle la zone de translucidité apparaît dépend de la composition du système et, plus particulièrement de la concentration en sel,
- l'ensemble du procédé peut être suivit par conductimétrie, comme illustré dans la Figure II.1.

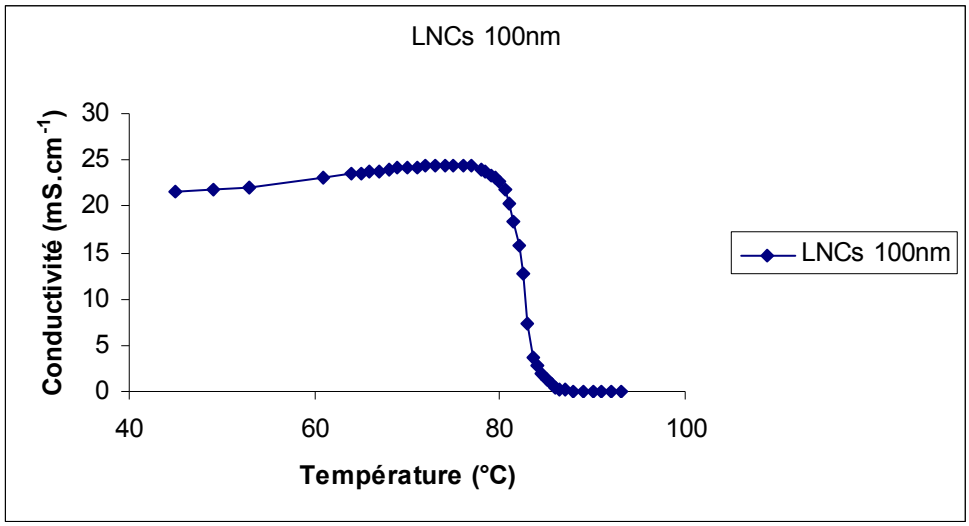

Figure II.1 : Suivi conductimétrique de la transition de phase sur laquelle s'appuie la formulation des LNCs de 100nm.

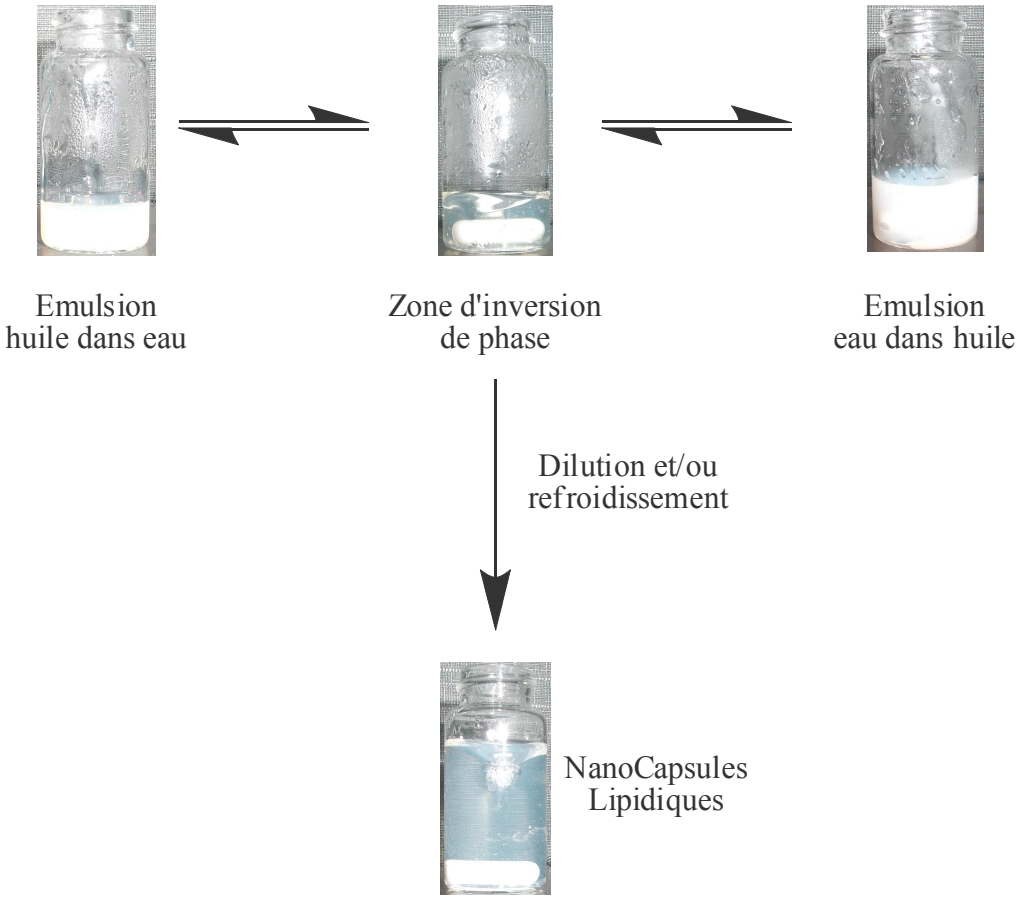

Figure II.2 : Description schématique du procédé de production des nanocapsules lipidiques.

Nous avons donc par ce procédé formulé une émulsion réversible avec la température :

- en effet, à température inférieure à la température d'inversion de phase, nous avons une émulsion huile dans eau.
- à température supérieure à la température d'inversion de phase, nous avons une émulsion eau dans huile.

La question qui se pose alors est la suivante : comment obtenir un système stable à partir de l'émulsion préparée par la méthode décrite ci-dessus ? L'approche expérimentale consiste à vouloir figer le système en refroidissant brutalement le mélange, sous sa forme translucide, soit par ajout d'eau froide soit par refroidissement direct du mélange dans de l'eau glacée.

Constituants	*Quantités en g.*		
	NL 20 nm	*NL 50 nm*	*NL 100 nm*
Solutol HS 15®	1.934	0.846	0.484
Lipoïd 75-3®	0.075	0.075	0.075
NaCl	0.089	0.089	0.089
Labrafac®	0.846	1.028	1.209
Eau	2.055	2.962	3.143
Eau à 4°C	12.5 ml	12.5 ml	12.5 ml
Volume total	**17,5 ml**	**17,5 ml**	**17,5 ml**
Concentration	**168 g/l**	**115 g/l**	**104 g/l**

Figure II.3 : Tableau des constituants des LNCs.

I) Etude de stabilité des nanocapsules lipidiques

Dans un premier temps, nous avons étudié l'impact de la nature de la phase dispersante sur la taille des nanocapsules lipidiques. Nous avons conduit une étude de stabilité

en fonction du pH et de la composition de la phase extérieure, à 4°C dans le but d'établir une charte pour le stockage des échantillons de nanocapsules lipidiques. La stabilité des nanocapsules lipidiques a été analysée par le biais de la diffusion dynamique de la lumière en fonction du temps.

I.1) Impact de la phase dispersante sur la formulation de nanocapsules de 50 nm

Nous avons choisi de diluer la zone d'inversion de phase avec une phase aqueuse de pH et de compositions variables. Nous avons utilisé trois pH différents (3 ; 7 ; 10) et des phases dispersantes contenant une concentration en sels (NaCl, KCl) ou en solutés (Glucose, tréhalose, saccharose) variable.

Les résultats sont consignés dans la Figure suivante :

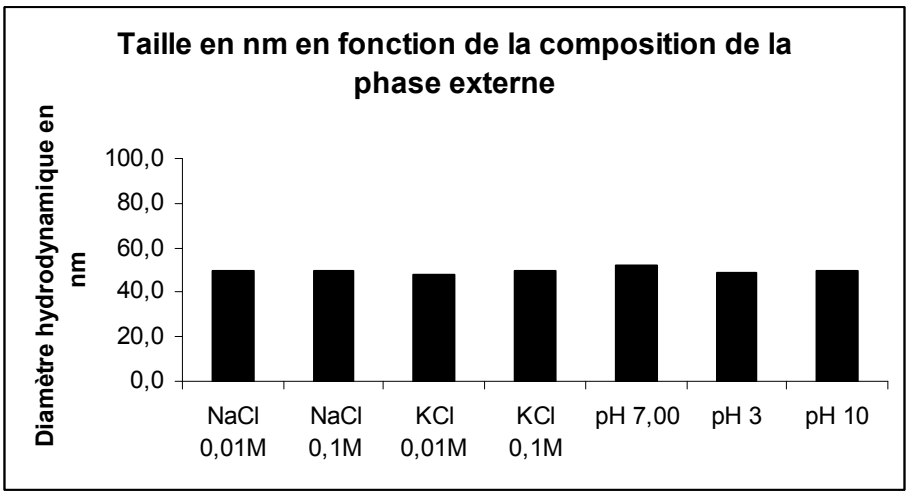

Figure II.4 : Diamètre hydrodynamique des LNCs en fonction de la concentration en sel et du pH de la phase dispersante.

Nous avons choisi d'utiliser des sucres comme solutés car ils peuvent être employés comme cryoprotecteurs, si les échantillons sont congelés lors du stockage.

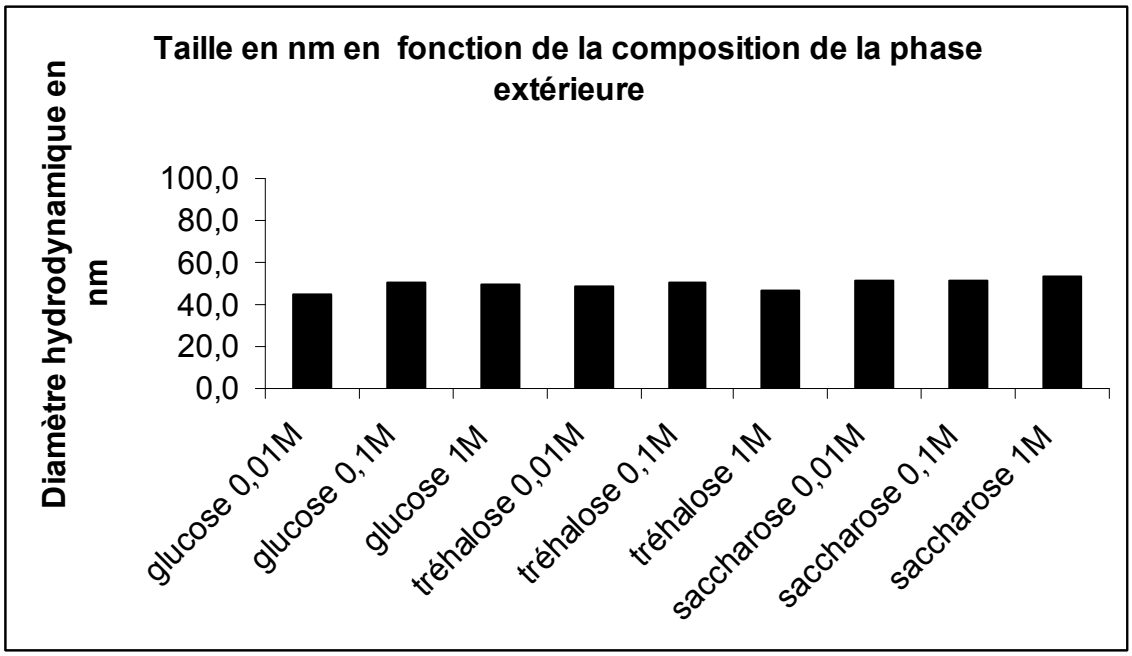

Figure II.5 : Diamètre hdyrodynamique des LNCs en fonction de la composition de la phase dispersante.

On peut affirmer que le pH, la salinité et la concentration en solutés n'influe pas sur le diamètre hydrodynamique des LNCs. Cependant, l'indice de polydispersité augmente pour les solutions de tréhalose 1M et l'eau à pH = 10.

I.2) Etude de la stabilité temporelle

L'étude a été conduite sur une période de 3 mois en utilisant des échantillons stockés à 4°C. Les résultats sont consignés dans les Figures II.6 et II.7.

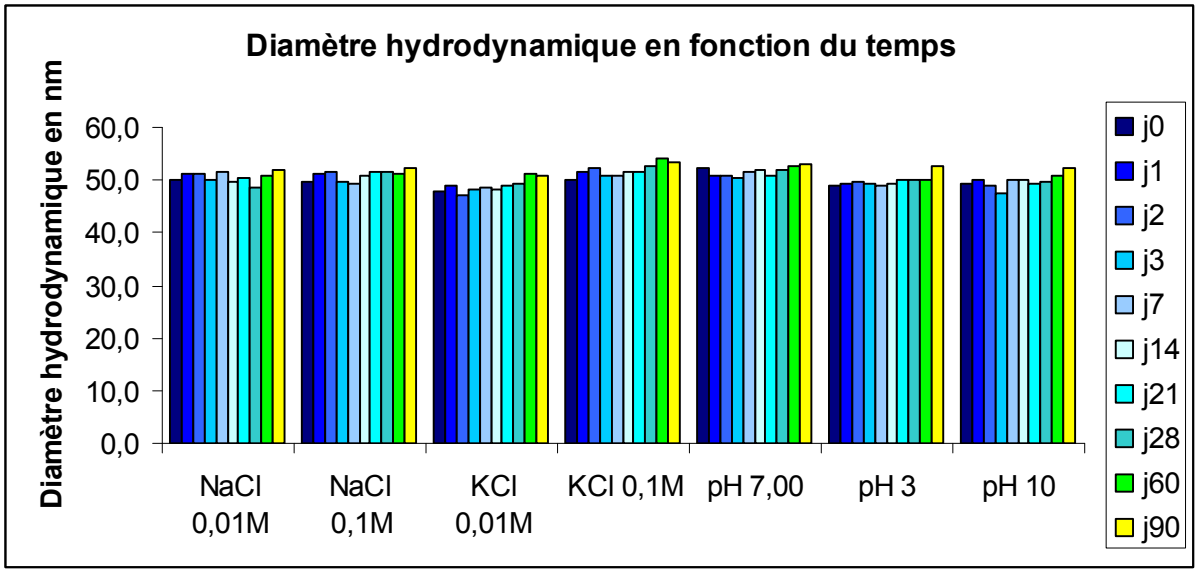

Figure II.6 : Evolution temporelle du diamètre hdyrodynamique des LNCs.

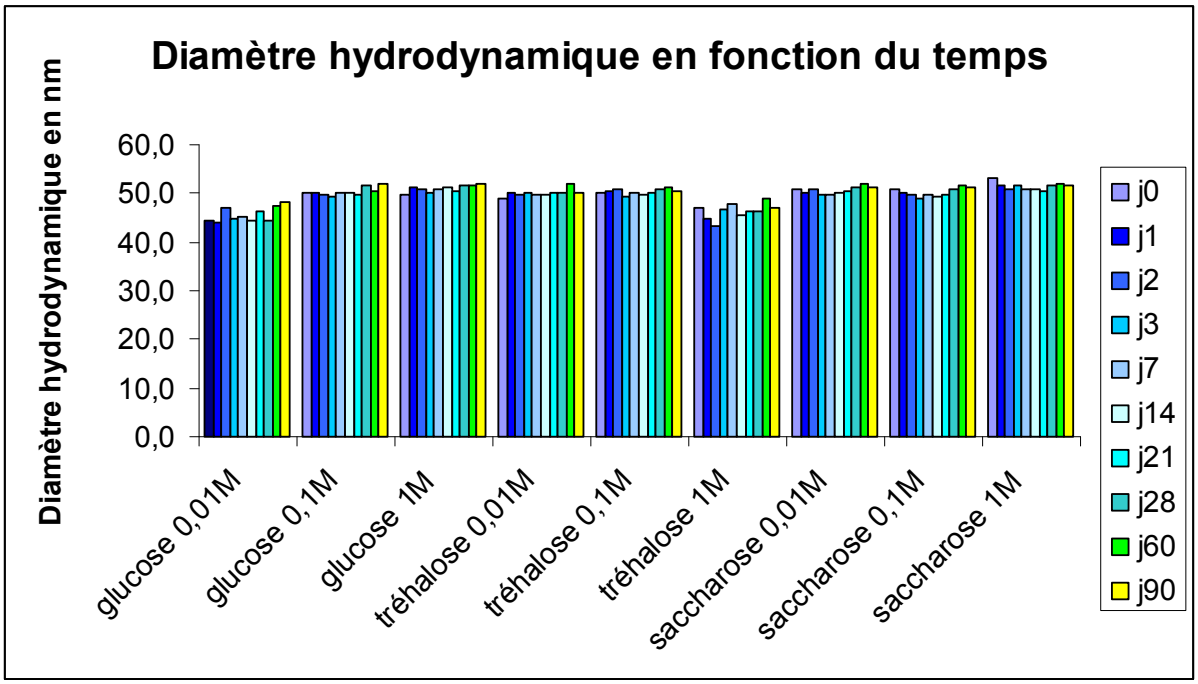

Figure II.7 : Evolution temporelle du diamètre hydrodynamique des LNCs.

Il apparaît que les nanocapsules lipidiques semblent être stables en suspension si elles sont stockées à 4°C quelle que soit la nature de la phase dispersante.

Par la suite nous avons étudié la stabilité des nanocapsules lipidiques en fonction du temps pour des températures supérieures. Un échantillon de nanocapsules blanches produit

selon la méthode développée au laboratoire et stocké à température ambiante semble avoir une stabilité comparable à celle obtenue à 4°C. Aucun phénomène de coalescence ou de murissement d'Ostwald ne semble se produire sur la période considérée. (Supérieure à 1 mois). Les nanocapsules lipidiques présentent une sensibilité thermique pour de températures supérieures à 60°C, proches des températures d'inversion de phase.

I.3) Facteurs de déstabilisation

Les LNCs sont détruites dans des milieux fortement acides (acide chlorhydrique et acide nitrique). De même, les LNCs sont détruites en présence de solvants organiques comme le chloroforme ou le tétrahydrofurane. Ces solvants sont des solvants des constituants des LNCs.

Nous allons donc par la suite caractériser physiquement le système obtenu par diffusion dynamique de la lumière et diffusion des neutrons aux petits angles. Cette étude se terminera par l'établissement d'un modèle physique des LNCs.

II) Etude des LNCs par diffusion des neutrons aux petits angles

LipidicNanoCapsules (LNCs) from structure to colloïdal properties, a study.

Thomas Perrier[1]*, Guillaume Bastiat[1], Annie Brûlet[2], Cédric Gaillard[3], Pascal Gayet[1], Jean-Pierre Benoît[1] and Patrick Saulnier[1]

(1) INSERM U646, Ingénierie de la vectorisation particulaire,

10, rue André Boquel, Université D'Angers, Angers, France

(2) Laboratoire Léon Brillouin, Commissariat à l'Energie Atomique de Saclay, bâtiment 563,

Gif-sur-Yvettes, France

(3) Inra - Site de Nantes, Rue de la Géraudière, BP 71627, 44316 Nantes cedex 3

*Corresponding author : To whom correspondance should be addressed. E-mail address : thomas.perrier@etud.univ-angers.fr

Abstract

Among available strategies of formulation, Phase Inversion Temperature (PIT) methods allow the rapid production of well defined nanoparticles (LipidicNanoCapsules) with interesting properties such as stability and narrow size distribution. Herein, we present the very specific parameters of the formulation process and the assessement of LNCs structure by

small angle scattering. Starting from those experimental facts, we explain the particular interfacial structure and the subsequent LNCs properties.

Introduction

This paper describes the structure of LipidicNanoCapsules (LNCs) obtained by dynamic light scattering (DLS), small angle neutron scattering(SANS) and transmission electronic microscopy (TEM). We demonstrate the singular structure of LNCs with an interface made of highly packed surfactants. This particular structure is a necessary condition to explain the outstanding colloïdal properties of LNCs such as temporal stability, cell uptake and biocompatibility.

Nanoparticles formulation has been extensively investigated in part because of their applications in sensing[166,167], imaging[168,169,170,171], delivery[172,173,174,175,176,177,178], and others

[166] Huang, C.-C., Yang, Z., Lee, K.-H., Chang, H.-T.
Synthesis of highly fluorescent gold nanoparticles for sensing mercury(II)
(2007) Angewandte Chemie - International Edition, 46 (36), pp. 6824-6828.
[167] Choi, Y., Ho, N.-H., Tung, C.-H.
Sensing phosphatase activity by using gold nanoparticles
(2007) Angewandte Chemie - International Edition, 46 (5), pp. 707-709.
[168] Mallidi, S., Larson, T., Tam, J., Joshi, P.P., Karpiouk, A., Sokolov, K., Emelianov, S.
Multiwavelength photoacoustic imaging and plasmon resonance coupling of gold nanoparticles for selective detection of cancer
(2009) Nano Letters, 9 (8), pp. 2825-2831.
[169] Javier, D.J., Nitin, N., Levy, M., Ellington, A., Richards-Kortum, R.
Aptamer-targeted gold nanoparticles as molecular-specific contrast agents for reflectance imaging
(2008) Bioconjugate Chemistry, 19 (6), pp. 1309-1312.
[170] Schuster, B.
Polymeric nanoparticles as imaging probes for protein kinase activity in cells
(2007) Angewandte Chemie - International Edition, 46 (46), pp. 8744-8746.
[171] Montet, X., Weissleder, R., Josephson, L.
Imaging pancreatic cancer with a peptide-nanoparticle conjugate targeted to normal pancreas
(2006) Bioconjugate Chemistry, 17 (4), pp. 905-911.
[172] Messerschmidt, S.K.E., Musyanovych, A., Altvater, M., Scheurich, P., Pfizenmaier, K., Landfester, K., Kontermann, R.E.
Targeted lipid-coated nanoparticles: Delivery of tumor necrosis factor-functionalized particles to tumor cells
(2009) Journal of Controlled Release, 137 (1), pp. 69-77.
[173] Chappell, J.C., Song, J., Burke, C.W., Klibanov, A.L., Price, R.J.
Targeted delivery of nanopartides bearing fibroblast growth factor-2 by ultrasonic microbubble destruction for therapeutic arteriogenesis
(2008) Small, 4 (10), pp. 1769-1777.
[174] Ghosh, P., Han, G., De, M., Kim, C.K., Rotello, V.M.
Gold nanoparticles in delivery applications
(2008) Advanced Drug Delivery Reviews, 60 (11), pp. 1307-1315.

technological uses[179,180]. Nanoparticles manufacturing processes could be divided into three main ways based on their origin :(i) physical processes (ii) chemical processes involved in the chemical synthesis of quantum dots[181,182,183] or in the synthesis of amphiphilic polymers self-associated into nanoparticles[184] (iii) cross processes, usually named physico-chemical processes[185,186,187], have been set up taking advantage of chemical parameters (nature of molecules, concentration) and physical parameters (properties varying with temperature or pressure). Biological architectures[188] like viruses[189], chylomicrons[190,191,192], high density

[175] Yuhua, H., Litwin, T., Nagaraja, A.R., Kwong, B., Katz, J., Watson, N., Irvine, D.J.
Cytosolic delivery of membrane-impermeable molecules in dendritic cells using pH-responsive core-shell nanoparticles
(2007) Nano Letters, 7 (10), pp. 3056-3064.
[176] Wang, Y., Gao, S., Ye, W.-H., Yoon, H.S., Yang, Y.-Y.
Co-delivery of drugs and DNA from cationic core-shell nanoparticles self-assembled from a biodegradable copolymer
(2006) Nature Materials, 5 (10), pp. 791-796.
[177] Yamada, T., Iwasaki, Y., Tada, H., Iwabuki, H., Chuah, M.K.L., VandenDriessche, T., Fukuda, H., Kondo, A., Ueda, M., Seno, M., Tanizawa, K., Kuroda, S.
Nanoparticles for the delivery of genes and drugs to human hepatocytes
(2003) Nature Biotechnology, 21 (8), pp. 885-890.
[178] Panyam, J., Labhasetwar, V.
Biodegradable nanoparticles for drug and gene delivery to cells and tissue
(2003) Advanced Drug Delivery Reviews, 55 (3), pp. 329-347.
[179] Wildgoose, G.G., Banks, C.E., Compton, R.G.
Metal nanoparticles and related materials supported on Carbon nanotubes: Methods and applications
(2006) Small, 2 (2), pp. 182-193.
[180] Reynolds, A.J., Haines, A.H., Russell, D.A.
Gold glyconanoparticles for mimics and measurement of metal Ion-mediated carbohydrate - carbohydrate interactions
(2006) Langmuir, 22 (3), pp. 1156-1163.
[181] Law, W.-C., Yong, K.-T., Roy, I., Ding, H., Hu, R., Zhao, W., Prasad, P.N.
Aqueous-phase synthesis of highly luminescent CdTe/ZnTe core/shell quantum dots optimized for targeted bioimaging
(2009) Small, 5 (11), pp. 1302-1310.
[182] Minbiao, J., Sungnam, P., Connor, S.T., Mokari, T., Yi, C., Gaffney, K.J.
Efficient multiple exciton generation observed in colloidal PbSe quantum dots with temporally and spectrally resolved intraband excitation
(2009) Nano Letters, 9 (3), pp. 1217-1222.
[183] Deka, S., Quarta, A., Lupo, M.G., Falqui, A., Boninelli, S., Giannini, C., Morello, G., De Giorgi, M., Lanzani, G., Spinella, C., Cingolani, R., Pellegrino, T., Manna, L.
CdSe/CdS/ZnS double shell nanorods with high photoluminescence efficiency and their exploitation as biolabeling probes
(2009) Journal of the American Chemical Society, 131 (8), pp. 2948-2958.
[184] Klaikherd, A., Nagamani, C., Thayumanavan, S.
Multi-stimuli sensitive amphiphilic block copolymer assemblies
(2009) Journal of the American Chemical Society, 131 (13), pp. 4830-4838.
[185] Motornov, M., Zhou, J., Pita, M., Tokarev, I., Gopishetty, V., Katz, E., Minko, S.
An Integrated multifunctional nanosystem from command nanoparticles and enzymes
(2009) Small, 5 (7), pp. 817-820.
[186] Xu, J., Liu, S.
Polymeric nanocarriers possessing thermoresponsive coronas
(2008) Soft Matter, 4 (9), pp. 1745-1749.
[187] Moughton, A.O., O'Reilly, R.K.
Noncovalently connected micelles, nanoparticles, and metal-functionalized nanocages using supramolecular self-assembly
(2008) Journal of the American Chemical Society, 130 (27), pp. 8714-8725.
[188] Williams, D.F.
On the nature of biomaterials
(2009) Biomaterials, 30 (30), pp. 5897-5909.
[189] Saini, V., Martyshkin, D.V., Mirov, S.B., Perez, A., Perkins, G., Ellisman, M.H., Towner, V.D., Wu, H., Pereboeva, L., Borovjagin, A., Curiel, D.T., Everts, M.
An adenoviral platform for selective self-assembly and targeted delivery of nanoparticles
(2008) Small, 4 (2), pp. 262-269.
[190] Bijsterbosch, M.K., Van Berkel, T.J.C.
Native and modified lipoproteins as drug delivery systems
(1990) Advanced Drug Delivery Reviews, 5 (3), pp. 231-251.

lipoproteins[193,194,195] have been taken out from their original media and modified. The convergency point of all these vectors is the nanometric scale, kept under the 200nm threshold, in most cases. However, many points of disagreement are still in balance : stealthiness towards immune system, active or passive targeting, stability or unstability under a variable set of conditions (production, storage, blood stream, local cell environnement, intracellular compartments). These nanoparticles can be loaded by different cargos depending on their hydrophilic, hydrophobic or amphiphilic characters. Herewith, we present a process based on thermal phase inversions of emulsionated systems[196,197] (under moderated magnetic stiring) composed by medium chain triglycerides (Labrafac® cc), salted water and a mix of phospholipids (Lipoïd® S75-3) and hydroxysterarate polyethyleneglycol (Solutol® HS-15). The feasability domain has been established before[198] where a high concentration of hydrophilic surfactants were required to obtain nanoparticles. The higher the solutol HS-15 amount is, the smaller particles are. First Dynamic Ligth Scattering and Transmission Electronic Microscopy analysis show nanoparticles with tunable sizes and narrow size distributions for a liquid phase formulation process (polydispersity index under 0.1).

However, the only intimate structure of these particles could be supposed because several points remained unknown at this stage of developpement. In brief, following questions

[191] Van Berkel Th., J.C.
Drug targeting: Application of endogenous carriers for site-specific delivery of drugs
(1993) Journal of Controlled Release, 24 (1-3), pp. 145-155.
[192] Rensen, P.C.N., Van Dijk, M.C.M., Havenaar, E.C., Bijsterbosch, M.K., Kruijt, J.K., Van Berkel, T.J.C.
Selective liver targeting of antivirals by recombinant chylomicrons - A new therapeutic approach to hepatitis B
(1995) Nature Medicine, 1 (3), pp. 221-225.
[193]Glickson, J.D., Lund-Katz, S., Zhou, R., Choi, H., Chen, I.-W., Li, H., Corbin, I., Popov, A.V., Cao, W., Song, L., Qi, C., Marotta, D., Nelson, D.S., Chen, J., Chance, B., Zheng, G.
Lipoprotein nanoplatform for targeted delivery of diagnostic and therapeutic agents
(2008) Molecular Imaging, 7 (2), pp. 101-110.
[194] Hellstrand, E., Lynch, I., Andersson, A., Drakenberg, T., Dahlbäck, B., Dawson, K.A., Linse, S., Cedervall, T.
Complete high-density lipoproteins in nanoparticle corona
(2009) FEBS Journal, 276 (12), pp. 3372-3381.
[195] Thaxton, C.S., Daniel, W.L., Giljohann, D.A., Thomas, A.D., Mirkin, C.A.
Templated spherical high density lipoprotein nanoparticles
(2009) Journal of the American Chemical Society, 131 (4), pp. 1384-1385.
[196] Heurtault, B., Saulnier, P., Pech, B., Proust, J.-E., Benoit, J.-P.
A novel phase inversion-based process for the preparation of lipid nanocarriers
(2002) Pharmaceutical Research, 19 (6), pp. 875-880.
[197] Anton, N., Benoit, J.-P., Saulnier, P.
Design and production of nanoparticles formulated from nano-emulsion templates-A review
(2008) Journal of Controlled Release, 128 (3), pp. 185-199.
[198] Heurtault, B., Saulnier, P., Pech, B., Venier-Julienne, M.-C., Proust, J.-E., Phan-Tan-Luu, R., Benoît, J.-P.
The influence of lipid nanocapsule composition on their size distribution
(2003) European Journal of Pharmaceutical Sciences, 18 (1), pp. 55-61.

should be addressed : (i) Is the whole amount of the excipients used for the formulation participate in the building of LNCs ? (ii) If the case, what is the physical structure for this particles ? (iii) What is the molecular organization at the interface between triglycerides and water ?

Discussion

We performed a formulation of nanoemulsion under constant stirring. Phase inversions were obtained and the system was described as followed : at high temperatures, the system was a water in oil emulsion and at lower temperatures, an oil in water one. Between these two extreme cases, specific phasesconstituting the so called phase inversion zone(PIZ)[199,200]. Differing in relation with different micellar topologies. These phases constitute the so called phase inversion zone (PIZ). Subsequent dilutions of the PIZ produced nanoparticles from translucent to opaque suspension with a marked Tyndall effect. Images of these colloïdal suspensions are presented in Figure II.8. TEM and Cryo-TEM analysis show round shaped nanoparticles with a diameter closed to 50nm.

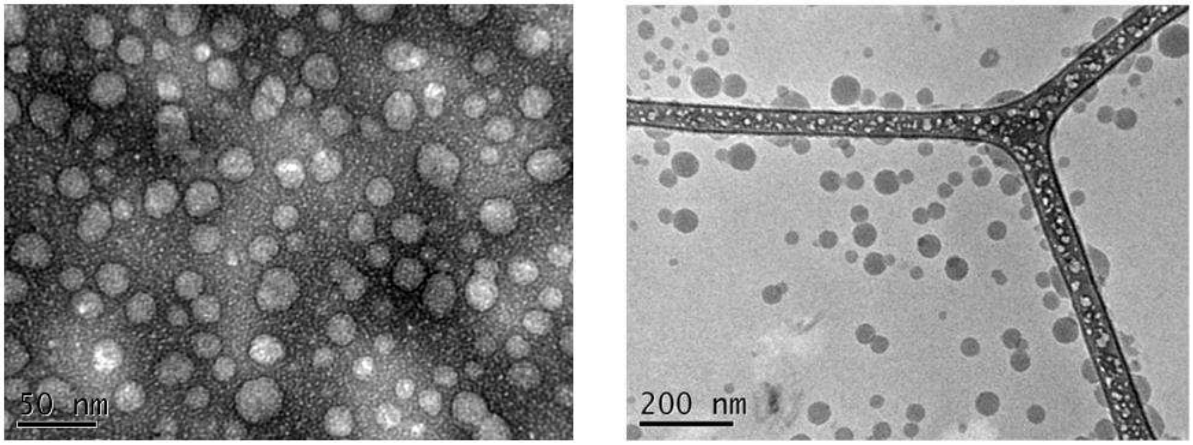

Figure II.8: Representative TEM (left) and Cryo-TEM (right) pictures for LNCs 50nm.

[199] Arai, H., Shinoda, K.
The effect of mixing of oils and of nonionic surfactants on the phase inversion temperatures of emulsions
(1967) Journal of Colloid And Interface Science, 25 (3), pp. 396-400.
[200] Kunieda, H., Shinoda, K.
Evaluation of the hydrophile-lipophile balance (HLB) of nonionic surfactants. I. Multisurfactant systems
(1985) Journal of Colloid And Interface Science, 107 (1), pp. 107-121.

A contrast agent, here uranyl acetate, is needed to see these nanoparticles and LNCs are not destroyed by the staining and the electron beam, even at low pressure. Cryo-TEM experiments show black nanoparticles with a well defined spherical shape. In both cases, polydisperisty of the nanoparticles is closed to the one obtained from dynamic ligth scattering experiments.

Nevertheless, LNCs seemed to be enough stable[201] to resist to both imaging methods. No aggregation or inter-particles fusion were detected. Dynamic light scattering experiments provided the hydrodynamic diameter for each formulation. LNCs with HD equal to 27, 50 and 100nm were produced just by modification of the whole composition as shown in the Table II.1.

Excipients	*LNCs 20nm*	*LNCs 50nm*	*LNCs 100nm*
Solutol HS 15®	1.934	0.846	0.484
Lipoïd 75-3®	0.075	0.075	0.075
NaCl	0.089	0.089	0.089
Labrafac®	0.846	1.028	1.209
Water (g)	2.055	2.962	3.143
Water 4°C (g)	12.5	12.5	12.5
Total volume (ml)	17.5	17.5	17.5
Concentration (g/l)	168	115	104

Table II.1: Amount of excipients for each formulation.

For each sample, autocorrelation functions were decreasing exponential function of time with excellent fitting parameters, indicating the samples monodispersity.

[201] Heurtault, B., Saulnier, P., Pech, B., Proust, J.-E., Benoit, J.-P.
Physico-chemical stability of colloidal lipid particles
(2003) Biomaterials, 24 (23), pp. 4283-4300.

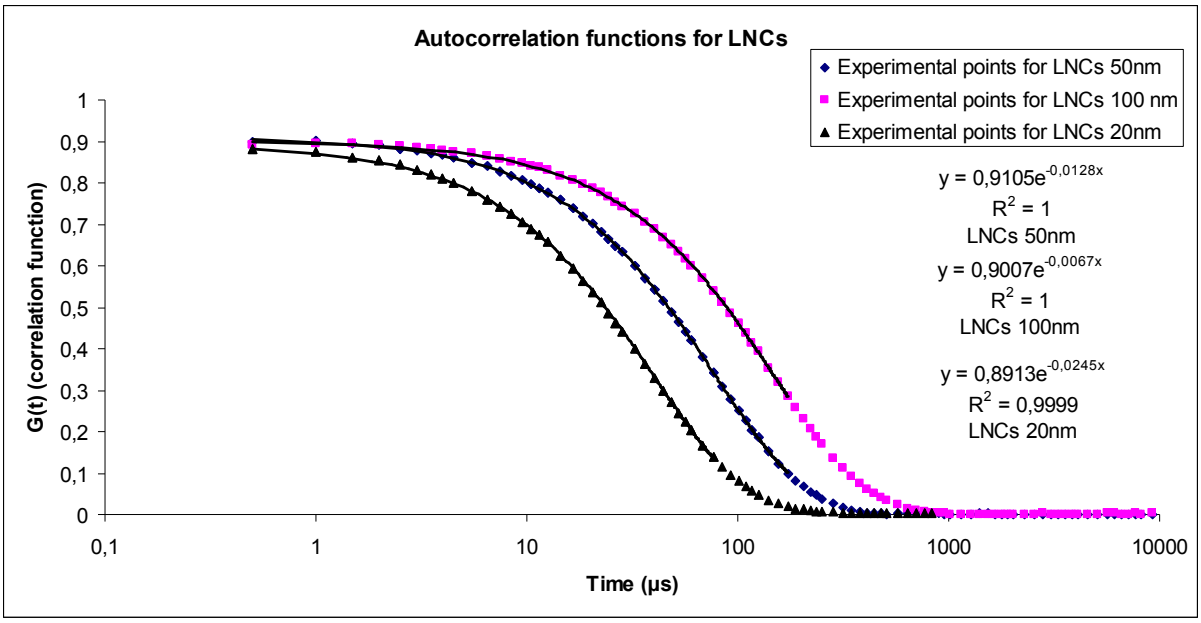

Figure II.9: Autocorrelation functions for each formulation.

Size distributions followed a log-normal law with an excellent matching with the theoritical distribution (log normality index inferior to 0.1). Before discussing on the intimate structure of LNCs, we have assessed if the whole amount of excipients was involved into the architecture of LNCs.

LNCs have been extensively dialysed against distilled water to remove putative excess of materials. The dialysed LNCs were dried and an amount of salted water was added and the formulation was redone. The result is the getting of LNCs with similar characteristics to those obtained before the dialysis step. Furthermore, we have simulated the impact of the loss of solutol HS-15 onto size distribution by making formulations with decreasing amount of solutol HS-15. Figure shows the influence of the amount of solutol HS-15 on the hydrodynamic diameter : it is obvious that the less Solutol HS-15, the bigger LNCs are. As the formulation is surfactant dependent and that no modification of LNCs sizes can be noticed after dialysis and reformulation, we can say that the whole amount of surfactants is involved in the forming of LNCs. As the amount is very important, surfactant molecules should be packed in a tight way. In order to evaluate the macroscopic organisation of our system as well

as the impact of the high amount of surfactants, thermodynamic equilibrium experiments have been made and permit to draw the phase diagram presented in Figure S1 (see supporting info). As shown in Figure S1 and on the basis of previous work, our system presents several molecular organizations, depending on temperature. The phase inversion consists in a transition between Windsor I to Windsor II macroscopic organisation through Windsor III system. Our system, at the temperatures of the phase inversion zone, has a Windsor IV organisation, when the magnetic stirring is stopped (equilibrium conditions). Classical other nano-emulsion processes present phase inversion for amount of surfactant close to 5-6%, the related system shows a Windsor III structure when the equilibrium is reached.

In order to propose a study on the molecular constitution of LNCs, we have calculated the number of LNCs in each samples, assuming on the base of dynamic light scattering experiments that LNCs are monodisperse spherical objects with a radius equal to 12.5, 25 and 50nm respectively. We have calculated the number of molecule of each excipients per LNCs. Results are presented in Table II.2.

	LNCs 20nm	LNCs 50nm	LNCs 100nm
R_2 (nm)	12.5	25	50
$V_{Labrafac}$ (ml)	0.454	1.105	1.3
$V_{Labrafac+Solutol+Lipoïd}$ (ml)	1.153	1.755	1.703
R_1 (nm)	9.16	21.42	45.68
R_2-R_1=thickness (nm)	3.33	3.57	4.31
N_{LNCs}	$1.41006*10^{23}$	$2.6819*10^{22}$	$3.2543*10^{21}$
$N_{Solutol}$ per LNC	3993	18254	86065
NLipoïd per LNC	126	1330	10962
$N_{Solutol}/N_{Lipoïd}$	31	13	7
$N_{Labrafac}$ per LNC	850	10860	105268
Molecular area Solutol (nm^2)	0.250	0.284	0.250

Table II.2: Calculated parameters for each formulation.

As the surface area of one LNC is known, we have evaluated the molecular area for one molecule of surfactant, Solutol HS-15 and phospholipids. We found a value closed to the molecular area obtained by means of Langmuir isotherms[202]. These values are closed to the molecular area of packed phospholipids assembled into liposomes. Both of these facts indicate that Solutol HS-15 and phospholipids coming from Lipoïd S75-3 form a mix monolayer at the interface between triglycerides and water.

[202] Minkov, I., Ivanova, Tz., Panaiotov, I., Proust, J., Saulnier, P.
Reorganization of lipid nanocapsules at air-water interface. Part 2. Properties of the formed surface film
(2005) Colloids and Surfaces B: Biointerfaces, 44 (4), pp. 197-203.

To confirm this fact, small angle neutron scattering (SANS) was performed for LNCs 50 and 100nm. As shown in Figures II.10 and II.11, experimental points were fitted against a homogeneous sphere model and a spherical core-shell model[203].

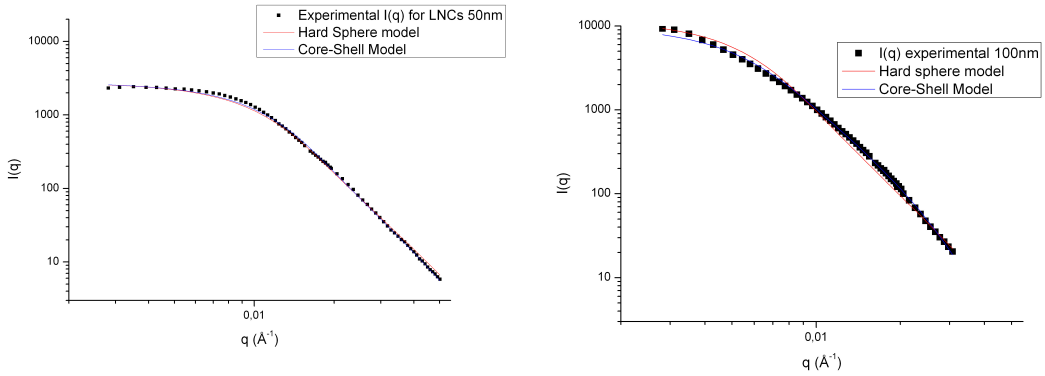

Figure II.10 and **Figure II.11:** Scattered intensity I(q) versus wave vector q for LNCs 50nm and LNCs 100nm.

LNCs 50nm	Homogeneous Sphere Model	Core-Shell Model
R_2 (nm)	21.7	21.1
R_1 (nm)		19.4
Standard Deviation (Normal law)	12.3	11.5
R^2	0.9884	0.9927

Table II.3: Physical parameters for LNCs 50nm calculated with SANS analysis software.

LNCs 100nm	Homogeneous Sphere Model	Core-Shell Model
R_2 (nm)	38.1	39.9
R_1 (nm)		31.8
Standard Deviation (Normal Law)	22.2	27.7
R^2	0.9805	0.9858

Table II.4: Physical parameters for LNCs 100nm calculated with SANS analysis software.

[203] Pedersen, J.S.
Analysis of small-angle scattering data from colloids and polymer solutions: Modeling and least-squares fitting
(1997) Advances in Colloid and Interface Science, 70 (1-3), pp. 171-210.

Experimental and theoritical values were compared with a least mean square method. Without ambiguity, as indicated by R^2 value for both models, LNCs can be considered as homogenous spheres and as well as spherical core-shell structures. This result is not surprising considering LNCs are spherical objects surrounded by a shell of surfactants.with a thickness comprised between 2 and 5nm. This thickness is very closed to the length of one surfactant molecule ; indicating here also a monolayer organisation in the shell. We propose the scheme, indicated in the Figure II.5, in order to illustrate the whole structure of LNCs. The monolayer is in closed relationship with the core, and hydrophobic tails of the surfactants interact with triglyceride molecule forming a continous assembly. Concerning the hydrophilic part, phospholipidic heads are hidden by the PEG chains ; these latters are interacting with water confering to LNCs a good colloïdal stability (Figure S5 ; see ESI).

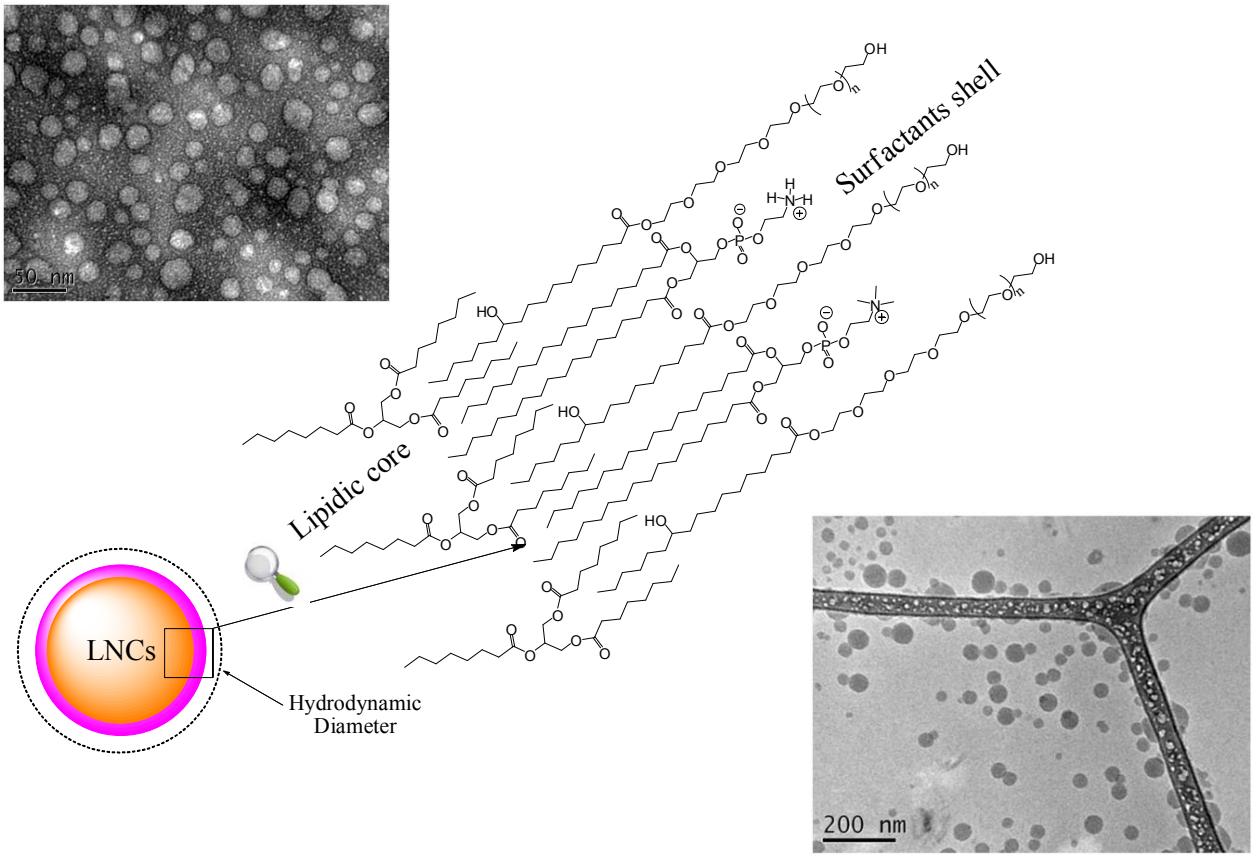

Figure II.5: Illustration of the interface between the oily core and the surfactants shell.

We have shown experimentally that LipidicNanoCapsules are spherical nanoparticles with an interface made of a mix of surfactants assembled into a monolayer. This supramolecular association is cohesive and leads to stable colloïdal nano-objects able to carry and protect drugs or dyes. Further studies will be now conducted to know the diffusion of surfactants into the interfacial monolayer. We are also working on the establishment of drug release model from the triglyceride core of LNCs.

Acknowledegment

This work was financially supported by The Région Pays de La Loire and by European Union through the NanoEar project.

Supporting info available :

Detailed materials and methods. Theoritical background concerning ligth and neutrons scattering and mathematical treatement of raw datas. This material is available free of charge via the Internet at http://pubs.acs.org.

Supporting Information

Experimental Details

Materials

Labrafac® WL 1349 (Gattefossé S.A., Saint-Priest, France) is a mixture of capric and caprylic acid triglycerides. NaCl was purchased from Prolabo (Fontenay-sous-Bois, France) and water was obtained from a Milli-Q-plus® system (Millipore, Paris, France). Lipoïd® S75-3 (Lipoïd GmbH, Ludwigshafen, Germany) is a soybean lecithin made of 69% of phosphatidylcholine, 10% phosphatidylethanolamine and other phospholipids, and Solutol® HS 15 (BASF, Ludwigshafen, Germany) is a mixture of free polyethylene glycol 660 (PEG) and polyethylene glycol 660 hydroxystearate. Dialysis membrane was purchased from Spectrapore and has a molecular weight cut off equal to 100000daltons.

Formulation process

After weighting, all components are mixed under magnetic stirring (200rpm) at room temperature and leading to a O/W emulsion. After progressive heating at a rate of 4°C/ min, a short interval of transparency at temperatures close to 70°C can be observed, and the inverted phase (water droplets in oil) is obtained at 85°C. At least three temperature cycles alternating from 60 to 85°C at the same rate are applied near the phase inversion zone. Thereafter, the mixture undergoes a fast cooling-dilution process: it is diluted 1:3.5 with 12.5ml cold water at 2°C and stirred for 30min, leading to the formation of LNC with the desired size. LNCs are liquid core nanocapsules made of medium chain triglycerides (Labrafac CC) surrounded by a surfactant shell assembled in a mix monolayer.

Establishement of phase equilibrium diagram

The phase diagram is constructed by mixing x wt.% of Labrafac with salted water containing y wt.% of Solutol HS-15 and Lipoïd S75-3, so that $x + y = 100$ wt.%. The Labrafac:Solutol :water mixtures with x:y composition is prepared in culture glass tubes sealed with caps. For x and y varying from 0 to 100wt.%, the samples are vigorously shaked by vortex and left resting for days or months depending if the sample is liquid or liquid crystalline, to attain equilibrium before analysis.

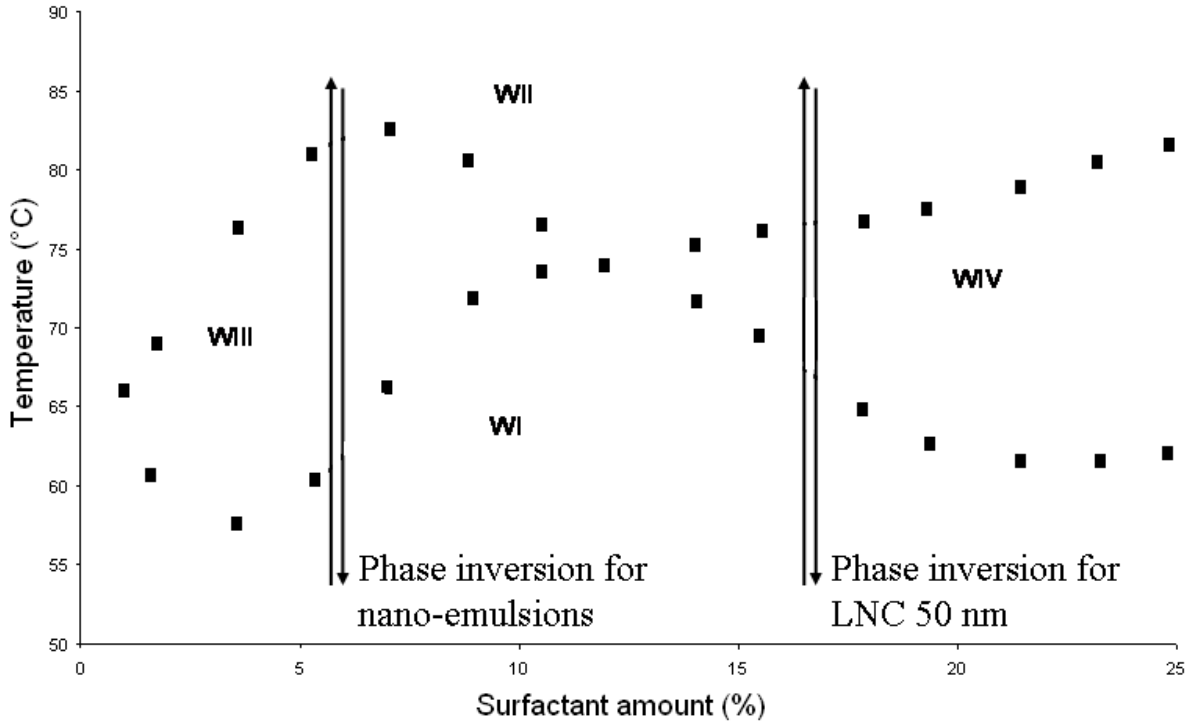

Figure S1: phase diagram for nano-emulsions and for LNCs 50nm.

Dynamic light scattering measurements

All the particles are characterized in term of size distributions using a NanoZS apparatus from Malvern Instruments after dispersion of 50µl of the mother suspension in 3ml of appropriated aqueous medium. Each measurement is made in triplicate.

The non-negative least squares (NNLS) algorithm, used in the Malvern software, allows extracting hydrodynamic radius R_H and the standard deviation σ of the measurement.

Statistical treatment of the curve fitting

To analyse the validity of the fit for the SANS curves and autocorrelation function in dynamic light scattering, the coefficient of determination R^2 was calculated as follows :

$$R^2 = 1 - \frac{SS_r}{SS_{tot}} \qquad \text{(eq. 1)}$$

with SS_r and SS_{tot} the residual and total sum of square respectively. Considering the n observable data (y_i,x_i) and the theoretical fit $y_{theo} = f(x)$ with the couple $(y_{i\ theo},x_i)$, the expression SS_r and SS_{tot} will be:

$$SS_r = \sum_{i=1}^{n} \left(y_i - y_{i\,theo}\right)^2 \qquad \text{(eq. 2)}$$

$$\text{and} \qquad SS_{tot} = \sum_{i=1}^{n} \left(y_i - \overline{y}\right)^2 \qquad \text{(eq. 3)}$$

with

$$\overline{y} = \frac{\sum_{i=1}^{n} y_i}{n}$$

Monomodal analysis

To ensure the validity of the measurement given by Malvern, 2 other approaches are applied, different from the classical NNLS treatment. After extraction of the autocorrelation functions for each size, these later are fitted with the classical monomodal model:

$$G(\tau) = A + B\, e^{-2\, q^2 D\, \tau} \qquad \text{(eq. 4)}$$

with q the wave vector and D the diffusion coefficient, in relation with R_H with the Stokes-Einstein equation (eq. 6).

$$q = \frac{4\,\pi\, n}{\lambda} \sin\left(\frac{\theta}{2}\right) \qquad \text{(eq. 5)} \qquad\qquad D = \frac{k\, T}{6\,\pi\,\eta\, R_H} \qquad \text{(eq. 6)}$$

n is the refractive index of the medium, λ is the laser wave length, θ is the scattering angle, k is the Boltzmann constant, T is the temperature and η is the medium viscosity.

Secondly, a Cumulant approach is applied and the exponential fitting expression is expanded to account for polydispersity or peak broadening effects:

$$G(\tau) = A + B\, e^{\left(-2\, q^2 D\, \tau + \mu\, \tau^2\right)} \qquad \text{(eq. 7)}$$

with q^2 D and μ the first and second cumulant or moment.

$$PdI = \frac{2\,\mu}{(q^2\, D)^2} \qquad \text{(eq. 8)} \qquad\qquad \sigma = \sqrt{PdI\; R_H} \qquad \text{(eq. 9)}$$

with PdI the polydispersity index and σ the standard deviation of the Gaussian distribution assuming a single size distribution.

NB: the values are commonly reported as hydrodynamic diameter D_H rather than as hydrodynamic radius R_H.

		LNC 25nm	LNC 50nm	LNC 100nm
Monomodal method	D_H (nm)	26.7	53.4	101.9
	R^{2a}	0.99997	0.99997	0.9931
Cumulant approach	D_H (nm)	26.7	53.4	101.9
	PdI	0.103	0.009	0.021
	Calculated σ (nm)[b]	8.5	5.0	14.9
	R^{2a}	0.99992	0.99996	0.99997
NNLS algorithm	D_H (nm)	28.7	54.4	100.6
	σ (nm)	7.6	7.8	19.3
	Calculated PdI[b]	0.071	0.021	0.037

a – Cf statistical part
b – Calculated form eq. 6.

Table S1: Hydrodynamic diameter D_H of LNC calculated with the 3 approaches: (i) monomodal method, (ii) Cumulant approach and (iii) NNLS algorithm, after autocorrelation curve fits.

LNC dialysis and simulation of the impact of a loss of Solutol onto the hydrodynamic size distribution

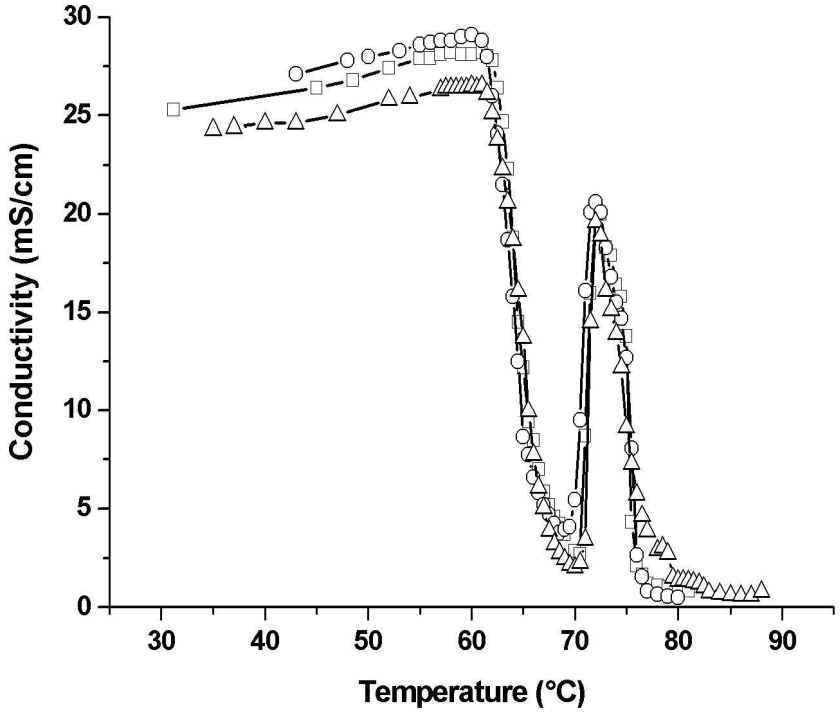

Figure S2: Conductivity *vs.* temperature for 25 nm LNCs: 1st(□), 2nd(△) and 3rd measurement (○). .

For 3 formulations (25, 50 and 100nm-diameter LNCs), the phase inversion zone has been followed by conductivity during the third cooling after 3 thermal cycles. Then, a 4th temperature cycle was performed and the cooling-dilution process was realized as previously described. Dialysis was performed on each sample during one week against pure water (obtained through a milli-Q apparatus, Millipore, France), changing water 2 times a day. Spectra/Por® Biotech Cellulose Ester Dialysis Membrane (Mw=100000Da) was used. After the end of dialysis, formulation volume was adjusted to obtain exactly the same volume that the initial formulation by mild evaporation (T < 35°C) as well as the same amount of NaCl. A new time, temperature cycles were performed by following the conductivity variations. Size measurements were performed at various steps: (i) at the beginning before dialysis, (ii) after dialysis and (iii) after the 2nd inversion phase cycle upon the nanoparticle suspension previously formulated as shown in Figure S3.

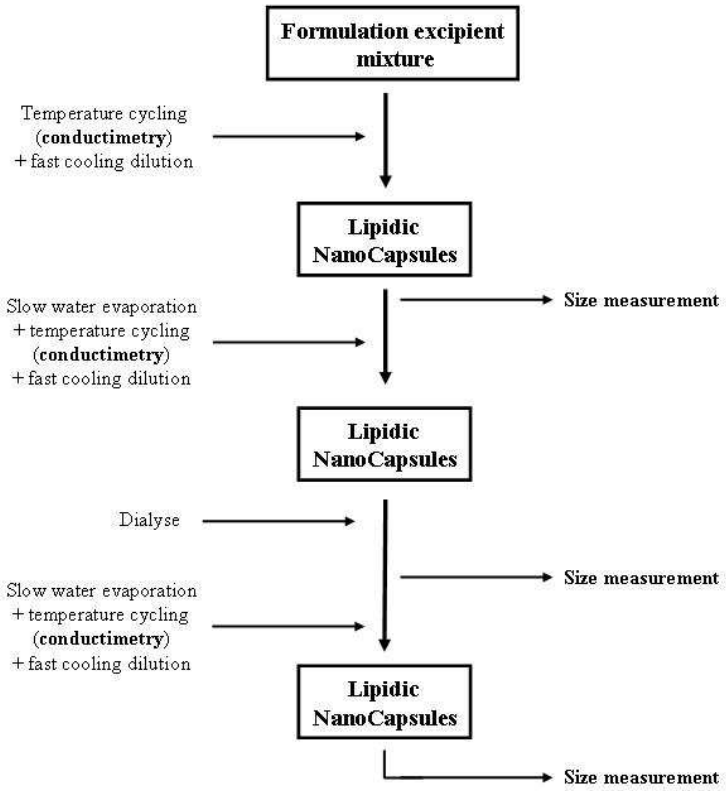

Figure S3: Schematic description of the dialysis experiments.

	Diameter ± standard deviation (nm)		
	LNC 20 nm	LNC 50 nm	LNC 100 nm
LNC before dialysis	24.1 ± 5.6	50.0 ± 10.3	91.2 ± 19.7
LNC after dialysis	23.6 ± 5.8	49.9 ± 13.6	93.1 ± 20.8
LNC after 3nd inversion cycle	24.1 ± 5.3	50.8 ± 12.0	90.7 ± 19.7

Table S2: LNC diameter before dialysis, after dialysis and after the 2nd inversion cycle.

No size variation was observed before and after dialysis, and after the new phase inversion process. After dialysis and water evaporation, inversion phase with temperature was always present and the position of the inversion phase temperature is similar (Figure S1). Dialysis simulations were performed. New formulations were prepared, decreasing the amount of Solutol-HS15 After formulation process, LNC sizes were measured and the size variation *vs.* the Solutol HS-15 simulated loss was reported in Figure S4.

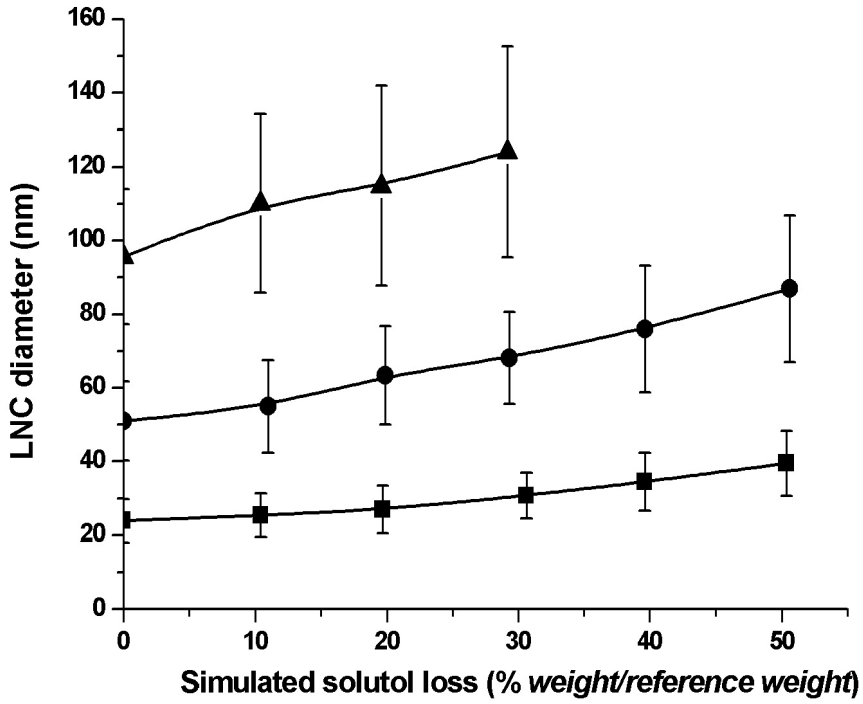

Figure S4: LNC hydrodynamic diameter *vs*. simulated Solutol loss for 25nm (■), 50nm (●) and 100nm (▲) - diameter LNCs. Error bars corresponded to standard deviation of the normal law used by NNLS treatment.

With a loss of Solutol HS-15, followed by phase inversions, LNC diameter increases whatever the formulation (PdI < 0.06 whatever the formulation). After dialysis and phase inversion, the LNC sizes kept constant. All surfactant molecules participate to the LNC formation and there was no free micelle for example in concurrence with LNC after a formulation process. More, it seems that the assembly was strong enough to resist to the dialysis.

Small angle neutron scatering measurments

Small-angle neutron scattering experiments were performed on the PACE spectrometer at LBB, Saclay. The wavelength of neutron beam l was 0.6nm with a spread $\Delta\lambda l/\lambda$ of 10% fwhm. Data were collected at BF_3 position sensitive multidetector made of 30 concentric rings of 1cm width. First ring radius : 3cm ; last ring radius : 32cm at distances of 3 and 4,7m from the sample, covering a range of the scattering vector q from 0.03 to 0.5Å. The samples were contained in standard 2-mm path length quartz cells. Data reduction was done with the LLB standard software package. Corrections were made for instrumental background, electronic noise, transmission, and empty cell. Incoherent background was determined with several H/D mixtures and interpolated for the desired concentrations. Normalization to absolute values of the scattered intensity (in cm^{-1}) was performed by measurements of the secondary calibration standard water (H_2O). All theoretical curves are convoluted with the resolution function for each sample-to-detector distance. This includes the angular resolution due to the finite collimation, the detector cells, and the wavelength spread of the mechanical velocity selector.

Samples were prepared as described previously replacing pure water by D_2O to increase contrast between LNCs and solvent.

Small angle neutron scattering models

The scattering curve I(q) vs. q was fitted

$$I(q) = K\ P(q)\ S(q) \qquad \text{(eq. 10)}$$

with P(q) and S(q) the form and structure factor. The prefactor K is a constant depending on (i) the number density of particles, (ii) the difference in scattering length density between LNC and solvent and (iii) the LNC volume.

Hard sphere potential was used for S(q) described by the following equations :

$$S(q) = \frac{1}{1 + \dfrac{24\,\eta\,G(2qR)}{2qR}} \qquad \text{(eq. 11)}$$

$$G(x) = \alpha\left(\sin(x) \_\, x\cos(x)\right)/x^2 + \beta\left(2x\sin(x) + (2-x^2)\cos(x) - 2\right)/x^3 + \gamma\left(-x^4\cos(x) + 4\left(\left(3x^2-6\right)\cos(x) + \left(x^3-6x\right)\sin(x) + 6\right)\right)/x^5$$

with

$$\alpha = \frac{(1+2\eta)^2}{(1-\eta)^4} \qquad \beta = \frac{-6\eta\,(1+\eta/2)^2}{(1-\eta)^4} \qquad \gamma = \frac{\eta\,\alpha}{2}$$

Two models were used for P(q). For spherical scattering objects, $P(q) = (F(q))^2$ where $F(q)$ is the amplitude of the form factor. The first model corresponded to a homogeneous sphere

$$F_{HS}(q) = 3\left(\frac{\sin qR - qR\cos qR}{(qR)^3}\right)^2 \qquad \text{(eq. 12)}$$

with R the radius of the homogeneous sphere.

The second model corresponds to spherical concentric shells simplified to a core-shell model:

$$F_{CS}(q) = \frac{1}{M_3}\left(\rho_1 V(R_1) F_{HS}(q,R_1) + (\rho_2 - \rho_1) V(R_2) F_{HS}(q,R_2)\right) \qquad \text{(eq. 13)}$$

$$M_3 = \rho_1 V(R_1) + V(R_2)(\rho_2 - \rho_1)$$

with R_1 and R_2 the internal and external radius. R_1 is the core radius with $V(R_1)$ the core volume and R_2 is the total LNC radius (core + shell) with $V(R_2)$ the LNC volume. ρ_1 and ρ_2 were the scattering length densities of the core and the shell respectively. For the parameter optimization, it was considered in 1st approximation that the core was composed of Labrafac and the shell was composed by Lipoid and Solutol.

In addition to the form factor, a normal law was added on $P(q)$.

$$P_{NL\,CS\,or\,HS}(q) = \int_{r=R-k}^{r=R+k} \frac{1}{\sigma\sqrt{2\pi}} e^{-0.5\left(\frac{k}{\sigma}\right)^2} P_{CS\,or\,HS}(q,r)\,dr \qquad \text{(eq. 14)}$$

with σ the standard deviation of the normal law and R the external LNC radius. Considering the probability density of the normal law $f(x)$, k was defined by the limit $f(r) / f(R) < 0.01$.

Fit of the experimental data

A Fortran program, based on a least square fitting and a traditional optimization method of simulated annealing, was used to fit the parameters. For autocorrelation function, R_H and *PdI* have been optimized for the various treatment models (classical method and cumulant approach, eq. 1 and 4 respectively). For the SANS curves, R_1 the radius of the homogeneous sphere form factor model (eq. 12), R_1 and R_2 the internal and external radius respectively of the core–shell form factor model (eq. 13), and σ the standard deviation of the normal law distribution applied to the form factor model (eq. 14) have been optimized.

Calculated physical parameters for LNCs

On the basis of SANS experiments, LNCs are spherical nanoparticles with a core-shell structure. R_1 and R_2 are the radius of the core and the whole LNCs respectively. $V_{Labrafac}$ is the volume of triglycerides used for each formulation. $V_{Labrafac+Solutol+Lipoïd}$ is the sum of the volume for the three component of LNCs and corresponds to the total volume of LNCs. N_{LNCs} is the number of LNCs in each formulation. R_2-R_1 is the thickness of the shell. Calculated parameters are listed in Table for each formulation.

$$V_{Labrafac} = N_{LNCs} * \frac{4}{3}\pi R_1^{\,3} \qquad \text{(eq. 15)}$$

$$V_{Labrafac+Solutol+Lipoïd} = N_{LNCs} * \frac{4}{3}\pi R_2^{\,3} \qquad \text{(eq. 16)}$$

	LNCs 20nm	LNCs 50nm	LNCs 50nm
R_2 (nm)	12.5	25	50
$V_{Labrafac}$	0.454	1.105	1.3
$V_{Labrafac+Solutol+Lipoïd}$	1.153	1.755	1.703
R_1 (nm)	9.2	21.4	45.7
R_2-R_1=thickness	3.3	3.6	4.3
N_{LNCs}	$1.41006*10^{23}$	$2.6819*10^{22}$	$3.2543*10^{21}$
$N_{Solutol}$ per LNC	3993	18254	86065
NLipoïd per LNC	126	1330	10962
$N_{Solutol}/N_{Lipoïd}$	31	13	7
$N_{Labrafac}$ per LNC	850	10860	105268
Molecular area Solutol (nm^2)	0,250	0.284	0.250

Transmission electronic microscopy

TEM analysis was performed using a Jeol 100CX instrument (JEOL-France, Paris, France). Before analysis, the nanoparticle suspensions were stained by a 2% phosphotungstic acid aqueous solution and were sprayed onto copper grids overlayed with 1% formwar in chloroform (Mikross, Paris, France).

LNC stability

25, 50 and 100nm-diameter LNCs were incubated at T=4, 25, 37 and 50°C, directly after formulation. LNC size was measured and the relative increase of LNC hydrodynamic diameter (RIHD) was evaluated as:

$$RIHD = \frac{D_{H\,t} - D_{H\,t_0}}{D_{H\,t}} \qquad \text{(eq. 17)}$$

.

with $D_{H\,t0}$ and $D_{H\,t}$ the hydrodynamic radius at t_0 (initial diameter) and t respectively.

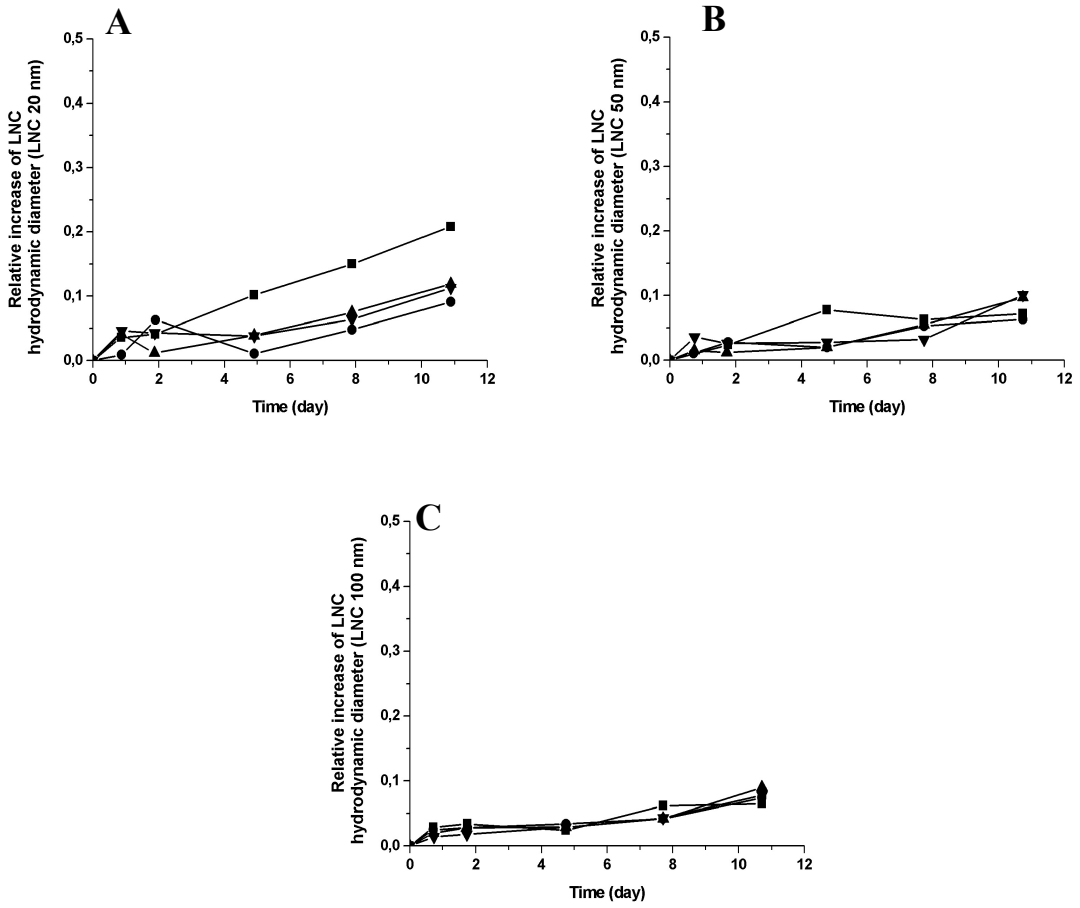

Figure S5. Relative increase of LNC hydrodynamic diameter *vs.* time for (A) 20, (B) 50 and (C) 100 nm-diameter LNC at (▼) 4, (▲) 25, (●) 37 and (■) 50°C.

As observed whatever the LNC size, the relative increase of the LNC diameter was always lower 0.1 after about a 10 days incubation, except for 20nm-diameter LNCs incubated at 50°C. This relative increase is very low, corresponding to an increase of 2.5, 5 and 10nm for 25, 50 and 100nm-diameter LNCs respectively. More, no temperature dependence was observed.

Chapitre III

Modifications post-formulation des LNCs

I) Etude du procédé de post-insertion

Post-insertion onto LipidicNanoCapsules (LNCs) : from experimental aspects to mechanisms.

Thomas Perrier*, Jean-Pierre Benoît and Patrick Saulnier

Inserm U646, Ingénierie de la vectorisation particulaire, Université d'Angers, 49100 Angers, France

*To whom correspondence should be addressed. E-mail address : thomas.perrier@etud.univ-angers.fr

Abstract

LipidicNanoCapsules (LNCs) were prepared using a phase inversion methodolgy. After the formulation, insertion of commercially available disteraoylphosphatidylethanolamine-peg amphiphile was performed using the known technique called post-insertion, initially developped on liposomes. First the impact of this method on the size and zeta potential distribution was monitored and shows clearly the insertion of amphiphile. Subsequently, the length of the hydrophilic part was investigated and was regarded versus hydrophilic-lipophilic balance of these amphiphiles. It establishes a correlation of size and zeta potential with the HLB of these surfactants. Finaly, after

comparison with other surfactants of same HLB, possible post-insertion mechanisms are discussed.

Introduction

In the field of nanomedecines (drug delivery systems formulated at the nanometric scale), nanoparticles should have a defined surface which is the support of many expected properties such as targeting[204,205,206,207] but also preventing the recognition and the capture by the immune system[208]. Among the available surfactants, a particular class has emerged, that is to say surfactants with variable amount of polyethylene glycol called PEG. Nevertheless, the introduction of such surfactants into established formulation processes forces the scientist to play with numerous formulation parameters to reach the desired structure, size range and polydispersity[209,210]. By the way, post-formulation strategies have emerged to use nanoparticles as a platform for modification. Organic chemistry has produced several strategies from classical coupling reaction, such as creation of amide[211] and ester[212] bonds, to

[204] Gupta, A.K., Gupta, M.
Synthesis and surface engineering of iron oxide nanoparticles for biomedical applications
(2005) Biomaterials, 26 (18), pp. 3995-4021.
[205] Pellegrino, T., Kudera, S., Liedl, T., Javier, A.M., Manna, L., Parak, W.J.
On the development of colloidal nanoparticles towards multifunctional structures and their possible use for biological applications
(2005) Small, 1 (1), pp. 48-63.
[206] Nasongkla, N., Bey, E., Ren, J., Ai, H., Khemtong, C., Guthi, J.S., Chin, S.-F., Sherry, A.D., Boothman, D.A., Gao, J.
Multifunctional polymeric micelles as cancer-targeted, MRI-ultrasensitive drug delivery systems
(2006) Nano Letters, 6 (11), pp. 2427-2430.
[207] Byrne, J.D., Betancourt, T., Brannon-Peppas, L.
Active targeting schemes for nanoparticle systems in cancer therapeutics
(2008) Advanced Drug Delivery Reviews, 60 (15), pp. 1615-1626.
[208] Fang, C., Bhattarai, N., Sun, C., Zhang, M.
Functionalized nanoparticles with long-term stability in biological media
(2009) Small, 5 (14), pp. 1637-1641.
[209] Heurtault, B., Saulnier, P., Pech, B., Venier-Julienne, M.-C., Proust, J.-E., Phan-Tan-Luu, R., Benoît, J.-P.
The influence of lipid nanocapsule composition on their size distribution
(2003) European Journal of Pharmaceutical Sciences, 18 (1), pp. 55-61.
[210] Anton, N., Saulnier, P., Béduneau, A., Benoit, J.-P.
Salting-out effect induced by temperature cycling on a water/nonionic surfactant/oil system
(2007) Journal of Physical Chemistry B, 111 (14), pp. 3651-3657.
[211] Acharya, S., Dilnawaz, F., Sahoo, S.K.
Targeted epidermal growth factor receptor nanoparticle bioconjugates for breast cancer therapy
(2009) Biomaterials, 30 (29), pp. 5737-5750.

more recent techniques based on metathesis[213,214] or cycloadditions like Diels-Alder reaction[215,216]. But in most cases, these processes require the use of organic solvent and/or the assistance or organometallics coumpounds, which necessit to be removed from the sample afterwards. New methodologies like copper catalyzed azide-alkyne coupling reaction, known as CuAAC[217,218], have established water as the reference solvent for the modification of nanoparticles. To date, efforts have been made to developpe re-usable and recoverable catalysts[219]. In a similar way, physicals methods have been applied. Among these strategies, post-insertion has been widely use to modify the surface of liposomes[220,221,222]. It consists in the incubation of liposomes with a micellar suspension of the employed surfactant. The result is an incorporation of such surfactant into the liposome lipidic bilayer. To date, no systematic studies have been published towards the nature of the surfactants that is to say, the required length of hydrophobic and hydrophilic part respectively, and if one or more aliphatic chains

[212] Ljubimova, J.Y., Fujita, M., Ljubimov, A.V., Torchilin, V.P., Black, K.L., Holler, E.
Poly(malic acid) nanoconjugates containing various antibodies and oligonucleotides for multitargeting drug delivery
(2008) Nanomedicine, 3 (2), pp. 247-265.
[213] Koenig, S., Chechik, V.
Shell cross-linked Au nanoparicles
(2006) Langmuir, 22 (11), pp. 5168-5173.
[214] Airaud, C., Ibarboure, E., Gaillard, C., Héroguez, V.
Nanostructured polymer composite nanoparticles synthesized in a single step via simultaneous ROMP and ATRP under microemulsion conditions
(2009) Journal of Polymer Science, Part A: Polymer Chemistry, 47 (16), pp. 4014-4027.
[215] Zhu, J., Kell, A.J., Workentin, M.S.
A retro-Diels-Alder reaction to uncover maleimide-modified surfaces on monolayer-protected nanoparticles for reversible covalent assembly
(2006) Organic Letters, 8 (22), pp. 4993-4996.
[216] Shi, M., Ho, K., Keating, A., Shoichet, M.S.
Doxorubicin-conjugated immuno-nanoparticles for intracellular anticancer drug delivery
(2009) Advanced Functional Materials, 19 (11), pp. 1689-1696.
[217] Hein, C.D., Liu, X.-M., Wang, D.
Click chemistry, a powerful tool for pharmaceutical sciences
(2008) Pharmaceutical Research, 25 (10), pp. 2216-2230.
[218] Lutz, J.-F., Zarafshani, Z.
Efficient construction of therapeutics, bioconjugates, biomaterials and bioactive surfaces using azide-alkyne "click" chemistry
(2008) Advanced Drug Delivery Reviews, 60 (9), pp. 958-970.
[219] Sirion, U., Yu, J.B., Byoung, S.L., Dae, Y.C.
Ionic polymer supported copper(I): A reusable catalyst for Huisgen's 1,3-dipolar cycloaddition
(2008) Synlett, (15), pp. 2326-2330.
[220] Iden, D.L., Allen, T.M.
In vitro and in vivo comparison of immunoliposomes made by conventional coupling techniques with those made by a new post-insertion approach
(2001) Biochimica et Biophysica Acta - Biomembranes, 1513 (2), pp. 207-216.
[221] Allen, T.M., Sapra, P., Moase, E.
Use of the post-insertion method for the formation of ligand-coupled liposomes.
(2002) Cellular & molecular biology letters, 7 (2), pp. 217-219.
[222] Moreira, J.N., Ishida, T., Gaspar, R., Allen, T.M.
Use of the post-insertion technique to insert peptide ligands into pre-formed stealth liposomes with retention of binding activity and cytotoxicity
(2002) Pharmaceutical Research, 19 (3), pp. 265-269.

are necessary. As PEG has a great interest in pharmaceutical applications[223,224], like increasing colloïdal stability and enhancing blood ciruclation time[225]by decreasing macrophage up-take and complement activation[226], we chose to use amphiphilic phospholipids-PEG to test the post-insertion process on LNCs. According to Table III.1, these surfactants have molecular weigths comprised between 1000 to almost 6000g/mol. Associated HLB values range from 5.44 (hydrophobic) to 17.14 (hydrophilic). Furthermore, we have verified that the use of these phospholipids-PEG surfactants during the formulation step modifies dramatically the feasability window in which the LNCs are produced. Here, we propose to study the feasability of post-insertion on LNCs and to analyze the effect of the length of hydrophilic part on this phenomena, as described in Figure 1. We also discuss the impact of post-insertion on the structure of the external part of LNCs using soft particles analysis[227,228,229], an electrokinetic method used to quantify the electrical charge density in the ionic accessible layer inside the nanoparticle shell.

Experimental section

Materials

Labrafac® WL 1349 (Gattefossé S.A., Saint-Priest, France) is a mixture of capric and caprylic acid triglycerides. NaCl was purchased from Prolabo (Fontenay-sous-Bois, France) and water

[223] Kim, J.-Y., Kim, J.-K., Park, J.-S., Byun, Y., Kim, C.-K.
The use of PEGylated liposomes to prolong circulation lifetimes of tissue plasminogen activator
(2009) Biomaterials, 30 (29), pp. 5751-5756.
[224] Zalipsky, S.
Synthesis of an end-group functionalized polyethylene glycol-lipid conjugate for preparation of polymer-grafted liposomes
(1993) Bioconjugate Chemistry, 4 (4), pp. 296-299.
[225] Vonarbourg, A., Passirani, C., Saulnier, P., Benoit, J.-P.
Parameters influencing the stealthiness of colloidal drug delivery systems
(2006) Biomaterials, 27 (24), pp. 4356-4373.
[226] Vonarbourg, A., Passirani, C., Saulnier, P., Simard, P., Leroux, J.C., Benoit, J.P.
Evaluation of pegylated lipid nanocapsules versus complement system activation and macrophage uptake
(2006) Journal of Biomedical Materials Research - Part A, 78 (3), pp. 620-628.
[227] Ohshima, H.
Electrophoresis of soft particles
(1995) Advances in Colloid and Interface Science, 62 (2-3), pp. 189-235.
[228] Ohshima, H.
Electrophoretic Mobility of Soft Particles
(1994) Journal of Colloid And Interface Science, 163 (2), pp. 474-483.
[229] Ohshima, H.
Electrokinetics of soft particles
(2007) Colloid and Polymer Science, 285 (13), pp. 1411-1421.

was obtained from a Milli-Q-plus® system (Millipore, Paris, France). Lipoïd® S75-3 (Lipoïd GmbH, Ludwigshafen, Germany) is a soybean lecithin made of 69% of phosphatidylcholine, 10% phosphatidylethanolamine and other phospholipids, and Solutol® HS 15 (BASF, Ludwigshafen, Germany) is a mixture of free polyethylene glycol 660 (PEG) and polyethylene glycol 660 hydroxystearate. Dialysis membrane was purchased from Spectrapore and has a molecular weight cut off equal to 100000 daltons.

1,2-Distearoyl-*sn*-Glycero-3-Phosphoethanolamine-*N*-[methoxy(Polyethylene-Glycol)] with peg length comprised between 350 and 5000g.mol^{-1}, corresponding to 7 to 113units of PEG, were furnished by Avanti® Polar Lipids Inc. (Alabaster, USA)

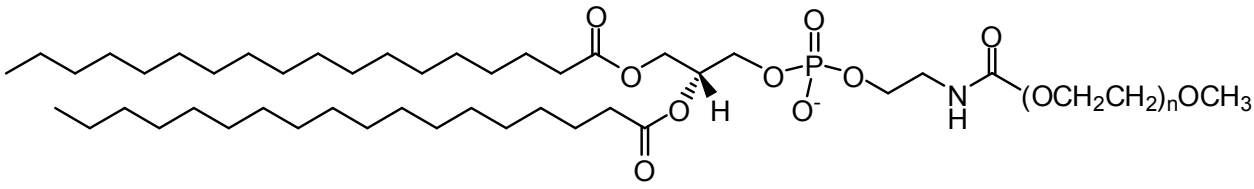

Figure III.1: Molecular structure of amphiphilic phospholipids used in this studies.

Hydrophilic Lipophilic Balance (HLB) was calculated according to Griffin's Formula[230,231,232]:

$$HLB = \frac{20 m_W}{M}$$

Where m_W is the molecular weight of PEG; M is the molecular weight of the whole molecule

[230] GRIFFIN, W.C. J. Soc. Cosmetic Chemists 1949, 1, 311
[231] GRIFFIN, W.C. J. Soc. Cosmetic Chemists 1954, 5, 4
[232] GRIFFIN, W.C. in Kirk-Othmer Encyclopedia of Chemical Technology, 3rd Edn.; Grayson, M. Ed.; J. Wiley & Sons: New York, 1979, Vol.8, pp.900-930 and pp. 620-628.

Surfactants	DSPE PEG 350	DSPE PEG 750	DSPE PEG 2000	DSPE PEG 3000	DSPE PEG 5000
MW of surfactants (g/mol)	1131	1527	2805	3774	5801
Nb of EO units	7	16	45	67	113
MW of PEG (g/mol)	308	704	1980	2948	4972
HLB	5,44	9,21	14,11	15,61	17,14

Table III.1: Physico-chemical parameters of the selected surfactants.

Preparation of Lipidic NanoCapsules (LNCs)

This formulation method was intensively described[233,234] and can be shortly presented as above. After weighting, all components were mixed under magnetic stirring at an agitation speed of 200rpm at room temperature leading to a O/W emulsion. After progressive heating at a rate of 4°C/min, a short interval of transparency at temperatures close to 70°C is observed, and the inverted phase (water droplets in oil) is obtained at 85°C. At least three temperature cycles alternating from 60 to 85°C at the same rate are applied near the phase inversion zone. Thereafter, the mixture underwent a fast cooling-dilution process: it was diluted 1:3.5 with 12.5ml cold water at 2°C and stirred for 30min, leading to the formation of LNC with the desired size. LNCs are liquid core nanocapsules made of medium chain triglycerides (Labrafac CC) surrounded by a surfactant shell assembled in a mix monolayer.

[233] Heurtault, B., Saulnier, P., Pech, B., Proust, J.E., Benoît, J.P.
Properties of polyethylene glycol 660 12-hydroxy stearate at a triglyceride/water interface
(2002) International Journal of Pharmaceutics, 242 (1-2), pp. 167-170.
[234] Heurtault, B., Saulnier, P., Pech, B., Proust, J.-E., Benoit, J.-P.
A novel phase inversion-based process for the preparation of lipid nanocarriers
(2002) Pharmaceutical Research, 19 (6), pp. 875-880.

Preparation of post-inserted LNCs

To reach a high density of PEG at the surface, 1.75ml LNC (10^{15} particles/ml) were incubated for 105min at 60°C with 1.3ml aqueous micellar solution (15mg/ml) of 1,2-Distearoyl-*sn*-Glycero-3-Phosphoethanolamine-*N*-[methoxy(Polyethylene-Glycol) (DSPE-PEG_{2000}-OCH_3) furnished by Avanti® Polar Lipids Inc. (Alabaster, USA). The suspension was vortexed every 15min and then quenched in an ice bath for 1min. The final DSPE-PEG concentration corresponded to 6mol % of total surface molecules. (Solutol HS-15 and Lipoïd S75-3).

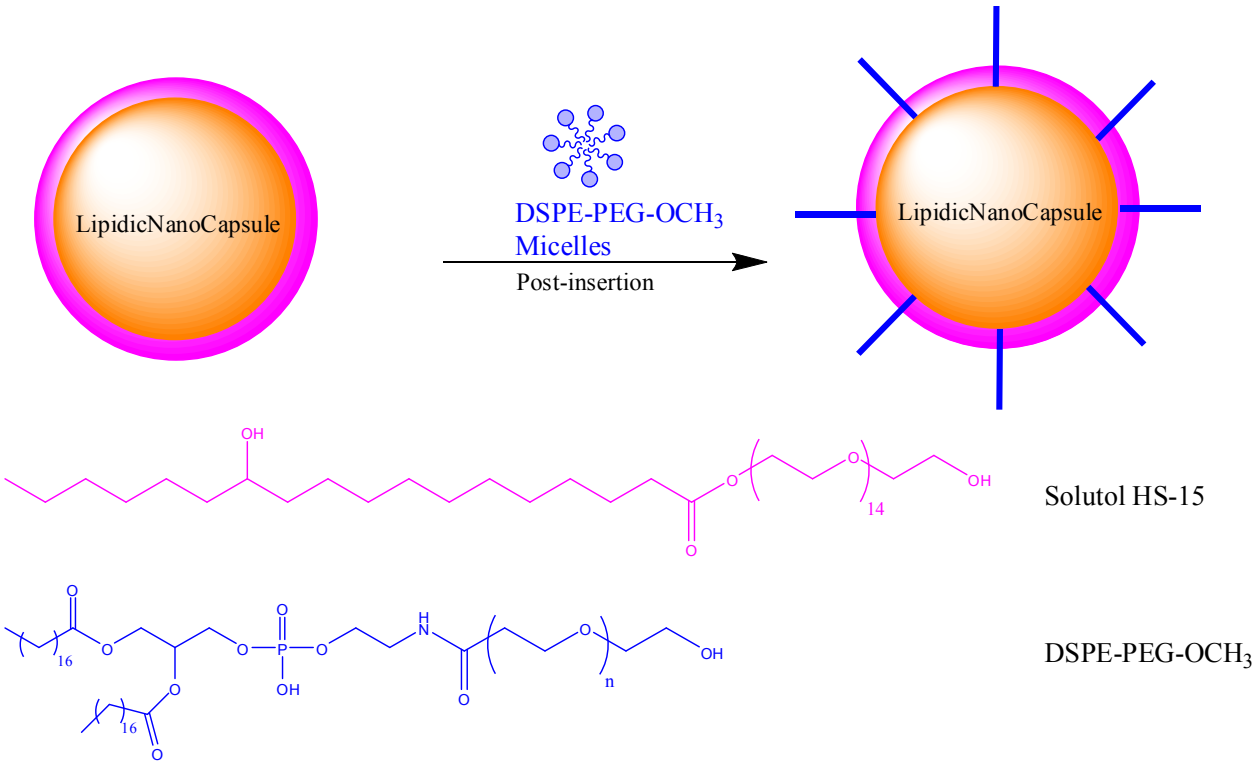

Figure III.2 : The post-insertion onto LipidicNanoCapsules (LNCs).

LNCs size and zeta potential distribution

All the particles are characterized in term of size and zeta potential using a NanoZS apparatus (Malvern Instruments) after dispersion of 50µl of the mother suspension in 3ml of appropriated aqueous medium. Each measurement (size and zeta potential) is made in

triplicate. All zeta potential values are comparable in relation with similar conductivity values.

Electrokinetic measurements-Soft particles analysis

To determine the electrokinetic behaviour of LNCs, we perform electrophoretic mobility measurements using a NanoZS instrument. 50µl samples (LNCs) are diluted into sodium chloride solution with [NaCl] up to 40mol/m^3. Measured values are the mean of five measurements. Experimental values were fitted to theorictical one according to the following equation (1) :

$$\mu = \frac{\varepsilon_r \varepsilon_0}{\eta} \frac{\frac{\psi_0}{\kappa_m} + \frac{1}{\lambda}\psi_{DON}}{\frac{1}{\kappa_m} + \frac{1}{\lambda}} + \frac{Rho_{fix}}{\eta}\left(\frac{1}{\lambda}\right)^2 (1)$$

Where ψ_0 is the potential for r=b and ψ_{DON} is the Donnan potential in the polyelectrolyte layer (see Figure) and are calculated according to equations (2) and (3) where A and κ_m are given by equations (5) and (6).

$$\psi_0 = \frac{kT}{e}\left\{\ln\left[A + \sqrt{1 + A^2}\right] + \frac{1 - \sqrt{1 + A^2}}{A}\right\} (2)$$

$$\psi_{DON} = \frac{kT}{e}\ln\left[A + \sqrt{1 + A^2}\right] (3)$$

$$A = \frac{N}{2n} (4)$$

$$\kappa_m = \kappa\sqrt[4]{1 + A^2} \ (5)$$

κ is Debye length and is calculated following equation (6) ; ε_0 is the electric permitivity of free space, ε_r is the electric permitivity of water, k is the Boltzmann's constant, T is the temperature, z_i is the charge number of ion species i, e is the elemental charge.

$$\kappa = \sqrt{\frac{\sum_{i=1}^{N} z_i^{\,2} e^2 n_i}{\varepsilon_0 \varepsilon_r kT}} \quad (6)$$

According to Figure III.3 : the particles have a hard core of radius a surrounded by a polylectrolyte layer, depicted here in blue. Rhofix is the ellectronic density inside the polyelectrolyte layer and 1/λ represents the accessibility to ions (Na^+, Cl^-) inside the polyelectrolyte layer[235,236,237,238].

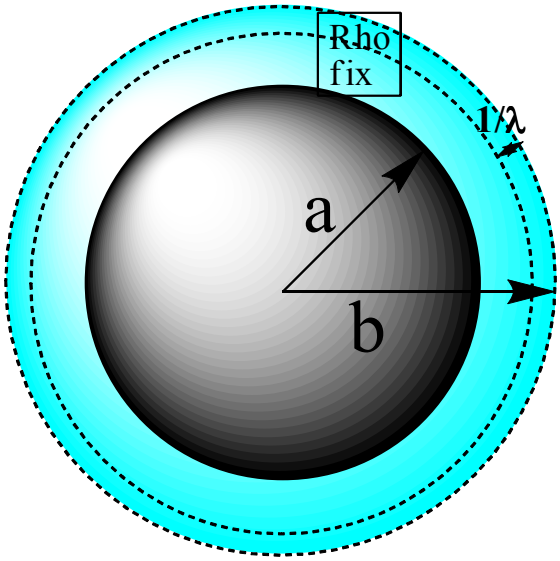

Figure III.3: Schematic illustration of a soft particle.

Results

Narrow size distribution are obtained (PDI<0.1) and, here, we formulate LNCs with a 54.6nm hydrodynamic diameter (H_D). As LNCs shell contains hydrophilic surfactant with PEG chains, solutol HS-15, LNCs display a zeta potential equal to –10mV identical to the

[235] Ohshima, H.
Electrophoresis of soft particles: Analytic approximations
(2006) Electrophoresis, 27 (3), pp. 526-533.
[236] Duval, J.F.L., Ohshima, H.
Electrophoresis of diffuse soft particles
(2006) Langmuir, 22 (8), pp. 3533-3546.
[237] Ohshima, H.
Electrokinetics of soft particles
(2007) Colloid and Polymer Science, 285 (13), pp. 1411-1421.
[238] Ohshima, H.
Electrostatic interaction between soft particles
(2008) Journal of Colloid and Interface Science, 328 (1), pp. 3-9.

previously obtained value and very close to the zeta potential (ZP) of other pegylated carrier (liposomes) or similar nanoparticles. First, post-insertion experiments were made by incubation of micellar suspension of DSPE-PEG_{2000}-OCH_3 with LNCs. The amount of DSPE-PEG_{2000}-OCH_3 is choosen in the range 0 or 10% (% in mol of Lipoïd S75-3 and Solutol HS-15) in order to analyse the effect on the LNCs size distribution and zeta potential. Figure III.4 presents the evolution of H_D and ZP versus the concentration of DSPE-PEG_{2000}-OCH_3.

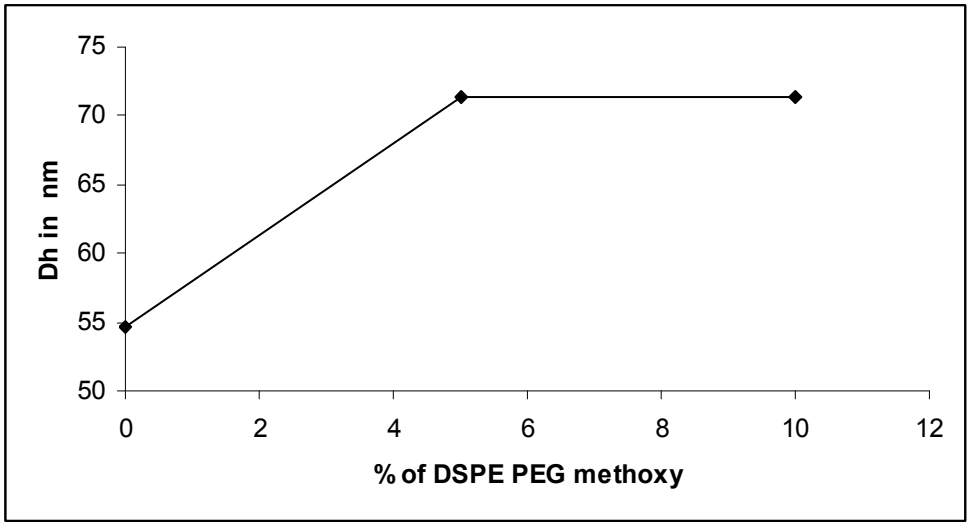

Figure III.4: Evolution of H_D versus the amount of DPSE-PEG_{2000}-OCH_3.

H_D is increased from 55nm to 70nm, corresponding to a 27% increase, if percentage of DSPE-PEG_{2000}-OCH_3 is equal to 5%. If [DSPE-PEG_{2000}-OCH_3] is superior to 5%, H_D does not grow and 70nm seems to appear as a limit of hydrodynamic size. In all cases, the theoritical NNLS theory fit well the experimental. ZP, based on experiments carried out in similar conditions, clearly decreased with the amount of DSPE-PEG_{2000}-OCH_3 in a linear way.

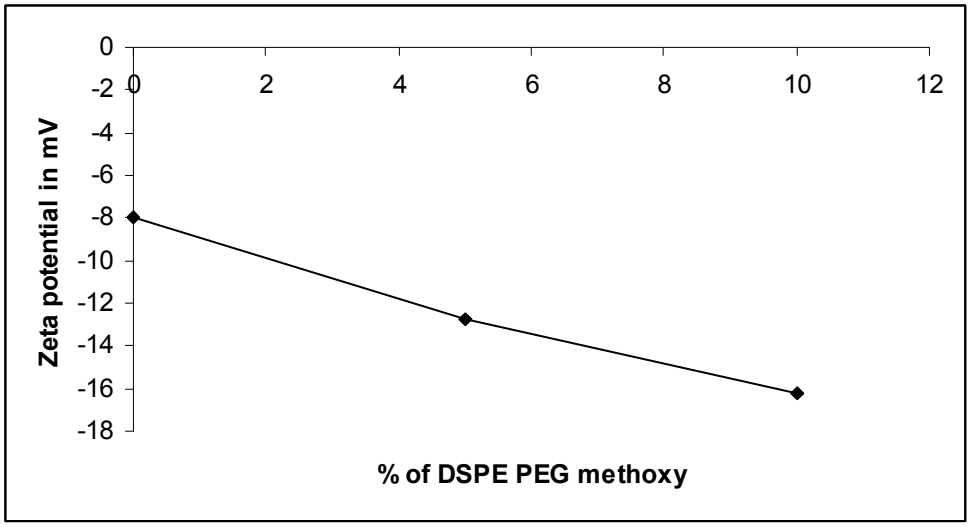

Figure III.5: Variation of ZP with the amount of DSPE-PEG_{2000}-OCH_3.

Control experiments are carried out by treatment of LNCs, in the same conditions of salinity and temperature, but without addition of DSPE-PEG_{2000}-OCH_3 and show minor modification of H_D and ZP (results not shown). So, LNCs are stable under experimentals conditions of post-insertion and variation of H_D and ZP during post-insertion is the fact of DSPE-PEG_{2000}-OCH_3 molecules.

Time of incubation superior to 100 minutes and temperature around 60°C have been found to be necessary in order to notice modifications through dynamic light scattering and zeta potential measurments. Relation between temperature and post-insertion duration is shown in Table III.2.

Post-Insertion temperature	Time to reach completion
25°C	No post-insertion
37°C	240 min
45°C	180 min
60°C	90 min

Table III.2: Relation between temperature and post-insertion duration.

The next experiments are carried out with a constant molar amount of DSPE-PEG$_X$-OCH$_3$ with a variation of the length of PEG moiety, between 500 to 5000Da. Figures III.6 and III.7 show the evolution of H_D and ZP for LNCs post-inserted in these conditions.

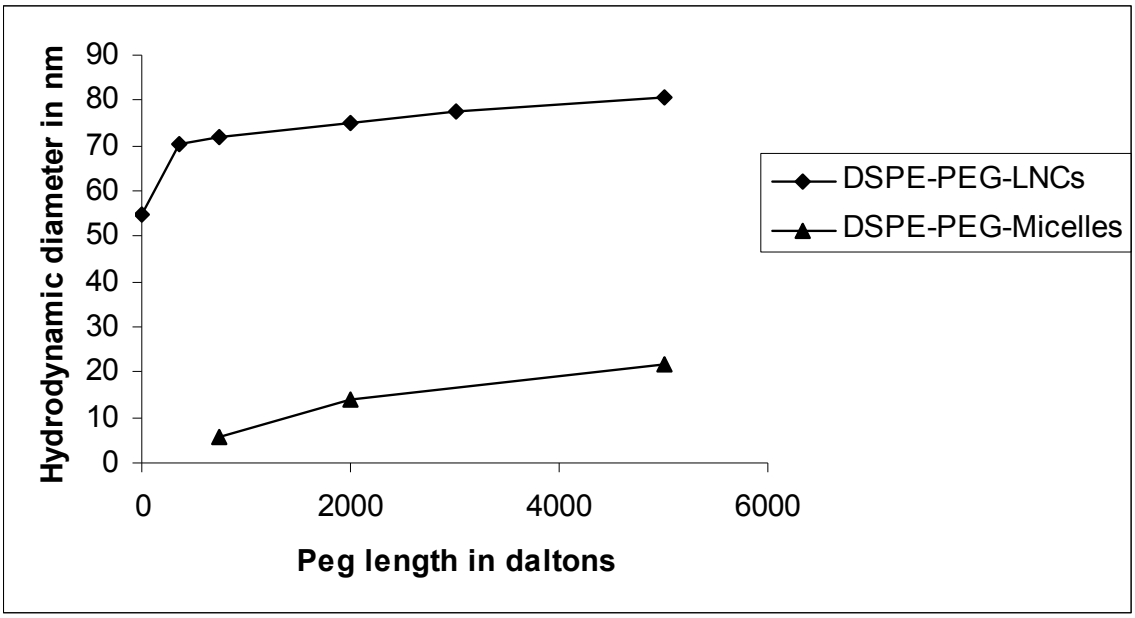

Figure III.6: Variation of H_D for post-inserted LNCs and DSPE-PEG micelles.

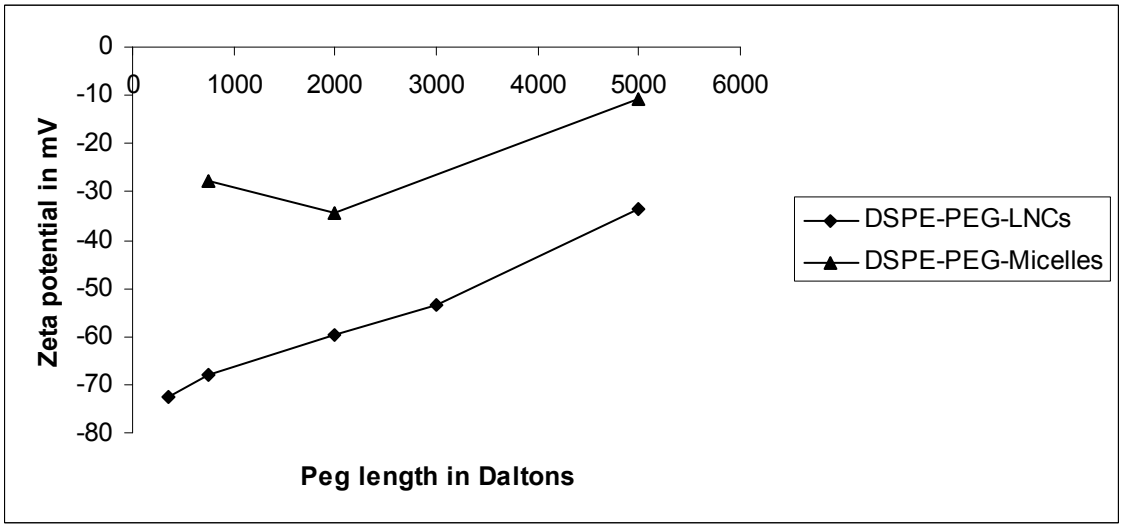

Figure III.7: Variation of ZP for post-inserted LNCs and DSPE-PEG micelles.

H_D increases linearly with the length of PEG chains in a range 350 to 5000Da. This progression is closed to the one observed for DSPE-PEG-micelles, reported previously in the literature. Concerning variation of ZP, negative ZPs (–72mV) are obtained for the shortest PEG chains. Absolute values of ZP decrease linearly with PEG lengths and ZP is equal to –33mV for DSPE-PEG_{5000}.

In order to determine the electrokinetic behaviour of LNCs as well as the values for both electronic density and accessibility to ions, we performed electrokinetic experiments for each post-inserted LNCs. Here, we present in Figure III.8 the variation of the electrophoretic mobility versus the concentration of sodium chloride [NaCl].

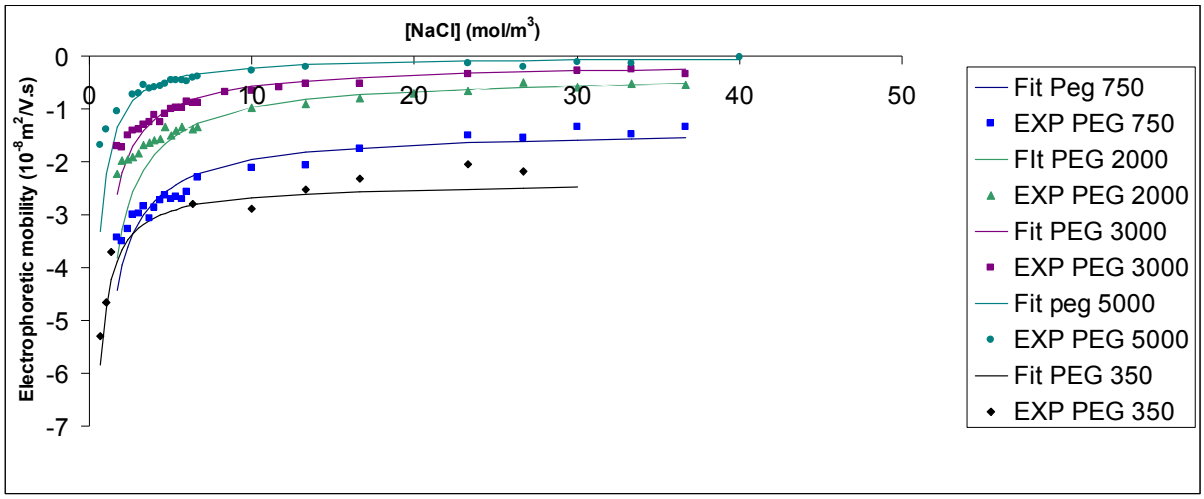

Figure III.8: Electrokinetic measurements for post-inserted LNCs.

Theoritical values were calculated using equation (1) which describes the electrophoretic mobility for a soft particle, according to the litterature. Electrophoretic mobilities have a hyperbolic variation versus [NaCl] in all cases and the experimental curves (points) follow the theoritical ones (continuous line). Measured electrophoretic mobilities are comprised between $–6.10^{-8}$ to almost $0m^2/V.s$. Figure show differences in the electrokinetic behaviour of LNCs as a function of PEG length. For example, electrophoretic mobility, for

high [NaCl], is closed to $3.10^{-8}m^2/V.s$ for PEG_{350} and is almost nil for PEG_{5000}. Subsequently, RhoFix and $1/\lambda$ were determined and variation of these two parameters are presented in Figures III.9 and III.10 as a function of PEG length.

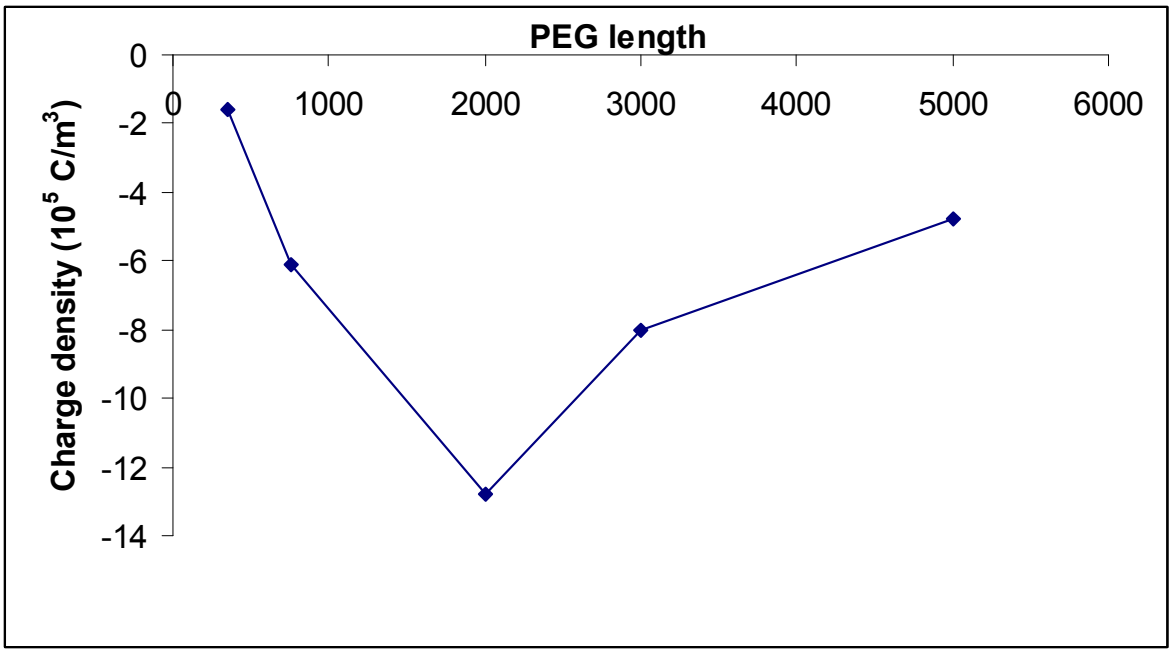

Figure III.9: Variation of charge density as a function peg length.

Rhofix varies from $-1.6.10^5 C/m^3$ for $DSPE\text{-}PEG_{350}$ to $-12.8 C/m^3$ for $DSPE\text{-}PEG_{2000}$. Rhofix for $DSPE\text{-}PEG_{5000}$ is closed to the one measured for $DSPE\text{-}PEG_{750}$. $1/\lambda$ decreases clearly with the PEG length with values comprised between 10.7nm for $DSPE\text{-}PEG_{350}$ to 0.1nm for $DSPE\text{-}PEG_{5000}$.

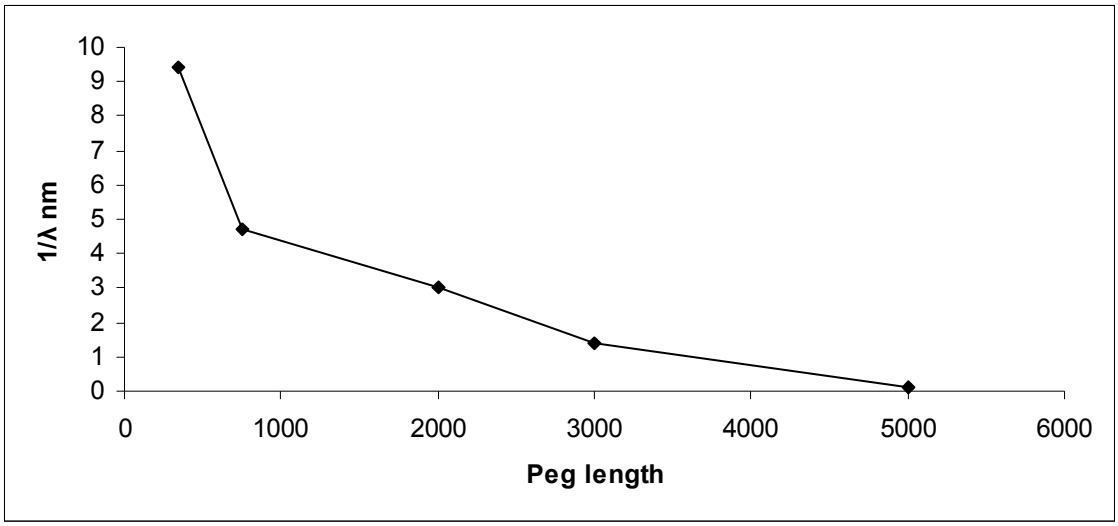

Figure III.10: Variation of the accessibility to ions 1/λ as a function of peg length.

Discussion

We have demonstrated that we can apply a post-insertion method for the modification of LNC outer parts. We have shown a gradual increase of HD for post-inserted molecules concentrations lower than 5%. Control experiments (without added micelles) show that this diameter growing is not due to Ostwald ripening or coalescence. HR3 (hydrodynamic radius) and 1/HR2 do not vary with time over periods superior to many weeks, even at temperature closed to 60°C. Nevertheless, HD is not modified by treatment of LNCs with amount of DSPE-PEG higher than 5%. In this case, ZP still decreases indicating that added molecules still incorporate the particle shell. For these concentrations, smooth dialysis is sufficient to remove these excess molecules indicating very weak inter-molecular interactions (results not shown).

We have indicated that the post-insertion method is temperature and time dependant, surely in relation with the interfacial fluidity of the host particle as well as the guest micelle. This interfacial fluidity surely controls the speed and the efficiency of the molecular transfer in a strong dynamic way.

The HD increase cannot be totally explained by an adsorption of DSPE-PEG_{2000}-OCH_3 micelles that should produce an HD increase in the order of two micelle diameters (around 30nm). For the same reasons, a hemi-micelle presence at the LNC surface is excluded and difficult to envisage in relation with the hydrophilic nature of the outer LNC part. Moreover, the LNC diameters are lower than the one predicted in the case of a single surfactant molecular adsorption. In other words, if we consider a length of 0.15nm for a C-C bound and 0.14nm for a C-O one, the length of the PEG moieties (in linear conformation) should produce post-inserted LNCs with higher diameter values (donner les tailles). These considerations involve that PEG chains strongly interact to produce interfacial associations closed to mushroom structures. Nevertheless, micelles and LNCs diameter variations are homothetic versus the surfactant head sizes. This indicates a similar self molecular association at the surface for both systems.

In another hand, measured ZP values are the result of several contributions: number of ethylene oxide units, statistic dipolar distribution leading to more or less pseudo apparent charges neutralized by the presence of counter ions in the Stern layers. To underline these facts, post-insertion with DSPE-PEG_{350}-OCH_3 produces LNCs with a -72mV ZP, much more negative than all the ones measured for surfactants with longer PEG chains where inter dipolar compensations prevail leading to lower pseudo apparent charges. One can also note that these LNC ZPs are much higher than all the values attributed to the corresponding micelles. This is in good agreement with a synergic association between the OH stearate of PEG dipoles and the added surfactant ones.

DSPE-PEG_{350}-OCH_3 molecules much smaller than the PEG_{660} OH-stearate ones, produce a higher number of active dipolar moments (no compensated) exposed at the particle surface. As the contrary, the DSPE-PEG_{5000}-OCH_3 surfactant (longer PEG chain) shows less negative ZP values. In this case, the active dipolar density exposed far from the particle

surface is lower and we can suppose important dipolar compensations in relation with the PEG chain length. If we take in consideration the ρfix values (not depending on the Stern layers properties), one can note that the post insertion of DSPE-PEG_{2000}-OCH_3 produces the higher negative apparent charge ($–13.10^5 C.m^{-3}$). This surfactant induces the higher synergic dipolar associations with minimum dipolar compensation. As the chain length increases, this phenomenon takes more and more importance. As a consequence the penetration depth of the added electrolytes in the hairy external LNC part decreases to values lower than 2 nm. Consequently the electronegative charge density is lower ($–8.10^5 C.m^{-3}$ for PEG_{3000} and $–6.10^5 C.m^{-3}$ for PEG_{5000}). It is noTable that PEG_{1000} and PEG_{350} surfactants exhibit the smaller negative charge density with a maximal penetration depth (1/λ).

Finally and for all the cases, micelle ZP values are always less negative than the ones found for LNCs. This confirms the synergic association of dipoles coming from the post-inserted surfactant and those coming from the PEG_{660}OH-stearate ones.

Furthermore, in order to precise the robstness of post-inserted LNCs, dialysis has been conducted on each batch. H_D is increased after dialysis due to changes in PEG chains hydratation, as dialysis was conducted versus salt free water. PEG chains are a little bit unpacked, involving a H_D increase. One particular case is for DSPE-PEG_{5000}-OCH_3, as H_D decreases after dialysis. Considering that this surfactant is very hydrophilic (HLB=17.14), post-inserted molecules can be removed for a part.

In addition, to evaluate if other surfactants could be used, we tried post-insertion with Solutol HS-15 micelles instead of DSPE-PEG_{2000}-OCH_3 ones. No modification of HD and ZP could be obtained even if Solutol HS-15 has a HLB value (HLB=13) closed to the one of DSPE-PEG_{2000}-OCH_3. This fact indicates that the hydrocarbon part needs to be composed by at least two aliphatic chains. We tried post-insertion with with cholesterol-PEG_{660} (datas not

shown). Here also, no variation of H_D and ZP were detected under the same experimental conditions. These additionnal experiments indicate that post-insertion is not possible with these surfactants, even if their molecular structure is closed to DSPE-PEG_{750}. Post-insertion parameters should be revised for surfactants bearing one single aliphatic chains or cholesterol as hydrophobic part.

Long PEG chains rigify the shell of LNCs as $1/\lambda$ is very small ; as $1/\lambda$ is also a resistance to the hydrodynamic flow.

Conclusion

Our work clarifies the conditions of DSPE-PEG_n-X post-insertion onto LNCs. It proposes a methodology for the setting up of feasability domains. From those experimental constrains arise several important points : as post-insertion is a temperature dependant process, variation of lipids fluidity on the surface of LNCs, changes in lipids solubility and conformation of PEG chains from Solutol HS-15 should be feavorable facts towards the transfer of DSPE-PEG molecule from micelles to LNCs. DSPE-PEG molecules have to be associated into micelles to promote a convenient post-insertion. The first experiments establish a base for the finding of optimal post-insertion conditions. It is obvious that the maximum amount of inserted DSPE-PEG has to be fixed. In our case, this value was found to be comprised between 5 and 10% of the amount of surfactants forming the shell. It is also necessary to highlight that post-insertion conditions can be adapted to specific constrains : in the case of thermosensible groups, post-insertion temperature can be diminished and a more important incubation time is required.

The second batch of experiments, with the variation of PEG length and the subsequent purification by dialysis, allows us to fix the limits for post-insertion in terms of the nature of transfered amphiphiles. Both short and long PEG chains surfactant can be used for post-

insertion. But, in the case of very hydrophilic molecules, post-insertion should be reversible and uncomplete. Furthermore, informations provided by zeta potential and electrokinetic measurements indicate that the conformation of the PEG chains is not the same for low HLB and high HLB amphiphiles. Accessibility to ions decrease with the PEG length and the PEG chains tend to be packed, the length of PEG should adapted for each applications.

Acknowledgment

We wish to thank European Union (Project NanoEar) and the Région Pays de la Loire for providing financial support for all this work. We are gratefull to Dr Guillaume Bastiat for helping us in the use of the fitting software and providing usefull advices.

II) Mise au point du procédé de transacylation sur LNCs

Transacylation onto LipidicNanoCapsules (LNCs). Application to the design of modified LNCs for siRNA delivery.

Thomas Perrier*, Jean-Pierre Benoît and Patrick Saulnier

Inserm U646, Ingénierie de la vectorisation particulaire, Université d'Angers, 49100 Angers, France

*To whom correspondence should be addressed. E-mail address : thomas.perrier@etud.univ-angers.fr

Abstract

In the field of drug delivery systems, nanoparticles are used to carry and deliver drugs to a specific target. To satisfy this goal, the drugs can be stored inside the particles or can be linked to their external part. The first strategy is based on formulation processes and the second one implies to synthesize drug conjugates or to develop processes for a convenient chemical coupling. Considering that LipidicNanoCapsules (LNCs) contain surfactants with ester groups, we chose to evaluate the feasibility of transacylation to modify their surfaces. Herein, we present the related results as well as the ability of LNCs to bind siRNA.

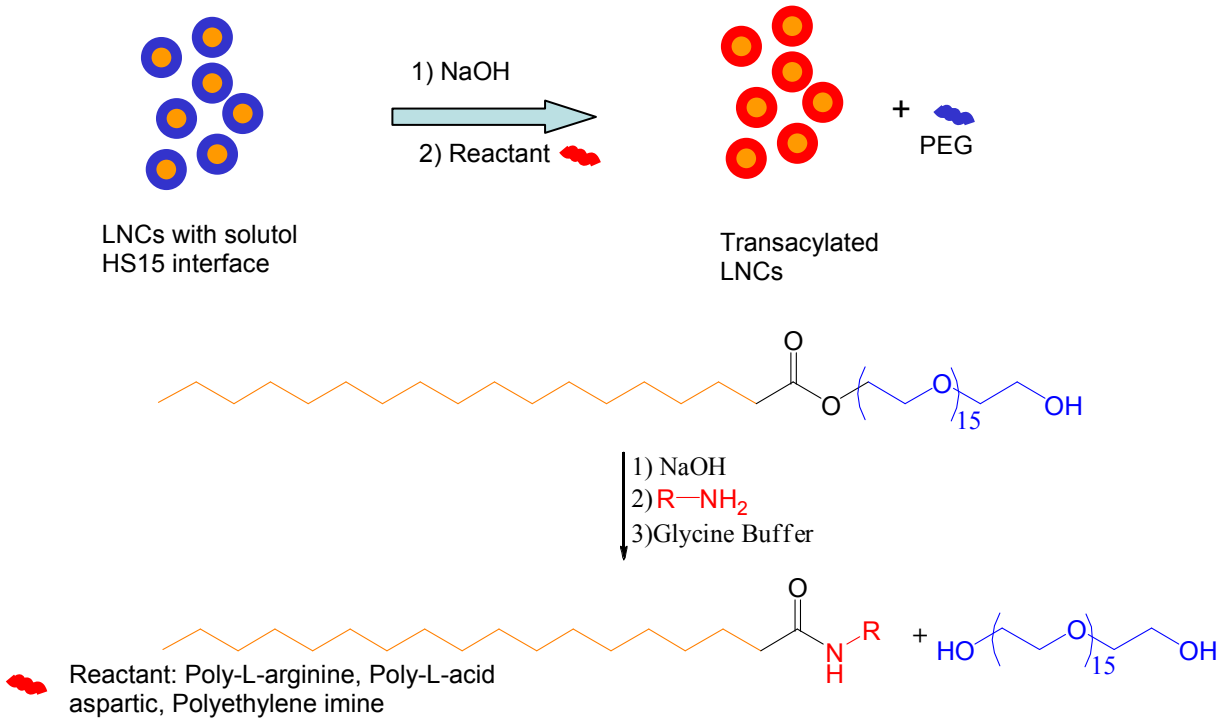

Figure III.11: Transacylation onto LipidicNanoCapsules (LNCs).

Introduction

Nowadays, multifunctional nanoparticles[239,240,241,242] can be prepared by a wide range of approaches leading to a broad range of nanoobjects such as liposomes, polymeric nanoparticles (nanospheres, Solid Lipid Nanoparticles SLNs), micelles, dendrimers and other vesicular like carriers (nanocapsules, polymersomes, niosomes, catanionique vesicles). By addition, manufacturing processes are limited by several constraints: (i) physical constrains such as solubility, miscibility and temperature (ii) formulation constrains such as feasibility

[239] Gindy, M.E., Prud'homme, R.K.
Multifunctional nanoparticles for imaging, delivery and targeting in cancer therapy
(2009) Expert Opinion on Drug Delivery, 6 (8), pp. 865-878.
[240] Kim, J., Piao, Y., Hyeon, T.
Multifunctional nanostructured materials for multimodal imaging, and simultaneous imaging and therapy
(2009) Chemical Society Reviews, 38 (2), pp. 372-390.
[241] Sajja, H.K., East, M.P., Mao, H., Wang, Y.A., Nie, S., Yang, L.
Development of multifunctional nanoparticles for targeted drug delivery and noninvasive imaging of therapeutic effect
(2009) Current Drug Discovery Technologies, 6 (1), pp. 43-51.
[242] Debbage, P.
Targeted drugs and nanomedicine: Present and future
(2009) Current Pharmaceutical Design, 15 (2), pp. 153-172.

domains, robustness towards the incorporation of amphiphilic molecules. All these constrain can dramatically affect the formulation. The manufacture of multifunctional nanoparticles is an intensively investigated field and is facing issues, very closed to the previously exposed constrains. By the way, the introduction of specific molecules at the interface (between nanoparticles and the surrounding medium) is likely to be performed in a post-formulation way. Few strategies are available, and we can cite the post-insertion or the chemical coupling reactions (carbodiimide chemistry, disulfide bonds, azide-alkyne click chemistry). Post-insertion has not been fully investigated for particles different from liposomes and lipidic nanocapsules. Coupling reactions need to use specific chemical groups that can be difficult to incorporate into the formulation processes. As LNCs contain a high percentage of hydrophilic surfactants bearing ester group (Solutol HS-15, PEG-ester of hyroxystearic acid), we have focused our research on the quest for a versatile reaction which could be done in aqueous medium and onto these esters. After screening the literature, it appears that transacylation reactions are unemployed towards their potentiabilities. Transacylation is the exchange of acyl groups between distinct molecules: starting from an ester, acyl groups can be transferred to another organic alcohol (transesterification) or to another substrate like organic amine, forming an amide. If acyl groups are blocked into a supramolecular assembly (micro or nanoparticles), transacylation leads to the modification of this supramolecular assembly. Furthermore, in spite of the fact that transacylation has been employed successfully on microparticles[243], little attention has been paid towards the use of this reaction on nanoparticles. In order to demonstrate the use of transacylation as a method to create LNCs able to bind and deliver hydrophilic drugs, we chose siRNA as a model drug. Indeed, it appears clearly that RNAs are playing a central role in the biology of living cells[244]. Since

[243] Coating alginate beads with cross-linked biopolymers: A novel method based on a transacylation reaction
(1996) Journal of Microencapsulation, 13 (2), pp. 169-183.
[244] Sharp, P.A.
The Centrality of RNA
(2009) Cell, 136 (4), pp. 577-580.

1999 and the discovery of post-transcritpionnal gene silencing in plants, small interfering RNA (small double stranded RNA) has been shown to be able to gene silencing into mammalian cultured cells[245,246]. The appealing interest of siRNA towards biomedical research and drug development[247,248] has accelerated the discovery of their mechanism of action. Nowadays, this mechanism is unambiguous and allows the scientific community to understand these phenomena at a molecular level. Thus, once siRNA are in the cytoplasm of cells they are loaded on the RNA Induced Silencing Complex (RISC) by the RLC with a concomitant removal of the sense strand. After what, the antisense strand guides the RISC to the complementary target RNA which is cleaved by the Ago2 protein. This latter has been analysed and shows a structure closed to RNAseH, a well known RNAse which is a useful tools for molecular biologists. By the way, due to their ability to modulate gene expression, and due to the fact that proteins are involved directly or undirectly in a wide range of pathologies, siRNAs have became a new class of potential therapeutical agents. However, as others therapeutics like anticancer drugs, synthetic siRNAs should cross many obstacles to reach the cytoplasm of the desired cells. That is the reason why, extensive interest has been focused on the development of nanocarriers able to deliver siRNA to the relevant cells.

To overcome these difficulties, several strategies have been set up. First, as siRNA should cross the plasmatic membrane, they have been conjugated to a wide range of lipophilic substances[249,250] such as cholesterol, bile acid and other lipids including saturated or

[245] Elbashir, S.M., Lendeckel, W., Tuschl, T.
RNA interference is mediated by 21- and 22-nucleotide RNAs
(2001) Genes and Development, 15 (2), pp. 188-200.
[246] Elbashir, S.M., Harborth, J., Lendeckel, W., Yalcin, A., Weber, K., Tuschl, T.
Duplexes of 21-nucleotide RNAs mediate RNA interference in cultured mammalian cells
(2001) Nature, 411 (6836), pp. 494-498.
[247] McManus, M.T., Sharp, P.A.
Gene silencing in mammals by small interfering RNAs
(2002) Nature Reviews Genetics, 3 (10), pp. 737-747.
[248] Hannon, G.J., Rossi, J.J.
Unlocking the potential of the human genome with RNA interference
(2004) Nature, 431 (7006), pp. 371-378.
[249] Jeong, J.H., Mok, H., Oh, Y.-K., Park, T.G.
SiRNA conjugate delivery systems
(2009) Bioconjugate Chemistry, 20 (1), pp. 5-14.

unsaturated aliphatic chains or lipophilic vitamins such as vitamin E (alpha tocopherol). The conjugation of siRNA with cholesterol seems to enhance cell uptake/penetration without the help of other transfection agents. Furthermore, conjugation improves in vivo pharmacokinetics mainly due to their interaction with high density lipoproteins (HDL) and light density lipoproteins (LDL) influencing both gene silencing efficacy and *in vivo* distribution. However, the requirement for high siRNA dose (50mg/kg) remains a big issue towards in vivo studies and transfer to preclinical and clinical trials. Another strategy was to conjugate siRNA with cell penetrating peptides[251] (CPP) such TAT, penetratin or transportan. In a similar way as lipophilic conjugates, CPP-conjugates show good transfection efficacies, as good as a commercial reference (lipofectamine®). However no improvement of siRNA stability has been demonstrated in comparison with naked siRNA. One step further was the formulation of multifunctional carriers[252,253,254] designed both for diagnostic and therapeutic purposes such as targeted liposomes, multifunctional micelles or polyplexes developed in a similar way as the one employed for plamsidic DNA delivery. Among available strategies, chemical conjugation by cleveable (disulfide, βthiopropionate) or uncleveable bonds (amide, pyrolidone, thioether) and ionic association with hydrophilic or lipophilic cationic substances are the most common ways.

[250] Akinc, A., Zumbuehl, A., Goldberg, M., Leshchiner, E.S., Busini, V., Hossain, N., Bacallado, S.A., Nguyen, D.N., Fuller, J., Alvarez, R., Borodovsky, A., Borland, T., Constien, R., De Fougerolles, A., Dorkin, J.R., Narayanannair Jayaprakash, K., Jayaraman, M., John, M., Koteliansky, V., Manoharan, M., Nechev, L., Qin, J., Racie, T., Raitcheva, D., Rajeev, K.G., Sah, D.W.Y., Soutschek, J., Toudjarska, I., Vornlocher, H.-P., Zimmermann, T.S., Langer, R., Anderson, D.G.
A combinatorial library of lipid-like materials for delivery of RNAi therapeutics
(2008) Nature Biotechnology, 26 (5), pp. 561-569.
[251] Moschos, S.A., Jones, S.W., Perry, M.M., Williams, A.E., Erjefalt, J.S., Turner, J.J., Barnes, P.J., Sproat, B.S., Gait, M.J., Lindsay, M.A.
Lung delivery studies using siRNA conjugated to TAT(48-60) and penetratin reveal peptide induced reduction in gene expression and induction of innate immunity
(2007) Bioconjugate Chemistry, 18 (5), pp. 1450-1459.
[252] Giljohann, D.A., Seferos, D.S., Prigodich, A.E., Patel, P.C., Mirkin, C.A.
Gene regulation with polyvalent siRNA-nanoparticle conjugates
(2009) Journal of the American Chemical Society, 131 (6), pp. 2072-2073.
[253] Fukushima, S., Miyata, K., Nishiyama, N., Kanayama, N., Yamasaki, Y., Kataoka, K.
PEGylated polyplex micelles from triblock cationers with spatially ordered layering of condensed pDNA and buffering units for enhanced intracellular gene delivery
(2005) Journal of the American Chemical Society, 127 (9), pp. 2810-2811.
[254] Yezhelyev, M.V., Qi, L., O'Regan, R.M., Nie, S., Gao, X.
Proton-sponge coated quantum dots for siRNA delivery and intracellular imaging
(2008) Journal of the American Chemical Society, 130 (28), pp. 9006-9012.

So, as LNCs are unadapted to carry hydrophilic substances, we modified the original LNCs by the chemical transacylation of solutol HS-15 with relevant polycationic polymers (Polyethylene imine, Poly-L-arginine, Poly-L-lysine). Herein, we present the feasibility of transacylation onto LNCs and demonstrate that transacylated LNCs with poly-L-lysine are able to bind siRNA in a nanomolar range, using electrostatic interactions between amino groups and phosphate groups.

Materials and methods

Materials

Labrafac® WL 1349 (Gattefossé S.A., Saint-Priest, France) is a mixture of capric and caprylic acid triglycerides. NaCl was purchased from Prolabo (Fontenay-sous-Bois, France) and water was obtained from a Milli-Q-plus® system (Millipore, Paris, France). Lipoïd® S75-3 (Lipoïd GmbH, Ludwigshafen, Germany) is a soybean lecithin made of 69% of phosphatidylcholine, 10% phosphatidylethanolamine and other phospholipids. Solutol® HS 15 and Polyethylene imine (Lupasol WF) was a gift from BASF (Ludwigshafen, Germany). Bovine Serum Albumin (BSA, 66kDa, reference A4503), Poly-L-aspartic acid (5-15kDa, reference P5387), Poly-L-arginine (70kDa, P3892) and Poly-L-lysine (30-70kDa, reference P3069) were purchased from Sigma-Aldrich (Sigma, Saint-Quentin de Fallavier, France).

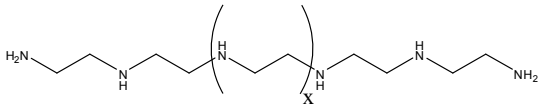

Polyethylene imine

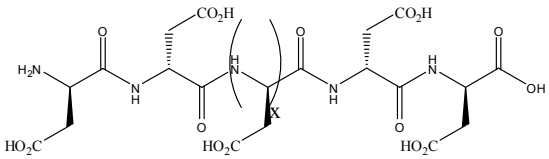

Poly-L-aspartci acid

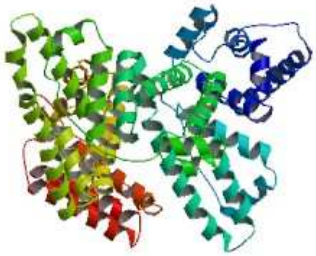

Bovine serum albumin

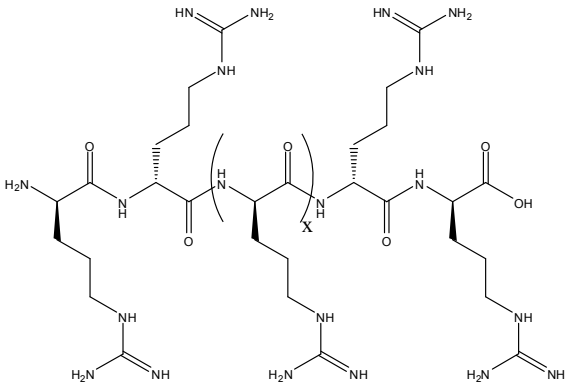

Poly-L-arginine

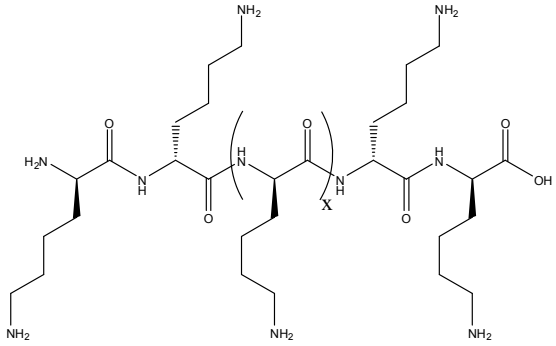

Poly-L-lysine

Figure III.12: Molecular structure of the reactants used for transacylation experiments.

LNCs formulation

The components Solutol HS 15® (mixture of free polyethylene glycol 660 and polyethylene glycol 660 hydroxystearate), Lipoid S75-3 (soybean lecithin at 69% of phosphatidylcholine), Labrafac® (caprylic-capric acid triglycerides), NaCl (sodium chloride) and water were stirred magnetically and heated to 90°C at a rate of about 4°C/min in order to obtain a water in oil (W/O) emulsion. A progressive cooling to 60°C at a rate of about 4°C/min then was performed in order to obtain an oil in water (O/W) emuslion). Three temperature cycles (90-60-90-60-90°C) were applied to cross several times the inversion phase. At the phase inversion temperature an irreversible shock was induced by dilution of the

formulation with cold water (4°C). This fast cooling-dilution led to the obtention of LNCs. Afterwards, a fast magnetic stirring was applied to the suspension for about 5 minutes.

Transacylation of LNCs

For the Transacylation step 20ml of LNCs were mixed with 1000µl NaOH 10N and 10µl or 400µl of a 5% (W/V) solution of the reactant (BSA, PLA, APA, PEI). The solution was stirred magnetically at 25°C during 15 minutes. Then 20ml of a Glycin-HCl buffer (pH 2,2) was added and the pH was adjusted to pH 7,4. Sample was immediately placed under dialysis conditions versus five liters of ultrapure water (pH=7.4).

Purification

Spectra/Por® Biotech Cellulose Ester Dialysis Membrane was used to perform the dialysis step. The molecular weight cut-off was adjusted to the molecular weight of the reactant (from 50000Da to 100000Da).

Size and zeta potential measurements

All the particles were characterized in term of size and zeta potential using a NanoZS apparatus (Malvern) after dispersion of 50µl of the mother suspension in 3ml of appropriated aqueous medium(MilliQ water, distilled water or buffer). All zeta potential values are comparable in relation with similar conductivity values and are the average of at least three measurements.

Stability versus time

To assess LNCs stability versus time and pH, LNCs suspensions with a defined pH were formulated. Size and zeta potential measurements were conducted as described above and over a period of three months at 4°C.

Preparation of LNCs-PLL-siRNA complexes

LNCs-PLL (pH=7.4) were filtered on a sterile 0.2µm syringe filters under sterile conditions. 1.5µl of LNCs-PLL were placed into Eppendorf tubes. Volumes of siRNA stock solution (1nmol/µl) were added to the corresponding tubes containing LNCs-PLL. After mixing LNCs-PLL and siRNA, solutions were diluted with the appropriate volume of water up to 1.5ml. Samples were used immediately for further experiments.

Results

In order to perform all the transacylation experiments on the same batch of LNCs, the original formulation process has been scaled-up by a factor of fifty. We obtain LNCs in the desired size ranges with low polydispersity index (0.06 and 0.05 for 20nm and 50nm LNCs respectively) and zeta potential closed to -10mV, a value very similar as the one obtained with the original process. LNCs suspensions were subsequently adjusted to pH 3 or 10 and stability studies done over a period of three months. pH=3 and 10 were chosen to access LNCs stability in acidic and basic suspensions mimicking reaction media; pH=10 is the pH of the transacylation medium. Results are summarized in Figure III.13 and Figure III.14.

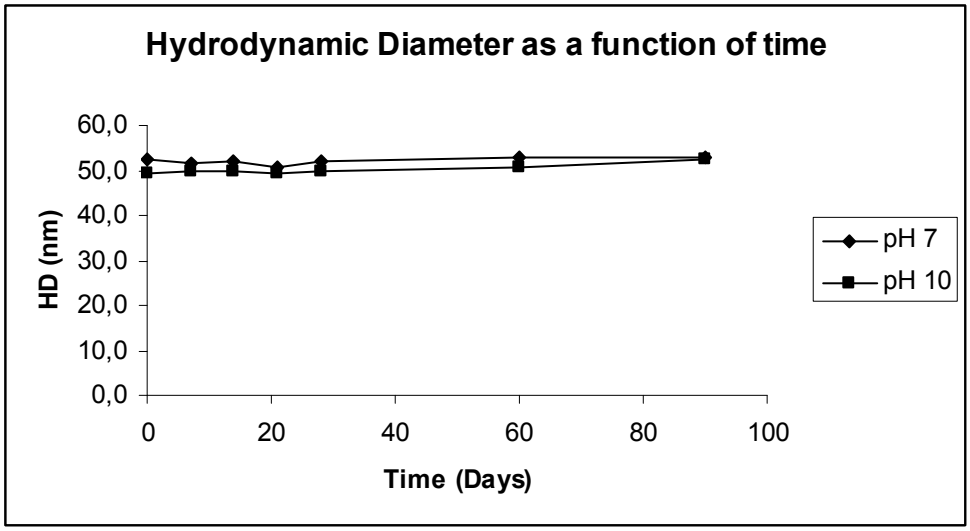

Figure III.13: Evolution of Hydrodynamic diameter versus time.

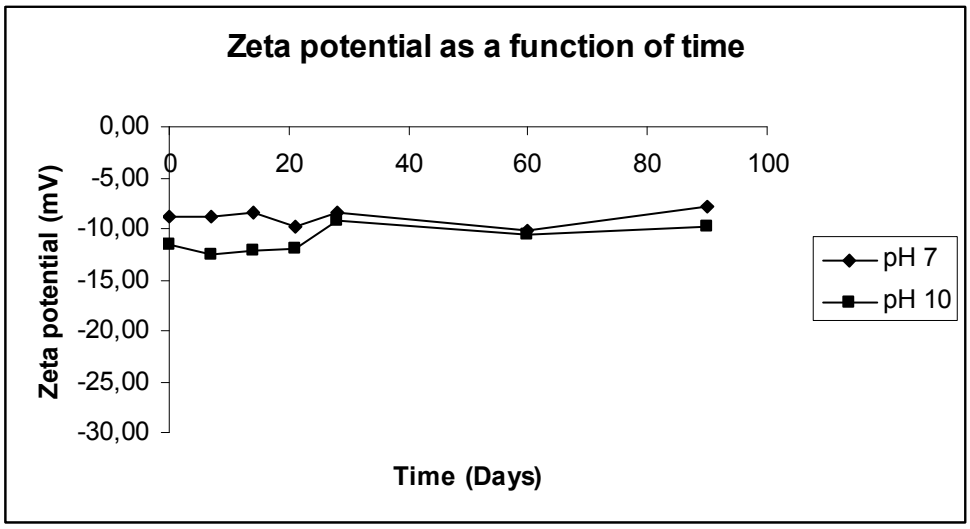

Figure III.14: Evolution of zeta potential versus time.

Figure III.13 shows the evolution of LNCs hydrodynamic diameter HD versus time. HD is constant over a period of three months even if the pH is acidic (pH=3) or basic (pH=10). In addition, as shown in Figure III.14, zeta potential is almost constant over the evaluated period of time, very closed to the starting values (-10mV). After the stability studies, transacylation experiments were carried out. 20ml of LNCs were taken up from their original medium and placed under vigorous stirring under constant temperature (water bath).

After the addition of sodium hydroxide solution to reach pH=10, the reactant bearing one or more amino groups was added. To prevent inter-LNCs cross-linking, the reaction time was fixed to 15 minutes. In order to stop the reaction, several methods were screened and it appears that the addition of glycin buffer (pH=2.2) seems to be the best, giving a pH value comprised between 5 and 6 pH units. pH was further adjusted with the appropriate solutions to 7.4. After this neutralization step, the whole sample was immediately put in a dialysis bag. Dialysis took place against milliQ water (pH=7.4) or appropriate buffer with an external volume of 5 liters for 40ml of neutralized transacylation medium. All the dialysis experiments were conducted at room temperature in the dark. After changing the external medium 3 times, for a total duration of 48 hours, transacylated LNCs were recovered, filtered using syringe filters (0.2µm) and placed into scintillation vials. Size measurements show clearly a displacement of the size distribution to the higher sizes. Results are listed in Table III.3 and III.4.

LNC 20nm			
	D_h (nm)	**PDI**	**Zeta potential (mV)**
LNC	26,6	0,062	-9,8
LNC + 400µl PLA	36,0	0,18	-15,7
LNC + 400µl APA	26,8	0,149	-31,1
LNC + 400µl BSA	25,4	0,146	-28,1
LNC + 400µl PEI	57,8	0,395	1,3

Table III.3: Results of transayclation for LNCs 25nm.

LNC 50nm			
	Dh (nm)	**PDI**	**Zeta potential (mV)**
LNC	55,7	0,051	-10,3
LNC + 400µl PLA	85,0	0,218	5,8
LNC + 400µl APA	62,7	0,087	-32,9
LNC + 400µl BSA	59,0	0,075	-30,4
LNC + 400µl PEI	110,9	0,061	30,4

Table III.4: Results of transacylation for LNCs 55nm.

It confirms that a reaction took place between the LNCs surface and the reactant. Both 26nm and 55nm LNCs undergo a HD increase. As shown in Table III.3 and III.4, HD can be raised up to 57nm and 110nm for LNCs 26nm and 55 nm respectively, if PEI is used during the transacylation step. For PLA, HD increase by a factor of 38% (LNCs 20nm) and 54% (LNCs 50nm). APA seems to react poorly with LNCs 50nm (HD increase=12.7%) and do not react with with LNCs 20nm. Zeta potential is modified up to a positive value when PEI and PLA are used (30mV and 5.8mV respectively for LNCs 50nm). Concerning LNCs 20nm, zeta potential is equal to 1.8mV (for PEI) and -15mV (for PLA). By the way, transacylation was tested on LNCs 50nm with another polycationic polymer, Poly-L-Lysine (PLL) labelled with fluoresceinisothiocyanate (FITC). As shown in Table III.5, HD is equal to 79.8nm (43% increase) and zeta potential is equal to 26mV.

LNCs PLL- FITC

	Hydrodynamic Diameter H_D [nm]	**PDI**	**ZETAPOTENTIAL [mV]**
LNC 50nm	**55.7**		**-10.3**
LNCs-PLL dialysed + filtrated	**94.8**		**18.5**
LNCs-PLL dialysed + filtrated (pH=7.4)	**79.8**		**26.6**

Table III.5: Transacylation of LNCs 55nm witl PLL-FITC.

To assess the amount of graft PLL, µBCA measurements were performed after dialysis with the appropriate controls following the manufacturer advices. PLL concentration was found to be equal to 46.2 µg/ml, corresponding to 9.2% of the starting PLL amount (Table III.6).

	PLL concentration	PLL maximum theoretical concentration	Grafted PLL
	µg/ml	µg/ml	(%)
LNC 50nm + 400µl PLL-FITC	46.2	500	9.2

Table III.6: Protein content assay, after transacylation and purification.

No additional PLL was removed from the dialysis bag, even if water was changed and dialysis time extended: the quantified amount of PLL, through µBCA assays, represents the PLL grafted on the LNCs surface.

In order to check if the introduced PLL was able to bind siRNA, we prepare LNCs-PLL suspension containing siRNA at a concentration comprised between 0 to 60nM.
Size measurements were performed and the results are presented in Figure III.15.

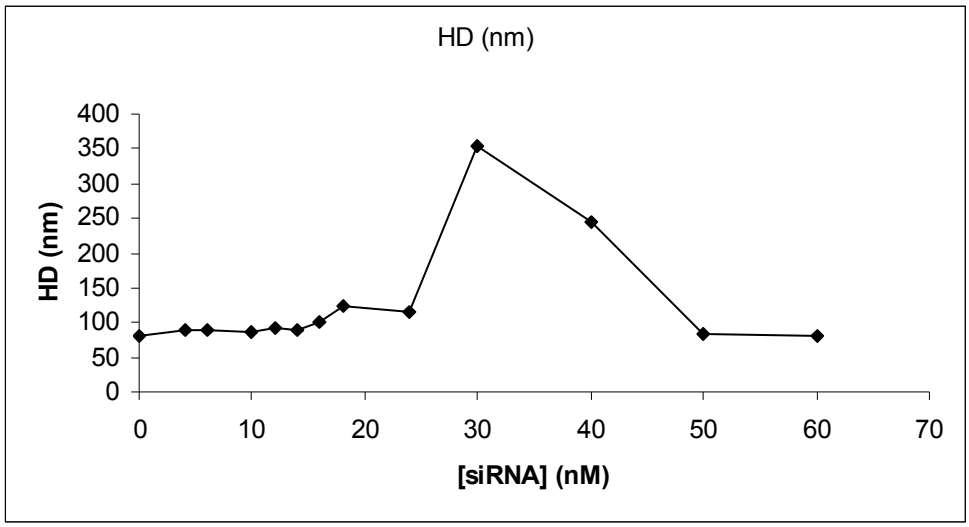

Figure III.15: Evolution of hydrodynamic diameter versus [siRNA].

Figure III.15 shows the evolution of HD versus the [siRNA]. HD is increased from 79nm ([siRNA]=0nM) to 113nm ([siRNA]=24nM). For [siRNA]=30nM, HD is equal to 354nm; in the same way HD is equal to 244nm for [siRNA]=40nM. For [siRNA]=50nM and [siRNA]=60nM, hd is closed to 80nm. Zeta potential measurements, performed on the same solutions, are summarized in Figure III.16.

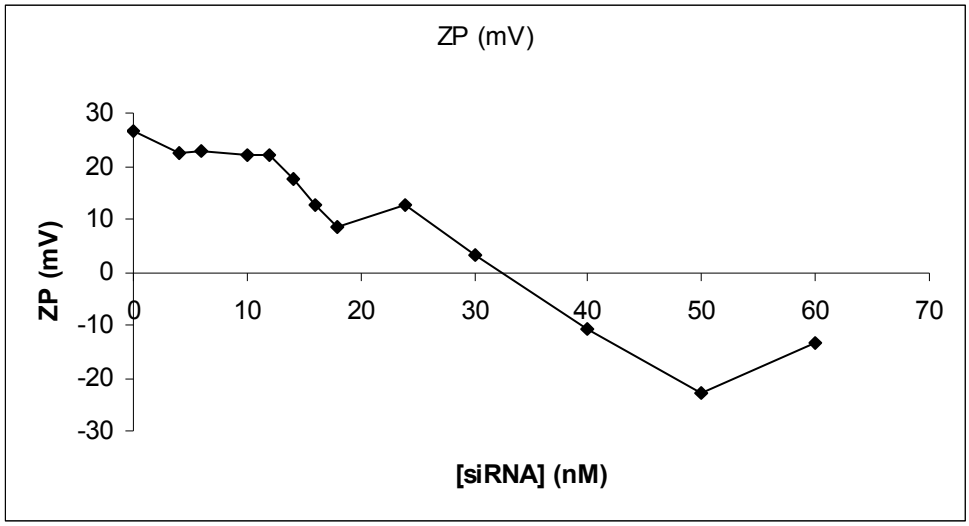

Figure III.16 : Evolution of zeta potential versus [siRNA].

ZP decreases with [siRNA], starting from 26 mV to –13mV. ZP is closed to 0mV for [siRNA]=30nM.

Discussion

As published before, LNCs can be produced with different HDs, depending on the amount of the formulation excipients. We have scaled up the formulation process up to 875ml; starting from a 17.5ml process without disturbing size distributions and PDI. It demonstrates that the formulation of LNCs is robust and easily scaled-up with common laboratories labware.

As HDs are modified by the experimental conditions employed here, we can say that a reaction occurred between LNCs surface and used molecules. As the only chemical functionality available on the LNCs surface is the ester group (coming from solutol HS-15) and that the nucleophilic character of the amine group from the reactant is strongly enhanced under basic conditions, it is clear that the only reaction that is likely to occur under these conditions is the nucleophilic attack of amine towards the ester group of solutol HS-15. In other words, the overall reaction is a transacylation.

In addition, LNCs are stable under basic conditions for several hours or days, depending on temperature of storage. This fact is a strong argument towards the fact that solutol HS-15 should not be cleaved under basic conditions in absence of nucleophilic species. Size analyses give us precious knowledge towards the functionalization degree obtained under these conditions, if we keep in mind that the measured size are hydrodynamic diameter and the chemical nature of the reactant. For example, hydrophilic polymers like PLA and PEI seems to access easily to the LNCs surface (20 and 50nm) and react in a more efficient way, causing a strong increase in size distribution. The case of APA is very interesting because APA is by nature as hydrophilic as PEI or PLA but it carries only one amine group (coming form the N-terminus) and the nucleophilic nature of these latter should be balanced by intra or intermolecular hydrogen bonds, reducing the reaction rate in this case. For LNCs 20nm no reaction seems to occur. In all cases, zeta potential measurements, carried out with care towards pH and conductivity, corroborate the previous noticed experimental fact. Zeta potential values are reversed when poly-amine such PLA or PEI are used.

However, differences exist between LNCs 20nm and 50nm. These differences could be explained by the fact that LNCs 20nm contain much more Solutol HS-15, and subsequently, their ester groups are less accessible to reactants.

On the basis of these first experiments, we performed transacylation with PLL in order to use LNCs-PLL to bind and carry siRNA. We limited this study to PLL because PLL have a lower toxicity than linear PEI and LNCs-PLL have a much more positive zeta potential than LNCs-PLA. We choose to limit this work to LNCs 50nm, as it seems that they have the best reactivity. We obtained LNCs able to bind siRNA, as shown in Figures III.15 and III.16. It appears that LNCs-PLL are able to bind siRNA as HD increases and zeta potential decreases. It could be illustrated by Figure III.17: zeta potential decrease as more and more siRNA are bind to the LNCs surface, mainly by electrostatic interactions between lysine side chains and phosphate groups.

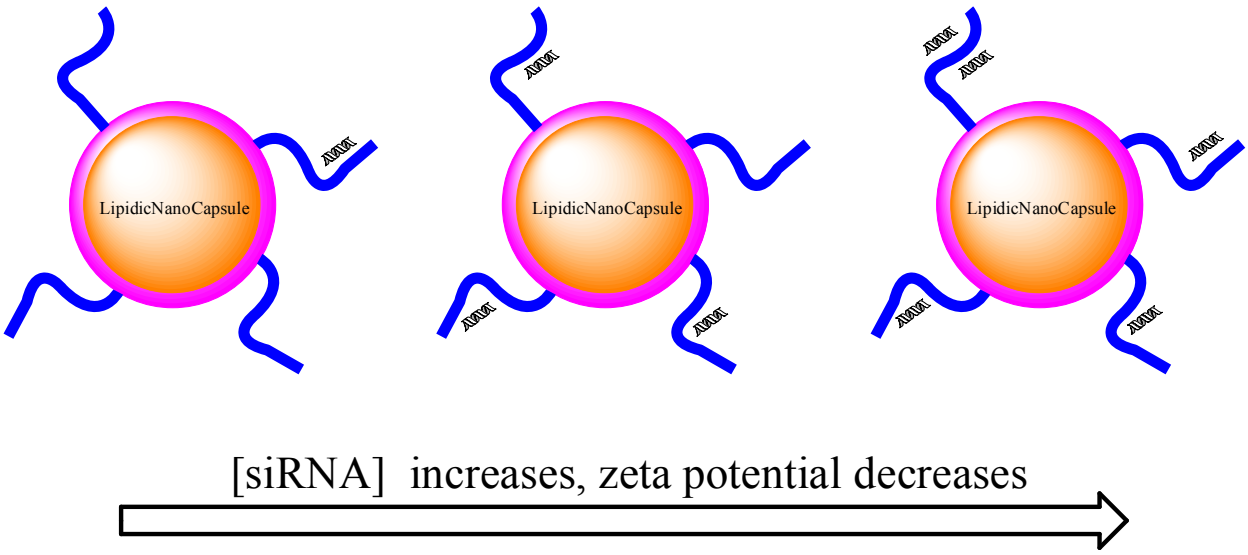

Scheme III.17: Binding of siRNA by LNCs-PLL.

In addition, the electric neutralization promotes the association of LNCs-PLL for [siRNA] close to 30nM, forming interparticle assemblies as illustrated in scheme III.18. These facts have to be taken in consideration if LNCs-PLL are used to deliver siRNA to cells.

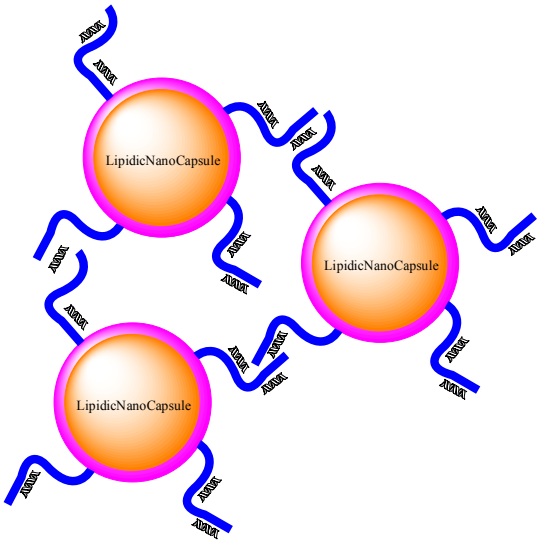

Scheme III.18: InterLNCs assemblies near electroneutrality.

Conclusion

Chemical modification of nanoparticles is a major drawback as nanoparticles are facing many obstacles and challenges. The presented work explored transacylation reaction to enable substrates to be anchored on the surface of LNCs. The work demonstrates clearly the feasibility of this process for grafting proteins and/or polymers. This strategy has strong advantages as the reaction is performed in aqueous medium with inexpensive reagents, under mild conditions. Moreover, reaction parameters can be easily tuned to satisfy specific constrains. A further advantage of this approach is that the introduced substrate is likely to be anchored onto the LNCs in an orthogonal orientation. By the way, no complicated chemistry is required to introduce attractive functionalities. In case of polymers, both cationic and anionic polymers can be grafted expanding the potent ability of use of transacylated LNCs. Both of these facts make transacylation a promising tool to create new architectures based on LNCs, able to be involved in projects from materials sciences to nanomedecine.

Acknowledgement

We wish to thank the Région Pays de La Loire for financial support.

III) Résultats complémentaires

Comme nous pouvons introduire des polymères possédant des groupements ionisables par transacylation, nous avons essayé de développer un système Layer-by-layer avec les LNCs transacylées par de l'acide poly-L-aspartique. Ces LNCs ont un diamètre hydrodynamique de 66,2 nm et un potentiel zeta égal à -31 mV. Par la suite nous avons incubé ces LNCs-APA avec une solution d'un polycation, la poly-L-lysine. Les résultats des mesures de potentiel zeta sont représentés dans la Figure. On voit très nettement une variation de potentiel zeta, ce dernier étant égal à +50 mV. De plus, le diamètre hydrodynamique des LNCs-APA augmente pour atteindre une valeur de 78 nm. L'ensemble des mesures confirment, dans ce cas, que la poly-L-lysine s'est déposée sur les LNCs-APA pour former un système layer-by-layer à deux couches. Par la suite, nous avons dialysé les LNCs-PLL-APA pour éliminer l'excès d'APA et pour évaluer la robustesse de l'association en couches. Les mesures de taille et de potentiel zeta après dialyse montrent peu d'évolution du diamètre hydrodynamique et du potentiel zeta. Ces résultats confirment que l'association en couche est assez robuste.

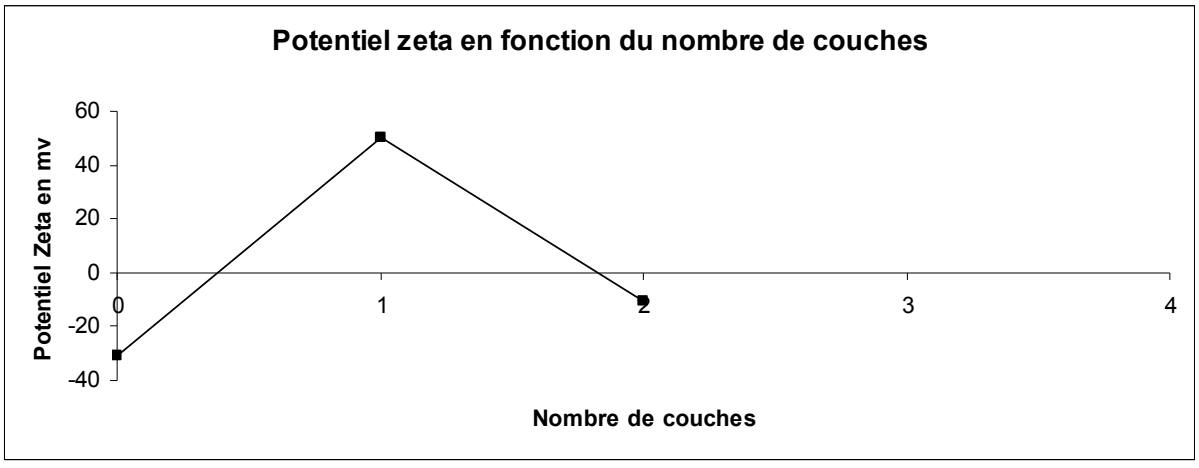

Figure III.19 : Potentiel zeta en focntion du nombre de couches.

Par la suite, nous avons souhaité rajouté une couche additionnelle en placant les LNCs-APA-PLL dans une solution d'APA. Dans ces conditions, la taille des particules augmente de façon importante jusqu'à atteindre 153 nm. Le potentiel zeta est quant à lui ramené autour de -10 mV. Du fait de la forte augmentation de diamètre hydrodynamique et du fait que le potentiel zeta est proche de la neutralité, cette expérience nous indique que les particules auraient tendance à s'aggréger.

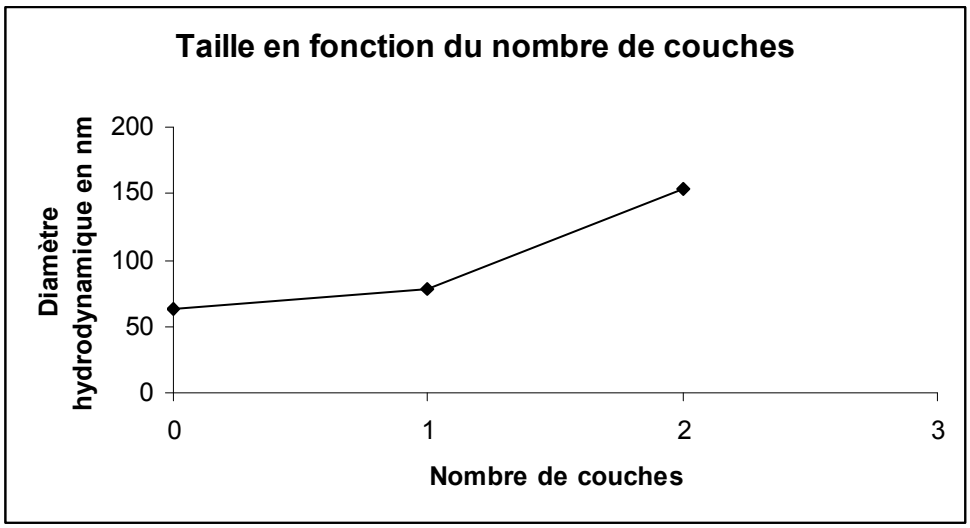

Figure III.20 : Diamètre hydrodynamique en focntion du nombre de couches.

IV) Conclusions

Nous avons développé deux méthodes pour la fonctionnalisation des LNCs en milieu aqeux. D'une part, la post-insertion a été analysée en démontrant qu'il existe une relation linéaire entre le diamètre hydrodynamique des LNCs et la longueur des chaînes de poly-oxyde d'éthylène. De plus, l'analyse des potentiels zeta a permis de comprendre l'influence de la répartition des dipôles électriques que sont les unités d'oxyde d'éthylène. En partant des tailles des micelles de DSPE-PEG et par l'apport des mesures de la mobilité electrophorétique

des particules, nous avons conclu que le bilan de la post-insertion était une insertion moléculaire dans l'interface huile-eau des LNCs.

Par la suite, nous avons étudié la faisabilité du procédé de transacylation sur les LNCs et démontré que ce procédé peut permettre l'introduction de polymères à l'interface huile-eau des LNCs. Ces polymères permettent, entre autre, de fixer des molécules d'intérêt pharmaceutiques comme les siRNA.

Les premières évaluations biologiques des LNCs modifiées par les procédés de post-insertion et de transacylation seront présentées dans le chapitre suivant.

Chapitre IV

Etude *in vitro* et *in vivo* des LNCs modifiées

Introduction

Dans ce chapitre, nous allons présenter les résultats de l'évaluation biologique des LNCs modifiées soit par le procédé de post-insertion soit par le procédé de transacylation sur deux modèles distincts qui seront décrits. Le modèle retenu pour l'évaluation des LNCs modifiées par post-insertion est le modèle de l'oreille interne étudié au travers du projet européen NanoEar. Concernant l'évaluation de l'aptitude des LNCs-PLL à transfecter des siRNA, nous avons choisi d'utiliser un modèle in vitro à base de cellules cancéreuses humaines issues de gliome, les cellules U87MG.

I) Evaluation des LNCs modifiées par post-insertion sur le modèle de l'oreille interne

I.1) Présentation du projet NanoEar[255]

Le but du projet NanoEar (Durée : 4 ans) est de développer de nouvelles nanoparticules multifonctionnelles qui seraient dirigeables à façon vers une population cellulaire donnée, biodégradables, traçables *in vitro* et *in vivo* et capables de relarguer un ou

[255] http://www.NanoEar.org/

plusieurs médicaments au niveau des cellules ciblées. Le projet NanoEar implique 26 partenaires européens, regroupés en huit sous-groupes appelés workpackages. Le projet s'articule autour de trois grands axes : la synthèse de nanoparticules de différents types, l'étude in vitro de ces dernières du point de vue de la cytotoxicité et de la pénétration cellulaire; et enfin, pour les particules les plus appropriées, l'étude *in vivo* chez le petit animal.

Figure IV.1: Description organisationnelle du projet NanoEar.

L'oreille interne est un enjeu clinique important, représentant bien les challenges propres au système nerveux central. Selon l'organisation mondiale de la santé, la perte d'audition ou la surdité touche au moins 250 millions de personnes à travers le monde. De plus, avec l'augmentation de la durée de vie et le vieillissement des populations, les troubles de l'audition sont devenus un challenge de santé public. Par ailleurs, l'exposition au bruit ainsi que l'usage grandissant de systèmes électroniques portatifs (téléphone, baladeur) contribuent à l'augmentation de l'incidence des problèmes d'audition. L'OMS estime, qu'en

2050, la perte d'audition touchera 900 millions de personnes à travers le monde. Au sein de l'union européenne, 44 millions de citoyens souffrent de problèmes d'audition et 40000 d'entres eux sont profondément sourds. L'oreille interne est isolée du reste du corps par de multiples barrières et est divisée en plusieurs compartiments eux-mêmes comportant plusieurs types cellulaires.

I.2) Présentation de l'oreille.

Globalement l'oreille dans son sens large peut-être décomposée en trois parties distinctes : l'oreille externe, l'oreille moyenne et l'oreille interne.

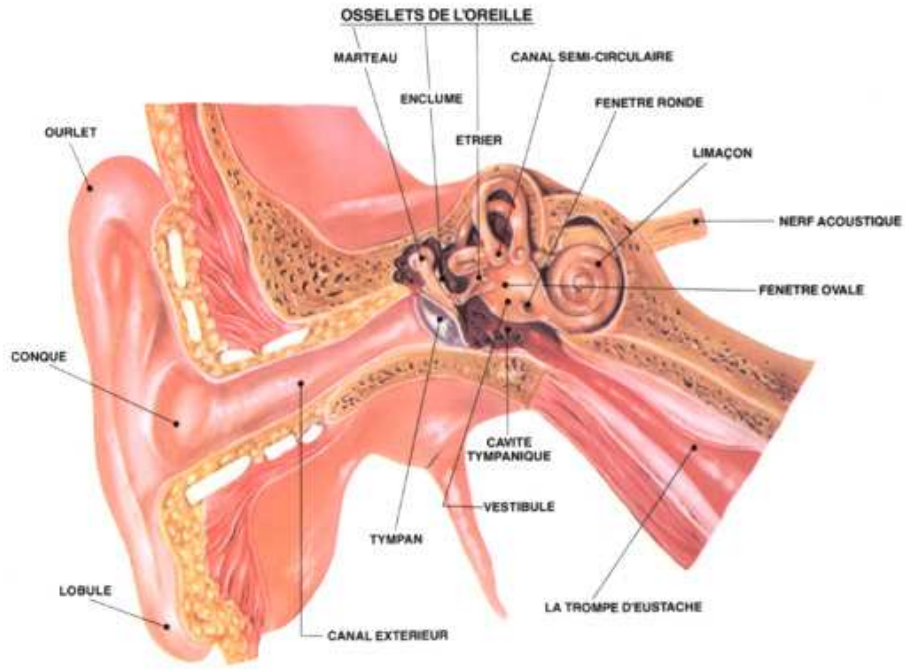

Figure IV.2 : Schéma générale de l'oreille humaine.

I.2.a) L'oreille externe

L'oreille externe est le point de départ du mécanisme physiologique de l'audition. Elle est principalement constituée du pavillon (ou pinna) qui capte et amplifie les sons. Certains mammifères peuvent bouger le pavillon pour diriger l'ouie. La plupart des êtres humains ont perdu cette capacité. Le pavillon humain amplifie de quelques décibels les fréquences autour de 2000 Hz et les fréquences plus aigues autour de 3000 Hz seront également amplifiées par le conduit auditif externe.

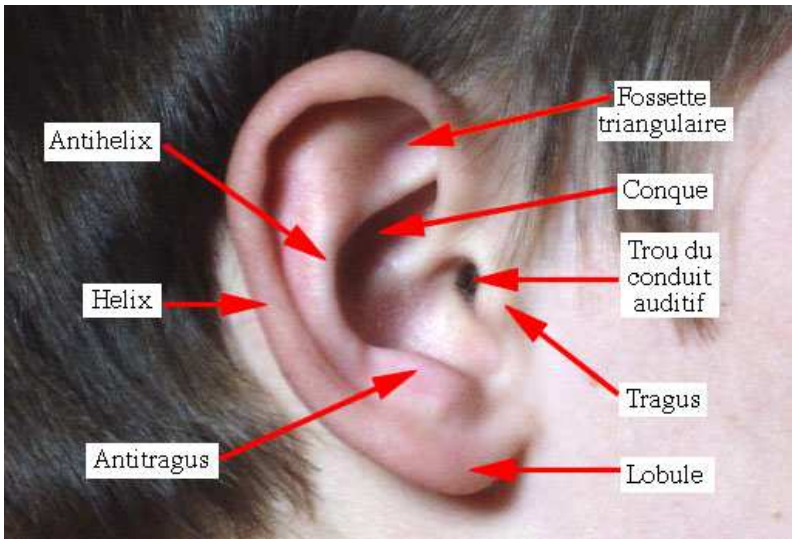

Figure IV.3 : Photo du pavillon humain.

L'oreille externe est ensuite formée par le conduit auditif externe et la face externe du tympan qui sont revêtus par la peau. La production de sérumen résulte de la sécrétion des glandes cérumineuses (variété de glandes apocrines) et des glandes sébacées présentes dans le derme de la peau du conduit auditif externe.

I.2.b) L'oreille moyenne

Elle comprend la face interne du tympan, les osselets (chaîne ossiculaire) et les parois osseuses de la caisse du tympan ainsi que celles des cavités mastoïdiennes.

Le tympan est constitué par un épithélium externe (épiderme) et un épithélium interne (épithélium pavimenteux ou cubique simple qui renferme quelques îlots de cellules ciliées et de cellules glandulaires muqueuses ou séro-muqueuses) séparés par une lame fibreuse dans l'épaisseur de laquelle se loge le manche du marteau.

Les osselets sont quatre petits os. Ils s'appellent respectivement le marteau, l'enclume, l'os lenticulaire et l'étrier. Ces noms proviennent de leurs formes caractéristiques. Le marteau et l'enclume forment une articulation peu flexible appelée bloc incudo-maléaire.

Puisque l'oreille moyenne est creuse, un environnement de haute pression (comme l'eau) poserait le risque de percer le tympan. Palier ce risque est la fonction des trompes d'Eustache. Descendantes évolutionnaires des ouïes respiratoires des poissons, ces trompes relient l'oreille moyenne aux fosses nasales afin de rétablir la pression au niveau de l'oreille moyenne.La muqueuse des trompes d'Eustache, dont l'épithélium est de type respiratoire, repose sur une armature cartilagineuse et fibreuse dans sa portion externe et osseuse dans sa portion interne.

I.2.c) L'oreille interne[256]

Elle contient non seulement l'organe de l'ouie, la cochlée ou limaçon (cochlea), mais aussi le vestibule, organe de l'équilibre, responsable de la perception de la position angulaire de la tête et de son accélération. Les mouvements de l'étrier sont transmis à la cochlée via la fenêtre ovale et le vestibule.

La cochlée est un organe creux rempli de deux liquides appelés endolymphe et périlymphe. Elle est tapissée de cellules ciliées, des cellules sensorielles coiffées de structures filamenteuses, les stéréo-cils, groupés en touffe ciliaire libre de vibrer. Ces cellules sont disposées le long d'une membrane (la membrane basilaire) qui vient partitionner la cochlée en deux chambres. L'ensemble des cellules ciliées et des membranes qui leur sont adjointes constitue l'organe de Corti. La membrane basilaire et les cellules ciliées qu'elle porte sont mises en mouvement par les vibrations transmises à travers l'oreille moyenne. Le long de la cochlée, chaque cellule répond préférentiellement à une certaine fréquence, permettant au cerveau de différencier la hauteur des sons. Ainsi, les cellules ciliées les plus proches de la base de la cochlée (fenêtre ovale) répondent préférentiellement aux aigus. Celles situées en son apex (dernier tour de la cochlée) répondent aux basses fréquences.

L'appareil vestibulaire se constitue de trois canaux semi-circulaires, disposés orthogonalement dans les 3 plans de l'espace. Ils sont remplis de la même endolymphe que la cochlée. Lorsque l'oreille est soumise à un mouvement, l'inertie de ce liquide rend ce mouvement détecTable par des cellules ciliées, tout à fait similaires à celles de la cochlée. La

[256] Shim, K.
The auditory sensory epithelium: The instrument of sound perception
(2006) International Journal of Biochemistry and Cell Biology, 38 (11), pp. 1827-1833.

disposition de trois canaux en trois plans orthogonaux permet de détecter la position angulaire de la tête dans toutes les directions possibles.

I.2.d) Détails structurels de l'oreille interne

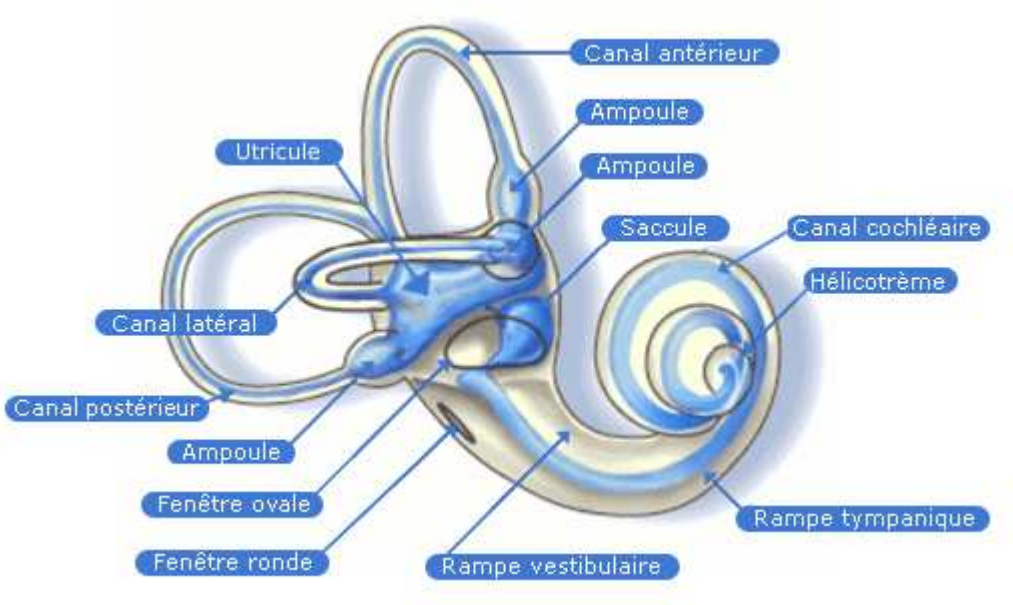

Figure IV.4 : Détails structurels de l'oreille interne (source : www.asc-csa.gc.ca/).

- Labyrinthe membraneux et labyrinthe osseux

Cavité close bordée par un épithélium et contenant l'endolymphe, le labyrinthe membraneux comprend plusieurs parties distinctes mais inter-communicantes : l'utricule, le saccule, les canaux semi-circulaires, le sac endolymphatiques et le canal cochléaire. Ultérieurement, l'épithélium pavimenteux ou cubique simple du labyrinthe membraneux subit en certains endroits des différenciations dont les trois principales sont celles qui donneront naissance aux zones réceptrices sensorielles (macules de l'utricule et du saccule, crêtes ampullaires des canaux semi-circulaires, organe de Corti), à la strie vasculaire sécrétant l'endolymphe et au sac endolymphatique le résorbant.

Autour du labyrinthe membraneux, la différenciation du mésenchyme conduit à la formation du labyrinthe osseux, coque osseuse moulant le labyrinthe membraneux dont il reste séparé par les espaces périlymphatiques contenant la périlymphe. Ainsi le vestibule osseux contient le saccule, l'utricule et les canaux semi-circulaires ; l'aqueduc du vestibule contient les canaux et le sac endolymphatiques ; la cochlée contient le canal cochléaire. La cochlée ressemble à une coquille d'escargot. Elle est constituée par un axe osseux conique, la columelle, autour de laquelle s'enroule en deux tours 3/4 de spires un tube osseux ou lame des contours. Ce tube osseux est longitudinalement divisé en deux compartiments par une lame spirale osseuse insérée sur la columelle où siège le ganglion spiral de Corti, et prolongée vers l'extérieur par la membrane basilaire s'insérant sur le ligament spiral. Ces deux compartiments, rampe tympanique en bas et rampe vestibulaire en haut communiquent entre eux par un petit orifice (hélicotrème) situé au sommet de la cochlée.

- Le canal cochléaire

Le canal cochléaire s'enroule en spirale entre les deux rampes précédentes. De section grossièrement triangulaire, sa face inférieure différenciée en organe de Corti, repose sur la membrane basilaire qui la sépare de la rampe tympanique. Sa face externe différenciée en strie vasculaire s'applique contre la partie supérieure du ligament spiral tandis que sa face supérieure constitue, avec les cellules mésenchymateuses périlymphatiques aplaties qui la recouvrent, la membrane de Reissner qui la sépare de la rampe vestibulaire.

- L’organe de Corti

L'organe de Corti est centré par le tunnel de Corti, de section triangulaire, dont la paroi externe et la paroi interne sont respectivement constituées par une rangée de piliers externes et une de piliers internes. Ces piliers sont des cellules de soutien contenant dans leur cytoplasme un volumineux trousseau de filaments intermédiaires. De part et d'autre de ce tunnel, se disposent les rangées de cellules sensorielles soutenues par les cellules de Deiters. En dehors, on trouve trois ou quatre rangées de cellules sensorielles externes et en dedans une rangée de cellules sensorielles internes. Les cellules de Deiters reposent par leur pôle basal sur la membrane basilaire tandis que leur partie supérieure enveloppe la base des cellules sensorielles ainsi que les terminaisons nerveuses adjacentes. Cette partie supérieure envoie un long prolongement dont l'extrémité supérieure aplatie (« phalange ») contribue à former avec ses homologues et les phalanges des piliers la « membrane réticulaire » qui enserre et maintient en place le pôle apical des cellules sensorielles. Ensuite, de part et d'autre de ces cellules, deux massifs de cellules de soutien assurent la continuité d'une part, avec l'épithélium recouvrant le bourrelet du ligament spiral et d'autre part, avec l'épithélium recouvrant la bandelette sillonnée. De celle-ci, naît la membrana tectoria (faite d'un matériel protéique fibrillaire voisin de la kératine) qui vient s'appliquer par sa face inférieure sur les stéréo-cils des cellules sensorielles.

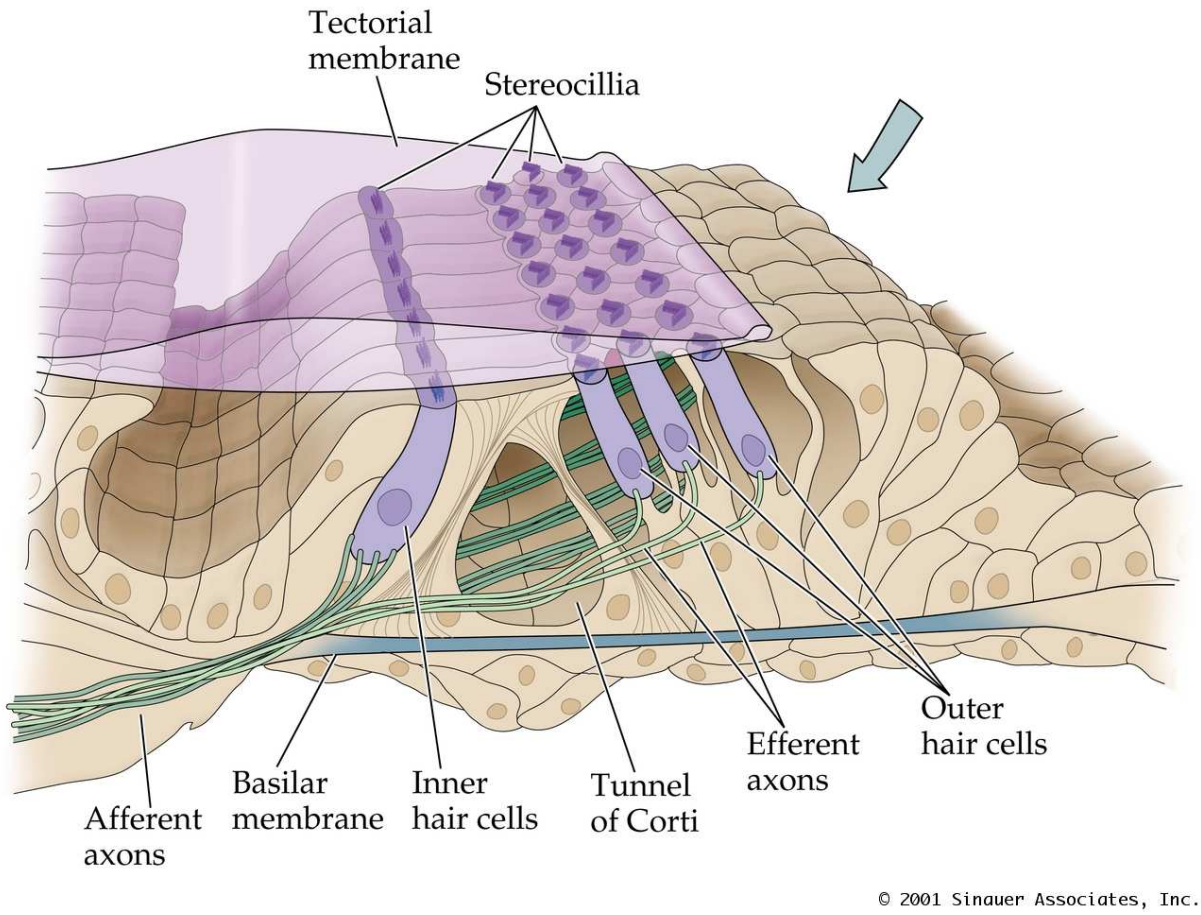

Figure IV.5 : Représentation schématique de l'organe de Corti (source : http://www.ncbi.nlm.nih.gov/bookshelf/)

- Les macules utriculaire et sacculaire

Siégeant l'une dans l'utricule, l'autre dans le saccule, les macules comportent des cellules sensorielles vestibulaires de type I et de type II dispersées au sein d'une couche de cellules de soutien. La membrane otolithique (couche de substance gélatineuse fondamentale contenant des faisceaux de fines fibrilles et dans sa zone superficielle des petites masses de carbonate de calcium, les otolithes) repose par sa face profonde sur les stéréo-cils apicaux des cellules sensorielles. Des terminaisons nerveuses afférentes (nerf vestibulaire) et efférentes entourent la base des cellules sensorielles. Les macules sont stimulées par la posture de la tête ; en effet, selon la position de la tête, les otolithes, du fait de la pesanteur, appuient plus

ou moins sur les stéréo-cils des cellules sensorielles dont la distorsion stimule les fibres nerveuses vestibulaires afférentes.

- Les crêtes ampullaires des canaux semi-circulaires

Elles ont une structure proche de celle des macules ; toutefois, leur forme générale est différente et la cupule (analogue de la membrane otolithique des macules) ne contient pas d'otolithes. Les crêtes ampullaires sont stimulées par les mouvements de la tête.

- Les cellules sensorielles vestibulaires et auditives

L'ultrastructure des cellules sensorielles, ainsi que les rapports étroits qu'elles affectent avec les terminaisons nerveuses permettent de distinguer trois types cellulaires : cellules sensorielles vestibulaires de type I, cellules sensorielles vestibulaires de type II et cellules sensorielles auditives. Retenons surtout ici leurs points communs essentiels : microvillosités à base étroite au pôle apical, présence d'un cil ou d'un résidu ciliaire sous forme d'un corpuscule basal, contacts avec des terminaisons nerveuses afférentes, entourage intime par des cellules de soutien.

Les cellules réceptrices de l'oreille interne sont organisées selon un même patron : il s'agit de cellules portant une rangée de stéréo-cils à leur extrémité apicale. Ces stéréo-cils baignent dans les liquides contenus dans les cavités de l'oreille interne.

Pour l'organe de Corti, deux types de cellules sont décrites : les cellules sensorielles auditives externes et internes. Ces cellules reposent sur la membrane basilaire. Le pôle apical des cellules auditives externes est solidaire d'une membrane protéique fixe, la membrane

tectoriale. Ainsi, lors de la perception sonore, le tympan vibre entraînant des oscillations de la membrane basilaire transmises par la chaîne des osselets. Il s'ensuit un déplacement des cellules sensorielles et de leurs stéréo-cils maintenus par la membrane tectoriale moins mobile que la membrane basilaire.

Dans l'utricule et le saccule, la partie apicale des cellules sensorielles est en contact avec une membrane protéique contenant de petites masses de carbonate de calcium, les otolithes. Ces otolithes sont sensibles à la pesanteur entraînant lors des modifications de la position de la tête des mouvements de la membrane et des stéréo-cils par rapport aux cellules sensorielles.

Enfin, les cellules des crêtes ampullaires sont en rapport à leur pôle apical avec une membrane protéique, la cupule. Celle-ci se déplace par rapport aux cellules sensorielles lors des mouvements de la tête qui produisent un mouvement du liquide des canaux semi-circulaires. En conclusion, pour toutes ces cellules, la réception de l'information sensorielle est secondaire à un mouvement affectant les stéréo-cils.

Les stéréo-cils des cellules sensorielles ne sont pas tous de même taille. Ils sont organisés en rangées de stéréo-cils de même taille et sont disposés sur une même cellule selon une taille croissante. Deux stéréo-cils voisins sont reliés par un filament protéique, le lien apical ou terminal (*tip link*)[257] qui mesure 150 nm. Sa composition protéique exacte est encore inconnue. La zone d'insertion du lien apical sur le stéréo-cil le plus haut se fait à proximité d'un canal ionique (canal K^+ mécano-sensible). Selon le type de mouvement des stéréo-cils, le lien apical sera plus ou moins tendu. Lorsqu'il est en tension maximale, il entraîne une ouverture du canal ionique normalement fermé. Il s'ensuit un courant cellulaire responsable d'une dépolarisation et d'un potentiel cellulaire. Ceci produit une transmission synaptique à la

[257] Gillespie, P.G., Dumont, R.A., Kachar, B.
Have we found the tip link, transduction channel, and gating spring of the hair cell?
(2005) Current Opinion in Neurobiology, 15 (4), pp. 389-396.

base de la cellule sensorielle qui entraîne un potentiel d'action dans les fibres nerveuses du nerf VIII.

L'oreille interne est isolée du reste du corps et est divisée en plusieurs compartiments comportant chacun plusieurs types cellulaires. Dans la cochlée, les mécanismes de mort cellulaire sont soit la nécrose cellulaire, soit l'apoptose qui résulte de l'activation des caspases, une famille de protéines à cystéine. Il a été démontré que les anti-oxydants protègent la cochlée des traumatismes acoustiques[258] mais aussi de l'exposition aux drogues comme le cisplatine ou les aminoglycosides[259]. Les anti-oxydants permettent de prévenir la formation de radicaux oxygénés réactifs, la neutralisation de produits toxiques et ainsi de bloquer les voies d'apoptose. De plus, un nombre important de maladies de l'oreille interne possède une origine génétique. Des vecteurs viraux ont été utilisés pour permettre l'expression de gènes qui régulent la différenciation des cellules de soutien en cellules ciliées[260]. Cependant, l'usage des ces vecteurs viraux pour le traitement des pathologies humaines n'est pas sans risque. De ce fait, il apparaît la nécessité de mettre au point des vecteurs combinant les avantages des vecteurs viraux et non viraux. Ces vecteurs doivent être plurifonctionnels, c'est-à-dire que l'on doit pouvoir suivre leur distribution au sein de l'organisme et de l'organe ciblé ; ils doivent transporter le principe actif et le libérer au sein des cellules cibles. Il faut préciser qu'à ce jour qu'aucun récepteur cellulaire spécifique des cellules ciliées n'a été utilisé pour réaliser un ciblage cellulaire à partir de vecteurs nanométriques. Il y a une nécessité à trouver des ligands spécifiques des cellules visées. Les

[258] Kopke, R.D., Weisskop, P.A., Boone, J.L., Jackson, R.L., Wester, D.C., Hoffer, M.E., Lambert, D.C., Charon, C.C., Ding, D.-L., McBride, D.
Reduction of noise-induced hearing loss using L-NAC and salicylate in the chinchilla
(2000) Hearing Research, 149 (1-2), pp. 138-146.
[259] Garetz, S.L., Altschuler, S.A., Schacht, J.
Attenuation of gentamicin ototoxicity by glutathione in the guinea pig in vivo
(1994) Hearing Research, 77 (1-2), pp. 81-87.
[260] Ballana, E., Wang, J., Venail, F., Estivill, X., Puel, J.-L., Arbonès, M.L., Bosch, A.
Efficient and specific transduction of cochlear supporting cells by adeno-associated virus serotype 5
(2008) Neuroscience Letters, 442 (2), pp. 134-139.

premiers tests consistent en une étude de la biodistribution des LNCs post-insérées dans l'oreille interne du rat (étude 1) et du cochon d'inde (étude 2). La deuxième étude évalue aussi l'impact des LNCs utilisées sur la fonction auditive. Ces LNCs portent des marqueurs fluorescents afin de pouvoir évaluer leur distribution au sein de l'oreille interne.

II) Production de LNCs porteuses de marqueurs fluorescents.

Pour les deux études, les LNCs ont été produites selon le schéma ci-dessous :

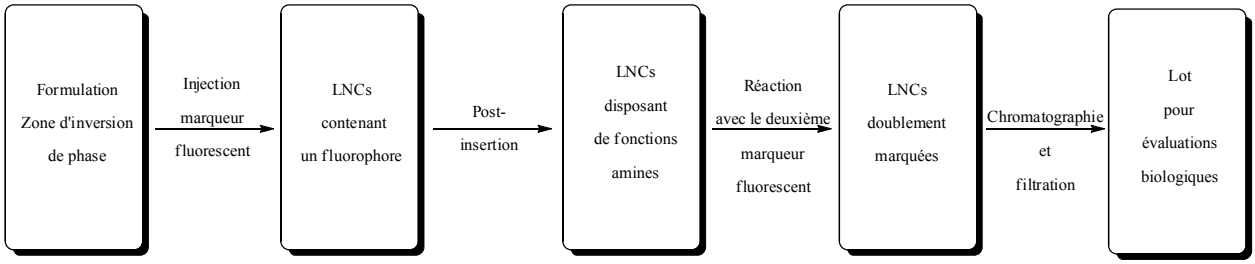

Schéma IV.6 : Représentation schématique de la production de LNCs doublement marquées.

A partir de la formulation de LNCs de 50 nm, nous avons étudié les moyens de charger les LNCs en marqueur fluorescent. Nous avons choisi d'introduire le marqueur fluorescent dans la zone d'inversion de phase, juste avant dilution[261]. Nous avons évalué l'impact de la quantité de marqueur fluorescent sur la taille des LNCs obtenues. Les résultats sont consignés dans la Figure IV.7.

[261] Saulnier Patrick, Benoît Jean-Pierre, Anton Nicolas : Methode for preparing lipidic nanocapsules. WO 2009004214 (AZ), 08/01/2009.

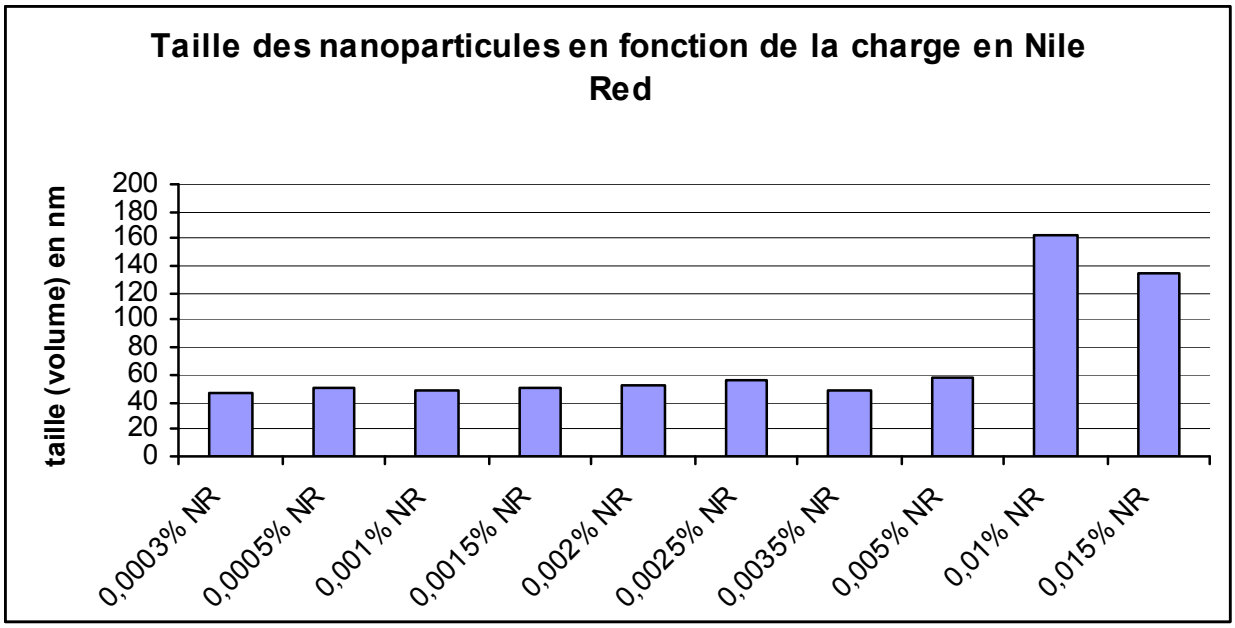

Figure IV.7 : Influence de la quantité de fluorophore (Nile Red) sur la taille des LNCs.

Il apparaît que pour une quantité de marqueurs fluorescents supérieure à 0,01% (masse de marqueur fluorescent/masse des excipients), l'ajout de marqueur fluorescent augmente de façon importante la taille des LNCs (+ 220%). Nous avons donc choisi de nous limiter à une quantité de marqueur fluorescent égale à 0,0005% en masse par rapport à la masse des excipients. Neanmoins, les études confirment que les LNCs peuvent être suivies par microscopie confocale lorsqu'elles sont chargées avec cette petite quantité de marqueur fluorescent.

Les LNCs ont ensuite été post-insérées, comme décrit au chapitre 3, avec du DSPE-PEG-2000-amino. Par la suite, nous avons réalisé un marquage au FITC (ou au RITC) en milieu aqueux (pH = 10), selon un protocole utilisé pour le marquage des protéines. Nous avons estimé que 60% des groupes amino sont marqués au FITC. Nous avons choisi la filtration sur membrane (0,2µm) comme méthode de stérilisation car elle est rapide, économique et est efficace sur une période de plusieurs semaines.

II.1) Première étude

Ce travail a été réalisé en collaboration avec l'équipe du Pr Ilmari Pykko de l'université de Tampere, Finlande. Nous avons choisi comme méthode d'administration des LNCs dans l'oreille interne, le dépôt des suspensions de LNCs fluorescentes sur la fenêtre ronde. Il apparaît que les LNCs sont capables de traverser la fenêtre ronde et de diffuser au sein de l'oreille interne. Il apparaît que, dès 30 minutes après l'administration des LNCs, celles-ci ont diffusées à travers la fenêtre ronde et ont atteint les cellules du ganglion spinal ainsi que les fibres nerveuses et les fibrocytes du ligament spiral. Il apparaît aussi une colocalisation des deux marqueurs fluorescents, ce qui laisse à penser que les LNCs sont intactes au sein de ces cellules. Cette étude a servi de base aux développements ultérieurs.

Distribution of Lipid Nanocapsules in Different Cochlear Cell Populations After Round Window Membrane Permeation

Jing Zou,[1] Patrick Saulnier,[2] Thomas Perrier,[2] Ya Zhang,[1] Tommi Manninen,[1] Esko Toppila,[1] Ilmari Pyykkö[1]

[1] Department of Otolaryngology, University of Tampere, School of Medicine, 33520 Tampere, Finland

[2] Université d'Angers-INSERM U646 Ingénierie de la Vectorisation Particulaire, 49100 Angers, France

Received 25 October 2007; revised 10 December 2007; accepted 18 December 2007
Published online 24 April 2008 in Wiley InterScience (www.interscience.wiley.com). DOI: 10.1002/jbm.b.31058

Abstract: Hearing loss is a major public health problem, and its treatment with traditional therapy strategies is often unsuccessful due to limited drug access deep in the temporal bone. Multifunctional nanoparticles that are targeted to specified cell populations, biodegradable, traceable *in vivo*, and equipped with controlled drug/gene release may resolve this problem. We developed lipid core nanocapsules (LNCs) with sizes below 50 nm. The aim of the present study is to evaluate the ability of the LNCs to pass through the round window membrane and reach inner ear targets. FITC was incorporated as a tag for the LNCs and Nile Red was encapsulated inside the oily core to assess the integrity of the LNCs. The capability of LNCs to pass through the round window membrane and the distribution of the LNCs inside the inner ear were evaluated in rats via confocal microscopy in combination with image analysis using ImageJ. After round window membrane administration, LNCs reached the spiral ganglion cells, nerve fibers, and spiral ligament fibrocytes within 30 min. The paracellular pathway was the main approach for LNC penetration of the round window membrane. LNCs can also reach the vestibule, middle ear mucosa, and the adjacent artery. Nuclear localization was detected in the spiral ganglion, though infrequently. These results suggest that LNCs are potential vectors for drug delivery into the spiral ganglion cells, nerve fibers, hair cells, and spiral ligament. © 2008 Wiley Periodicals, Inc. J Biomed Mater Res Part B: Appl Biomater 87B: 10–18, 2008

Keywords: nanoparticles; inner ear; drug delivery; neuron; biological barrier

INTRODUCTION

Hearing loss is a major public health problem that ranks 8th among common diseases in the EU. The traditional treatment strategy for sensorineural hearing loss (SNHL) has not been very successful. The human cochlea is deeply buried in the temporal bone, and its access is limited by membranous partitions. The blood supply derived from the intracerebral vessels hampers any efforts for intravascular treatment. Cochlear implantation (CI) bypasses the membranous borders and provides direct contact with cochlear partitions. Thus far, only electrical stimulation has been used in hearing rehabilitation, and CI is a well-established method for restoring severe or profound hearing loss. However, hearing performance after implantation is variable due to several causes.[1–4] A cure for SNHL would thus depend on novel concepts such as successful gene or drug delivery alone or in combination with CI.[5]

To achieve an ideal outcome with a minimum amount of adverse effects, novel multifunctional nanoparticles (MNPs) could be used. These must possess special characteristics such as the ability to be targeted to specified cell populations, as well as being biodegradable, traceable *in vivo*, and equipped with controlled drug/gene release. In clinical practice, a minimally invasive delivery approach is desired. One such method is round window membrane permeation, which is an efficient and minimally invasive method of administering substances into the inner ear, as has been proved in both animal and human studies.[6,7] The method is also feasible, as suggested by reports on gene delivery through intact round window membranes and expression in the cochlea.[8,9] Reports from clinical observation of transtympanic steroid treatments for SNHL indicate that the presence of a controlled sustained release of drug into the inner ear can determine the outcome of patients.[10–12] According to Praetorius et al., silica nanoparticles can reach all cell populations of the inner ear upon delivery onto the round window membrane.[13] Hitherto, silica nano-

Correspondence to: J. Zou (e-mail: Jing.Zou@uta.fi)
Contract grant sponsor: EU project Nanoear; Grant numbers: NMP4-CT-2006-026556

particles face problems in loading and releasing drugs in a controlled fashion.

Lipid core nanocapsule (LNC) possesses sustained release property for amiodarone.[14] For this study, the LNC was further modified to be made visible in tissues by incorporating FITC into the LNC to serve as a tag. Nile Red was encapsulated inside the oily core to assess the integrity of the LNC *in vivo*. If FITC and Nile Red co-localize inside the tissues, the LNC must be intact; otherwise it is considered degraded. The aim of the present work is to demonstrate that the LNC can permeate the round window membrane, pass the cochlear partitions, and address inner ear cell populations.

TABLE 1. Grouping of the Ear for Round Window Membrane Delivery of LNC

Groups[a]	Side of the Ear	Number of Animals	Number of the Ear
30 min	Left side	5	5
60 min	Right side		4
180 min	Right side		1
1 day[b]	Both side	2	4
7 day[b]	Both side	2	4

[a] The time between sampling and the administration of LNC.
[b] Left ear with transient administration of LCN (30 min), right side with constant delivery.

MATERIALS AND METHODS

Materials and Animals

Materials for LNC manufacturing include: the lipophilic Labrafac_WL 1349 (caprylic-capric acid triglycerides; European Pharmacopeia, IVth, 2002) which was kindly provided by Gattefossé S.A. (Saint-Priest, France), Lipoïd S75-3 (soybean lecithin with 69% of phosphatidylcholine), and Solutol HS 15 (mixture of free polyethylene glycol 660 and polyethylene glycol 660 hydroxystearate, European Pharmacopeia, IVth, 2002), which were gifts from Lipoïd Gmbh (Ludwigshafen, Germany) and BASF (Ludwigshafen, Germany), respectively. Because of the complex composition of each product, the brand names will be used in the following text. NaCl was obtained from Prolabo (Fontenay-sous-Bois, France). Water was obtained from a Milli RO System (Millipore, Paris, France). Fluorescein-5-isothiocyanate (FITC) was purchased from Fluorescéine IsoThioCyanate (France), Nile Red and 3,3′-Dioctadecyloxacarbovyanine perchlorate (DiO) were purchased from Sigma-Aldrich (USA), and Rhodamine B was purchased from ChemExper Inc. (Belgium). 1,2-Distearoyl-*sn*-Glycero-3-Phosphoethanolamine-*N*-[Amino(PolyethyleneGlycol)2000] (called DSPE-PEG2000-amino in the text) was furnished by Avanti® Polar Lipids, Inc (Alabaster, USA).

Materials for animal testing included elastase (Sigma-Aldrich, USA), collagenase type I (Sigma-Aldrich, USA), trypsin (Sigma-Aldrich, USA), fetal calf serum (Invitrogen, USA), paraformaldehyde (Sigma-Aldrich, USA), FITC-labeled phalloidin (Sigma-Aldrich, USA), rabbit anti-neurofilament 200 polyclonal antibody (Sigma-Aldrich, USA), FITC-labeled goat anti-rabbit IgG (Sigma-Aldrich, USA), 4′,6-Diamidino-2-phenylindole (DAPI) (Sigma-Aldrich, USA), Gel Mount™ Aqueous Mounting Medium (Sigma-Aldrich, USA), O.C.T. (Electron Microscopy Sciences, USA), medetomidine hydrochloride (Orion, Finland), atipamezole hydrochloride (Orion, Finland), Ketamine (Pfizer, USA), L-Polamivet (Intervet, Finland), and ofloxacin (Aventis Pharmacy, Finland).

Nine male Sprague-Dawley rats with normal Pryer's reflex (supplied by the experimental animal unit, University of Tampere) were used in the study in accordance with the local ethics committee of University of Tampere standards (permission no: 985/2003). They were divided into five groups according to their time points (Table 1). All animal experiments were approved by the Ethical Committee of the University of Tampere. Animal care and experimental procedures were conducted in accordance with European legislation.

LNC Preparation

The first step of the formulation was an emulsion consisting of Labrafac® WL 1349, an oil made of capric and caprylic acid triglycerides (average molecular weight of 512); Lipoid® S75-3, a soybean lecithin made of 69% phosphatidylcholine and other phospholipids; Solutol® HS 15, another surfactant; a mixture of polyethylene glycol 660 hydroxystearate (C18E15); and free polyethylene glycol 660. The optimal amounts of ingredients for preparation of 50 nm LNC were: Labrafac® (1.028 g), Lipoïd® (0.075 g), Solutol® (0.846 g), NaCl (0.089 g) and pure water (2.962 g). This mixture was prepared under magnetic stirring at room temperature to obtain an emulsion of oil in water. After progressive heating at a rate of 4°C/min under magnetic stirring, we observed a short interval of transparency at temperatures close to 70°C, and the inverted phase (water droplets in oil) was obtained at 85°C. Then, three cycles of cooling and heating were applied between 85°C and 60°C at the same rate of 4°C/min (near the phase inversion zone), and finally a fast dilution in cold water at a temperature close to 0°C produced a suspension of nanocapsules.[15,16]

DSPE-PEG2000-Amino Postinsertion

LNCs were incubated for 90 min with an aqueous micellar solution of DSPE-PEG-amino at 60°C. The suspension was vortexed every 15 min and then quenched in an ice bath for 1 min. The final DSPE-PEG concentration corresponded to 6 mol % of total surface molecules (i.e., Solutol and Lipoïd).[17]

Nile Red and DiO Encapsulation

A volume of 55 μL (0.18 μmol) of a Nile Red in ethanol solution (1 mg/mL) was added to the LNC emulsion, just before diluting the system with cold water. The Nile Red was totally encapsulated in the oily core, with the final concentration of 174 μmol/L. For DiO encapsulation, Nile Red was replaced by 153 μg DiO and the final concentration was 174 μmol/L.

FITC and Rhodamine B Labeling

After the postinsertion process, 2 mg of FITC isothiocyanate (5.13 μmol) was added to 2.95 mL of LNC suspension and the pH was increased to 10 by adding of a few drops of 0.1*M* Na_3PO_4 solution. The sample was protected from light and placed in a water bath under magnetic stirring at 35°C for 45 min. After the sample was cooled in an ice bath for 3 min in order to stop the reaction, size exclusion chromatography on a sephadex G-15 column was performed to separate free FITC from labelled LNCs. Optical density (FITC detection) as well as turbidity at 680 nm (LNC detection) was measured for each fraction [Figure 1(A)]. Fractions corresponding to the FITC labeled LNCs were analysed by dynamic light scattering. Electrokinetic measurements were performed at a constant conductivity (0.03 μs cm ^{1}). These measurements indicated a hydrodynamic diameter of 52 $\pm$ 5 nm and a zeta potential of -55 ± 7 mV (for non labelled LNCs we obtained -7 ± 3 mV) [Figure 1(B)]. Only fractions with a polydispersity index lower than 0.2 were pooled and used for animal testing [Figure 1(C)]. For Rhodamine B labeling, FITC was replaced by 2 mg Rhodamine B.

Round Window Membrane Delivery of LNCs

Animals were fully anesthetized with medetomidine hydrochloride (0.5 mg/kg) and ketamine (75 mg/kg). The operation was performed under sterile conditions. After local analgesia with lidocaine, a retro-auricular incision was used to expose the left bulla. A hole was drilled on the bulla with a 2 mm diameter burr. After visualizing the stapes artery, the round window membrane was identified above the artery. A small piece of gelfoam (around 8 mm^3) was saturated with LNC and placed on the round window membrane (LNC concentration: 20.5 g/L, stored at 4°C for 3 months). The ears were divided into five groups of 30 min, 60 min, 180 min, 1 day, and 7 days according to the sampling time post-LNC administration (Table 1). For the 1 day and 7 day groups, gelfoam was placed on the left ear for 30 min and then removed, whereas gelfoam was placed on the right ear constantly until the end of the experiment. The hole on the bulla was sealed with muscle and the wound was sutured in the 1 day and 7 day groups. Atipamezole hydrochloride (2 mg/kg) was injected i.p. immediately after the operation to accelerate recovery from anaesthesia of the animals. Saline (2 mL) was administered through subcutaneous injection on the neck. L-Polamivet (0.4 mL/kg) was injected b.i.d. to relieve the pain. Ofloxacin (20 mg/kg) was injected b.i.d. in the 1 day and 7 day groups after operation.

Whole Mount Sample Preparation

Following i.p. injection of pentobarbital (60 mg/kg), 2–3 mL of air was cardio injected to sacrifice the animals. The bulla was removed and fixed in 4% paraformaldehyde for 1 h. The cochlea was thoroughly washed with tap water for 30 s and then opened by breaking the bony wall under a stero-microscope, and washed again with PBS for 2 $\times$ 5 min. The bulla was counter stained with DAPI (10 μg/mL) for 10 min, and further washed three times for 5 min each with PBS in a dark room. The middle ear mucosa, stapes artery, round window membrane, lateral wall, and modiolus from the basal turn, cochlear nerve, and ampulla of the semi-circular cannel were taken under a stereo-microscope, placed on glass slide, and mounted with Gel Mount™ Aqueous Mounting Medium for confocal microscopy.

Cochlear Cell Isolation

To confirm the cellular internalization of LNCs, one small piece of tissue, each from the cochlear modiolus and lateral wall (fixed with 4% paraformaldehyde), was treated with elastase (1 mg/mL), collagenase type I (1 mg/mL) and trypsin (0.5 mg/mL) at 37°C for 15 min. The enzymes were inactivated through incubation with DMEM containing 5% fetal calf serum at room temperature for 5 min. The isolated cells were placed on glass slides and mounted with Gel Mount™ Aqueous Mounting Medium for confocal microscopy.

Cryosectioning

For clarification of the cellular population in the lateral wall, one piece of the fixed lateral wall was embedded with O.C.T., sectioned by a cryostat (Leica CM3050S, Germany) in 5-μm sections, and mounted with Gel Mount™ Aqueous Mounting Medium.

Cellular Specific Staining

To confirm the cell population of the cochlea with regard to the LNCs distribution, immunofluorescent staining was applied to visualize neurofilament in the cochlear nerve tissue, and FITC-labeled phalloidin was used to probe F-actin in the organ of Corti and lateral wall. After fixation and washing as stated above, permeation with 0.3% Triton X-100 PBS for 5 min, and washing again with PBS, lateral wall soft tissue was isolated from the bone and incubated in FITC-labeled phalloidin (50 μg/mL) for 40 min and then in DAPI for 10 min. After washing with PBS for 2 $\times$ 5 min, stria vascularis was isolated from the spiral ligament and both tissues were mounted as stated above. After incubation with preimmunized goat serum (1:20), the modiolus

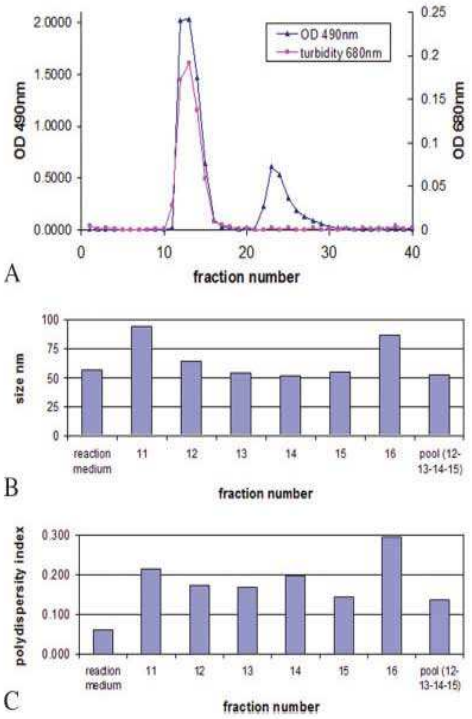

Figure 1. Characterization of FITC labeled LNCs. A: Separation of free FITC from labeled LNCs with Sephadex G15. The first peak showed absorbance at both 490 nm and 680 nm, indicating FITC-conjugated LNCs with encapsulated Nile Red. The second peak showed only absorbance at 490 nm, indicating free FITC. B: LNC size for each fraction after chromatography on Sephadex G-15. C: Polydispersity index for each fraction after chromatography on Sephadex G-15. [Color figure can be viewed in the online issue, which is available at www.interscience.wiley.com.]

including basilar membrane was incubated with rabbit anti-neurofilament 200 polyclonal antibody (1:1000) overnight at 4°C, washed with PBS containing 0.2% Tween 20 (PBS-T), and counterstained with DAPI for 10 min; the basilar membrane, together with bony spiral laminar, was isolated from the modiolus and mounted as stated above.

Confocal Microscopy

The whole mount samples and cryosectioned slices were observed under an Olympus microscope IX70 installed with ANDOR IQ. The excitation filters were 488 nm (blue excitation) and 568 nm (green excitation), with an Ar-Kr laser as the excitation source. The corresponding emission filters were 525/50 (FITC and DiO) and 607/45 (Nile Red and Rhodamine B). DAPI was excited with a 340–380 nm filter and detected using a 500 LP filter. For 3D scanning, the inter slice thickness was 0.5 μm. The image data was rendered with ImageJ 1.32j software.

RESULTS

Thirty minutes after administration of the LNC in the tympanic cavity on the round window membrane, abundant LNCs were found in the spiral ganglion cells [Figure 2(A–C)]. LNCs also attached to the outer surface of nerve fibers of the spiral ganglion; this was confirmed by neurofilament staining [Fig. 2(D)]. Nuclear localization was detected in the spiral ganglion, though infrequently [Figure 2(D)]. However, the spiral ganglion distribution intensity of LNCs after thorough treatment including washing with surfactant (Tween-20) during neurofilament staining was much lower than without the staining. LNCs were also visible in the inner hair cells and pillar cells as confirmed by F-actin staining [Figure 2(E–G)]. Again as a result of staining for neurofilament, LNCs were totally invisible in the organ of Corti [Figure 2(H)]. The distribution of LNCs in the lateral wall was found in both the spiral ligament and stria vascularis [Figure 2(I–L)]. The surface appearance of marginal cells of the stria vascularis after F-action staining showed that the intercellular complexes corresponded to the scanning electron microscopy report.[18] LNCs were frequently detected in the intercellular junction area of the marginal cells [Figure 2(K)]. Visualization of LNCs in a single cell isolated from the lateral wall confirmed the internalization of LNCs [Figure 2(N)]. After long incubations with various solutions and many washes during F-actin staining, LNCs disappeared from the spiral ligament while still remaining visible in the stria vascularis. There was also a gradient distribution in the stria vascularis in that more LNCs appeared in the second turn than the basal turn [Figure 2(K,L)]. The amount of LNCs in the cochlea as shown by F-actin staining was much lower than that in the cochlea without the specific staining. These further proved that long time processing swept the extracellular LNC away and the internalization occurred mainly in the stria vascularis rather than the spiral ligament. There was also uptake of LNCs in the stapedial artery, which has been shown to pass by the round window in rats [Figure 2(M)]. The loss of co-localization of Nile Red and FITC indicates the degradation of some LNCs.

One hour postround window membrane delivery, LNCs appeared in the tunnel fibers in the organ of Corti [Fig 3(A)]. LNCs went further distally and were also detectable in the outer hair cells [Figure 3(B,C)]. The internalization of LNCs in the cochlear hair cells was confirmed by isolated single cell imaging [Figure 3(G–I)]. LNCs inside the spiral ligament spread to the type V fibrocytes, which is adjacent to the perilymph of the scala vestibule [Figure 3(D,E)]. LNCs were also found in the spiral prominence and outer sulcus cells [Figure 3(F)].

The possibility of a paracellular pathway for penetration of LNCs through the round window membrane was indicated by the different behavior of LNCs 24 h after transient delivery (LNCs were placed on the round window membrane for 30 min and then removed) and constant administration (LNCs were constantly placed on the round window mem-

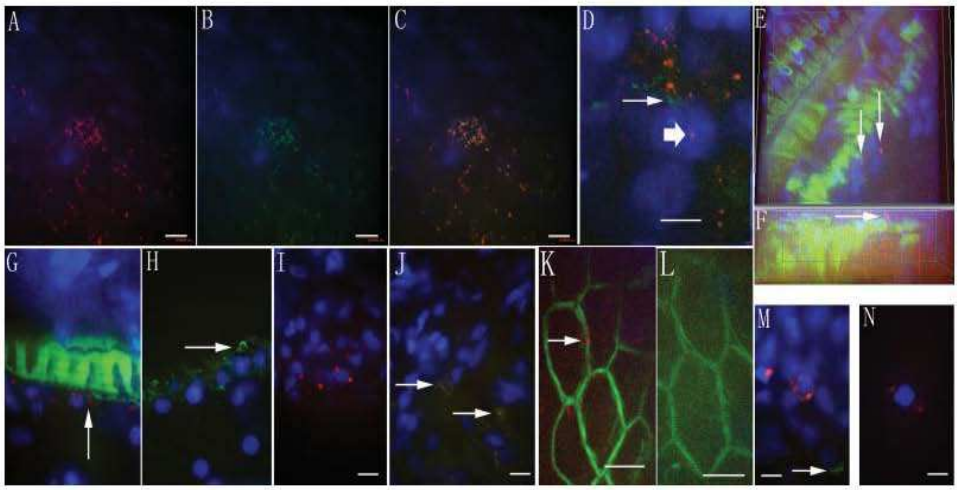

Figure 2. Localization of LNCs in different cell populations in the cochlea 30 min post-round window membrane administration. There were abundant nanoparticles in the spiral ganglion cells as shown by whole mount confocal microscopy (A. Nile Red signal; B. FITC signal; C. merged signal). Neurofilament of the spiral ganglion cell was seen with a specific antibody using a whole mounting method (arrow), nuclear localization of LNCs was detected, though infrequently (broad arrow) (D). LNCs reached the inner hair cells as shown by three-dimensional imaging using F-actin staining (arrow) (E, front view; F, lateral view). There was also uptake in the pillar cells as shown by F-actin staining (arrow) (G). However, after neurofilament staining (arrow), LNCs were invisible in the organ of Corti (H). There was also a distribution of LNCs in the lateral wall (I–K). Spiral ligament localization was confirmed by cryosection (arrow) (J); localization in the second turn of stria vascularis, especially intercellular junction site (arrow), was confirmed by F-actin staining (K, whole mount). LNCs were not visible in the basal turn after staining for F-actin (L, whole mount). Coagulated LNCs were detected in the stapes artery (M, whole mount). Only FITC was visible in some places, indicating the degradation of LNCs (arrow). The single cell image proved that the nanoparticles entered the cells (N). Scale bar = 8.5 μm.

brane until the end of the experiment). The abundant accumulation of LNCs in the round window membrane including the matrix and cytoplasm was detected on the constant delivery side [Figure 4(A)], while only a few LNCs were visible inside the cytoplasm after transient delivery [Figure 4(B)]. Concomitantly, more LNCs reached the hair cells which were continuous with the tunnel fibers [Figure 5(A–D)]. The number of LNCs in the spiral ganglion cells and spiral ligament also increased. Most LNCs accumulated around (but did not enter) the nuclei, although spiral ganglion cells had the quickest uptake during the first 30 min [Figures 2(A–C) and 5(E–H)]. LNCs were also detected in the vestibule, including the semicircular canal and macula utricle.

LNCs remained in the spiral ganglion, including the neuron and nerve fibers, organ of Corti, and lateral wall seven days after round window membrane delivery (Fig 6). Some of the Nile Red and FITC lost co-localization, which indicated degradation of the LNCs.

DISCUSSION

In the present study, we demonstrate that LNCs pass the round window membrane, penetrate the cochlear membranous partitions, and are incorporated into various cell types within the cochlea. The pathway that the nanoparticles use in passing through the round window membrane could be either via endocytosis or through a nonendocytotic pathway such as those seen in nonviral gene delivery.[19] Our data showed that there was abundant accumulation of LNCs in the round window membrane, including the matrix and cytoplasm on the side of constant delivery [Figure 4(A)], while few LNCs were visible inside the cytoplasm after transient delivery. We suppose that the nonendocytosis pathway, the so-called "paracellular pathway," seems to be the main channel for the LNCs to penetrate the round window membrane. The rapid incorporation of LNCs in the spiral ganglion cells, organ of Corti, and lateral wall upon delivery to the round window membrane can be explained by a paracellular pathway.

The rapid accumulation of LNCs in the spiral ganglion cells indicated that the most likely pathway is directly through the porous modiolar wall of the scala tympani.[20] The uptake of LNCs in the tunnel fibers may originate from either the spiral ganglion or the basilar membrane. The inner and outer hair cells are innervated by afferent nerve fibers that come from spiral ganglion cells and efferent nerve fibers that come from the superior olivary complex. Approximately 90% of the afferent nerve fibers end in synaptic boutons on the inner hair cell bodies (the inner

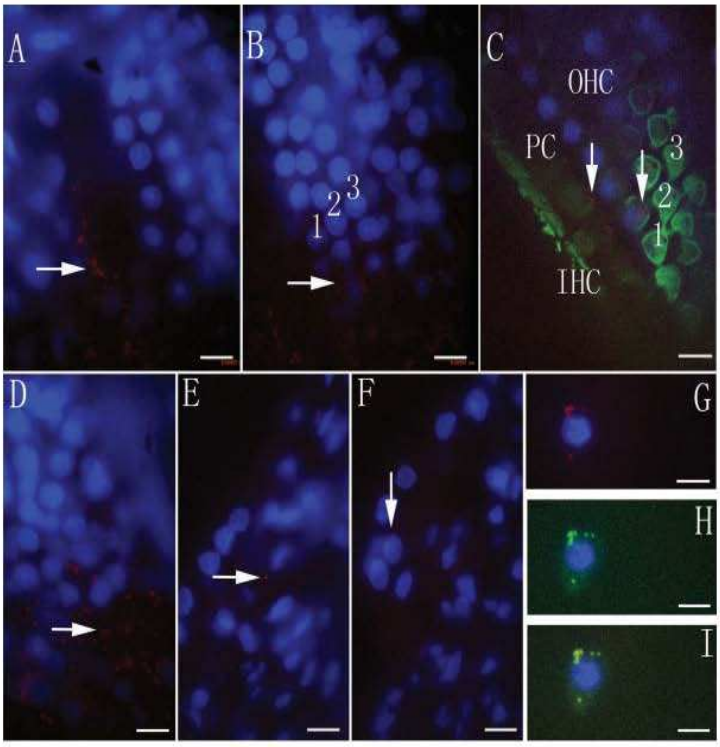

Figure 3. Nanoparticles diffused further 1 h after administration. LNCs were visible in the tunnel fibers (arrow) (A), pillar cells (PC) and the outer hair cells (OHC) in the organ of Corti (arrow) (B, C), and lateral wall (D–F). The cell population was confirmed by F-actin staining (C). LNCs were primarily located in the matrix of the lateral wall (arrow) (D). The spiral ligament fibrocytes type V, which are adjacent to the scala vestibuli, showed uptake of nanoparticles (arrow) as demonstrated by cryosection (E). LNCs also diffused to the spiral prominence (arrow) as showed by cryosection (F). The uptake of nanoparticles in the inner hair cells was further demonstrated by isolated single cell imaging (G, Nile Red signal; H, FITC signal; I, merged signal). IHC, inner hair cells; the numbers 1, 2, and 3 refer to the outer hair cells row 1, row 2, and row 3. Scale bar = 8.5 μm. [Color figure can be viewed in the online issue, which is available at www.interscience.wiley.com.]

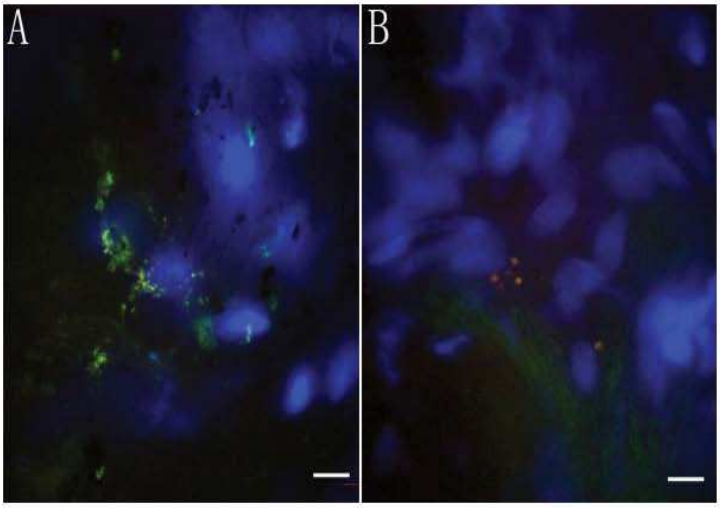

Figure 4. Round window membrane permeation of LNCs. Abundant LNCs were present throughout the round window membrane during constant 24 h administration (A). Only a few particles were detectable 24 h after transient delivery (LNCs were placed on the round window membrane for 30 min) (B). Scale bar = 6.8 μm. [Color figure can be viewed in the online issue, which is available at www.interscience.wiley.com.]

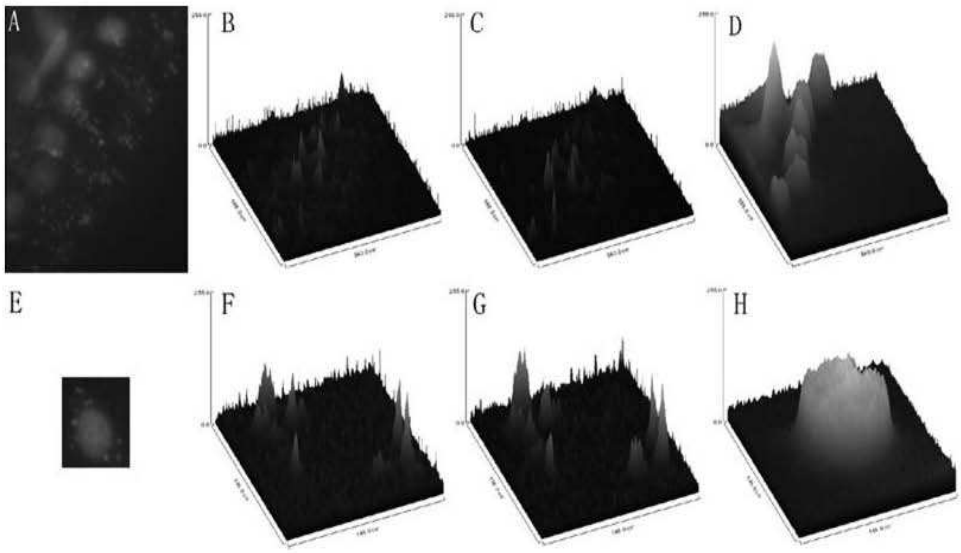

Figure 5. Distribution of LNCs in the organ of Corti and spiral ganglion cells was demonstrated by 3D scanning. Continuing through the tunnel fibers, nanoparticles reached the inner hair cells (A). Surface plot from a single slice showed the close spatial relationship between LNCs (B. FITC signal; C. Nile Red signal) and the nuclei of inner hair cells (D. DAPI of the nuclei). The perinuclear localization of LNCs in the spiral ganglion cell (E) was proven by surface plot of a single slice (F, FITC signal; G, Nile Red signal; H, DAPI signal of the nucleus). The samples were taken 24 h post-round window membrane administration of LNCs.

radial bundles). Only 10% of the afferent nerve fibers innervate the outer hair cells (the tunnel radial bundles, tunnel crossing bundles).[21] Efferent innervation of auditory hair cells is provided by the fibers of the lateral olivocochlear bundle to inner hair cells and the medial olivocochlear bundle (also referred to as efferent tunnel fibers) to outer hair cells. Efferent nerve fibers of the lateral system contact the synapses of the radial afferents on the inner hair cells and the medial system the outer hair cells directly (reviewed by Raphael and Altschuler).[22] Because it is hard to verify the different bundles with whole mount material imaging and their role for LNC transport is potentially the same, we can simply call the nerve fibers passing through the inner tunnel of the organ of Corti "tunnel fibers." Tunnel fibers, together with nerve fibers innervating the inner hair cells, pass through Rosenthal's canal. LNCs on the surface of nerve fibers can also freely diffuse between different fibers including afferent and efferent nerve fibers and migrate along the longitude of the nerve fibers. The disappearance of LNCs from the tunnel fibers after long time incubation with solu-

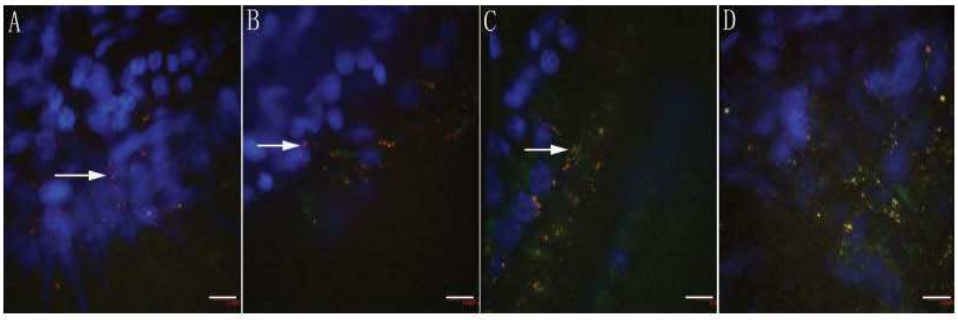

Figure 6. LNCs remained in the cochlea 7 days post-transient round window membrane administration. The LNCs were placed on the round window membrane for 30 min and then removed. LNCs presented along the neurofilaments from Rosenthal's canal (arrow) (A) to the tunnel fibers and were in contact with hair cells (arrow) (B, C). There was also rich accumulation of LNCs in the lateral wall (D). Scale bar = 8.5 μm. [Color figure can be viewed in the online issue, which is available at www.interscience.wiley.com.]

tions indicates their surface location. The delayed distribution of LNCs in the hair cells may come from the spiral ganglion, the tunnel fibers, and the Corti's liquid. The gradient uptake of LNCs from the inner hair cells to the outer hair cells (i.e., quicker and greater uptake in the inner hair cells than that in the outer hair cells) suggests that LNCs chiefly comes from the spiral ganglion area via Rosenthal's canal because of more intense innervation and a shorter distance to the inner hair cells. We call this the "nerve pathway." The recirculation of potassium from hair cells back to endolymph mainly takes a pathway from the supporting cells to the stria vascularis via different channels.[23] LNCs may also travel through the retrograde pathway from the stria vascularis to Corti's liquid because there is a rapid, intense uptake of LNCs in the stria vascularis. This possible pathway seems to be much slower than the "nerve pathway" because we did not find LNCs inside Hensen's cells, Deiter's cells, and outer hair cells, while they appeared in the inner hair cells at the 30-min time point. Our results suggest that LNC is a promising vector to deliver drugs to the spiral ganglion cells and hair cells.

The vestibular distribution of LNCs may originate from the spiral ligament, which was shown in MRI using Gd-DTPA-BMA as a tracer.[6] The uptake of LNCs in the spiral ligament fibrocyte type V, which is in contact with the perilymph in the scala vestibule, provides evidence for this pathway.[24,25] There is a possibility that drugs can also reach the vestibule by applying LNCs to the round window membrane.

A slower communication between different winding was reported in the guinea pig cochlea using Gd-DTPA-BMA enhanced MRI.[6] The present data acquired from rat cochlea using LNCs and confocal microscopy suggests a much faster longitudinal communication. This can be explained by different behaviors of the LNCs and a more sensitive detection by confocal microscopy.

The distribution of LNCs in the middle ear mucosa and stapes artery wall compromises the relative cell population selectivity of our LNCs. This can be further overcome by limiting the LNCs in the area of the round window. It is easier to achieve in humans because the round window area is much larger than that in rats.

CONCLUSIONS

This study describes the migration of LNCs through the round window membrane and cochlear partitions, finally reaching the inner ear cell populations. LNCs were manufactured by a novel phase inversion-based process. After round window membrane administration, LNCs reached the spiral ganglion, including the neuron and nerve fibers, organ of Corti, and lateral wall, within 30 min. The main pathway for LNCs to reach hair cells was the "nerve pathway," that is, diffusion from perilymph in the scala tympani to the spiral ganglion, continuing with nerve fibers inside Rosenthal's canal to approach the inner hair cells and pillar cells, and finally the outer hair cells. The "paracellular pathway" is the main approach for LNC penetration of the round window membrane. LNCs can also reach the vestibule, middle ear mucosa, and the adjacent artery. This suggested that LNC is a potential vector for delivery of drugs and proteins to the spiral ganglion, hair cells, and the lateral wall.

We are grateful to Mr. Peter Martinsson for his technical support in confocal microscopy.

REFERENCES

1. El-Hakim H, Abdolell M, Mount RJ, Papsin BC, Harrison RV. Influence of age at implantation and of residual hearing on speech outcome measures after cochlear implantation: binary partitioning analysis. Ann Otol Rhinol Laryngol Suppl 2002;189:102–108.
2. Gantz BJ, Woodworth GG, Knutson JF, Abbas PJ, Tyler RS. Multivariate predictors of audiological success with multichannel cochlear implants. Ann Otol Rhinol Laryngol 1993; 102:909–916.
3. Osberger MJ, Zimmerman-Phillips S, Koch DB. Cochlear implant candidacy and performance trends in children. Ann Otol Rhinol Laryngol Suppl 2002;189:62–65.
4. Geers A, Brenner C, Nicholas J, Uchanski R, Tye-Murray N, Tobey E. Rehabilitation factors contributing to implant benefit in children. Ann Otol Rhinol Laryngol Suppl 2002;189:127–130.
5. Rejali D, Lee VA, Abrashkin KA, Humayun N, Swiderski DL, Raphael Y. Cochlear implants and ex vivo BDNF gene therapy protect spiral ganglion neurons. Hear Res 2007;228(1-2):180–187.
6. Zou J, Pyykko I, Bjelke B, Dastidar P, Toppila E. Communication between the perilymphatic scalae and spiral ligament visualized by *in vivo* MRI. Audiol Neurootol 2005;10:145–152.
7. Salt AN. Pharmacokinetics of drug entry into cochlear fluids. Volta Rev 2005;105:277–298.
8. Jero J, Mhatre AN, Tseng CJ, Stern RE, Coling DE, Goldstein JA, Hong K, Zheng WW, Hoque AT, Lalwani AK. Cochlear gene delivery through an intact round window membrane in mouse. Hum Gene Ther 2001;12:539–548.
9. Maeda Y, Fukushima K, Kawasaki A, Nishizaki K, Smith RJ. Cochlear expression of a dominant-negative GJB2(R75W) construct delivered through the round window membrane in mice. Neurosci Res 2007;58:250–254.
10. Hoffer ME, Balough B, Henderson J, DeCicco M, Wester D, O'Leary MJ, Kopke R. Use of sustained release vehicles in the treatment of Meniere's disease. Otolaryngol Clin North Am 1997;30:1159–1166.
11. Kopke RD, Hoffer ME, Wester D, O'Leary MJ, Jackson RL. Targeted topical steroid therapy in sudden sensorineural hearing loss. Otol Neurotol 2001;22:475–479.
12. Van Wijck F, Staecker H, Lefebvre PP. Topical steroid therapy using the Silverstein Microwicktrade mark in sudden sensorineural hearing loss after failure of conventional treatment. Acta Otolaryngol 2007;127:1–6.
13. Praetorius M, Brunner C, Lehnert B, Klingmann C, Schmidt H, Staecker H, Schick B. Transsynaptic delivery of nanoparticles to the central auditory nervous system. Acta Otolaryngol 2007;127:486–490.
14. Lamprecht A, Bouligand Y, Benoit JP. New lipid nanocapsules exhibit sustained release properties for amiodarone. J Control Release 2002;84(1-2):59–68.

15. Heurtault B, Saulnier P, Pech B, Proust JE, Richard J, Benoit JP. Nanocapsules lipidiques, procédé de préparation et utilisation comme médicament, Patent No. 0002688000, 2000.
16. Heurtault B, Saulnier P, Pech B, Proust JE, Richard J, Benoit J-P. A novel phase inversion-based process for the preparation of lipid nanocarriers. P Pharmaceutical Res 2002;19:875–880.
17. Khalid MN, Simard P, Hoarau D, Dragomir A, Leroux JC. Long circulating poly(ethylene glycol)-decorated lipid nanocapsules deliver docetaxel to solid tumors. Pharm Res 2006;23:752–758.
18. Araki S, Mizuta K, Takeshita T, Morita H, Mineta H, Hoshino T. Degeneration of the stria vascularis during development in melanocyte-deficient mutant rats (Ws/Ws rats). Eur Arch Otorhinolaryngol 2002;259:309–315.
19. Khalil IA, Kogure K, Akita H, Harashima H. Uptake pathways and subsequent intracellular trafficking in nonviral gene delivery. Pharmacol Rev 2006;58:32–45.
20. Rask-Andersen H, Schrott-Fischer A, Pfaller K, Glueckert R. Perilymph/modiolar communication routes in the human cochlea. Ear Hear 2006;27:457–465.
21. Santi PAMP. Cochlear anatomy and central auditory pathways. In: Cummings CW, Fredrickson JM, Harker LA, Krause CJ, Richardson MA, Schuller DE, editors. Otolaryngol Head Neck Surg 1998;4:2803–2830.
22. Raphael Y, Altschuler RA. Structure and innervation of the cochlea. Brain Res Bull 2003;60(5/6):397–422.
23. Hibino H, Kurachi Y. Molecular and physiological bases of the K+ circulation in the mammalian inner ear. Physiol (Bethesda) 2006;21:336–345.
24. Spicer SS, Schulte BA. Differentiation of inner ear fibrocytes according to their ion transport related activity. Hear Res 1991;56(1/2):53–64.
25. Spicer SS, Schulte BA. The fine structure of spiral ligament cells relates to ion return to the stria and varies with place-frequency. Hear Res 1996;100(1/2):80–100.

II.2) Deuxième étude

Cette étude est le fruit de la collaboration entre notre équipe et l'équipe du Pr Timo Stover de l'université de Hanovre, Allemagne. Tout d'abord l'aptitude des LNCs à pénétrer les cellules a été évaluée sur culture de cellules L929 (fibroblastes de souris). Les LNCs pénètrent dans les cellules quelle que soit leur étape du cycle cellulaire et sont présentes dans le cytoplasme des cellules. Aucune présence dans le noyau n'a été détectée, ce qui est analogue aux résultats obtenus au sein de notre laboratoire. La quantité de LNCs pénétrant les cellules est comprise entre 1,4% et 2,4% du total des LNCs introduites (pour des dilutions au 1/10 et au 1/1000 de la suspension initiale, respectivement). La vitalité cellulaire n'est pas modifiée pour des dilutions au 1/300 et au 1/1000. Par contre, pour des suspensions plus concentrées de LNCs, une chute de la vitalité cellulaire est observée et laisse à penser que les LNCs sont toxiques : ceci n'est pas étonnant en regard de la quantité de molécules tensioactives mise en jeu.

En ce qui concerne la distribution des LNCs au sein de l'oreille interne, la microscopie confocale de fluorescence nous permet d'affirmer que les LNCs ont pénétré les cellules de la strie vasculaire, les cellules de soutien de la membrane basilaire ainsi que les cellules ciliées, quelles soient internes (Inner Hair Cells-IHCs) ou externes (Outer Hair Cells-OHCs).

Une observation rapprochée des cellules ciliées confirme que les LNCs sont dans le cytoplasme sans aucune pénétration nucléaire et que LNCs n'ont pas entraîné de mort cellulaire au sein des cellules ciliées, les échantillons observés ne présentant pas de trous dans les rangées de cellules ciliées.

De plus, les études de physiologie auditive montrent que les seuils d'audition ne sont pas perturbés suite à l'exposition aux LNCs. L'ensemble de ces arguments nous permet de

penser que les LNCs sont un vecteur de choix pour la délivrance de médicaments au sein de l'oreille interne, tout au moins chez l'animal.

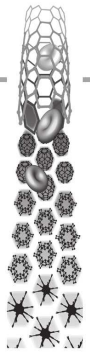

RESEARCH ARTICLE

Potential novel drug carriers for inner ear treatment: hyperbranched polylysine and lipid nanocapsules

Treatment of sensorineural hearing loss could be advanced using novel drug carriers like hyperbranched polylysine (HBPL) or lipid nanocapsules (LNC). This study examined HBPL and LNC for their cellular uptake and possible toxicity *in vitro* and *in vivo* as the first step in developing novel nanosized multifunctional carriers. Having incubated HBPL and LNC with fibroblasts, nanoparticle uptake and cell viability were determined by confocal laser scanning microscopy, fluorescence measurements and neutral red staining. *In vivo*, electrophysiology, confocal laser scanning microscopy and cytocochleograms were performed for nanoparticle detection and also toxicity studies after intracochlear application. Both nanoparticles were detectable in the fibroblasts' cytoplasm without causing cytotoxic effects. After *in vivo* application they were visualized in cochlear cells, not leading to a change of hearing threshold or loss of hair cells. Biocompatibility and traceability were demonstrated for HBPL and LNC. Thus, they comply with the basic requirements for drug carriers for potential application in the inner ear.

KEYWORDS: acoustically evoked auditory brainstem response biocompatibility cochlear drug carrier gene delivery hair cells inner ear nanoparticle

Verena Scheper[1*†], Melanie Wolf[1*], Markus Scholl[2], Zuzana Kadlecova[2], Thomas Perrier[3], Harm-Anton Klok[2], Patrick Saulnier[3], Thomas Lenarz[1] & Timo Stöver[1]

[†]Author for correspondence:
[1]Department of Otolaryngology, Medical University Hannover, Carl-Neuberg-Str. 1, 30625 Hannover, Germany
Tel.: +49 051 1532 4369; Fax: +49 051 1532 3293; scheper.verena@mh-hannover.de
[2]École Polytechnique Fédérale de Lausanne, Institut des Matériaux, Laboratoire des Polymères, MXD 135 (Bâtiment MX-D), Switzerland
[3]Université Angers – INSERM U646, Laboratoires Annuaires Ingénierie de la Vectorisation Particulaire, France
**Both contributed equally to this work.*

Damage to sensory hair cells, nerve fibers and/or the supporting cells (pillar cells or cells of stria vascularis) of the inner ear is one of the leading causes of hearing loss. Clinically, up to the present day, no treatment has been made available for patients suffering from hair cell loss to physically regenerate these cells in order to restore hearing function.

In order to develop cause-related therapy strategies to treat these disorders, local inner ear delivery of drugs or genes is required. Potential biological molecules for future local inner ear therapies may include nucleic acids (e.g., plasmid DNA, antisense oligonucleotides or siRNAs) [1,2] or proteins (monoclonal antibodies, growth factors or hormones) [3].

In animal experiments, viral vectors have been identified that successfully deliver encoded genes, neurotrophic factors or cell cycle proteins to the inner ear [4,5]. These interventions demonstrate protective and even regenerative effects on inner ear cells [6]. Although effective, these adenoviral vectors also present many disadvantages. First, they deliver their genes nonspecifically to a restricted number of cochlear cell types, resulting in a limited distribution of the gene inside the cochlea. Second, viral vectors have the potential to induce inflammatory and immunological reactions following inner ear application [7,8]. In addition, multiple viral applications to the inner ear will be required to maintain the biological effect, because the transgene expression is transient. Thus, alternative drug or gene carriers for inner ear application are required.

Nonviral vectors present an interesting alternative to viral vectors to deliver drugs or genes to the inner ear structures [9,10]. Chemically synthesized from lipids, peptides or polymers, they combine many advantages [11]. They are noninfectious, safe, cheap to manufacture and can be produced in large quantities. These constructs can be modified for surface and core charge to affect the surface adhesion and drug-carrying characteristics. These capabilities allow them to vary their biological behavior to a large extent. In addition, these particles can be synthesized with nanosized dimensions, so-called 'nanoparticles' (NPs), allowing them to directly interact with cell components. Finally, NPs can be biologically functionalized by attaching receptor-binding ligands for cell targeting and labeling onto the particle surface [12].

One of the limitations of nonviral gene delivery systems is their toxicity, and therefore much effort is involved in preparing carriers that have lower or no toxicity.

Previously, poly(lactic-co-glycolic acid) [13] and silica NPs have been applied intravenously, intravitreously and to the round window as nonviral vectors with no toxicity observed [14–17]. Lipid nanocapsules (LNCs) have already been evaluated concerning their biocompatibility and stealth properties by measuring complement

10.2217/NNM.09.41 © 2009 Future Medicine Ltd *Nanomedicine* (2009) **4**(6), xxx–xxx ISSN 1743-5889

activation and macrophage uptake [18,19]. In these first studies, LNCs were found to be attractive for intravenous and intraperitoneal applications because of their monodispersed submicron-sized structure and biocompatibility. Very low complement activation and macrophage uptake, combined with high drug loading possibilities and prolonged drug release over a significant period of time in the case of amiodarone, led to inner ear application research [20]. Zou and colleagues were able to detect LNCs in the inner ear tissue after round window membrane permeation assuming a paracellular pathway [21].

This study represents *in vitro* and *in vivo* experiments assessing the cell uptake and toxicity, as well as the influence on inner ear functionality, of hyperbranched polylysine (HBPL) compared with LNCs. The morphological and functional results of this study provide evidence for the potential of these NPs as novel drug carriers for inner ear treatment.

Materials & methods

Experimental design

In this study, two fluorescein-5-isothiocyanate (FITC)-tagged NPs, HBPL and LNCs, were examined for their cell uptake and toxic effects in *in vitro* and *in vivo* experiments.

In vitro experimental design

For visualization of FITC-tagged particles in cultured cells, confocal laser scanning microscopy (CLSM) was used. Cells were fixed with paraformaldehyde and stained with rhodamine phalloidin and 4′,6-diamidino-2-phenylindol (DAPI). Sequential excitation of the three dyes was used to detect the NPs (FITC), the cell nucleus (DAPI) and the actin filaments (rhodamine phalloidin). Furthermore, concentration-dependent fluorescence measurements were performed with a microplate fluorometer. NP uptake was calculated and the cell viability was examined using vital staining with neutral red.

Table 1. Different experimental groups and their treatments.

Groups	Acoustically evoked auditory brainstem response			
	Experimental day			
	Day 0	*Day 2*	*Day 14*	*Day 28*
HBPL day 2	X	X, †		
HBPL day 14	X	X	X, †	
HBPL day 28	X	X	X	X, †
LNC day 2	X	X, †		
LNC day 14	X	X	X, †	
LNC day 28	X	X	X	X, †

HBPL and LNCs were delivered unilaterally into the left scala tympani of n = 18 guinea pigs for each nanoparticle on experimental day 0. In all animals the contralateral (right) ear underwent the same surgical approach and phosphate-buffered saline was applied. The survival period was 2 days (n = 6), 14 days (n = 6) and 28 days (n = 6). Auditory brainstem response measurements (indicated as 'X') were performed for all groups before surgery on day 0 and on day 2; for the 14-day and 28-day groups on day 14 and for the 28-day survival group on day 28. The day of sacrifice for each experimental group is marked †.
HBPL: Hyperbranched polylysine; LNC: Lipid nanocapsules.

In vivo experimental design

In this study we examined two nanosized structures for their distribution and toxicity in the inner ear at three different time points following inner ear application. Guinea pigs underwent unilateral injection of LNCs or HBPL via a cochleostomy. In parallel, phosphate-buffered saline (PBS) was applied to the contralateral ear of the same animal, in order to control for potential hearing loss due to the surgical intervention itself (control ear).

Animals received either LNCs (n = 18) or HBPL (n = 18). In each of these two groups, six animals were sacrificed after 2, 14 and 28 days. Table 1 presents an experimental design overview of the *in vivo* experiments. Determination of possible toxic effects to the inner ear structures was performed by measuring the acoustically evoked auditory brainstem response (AABR) and counting lost hair cells quantitatively (cytocochleogram). In addition, CLSM was used to detect NPs in the cochlear cells.

Lipid nanocapsules

The 'Laboratoires Annuaires Ingénierie de la Vectorisation Particulaire' of the University of Angers (Angers, France) used a novel phase inversion-based method [22] to formulate LNCs that were composed of a liquid core surrounded by a cohesive interface and were dispersed in an aqueous medium (Figure 1). The oily phase was composed of the lipophilic Labrafac® WL 1349 (Gattefossé SA, Saint-Priest, France) made of capric and caprylic acid triglycerides. The aqueous phase consisted of NaCl purchased from Prolabo (Fontenay-sous-Bois, France) and water obtained from a Milli-Q-plus® system (Millipore, Paris, France). Two tensioactive surfactants were necessary for LNC preparation: Lipoïd® S75–3 (Lipoïd GmbH, Ludwigshafen, Germany), a soybean lecithin made of 69% phosphatidylcholine, 10% phosphatidylethanolamine and other phospholipids; and Solutol® HS 15 (BASF, Ludwigshafen, Germany), a mixture of free polyethylene glycol (PEG) 660 and PEG 660 hydroxystearate. The optimal amounts of ingredients for preparation of 50 nm LNCs were: 1.028 g of Labrafac®, 0.075 g of Lipoïd®, 0.846 g of Solutol®, 0.089 g of NaCl and 2.962 g of pure water. To obtain

an emulsion of oil-in-water, all components were mixed under magnetic stirring at an agitation speed of 200 r.p.m. at room temperature. After progressive heating at a rate of 4°C/min, a short interval of transparency at temperatures close to 70°C could be observed, and the inverted phase (water droplets in oil) was obtained at 85°C. At least three temperature cycles, alternating from 60 to 85°C at the same rate, were applied near the phase inversion zone to obtain a stable water-in-oil emulsion. Thereafter, the mixture underwent a fast-cooling dilution process: it was diluted 1:3.5 with 12.5 ml cold water at 2°C and stirred for 30 min, leading to the formation of LNCs with the desired size.

To reach a high density of PEG at the surface, 1.75 ml LNCs (10^{17} particles/ml) were incubated for 105 min at 60°C with 1.3 ml aqueous micellar solution (15 mg/ml) of 1,2-distearoyl-*sn*-glycero-3-phosphoethanolamine-*N*-[amino(polyethylene-glycol)2000] (DSPE–PEG2000–amino) furnished by Avanti® Polar Lipids, Inc. (Alabaster, USA) [23]. The suspension was vortexed every 15 min and then quenched in an ice bath for 1 min. The final DSPE–PEG concentration corresponded to 6 mol% of total surface molecules.

After this DSPE–PEG2000–amino post-insertion process, the LNCs have to be labeled with FITC, purchased from Fluorescéine IsoThioCyanate (France). Therefore, FITC was added to 2.95 ml of LNC suspension and the pH was increased to 9 by adding a few drops of 0.1 M Na_3PO_4 solution. The sample was protected from light and placed in a water bath under magnetic stirring at 37°C for 45 min. After the sample was cooled in an ice bath for 3 min in order to stop the reaction, size exclusion chromatography on a sephadex G-25 column was performed to separate free FITC from labeled LNCs. Optical density (FITC detection) as well as turbidity at 680 nm (LNC detection) was measured for each fraction. Dynamic light scattering analysis and electrokinetic measurements finally indicate a hydrodynamic diameter of 52 ± 5 nm and a ζ-potential of -55 ± 7 mV, whereas only fractions with a polydispersity index lower than 0.2 were pooled and finally used for experiments, so that absolute NP numbers could be given. The final concentration of the LNC solution is 9.5×10^{14} particles/ml.

The LNC suspensions were kept in different electrolyte solutions (NaCl, $CaCl_2$, KCl and phosphate buffer) for concentrations in the range 10^{-5}–10^{-2} M. The aging was also evaluated at different pH (3, 7.4 and 10). No hydrodynamic size and ζ-potential modification (data not shown) prevail over a period of 3 months, indicating a colloidal stability without flocculation or Ostwald ripening in these conditions.

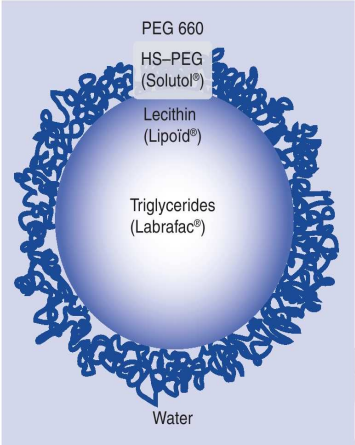

Figure 1. Fluorescein-5-isothiocyanate-modified lipid nanocapsule.
HS: ; PEG: Polyethylene glycol.

Hyperbranched polylysines

A sample of HBPL (M_n: 24600 g/mol, PDI: 12.5, hydrodynamic radius: 10 nm) was synthesized according to the procedure described by Scholl *et al.* [24]. The HBPL was modified with the fluorescent dye, FITC, following the manufacturer's recommendations: HBPL (500 mg, 0.034 mmol) was dissolved into stirring water (10 ml) and subsequently FITC (13.3 mg, 0.034 mmol) dissolved in dimethylformamide (2 ml) was added. The reaction mixture was stirred for 1 h at room temperature. Subsequent purification was carried out according to the procedure recommended by Seib *et al.* [25]. The final product was recovered in 85% yield as an orange powder. Before usage *in vitro* or *in vivo*, the powder was dissolved in PBS 1 mg/ml resulting in a molecular concentration of 4.1×10^{-5} mol/l. Because of the polydispersity of HBPL, the NP amount in the used solutions is given as a mole fraction and not as an absolute number. The sample of HBPL was analyzed by ^{1}H-NMR with Bruker Avance 400 spectrometer: ^{1}H-NMR (400 MHz, CD_3OD, 298 K): 7.42–7.30 (10 H, arom.), 4.24 (br, 1 H, COC<u>H</u>(R)NαH), 4.02 (br, 1 H, COC<u>H</u>(R)NαH), 3.33 (br, 1 H, COC<u>H</u>(R)N<u>α</u>H_2), 3.25 (br, 1 H, COC<u>H</u>(R)N<u>α</u>H_2), 3.18 (m, 2 H, C<u>H_2</u>-NεH), 2.74 (m, 2 H, C<u>H_2</u>-N<u>ε</u>H_2), 1.92–1.3 (br m, 6 H, CH_2). Steric exclusion chromatography was carried out

in 0.1 M $NaHCO_3$ eluent using Viscotek TDA Model 300 instrument and: M_N = 24600 g/mol; PDI = 10.

FIGURE 2 depicts the structure of HBPL labeled with fluorophore (fluorescein, highlighted with a box) via a thiourea bond (highlighted with an ellipse). It shows that fluorescein is attached via covalent bonds and not encapsulated in the structure of the carrier, nor entrapped by any other type of noncovalent interactions. This fact is important for the experiments, where tracking of the fluorophore is the only method to detect and localize HBPL. Covalent bonding is relatively the most stable attachment of fluorophore to HBPL, and allows fluorescent measurements and imaging over a relatively extensive period of time [25,26].

Cell culture experiments

Uptake and toxicity of NPs was first examined *in vitro* using the fibroblast cell line L929 (Gibco, Paisley, Scotland, UK). The cells were kept in Dulbecco's modified Eagle medium (Gibco) containing 10% fetal bovine serum, 2 mmol/l L-glutamic acid, 100 IU/ml penicillin and 100 kg/ml streptomycin (all components from Biochrom AG, Berlin, Germany) at 37°C and 5% CO_2.

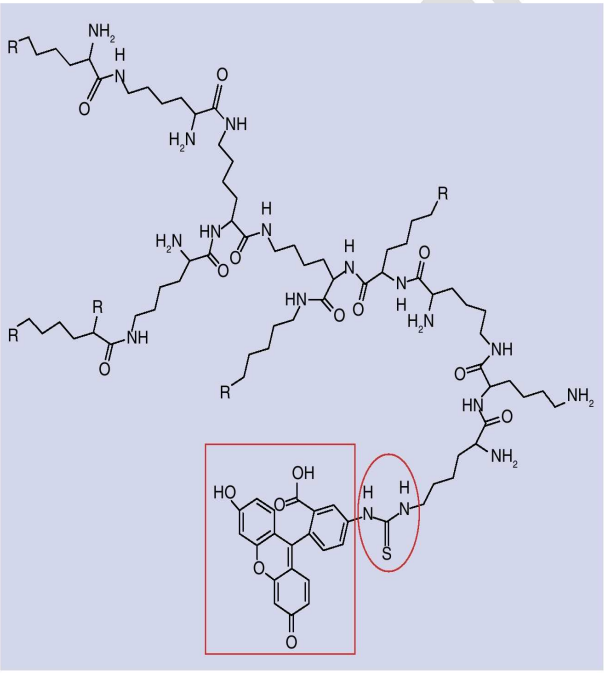

Figure 2. Hyperbranched poly-L-lysine labeled with fluorophore (fluorescein, highlighted with a box) via thiourea bond (highlighted with an ellipse).

Cell culture for CLSM

L929 cells were seeded at a density of 10^5 cells per well into 48-well plates (Becton Dickinson, Meylan Cedex, France) with glass platelets at the bottom (0.13 mm thickness). Cells were incubated for 24 h in 300 µl medium per well. To six wells 1.22×10^{-7} mmol HBPL and 2.85×10^{12} mmol LNCs (1:100 dilution of stock solution) were added. After 48 h of incubation at 37°C, the medium was evacuated and the wells were rinsed twice with PBS (Invitrogen, Gibco) before fixation for 10 min in 4% paraformaldehyde (Merck, Darmstadt, Germany). The cell membranes were permeabilized with Triton X-100 0.1% (Sigma-Aldrich Chemie GmbH Munich, Germany) for 3 min, whereupon the actin-filaments of the cells were stained with rhodamine phalloidin (Invitrogen, Eugene, Oregon, USA) by adding 200 µl PBS and 5 µl phalloidin per well and incubating for 30 min at room temperature. Finally, after rinsing twice with PBS, the glass platelets were removed from the wells and covers slipped on microscope slices with Prolong® Gold antifade reagent with DAPI (Invitrogen). After a 24 h drying period, the slides were used for CLSM.

Confocal laser scanning microscopy

Cells prepared as described previously were examined using CLSM (Leica TCS SP2, Leica Microsystems GmbH, Heidelberg, Germany) and sequential analysis was performed to visualize the three dyes. The following excitation filters were chosen: 405 nm for DAPI-stained nuclei; 488 nm for the FITC-labeled NPs; and 543 nm for the rhodamine-phalloidin-stained actin filaments. The corresponding emission spectra were 430–470 nm for DAPI, 500–540 nm for FITC and 570–610 nm for rhodamine-phalloidin. Finally, the different channels were overlain to detect the exact localization of the uptake of NPs. Photographs were taken electronically and saved as electronic files.

Fluorescence measurements

To quantify NP uptake by L929 cells, concentration-dependent fluorescence measurements with the microplate fluorometer Fluoroskan Ascent® and Ascent Software (Thermo Scientific, Milford, MA, USA) were performed at 480 nm excitation and 520 nm emission. The cells were seeded at a density of 10^4 per well into 96-well plates (Becton Dickinson, Meylan Cedex, France) and incubated for 24 h in 100 µl medium as described previously. Five different NP concentrations were applied to the cells: 1:10, 1:30, 1:100, 1:300 and 1:1000

(diluted in the medium) relating to the initial concentration of 4.1×10^{-8} mol/ml HBPL and 9.5×10^{14} LNCs/ml. The medium was removed after 24 h and replaced with PBS after rinsing all wells at least twice to eliminate all NPs not taken up by the cells. To calculate the number of NPs taken up, a dilution series of the original solution was measured and a calibration curve was generated based on these data. The slope of this graph was used to compute the NP number from the measured emission in the cells. Four replicate tests of fluorescence measurement were performed, each containing six wells per concentration for each NP.

Cytotoxicity test with neutral red assay

The experimental approach was the same as for the fluorescence measurements: 10^4 cells per well were seeded in a 96-well plate with 100 µl medium and the concentrations of NPs described previously, with the addition of a control group incubated without NPs. The neutral red solution was prepared by diluting the stock solution (4 mg/ml in water [Merck]) 1:50 with the medium. The medium in the well plate was removed 24 h after seeding and 100 µl neutral red solution was pipetted into the wells for a 3-h incubation period at 37°C. Afterwards, the staining solution was removed and the cells were fixed with 100 µl of a solution containing 0.5% formaldehyde and 1% $CaCl_2$ (both Merck) in distilled water. Having centrifuged the well plates for 5-min at 1000 G, the solution was changed: 100 µl per well with 1% acetic acid and 50% ethanol in distilled water was used for extraction. Good dispersion was reached by using an orbital shaker for 30 s and subsequently incubating for 10 min in the refrigerator. Photometric measurements were performed using an Ascent Multiskan with a 570 nm filter and Ascent Software (Thermo Scientific). To evaluate the cytotoxicity of the NPs, the measured values were compared with the control assay so that the quotient declared the percentage of vital cells in the assay. The averages for each NP concentration (four replicate tests, six wells per concentration) were finally compared with the values measured with the medium using two-sample t-test.

In vivo animal study

Animals

A total of 36 pigmented guinea pigs (Charles River WIGA GmbH, Sulzfeld, Germany), with normal Preyer reflexes were used for this study. All animal procedures were performed in accordance to the German law on protecting animals and the European Communities Council Directive 86/609/EEC for the protection of animals used for experimental purposes. All experiments were approved by the Institutional Animal Care and Research Advisory Committee at the Medical University Hannover and permitted by the regional government (LAVES, registration number 07/1266).

Anesthesia for animal procedures

The animals were anaesthetized with xylazine (10 mg/kg intramuscularly, Rompun® 2%, Bayer, Leverkusen, Germany) and ketamine (40 mg/kg intramuscularly, Ketamin Gräub®, Albrecht, Aulendorf, Germany) before surgery. All electrophysiological measurements and the sacrification of the animals were done with the same general anesthesia. In addition, local anesthesia with prilocain was used for the comfort of the animals (Xylonest®, AstraZeneca GmbH, Wedel, Germany).

Acoustic auditory brainstem responses

Hearing thresholds of the animals were determined just before NP application as well as at 2, 14 and 28 days after intervention. The animals were anaesthetized as described previously and placed on a heating pad in a soundproof chamber where they were exposed to tones via an ear speaker-tip system. The ear speaker-tip system was calibrated using a 0.25-inch pressure field microphone (ACO Pacific Inc., Belmont, CA, USA). The neurological responses were recorded using subdermal needle electrodes (1.0 M, Nicolet Biomedical, Inc., WI, USA) placed at the vertex (positive pole), at the left and right mastoid (negative pole) and in the neck (ground).

For frequency-specific AABR measurement, stimuli were controlled by a computer interfaced with TDT hardware (Tucker-Davis Technologies, Alachua, FL, USA) using Hugh Phonics software [27]. Two channels were chosen for stimulation, one for each ear, and six different frequencies were applied to acquire the hearing thresholds: 1, 4, 8, 16, 32 and 40 kHz. The acoustic tone pips were 10 ms in duration with a cosine-squared rise–fall time of 1 ms (200 kHz D/A sampling rate, 24-bit sigma-delta modulation). The recorded neural signals were digitized at a sampling rate of 24 kHz (16 bit) and bandpass filtered between 0.3 and 3 kHz. Depending on the hearing status of the animals, eight different levels were recorded between 0 and 100 dB sound pressure level (SPL) in 10 dB steps; 200–250 sweeps per stimulation were recorded and averaged. For visual data

interpretation on screen the single and double standard deviation (SD) for each measurement was calculated and the third peak of the signal evaluated. Hearing threshold was defined as the lowest stimulus level that generated a third peak exceeding two times SD.

NP application to the inner ear

The injection tube was prepared as described earlier [28]. After AABR measurement, animals were placed on a heating pad under aseptic conditions. A postauricular incision was made, the middle ear was opened to expose the middle ear cavity and the cochlea was visualized with the microscope OPMI®-6-M (Carl Zeiss AG, Oberkochen, Germany). Using a small lancet, a hole was drilled into the basal turn of the cochlea into the scala tympani. The tube and a 10 µl-Hamilton syringe (Hamilton Bonaduz AG, Bonaduz, Switzerland) were filled with the solution: PBS (Invitrogen, Gibco) for the right (control) ear and the NP solution diluted 1:100 with PBS for the left ear. The small polyimide tube was inserted into the scala tympani and 5 µl (PBS or 2.0×10^{-12} mol HBPL or 4.7×10^{10} LNCs) were injected over a time period of 10 min. The bony cochlear defect and the bulla were closed with carboxylate cement (Durelon®, ESPE Dental AG, Seefeld, Germany) before the wound was sutured in two layers.

Histology

To determine the survival of hair cells and to visualize potential cell uptake of NPs into cochlear cells, the inner ear tissue was examined histologically 2, 14 and 28 days after NP application. Following extraction of the temporal bone, the bulla wall and the bony cochlear wall were removed. After opening the round and oval window, the cochleae were fixated for 30 min in paraformaldehyde 4%, permeabilized in 0.1% Triton X-100 for 5 min, washed with PBS and stained for 1 h with rhodamine phalloidin (Invitrogen). For tissue preparation, the spiral ligament with the stria vascularis, as well as the basilar membrane (with removed excessive bone, Reissner membrane and tectorial membrane) were extracted in turn, put on a glass slide and coverslipped with ProLong® Gold antifade reagent with DAPI (Invitrogen). NP uptake was determined by CLSM, as described earlier. Potential toxicity to hair cells was determined by generating a cytocochleogram. Cells were visualized using a motorized fluorescence system (Olympus Europe GmbH, Hamburg, Germany) consisting of an inverted microscope (Olympus IX 81) equipped with a power supply unit (Olympus U-RFL-T) and a control box (Olympus IX2-UCB) connected to an imaging software (Analysis®, Soft Imaging System GmbH). Absence or presence of hair cells was assessed for the entire cochlea from the apex to the base, beginning at the point where the hair cells begin to display typical organization after 2 mm. According to Linss *et al.*, the mean basilar membrane length in guinea pig cochleae is 16.4 ± 1.4 mm (mean ± SD) containing an averaged hair cell density of 0.389 outer hair cells/µm (all three rows) and 0.101 inner hair cells/µm [29]. The basilar membrane was divided into 2 mm sections to be able to determine the percentage of missing hair cells in relation to the distance from the apex. Data were entered into a computer program (MS Excel) and mean and SD data were calculated for hair cell loss in each experimental group for NP-treated and PBS-treated ears for the different cochlear regions.

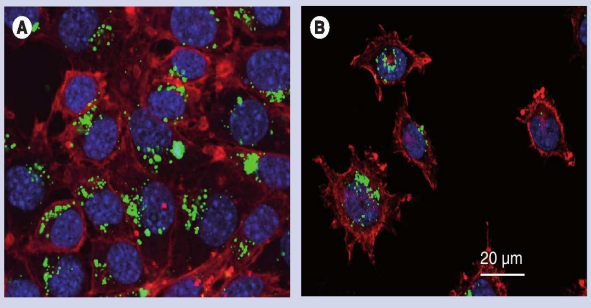

Figure 3. TITLE. Representative images of the uptake of fluorescein-5-isothiocyanate-labeled (green) hyperbranched polylysine **(A)** and lipid nanocapsules **(B)** in L929 mouse fibroblasts after 24 h incubation. Nuclei stained with 4′,6-diamidino-2-phenylindol (blue) and actin-filaments with rhodamine phalloidin (red).

Results

Cell culture study

Confocal laser scanning microscopy

A total of 24 h after particle application to L929 cell culture, HBPL and LNCs appeared in the cytoplasm near the nucleus. Particles seemed to form clusters and did not enter the nucleus, but appeared around it (Figure 3). Almost all cells were invaded by LNCs and HBPL, independent from the phase of cell cycle they were in and independent from other concentrations that were tried before.

Fluorescence measurement

Considering the absolute values, a decrease of NPs taken up by the fibroblasts was observed in relation to the dilution used. At a dilution of

1:10, 2.7×10^{-11} mol HBPL and 1.3×10^{11} LNCs were taken up by the cells. At a dilution of 1:1000 a decreased number of HBPL (4.1×10^{-13} mol) and LNCs (2.7×10^{9}) were taken up. By relating these numbers to the NP concentration in the incubating medium, it became obvious that the proportion of particles taken up by the cells did not decrease with further dilution of the NP solution, but remained constant (Figure 4). The amount of HBPL taken up by fibroblasts varies between 6.6% (SD ± 2.6%) at a dilution of 1:10 and 11.9% (SD ± 6.0%) at a dilution of 1:100, whereas the LNC uptake is between 1.4% (SD ± 1.2%) at a 1:10 dilution and 2.8% (SD ± 2.1%) at a 1:1000 dilution. There were no significant differences between the concentration-dependent NP uptakes; neither an increase nor decrease of NP uptake could be demonstrated.

Neutral red staining

The vitality tests with neutral red showed a reduction of vitality at high NP concentrations whereas lower concentrations had no toxic effect on cultured fibroblasts (Figure 5). Cells incubated with 9.51×10^{12} LNCs (dilution 1:10) reached a 39% vitality (SD ± 13%, $p = 0.001$), a dilution of 1:30 caused a cell vitality of 79% (SD ± 20%, $p = 0.001$) and cells incubated with a LNC dilution of 1:100 survived with a $p < 0.01$, statistically significant reduction of viability (89%, SD ± 22%). Higher LNC dilution did not result in statistically significant differences from the control assay ($p > 0.05$).

Incubated with 4.1×10^{-10} mol HBPL (dilution 1:10) the fibroblasts reached a 33% vitality related to the control group (SD ± 15%, $p < 0.001$), a 1:30 dilution led to 53% cell vitality (SD ± 14%, $p < 0.001$) and a 1:100 NP dilution led to 73% cell vitality, which is also a statistically significant reduction of cell viability (SD ± 10%, $p < 0.001$). Further HBPL dilution had no significant toxic effect on the incubated cells.

Additionally, the fibroblasts incubated with high NP concentrations presented morphological changes: the cells appeared smaller, rounded and more granulated than the more vital ones, but the cell number was nearly the same.

From these findings, it was concluded that a dilution of 1:100 for the NP stock solution would be appropriate for cochlear application in the following animal experiments. Therefore, enough NPs were applied to the scala tympani to ensure their visualization in the tissue and cell vitality may potentially not be decreased *in vivo*.

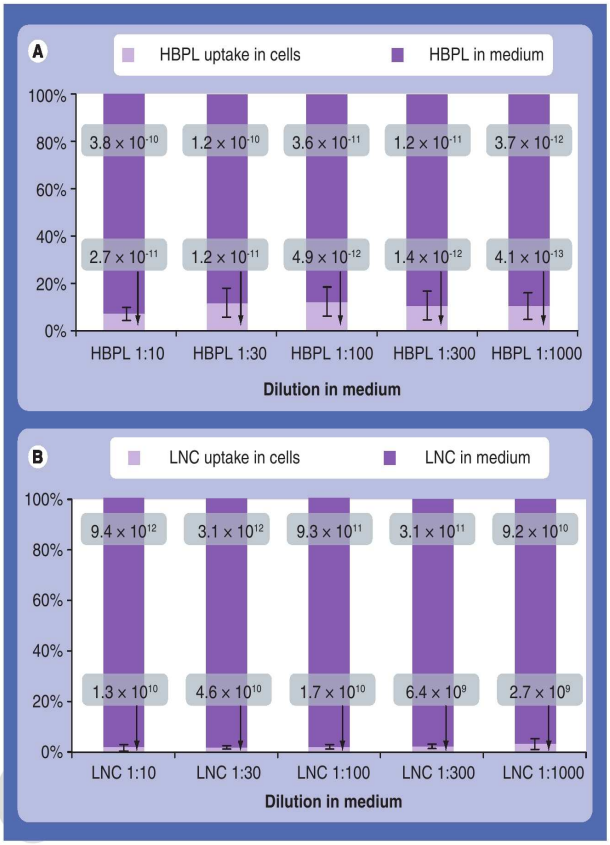

Figure 4. Quantification of nanoparticle uptake into the L929 fibroblasts by fluorescence measurements. The the absolute number of nanoparticles (NPs) taken up decreases with higher dilution, but in relation to the NP concentration in the incubating medium the NP uptake remains constant. **(A)** Uptake of HBPLs in L929. **(B)** Uptake of LNCs in L929. The upper small boxes contain the measured NP concentration in the medium, whereas the lower small boxes indicate the concentration of NPs which were incorporated in the cells.
HBPL: Hyperbranched polylysine; LNC: Lipid nanocapsule.

Animal study

Six out of 36 animals had to be excluded from the study owing to middle ear infection. One animal of each group was affected so that in the end five guinea pigs per group could be analyzed for each NP (HBPL and LNCs) and each time period (2, 14 and 28 days) – altogether 30 animals.

Confocal laser scanning microscopy

In all animals sacrificed after 2 days, we observed internalization of NPs under CLSM, which shows the uptake of HBPL and LNCs into inner and outer hair cells, pillar cells and cells of the stria vascularis. The uptake into inner hair cells seemed to exceed the uptake into outer hair cells, but was equivalent to the fluorescence detected in the supporting cells or stria vascularis when

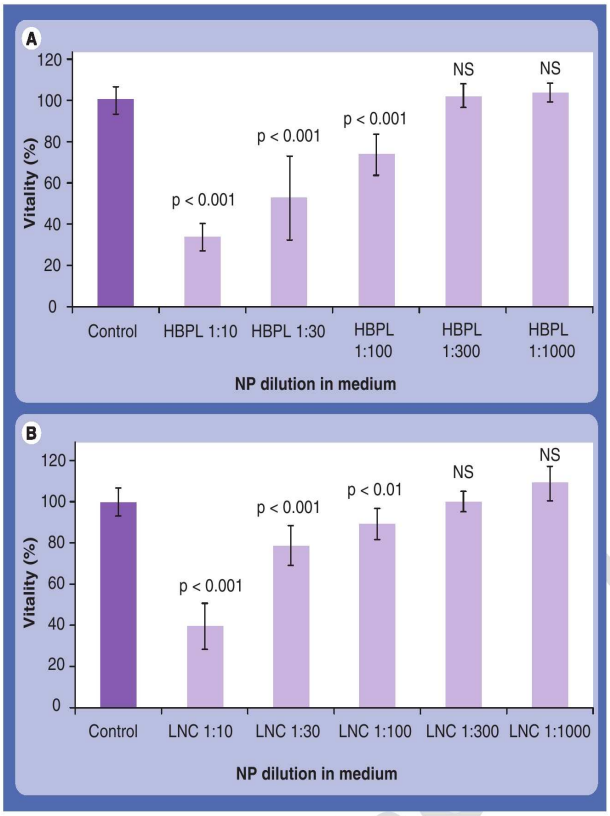

Figure 5. Results of the cell vitality tests with neutral red assay after NP application. (A) Cell vitality after incubation with HBPL. **(B)** Cell vitality after incubation with LNC. The cytotoxicity tests show toxic effects in high NP concentrations that are significant up to a dilution of 1:100 for LNCs as well as for HBPL. Further NP dilution did not lead to a significant reduction in cell vitality (NS). Statistically significant differences in cell viability compared with the controls are plotted as p-values above each column.
HBPL: Hyperbranched polylysine; LNC: Lipid nanocapsule; NP: Nanoparticle; NS: Not significant.

visually comparing the different cell populations. Both particles maintained fluorescence in these inner ear structures after 14 and 28 days, without any difference in distribution (Figure 6). Overlay of images taken at different excitation and emission wavelengths made it possible to detect the uptaken NPs accumulated in the cytoplasm near the nucleus, where they appeared to form clusters. No uptake to nuclei was observed.

Quantitative assessment of hair cell loss (cytocochleogram)

The cytocochleograms obtained from the HBPL-treated left cochleae revealed a mean hair cell loss of 0.003% ± 0.007% SD in the 2-day group, 0% in the 14-day group and 0.101 ± 0.119% in the 28-day group (Figure 7). The LNC-treated cochleae exhibited a mean inner and outer hair cell loss of 0.018 ± 0.031% in the cytocochleogram of the 2-day survival group, 0.024 ± 0.023% in the 14 day group and 0.021 ± 0.023% in the 28 day group. The hair cell loss appeared to be more evident near the apex, but did not exceed a maximum of 0.36% for HBPL and 0.07% for LNCs. There was no statistically significant difference between the NP-treated (left) and PBS-manipulated (right) cochleae in any of the experimental groups at any time point examined. Similarly, there were no statistically significant differences between data obtained from the two groups treated with HBPL and LNCs compared at each time point (day 2, 14 and 28 after application; Figure 7).

Acoustically evoked auditory brainstem response

Averaging the hearing thresholds of both ears for the measured frequencies of all 30 guinea pigs on experimental day 0, before surgery, the following mean hearing thresholds and SDs were received: at 1 kHz, the threshold was 59.2 ± 2.48 dB; at 4 kHz, 50.8 ± 3.12 dB; at 8 kHz, 33.8 ± 4.70 dB; at 16 kHz, 34.5 ± 3.08 dB; at 32 kHz, 41.5 ± 3.72 dB; and at 40 kHz, 53.5 ± 3.82 dB. The mean thresholds between the right and left ear differed by an average of 3.7 dB. The HBPL-treated animals showed an averaged increase in hearing threshold when compared with the threshold detected on day 0 of 14 dB after 2 days, 12 dB after 14 days and 9.7 dB after 28 days (Figure 8). Frequency-specific evaluation showed the increase differing from 0 dB (28-day group administered with HBPL, 1 kHz) up to 32 dB (2-day group administered with HBPL, 32 kHz). Additionally, the PBS-treated right ears showed an average increase in threshold of 14.3 dB after 2 days, 11 dB after 14 days and 9.7 dB after 28 days (Figure 8). The difference between the left and right ear was not statistically significant. LNC-treated animals also showed an increase of the hearing threshold after NP injection. After 2 days there was a mean increase of 5 dB, after 14 days, 21.3 dB and after 28 days, 4.7 dB (Figure 5). The frequency-specific analysis complies with the HBPL data: at high frequencies the thresholds rise much higher (up to 28 dB at 32 and 40 kHz, 14-day group) compared with the low or middle frequencies (0 dB at 1 or 4 kHz, 2-day group). The right ears treated with control PBS solution presented the following mean thresholds: 4 dB after 2 days, 23.7 dB after 14 days and only 0.3 dB after 28 days. The difference between both ears was not statistically significant.

Discussion

In the present study, we demonstrated that cells incubated with HBPL and LNC NPs neither induced visible signs of cell toxicity in morphology (blebbing and apoptosis) nor in neutral red assay, using a dilution of 1:300 or higher (3.1×10^{11} LNCs or 1.36×10^{-11} mol HBPL). Higher concentrations resulted in cell viability around 30–40%, with obviously different cell appearance: smaller cells which were rounded and granulated. This observation has already been described for polylysine by Santini *et al.* [30] who accounted for it because of the net positive charge and the ionic environment of the cell membrane. Following this, polylysine alters the active ionic transport and the type, quantity or distribution of membrane components such as lipids, proteins and polysaccharides, which are of great importance to maintain cell integrity. Concerning the effects of LNCs in high concentrations no explanation is found. Until now LNCs have always shown good biocompatibility and stealth properties [19]. Based on these data, we decided to inject a dilution of 1:100 *in vivo* as a compromise to gain good NP visualization and low toxicity.

The concentration-dependent fluorescence measurements verified that the cell uptake of HBPL and LNC positively correlated with the NP concentration in the incubating medium. Lower NP concentration in the medium led to lower absolute values of cell uptake. Relating the cell uptake to the incubating NP concentration, a nearly constant proportion was demonstrated. For HBPL, the percentage uptake was between 6.6 and 11.9%, and for LNCs it was between 1.4 and 2.8%. Thus, no decrease, increase or sign of saturation were detected.

Furthermore, our results have demonstrated that both of the tested NPs were capable of entering a broad variety of inner ear cell types, including inner and outer hair cells, pillar cells and cells located in the stria vascularis, by leaving the scala tympani perilymphatic space. These findings clearly show the different NP characteristics in comparison to previous work on viral vector application in the inner ear. Those studies reported gene expression restricted to the perilymphatic fluid spaces, likely due to the vector application into the scala tympani [31–34]. The NPs in the present study were also injected into the scala tympani, but particles were detected in perilymphatic and endolymphatic liquor spaces. Therefore, the distribution pathway of vectors, including the particles used in this study, focusing on vector size, surface charge and/or membrane passage and paracellular pathways, are of interest and should be investigated in future studies. However, the examined NPs were incorporated by various cell types within the cochlea without causing structural or functional damage. Thus, the two tested NPs are promising candidates as vehicles to transport drugs or genes into the inner ear.

Frequency-specific evaluation of the inner ear function showed increasing hearing thresholds differing from 0 dB (28-day group administered with HBPL, 1 kHz) up to 32 dB (2-day group administered with HBPL, 32 kHz). Obviously, the rise of hearing threshold was small in the

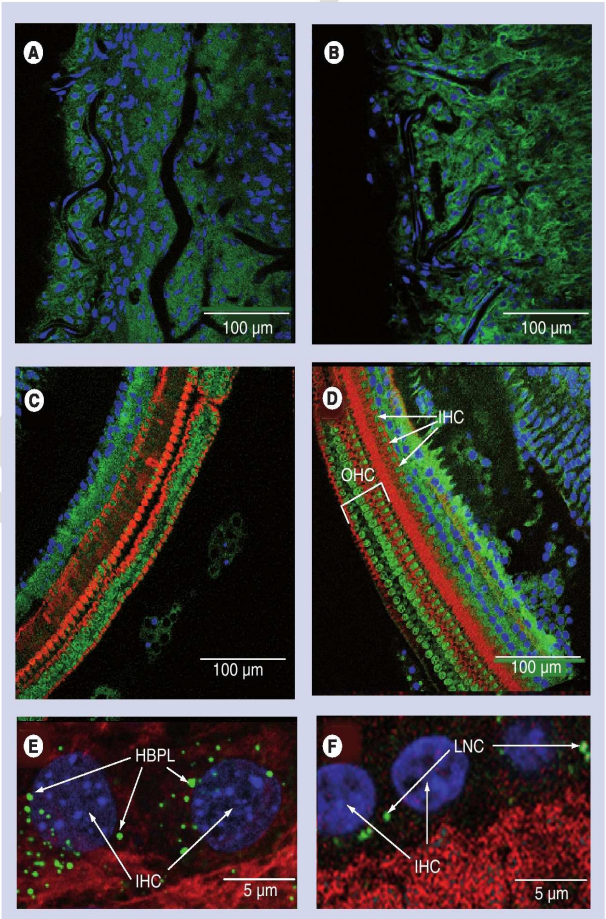

Figure 6. TITLE. Localization of fluorescein-5-isothiocyanate-labeled (green) HBPL **(A,C & E)** and LNCs **(B,D & F)** in different cell populations of the stria vascularis **(A & B)** and basilar membrane **(C & D)** 28 days after application. **(E & F)** are representative pictures of IHCs at higher magnification, illustrating the nanoparticle uptake in these cell types. Actin filaments of cells are visualized with rhodamine-phalloidin (red) and cell nuclei with 4′,6-diamidino-2-phenylindol (blue). HBPL and LNCs were taken up by IHCs and OHCs, supporting cells of the basilar membrane and cells of the stria vascularis.
HBPL: Hyperbranched polylysine; IHC: Inner hair cell; LNC: Lipid nanocapsule; OHC: Outer hair cell.

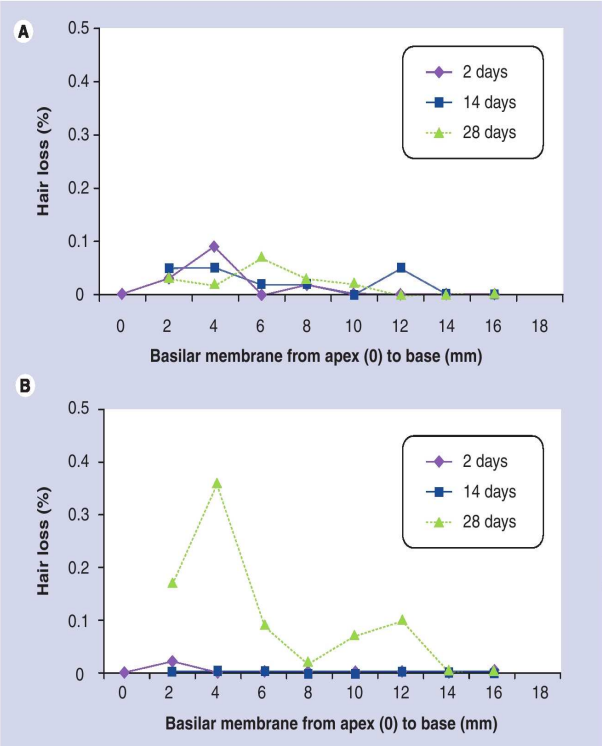

Figure 7. Cytocochleograms for both nanoparticle types for each time period. (A) Cytocochleogram after lipid nanocapsule injection. Demonstrates the mean percentage of hair cell loss observed in hyperbranched polylysine-treated cochleae 2, 14 and 28 days after nanoparticle application. **(B)** Cytocochleogram after hyperbranched polylysine injection. The mean percentages of hair cell loss 2, 14 and 28 days after lipid nanocapsule application are plotted in figure.

middle frequencies and particularly high in the high frequencies, although the NPs could be detected via CLSM in all cochlear turns. Additionally, the PBS-treated right ears also showed an increase in threshold of averaged 14.3 dB after 2 days, 11 dB after 14 days and 9.7 dB after 28 days. The difference between left and right ear was not statistically significant, therefore we assume that the manipulation itself and not NP toxicity was the cause for these results. Opening the middle ear cavity, drilling a cochleostomy in the basal turn, applying 5 µl of fluid into the scala tympani and closing the cochlear defect with carboxylate cement can induce increased hearing thresholds, especially in the high frequencies, independent of the solution injected. However, this temporary effect was reversible as hearing thresholds recovered partially over the experimental time in all groups. Thus, this effect is most likely related to the surgery itself and not the NP solution. Moreover, the cytocochleogram (hair cell counts) did not show any significant hair cell loss in NP-treated versus untreated ears.

In our study, FITC fluorescence (NP surface label) was found in the cytoplasm of the inner ear cells forming small clusters surrounding the nucleus. It can be assumed that the usual incorporation process of nonviral particles into cells is phagocytosis or pinocytosis. Phagocytosis is mainly seen with specialized cells that have to eliminate large particles, such as pathogens. Pinocytosis occurs as clathrin-mediated endocytosis, via caveolae, as micropinocytosis or as clathrin- and caveolae-independent endocytosis [35]; a nonendocytotic pathway is also possible. However, the mechanism of NP uptake into the cells may be of great importance, because this knowledge determines the ligand, tag or payload of the NP. Drugs, plasmids, genes or siRNA have to be integrated into the cells or even into the cell nucleus in order to transfect the cell or control the cell function. Neurotrophic factors only have to activate special receptors such as Trk-B [36] which are located on the cell surface, without entering the cells. This demonstrates that the drug carried by the NP determines the target (cell type and compartment) and the NP structure or additional receptors or peptides on the NP surface determine the pathway, final localization and release. If a complete gene sequence is intended to be expressed, the gene has to be carried into the cell nucleus. Transport across the nuclear envelope is mediated by supramolecular structures, called nuclear pore complexes, accommodating both passive diffusion and active transport. Whereas particles with a diameter up to 10 nm freely diffuse through the channels, most macromolecules are transported through a gated channel by signal-dependent mechanisms. In general, nuclear localization sequences specify the mediated import of particles with a diameter up to approximately 30 nm into the nucleus [37].

Zou *et al.* assumed a paracellular nerve-related pathway as the main approach for LNC penetration from the round window membrane to the cells of the organ of Corti [21]. They demonstrated that this nerve pathway started with the NP diffusion from the perilymph of the scala tympani to the spiral ganglion, continuing with nerve fibers inside Rosenthal's canal to reach the inner hair cells and pillar cells, and finally the outer hair cells. The present study additionally investigated a stronger NP fluorescence in the inner hair cells than in the outer hair cells, but there was no change over 28 days. Finally, the distribution and incorporation process for LNCs and HBPL is not identified yet and presents future work.

Hyperbranched polylysine and LNCs were visualized in all inner ear cell types, providing great variability of delivery possibilities. HBPL has a mean radius of 10 nm and thus qualifies as a gene carrier into the cell nucleus, although they do not enter the nucleus as our data demonstrate. LNCs, with a mean diameter of 52 ± 5 nm, are also possible gene carriers. Although HBPL and LNCs need mediated transport, they are still small enough to move to the vicinity of the central channel, translocate into the nucleus after channel gating, release into the nucleoplasm and deliver the gene at the destination.

The tested NPs show good biocompatibility in low concentrations *in vitro* and *in vivo* and nondirectional uptake in different cochlear cell types.

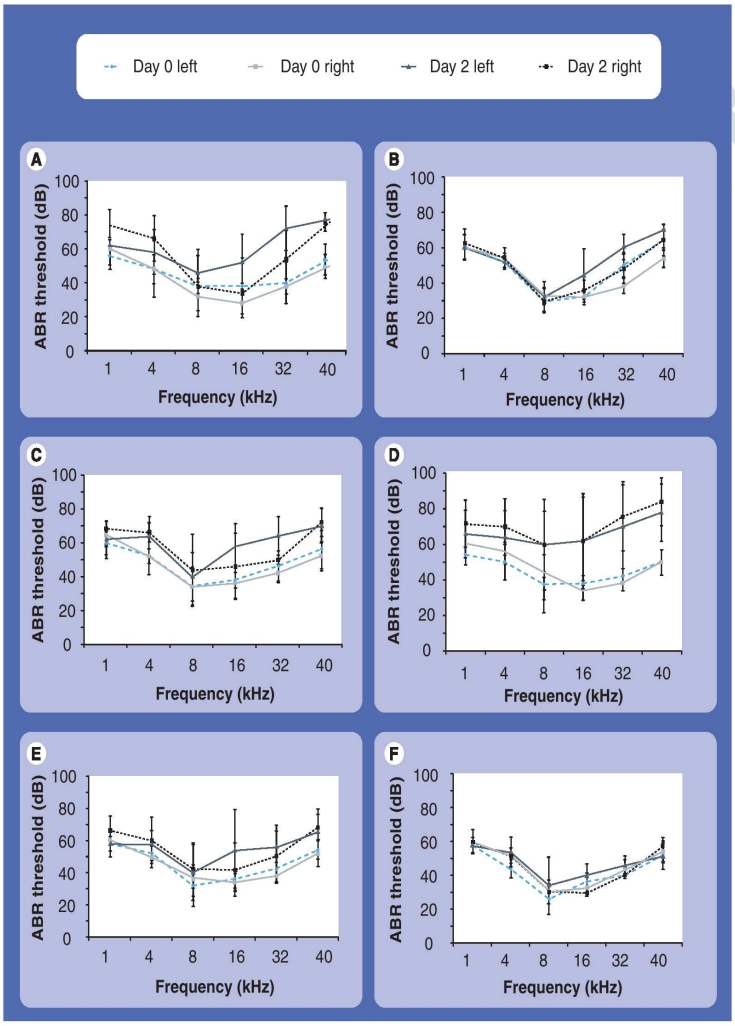

Figure 8. TITLE. (A) AABR measurements 2 days after hyperbranched polylysine (HBPL) injection. **(B)** AABR measurements 2 days after LNCL injection. **(C)** AABR measurements 14 days after HBPL injection. **(D)** AABR measurements 14 days after LNCL injection. **(E)** AABR measurements 28 days after HBPL injection. **(F)** AABR measurements 28 days after LNCL injection. Frequency-specific hearing thresholds 2, 14 and 28 days after HBPL (left) or lipid nanocapsules (LNC) (right) injection into the inner ear compared with day 0 before surgery and compared with phosphate buffered saline-treated control right ears. Each graph represents the average hearing threshold of the left and right (control) ears of one test set.
AABR: Acoustically evoked auditory brainstem response.

Conclusion

In this study we demonstrated that fluorescence labeled HBPL and LNCs are detectable in cultured fibroblasts after incubation and in inner ear cells of animals following local inner ear application. Using HBPL and LNCs (1:300 dilution), no toxic effect on cultured cells or hair cells of guinea pigs was observed. The hearing function of the NP-treated animals was completely preserved and neither neutral red assay *in vitro* nor cytocochleograms *in vivo* showed pathological alterations in lower concentrations. Altogether, the tested NPs showed good biocompatibility and are potentially suitable carriers for inner ear drug delivery.

Future perspective

Future work has to focus on the identification of the internalization mechanisms of HBPL and LNCs to ensure controlled uptake into cochlear cells. Furthermore, the use of NPs to realize inner ear treatment has to be shown. Nevertheless, at present, HBPL and LNCs present very promising tools to deliver drugs or genes to the inner ear, since they have been shown to be nontoxic *in vitro* and *in vivo*, and detectable in inner ear sensory cells. This opens up the exciting possibility of using these tools to intervene with inner ear structures on a nanoscale range, which has not been possible until now. Thus, HBPL and LNCs can be considered in the development of future inner ear therapies to protect, restore or even regenerate hearing function in mammals.

Financial & competing interests disclosure

This study was supported by the European Community 6th Framework Programme on Research, Technological Development and Demonstration (Nanotechnology-based Targeted Drug Delivery. Contract number: NMP4 -CT-2006–02556, Project acronym: NANOEAR). The authors have no other relevant affiliations or financial involvement with any organization or entity with a financial interest in or financial conflict with the subject matter or materials discussed in the manuscript apart from those disclosed.

No writing assistance was utilized in the production of this manuscript.

Ethical conduct of research

The authors state that they have obtained appropriate institutional review board approval or have followed the principles outlined in the Declaration of Helsinki for all human or animal experimental investigations. In addition, for investigations involving human subjects, informed consent has been obtained from the participants involved.

Executive summary

- Incubation of L929 fibroblasts with hyperbranched polylysine (HBPL) and lipid nanocapsules (LNCs) led to nanoparticle (NP) internalization into the cytoplasm around the nucleus in almost all cells.
- Fluorescence measurements demonstrated a positive correlation between NP concentration in the incubating medium and uptake into the cells.
- Neutral red assay showed a reduction in cell vitality at high NP concentrations, but no cytotoxic effect at a higher dilution than 1:100.
- Up to 28 days after intracochlear application, HBPL and LNCs were localized in all observed cell types of the inner ear.
- Cytocochleograms did not show significant hair cell loss or damaged cells.
- Electrophysiological measurements resulted in a slight increase of hearing threshold that was partially reversible and equivalent on both ears, presumably due to the surgical procedure itself and not related to the NP application.
- Having demonstrated biocompatibility and traceability for HBPL and LNCs, future work will focus on targetability and controlled drug release for these potential drug carriers.

Bibliography

1 Kawamoto K, Ishimoto S, Minoda R, Brough DE, Raphael Y: *Math1* gene transfer generates new cochlear hair cells in mature guinea pigs *in vivo*. *J. Neurosci.* 23, 4395–4400 (2003).

2 Izumikawa M, Minoda R, Kawamoto K *et al.*: Auditory hair cell replacement and hearing improvement by *Atoh1* gene therapy in deaf mammals. *Nat. Med.* 11, 271–276 (2005).

3 Miller JM, Miller AL, Yamagata T, Bredberg G, Altschuler RA: Protection and regrowth of the auditory nerve after deafness: neurotrophins, antioxidants and depolarization are effective *in vivo*. *Audiol. Neurootol.* 7, 175–179 (2002).

4 Raphael Y, Frisancho JC, Roessler BJ: Adenoviral-mediated gene transfer into guinea pig cochlear cells *in vivo*. *Neurosci. Lett.* 207, 137–141 (1996).

5 Suzuki M, Yamasoba T, Suzukawa K, Kaga K: Adenoviral vector gene delivery via the round window membrane in guinea pigs. *Neuroreport* 14, 1951–1955 (2003).

6 Duan ML, Ulfendahl M, Laurell G *et al.*: Protection and treatment of sensorineural hearing disorders caused by exogenous factors: experimental findings and potential clinical application. *Hear. Res.* 169, 169–178 (2002).

7 Stover T, Yagi M, Raphael Y: Transduction of the contralateral ear after adenovirus-mediated cochlear gene transfer. *Gene Ther.* 7, 377–383 (2000).

8 Kho ST, Pettis RM, Mhatre AN, Lalwani AK: Safety of adeno-associated virus as cochlear gene transfer vector: analysis of distant spread beyond injected cochleae. *Mol. Ther.* 2, 368–373 (2000).

9 Parker AL, Newman C, Briggs S, Seymour L, Sheridan PJ: Nonviral gene delivery: techniques and implications for molecular medicine. *Expert Rev. Mol. Med.* 5, 1–15 (2003).

10 Panyam J, Labhasetwar V: Biodegradable nanoparticles for drug and gene delivery to cells and tissue. *Adv. Drug Deliv. Rev.* 55, 329–347 (2003).

11 Dincer S, Turk M, Piskin E: Intelligent

polymers as nonviral vectors. *Gene Ther.* 12(Suppl. 1), S139–S145 (2005).

12 Gref R, Couvreur P, Barratt G, Mysiakine E: Surface-engineered nanoparticles for multiple ligand coupling. *Biomaterials* 24, 4529–4537 (2003).

13 Bala I, Hariharan S, Kumar MN: PLGA nanoparticles in drug delivery: the state of the art. *Crit. Rev. Ther. Drug Carrier Syst.* 21, 387–422 (2004).

14 Bourges JL, Gautier SE, Delie F *et al.*: Ocular drug delivery targeting the retina and retinal pigment epithelium using polylactide nanoparticles. *Invest. Ophthalmol. Vis. Sci.* 44, 3562–3569 (2003).

15 Bejjani RA, BenEzra D, Cohen H *et al.*: Nanoparticles for gene delivery to retinal pigment epithelial cells. *Mol. Vis.* 11, 124–132 (2005).

16 Tamura T, Kita T, Nakagawa T *et al.*: Drug delivery to the cochlea using PLGA nanoparticles. *Laryngoscope* 115, 2000–2005 (2005).

17 Praetorius M, Brunner C, Lehnert B *et al.*: Transsynaptic delivery of nanoparticles to the central auditory nervous system. *Acta Otolaryngol.* 127, 486–490 (2007).

18 Vonarbourg A, Passirani C, Saulnier P, Benoit JP: Parameters influencing the stealthiness of colloidal drug delivery systems. *Biomaterials* 27, 4356–4373 (2006).

19 Vonarbourg A, Passirani C, Saulnier P, Simard P, Leroux JC, Benoit JP: Evaluation of pegylated lipid nanocapsules versus complement system activation and macrophage uptake. *J. Biomed. Mater. Res. A* 78, 620–628 (2006).

20 Lamprecht A, Bouligand Y, Benoit JP: New lipid nanocapsules exhibit sustained release properties for amiodarone. *J. Control. Release* 84, 59–68 (2002).

21 Zou J, Saulnier P, Perrier T *et al.*: Distribution of lipid nanocapsules in different cochlear cell populations after round window membrane permeation. *J. Biomed. Mater. Res. B Appl. Biomater.* (2008).

22 Heurtault B, Saulnier P, Pech B, Proust JE, Benoit JP: A novel phase inversion-based process for the preparation of lipid nanocarriers. *Pharm. Res.* 19, 875–880 (2002).

23 Beduneau A, Saulnier P, Anton N *et al.*: Pegylated nanocapsules produced by an organic solvent-free method: evaluation of their stealth properties. *Pharm. Res.* 23, 2190–2199 (2006).

24 Scholl M, Nguyen TQ, Bruchmann B, Klok H-A: The thermal polymerization of amino acids revisited; synthesis and structural characterization of hyperbranched polymers from L-Lysine. *J. Polym. Sci. A1* 45, 5494–5508 (2007).

25 Seib FP, Jones AT, Duncan R: Comparison of the endocytic properties of linear and branched PEIs, and cationic PAMAM dendrimers in B16f10 melanoma cells. *J. Control. Release* 117, 291–300 (2007).

26 Banks PR, Paquette DM: Comparison of three common amine reactive fluorescent probes used for conjugation to biomolecules by capillary zone electrophoresis. *Bioconjug. Chem.* 6(4), 447–458 (1995).

27 Lim HH, Anderson DJ: Auditory cortical responses to electrical stimulation of the inferior colliculus: implications for an auditory midbrain implant. *J. Neurophysiol.* 96, 975–988 (2006).

28 Prieskorn DM, Miller JM: Technical report: chronic and acute intracochlear infusion in rodents. *Hear. Res.* 140, 212–215 (2000).

29 Linss V, Linss W, Emmerich E, Richter F: The cochleogram of the guinea pig. *Eur. Arch. Otorhinolaryngol.* 264, 369–375 (2007).

30 Santini MT, Cametti C, Indovina PL, Morelli G, Donelli G: Polylysine induces changes in membrane electrical properties of K562 cells. *J. Biomed. Mater. Res.* 35, 165–174 (1997).

31 Han JJ, Mhatre AN, Wareing M *et al.*: Transgene expression in the guinea pig cochlea mediated by a lentivirus-derived gene transfer vector. *Hum. Gene Ther.* 10(11), 1867–1873 (1999).

32 Stöver T, Yagi M, Raphael Y: Cochlear gene transfer: round window versus cochleostomy inoculation. *Hear. Res.* 136(1–2), 124–130 (1999).

33 Suzuki M, Yagi M, Brown JN, Miller AL, Miller JM, Raphael Y: Effect of transgenic *GDNF* expression on gentamicin-induced cochlear and vestibular toxicity. *Gene Ther.* 7(12), 1046–1054 (2000).

34 Tan BT, Foong KH, Lee MM, Ruan R: Polyethylenimine-mediated cochlear gene transfer in guinea pigs. *Arch. Otolaryngol. Head Neck Surg.* 134(8), 884–891 (2008).

35 Khalil IA, Kogure K, Akita H, Harashima H: Uptake pathways and subsequent intracellular trafficking in nonviral gene delivery. *Pharmacol. Rev.* 58, 32–45 (2006).

36 Qun LX, Pirvola U, Saarma M, Ylikoski J: Neurotrophic factors in the auditory periphery. *Ann. NY Acad. Sci.* 884, 292–304 (1999).

37 Melchior F, Gerace L: Mechanisms of nuclear protein import. *Curr. Opin. Cell Biol.* 7, 310–318 (1995).

II.3) Etudes complémentaires

Ces études sont le fruit d'un travail collaboratif entre notre équipe et l'équipe du Pr Jean-Luc Puel de l'Institut des Neurosciences de Montpellier, France. Ces études ont été réalisées sur des cochlées entières en culture, issues de jeunes rats. Ces manipulations sont donc des manipulations *ex-vivo*.

Afin de démontrer une efficacité dans la délivrance de principe actif au sein de l'oreille interne, nous avons mis au point des LNCs capables de transporter des siRNA selon le schéma suivant :

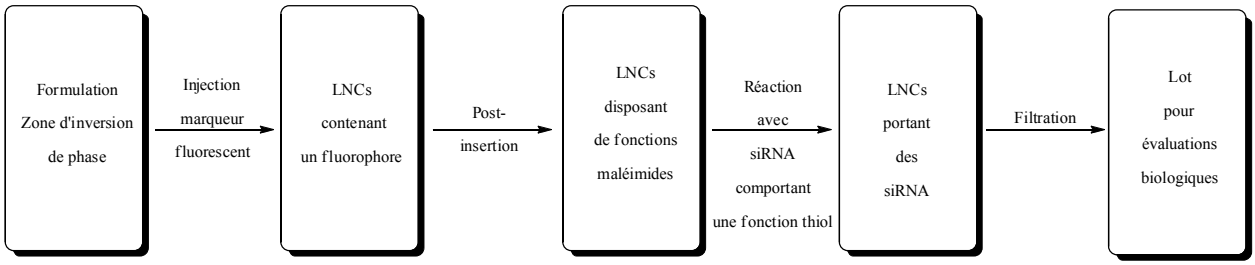

Schéma IV.8 : Représentation schématique de la production de LNCs porteuses de siRNA.

A partir de LNCs chargées en Nile Red, nous avons procédé à des post-insertions soit de DSPE-PEG-2000-maléimide soit de DSPE-PEG-2000-carboxy afin de pouvoir conjuguer les siRNA, comportant une fonction thiol, soit sur la fonction maléimide (liaison irréversible) soit par formation de ponts disulfures (liaison réversible).

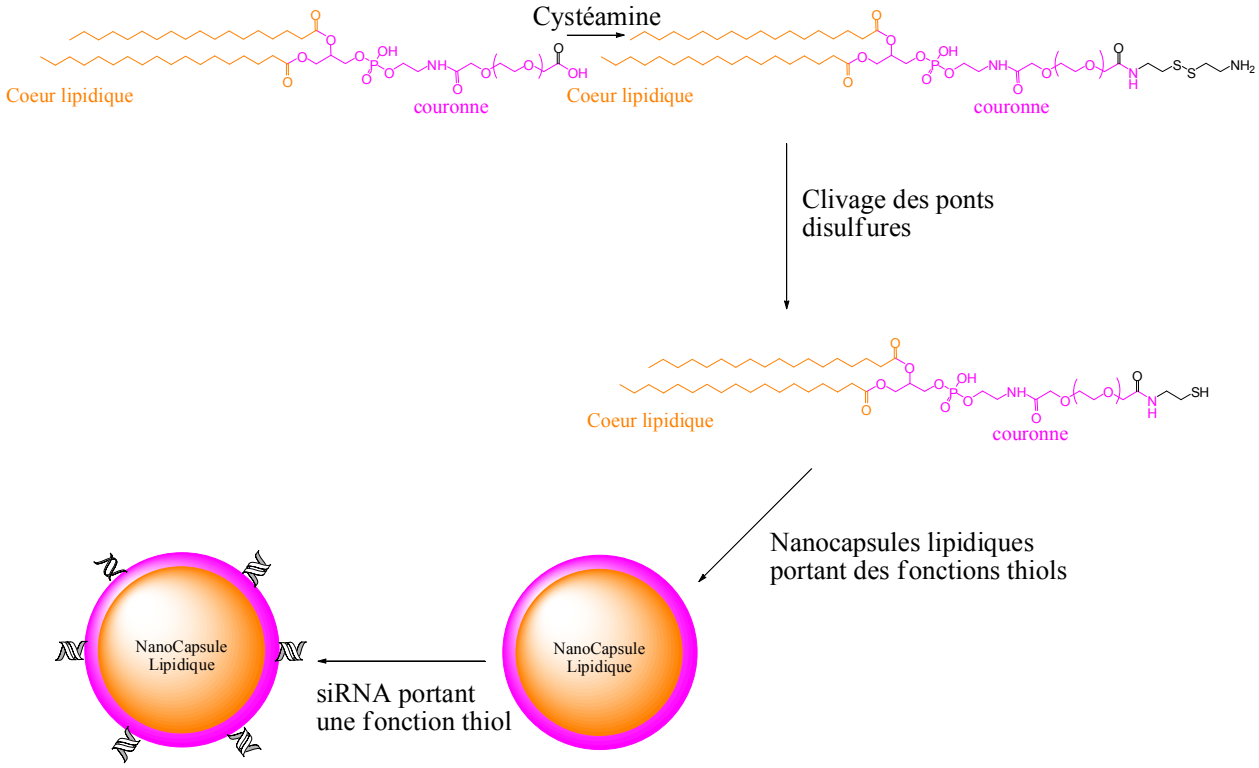

Figure IV.9 : Production de LNCs porteuses de fonction thiols.

Ces LNCs ont été testées sur des cochlées de rat en culture (manipulations *ex-vivo*) et l'évaluation consiste en la quantification de l'expression de la protéine d'intérêt.

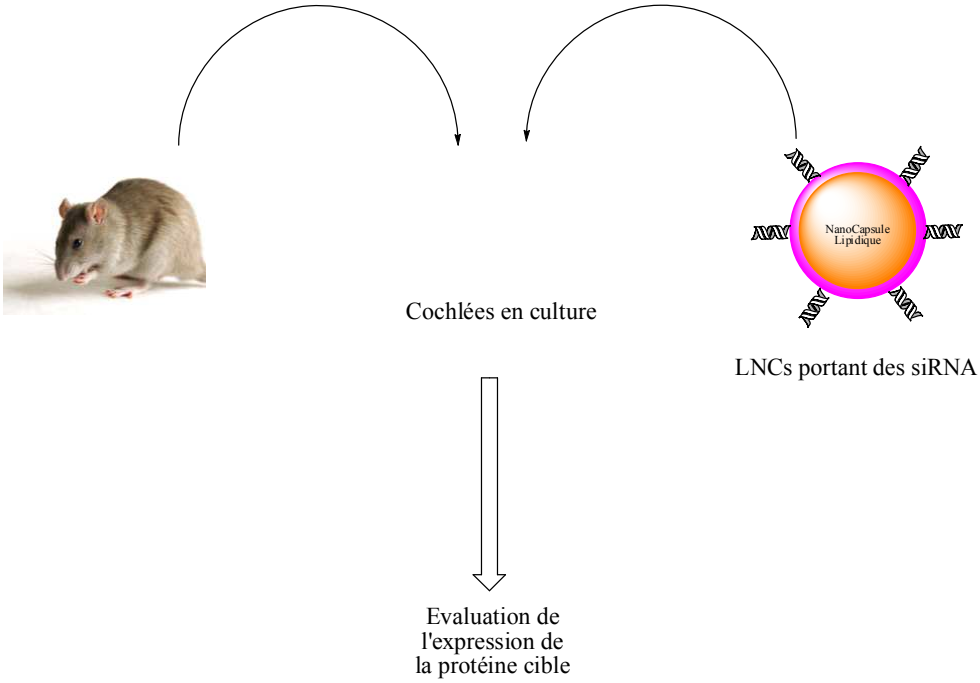

Figure IV.10 : Schéma du principe de l'évaluation biologique des LNCs porteuses de siRNA.

Ici, nous avons utilisé un siRNA dirigé contre l'ARN messager codant la protéine p27 impliquée dans le cycle cellulaire. Si l'expression de cette dernière est inhibée, il a été montré que les cellules de soutien de l'oreille interne peuvent se transdifférencier et peut-être produire de nouvelles cellules ciliées.

Concernant les LNCs portant des siRNA fixés sur le groupe maléimide, l'analyse de l'expression de la protéine p27 montre que les LNCs sont inefficaces pour diminuer l'expression de cette dernière. Par contre, les LNCs portant des siRNA fixés par une fonction thiol semblent être capables de transporter les siRNA au sein des cellules de l'oreille interne et d'induire une diminution dans l'expression de la protéine p27.

Les études de distribution des LNCs au sein de l'oreille interne ont montré qu'il n'y a aucune spécificité dans la répartition des LNCs au sein des cellules de l'oreille interne, c'est pourquoi nous avons développé des LNCs portant des peptides d'adressage spécifiques de récepteurs tyrosine-kinase dépendant comme décrit ci-dessous :

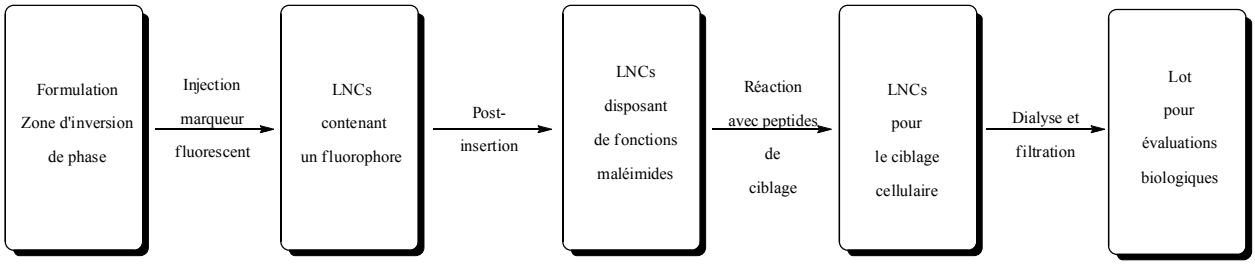

Schéma IV.11 : Représentation schématique de la production de LNCs porteuses de peptides d'addressage.

Nous avons optimisé l'étape de fixation des peptides pour obtenir un rendement compris entre 60 et 85%.

III) Evaluation in vitro de l'aptitude des LNCs modifiées par le procédé de transacylation à délivrer des siRNA au sein de cellules cancéreuses humaines

III.1) Cellules U87MG comme modèle de cancer humain et choix des cibles moléculaires

Les cellules U87MG (Human Glioblastoma-astrocytoma, epithelial-like cell line) ont été choisies comme un modèle in-vitro des tumeurs cérébrales humaines. En effet, le glioblastome est la forme la plus dédifférenciée des tumeurs astrocytiques et est réfractaire à la chimiothérapie dans la majeure partie des cas. De plus, sur la base de la littérature[262,263,264,265] et de l'expérience du laboratoire, les cellules U87MG expriment récepteur le récepteur à l'EGF (epithelial growth factor) qui a été notre cible dans cette étude. En effet, si l'on peut inhiber l'expression de cette protéine pour toute ou partie, cela permettrait de diminuer la croissance tumorale. Nous avons donc choisi d'employer un siRNA dirigé contre l'ARNmessager correspondant à l'EGFR. L'efficacité des LNCs-PLL à transfecter les cellules U87MG sera donc évaluer par quantification par qPCR du contenu en ARNm correspondant pour chaque condition expérimentale. Afin de pouvoir comparer les résultats, les analyses par qPCR ont été normalisées par rapport à l'expression d'un gène de ménage, ici la G3PDH (Glyceraldehyde-3-Phosphate Dehydrogenase).

[262] Shibuya, M.
Brain angiogenesis in developmental and pathological processes: Therapeutic aspects of vascular endothelial growth factor(2009) FEBS Journal, 276 (17), pp. 4636-4643
[263] Miletic, H., Niclou, S.P., Johansson, M., Bjerkvig, R.
Anti-VEGF therapies for malignant glioma: Treatment effects and escape mechanisms
(2009) Expert Opinion on Therapeutic Targets, 13 (4), pp. 455-468.
[264] Chen, K., Cai, W., Li, Z.-B., Wang, H., Chen, X.
Quantitative PET imaging of VEGF receptor expression
(2009) Molecular Imaging and Biology, 11 (1), pp. 15-22.
[265] Norden, A.D., Drappatz, J., Wen, P.Y.
Novel anti-angiogenic therapies for malignant gliomas
(2008) The Lancet Neurology, 7 (12), pp. 1152-1160.

III.2) Evaluation in vitro l'aptitude des LNCs-PLL à délivrer des siRNA au sein de cellules U87MG

Les cellules U87MG ont été cultivées dans du DMEM supplémenté à 10% en sérum fœtal de veau et en présence d'antibiotiques à une concentration de 1%. Pour les expériences de transfection, nous avons placé 50000 cellules par puits puis cultivé les cellules pendant 72 heures. Les cellules ont ensuite été mises en contact avec les complexes LNCs-PLL/siRNA préalablement préparés. Quatre concentrations en LNCs-PLL ont été utilisées, avec à chaque fois la même gamme de concentration en siRNA. Toutes les conditions opératoires ont été réalisées en duplicat.

Après 48 heures de contact entre cellules et complexes de siRNA, les cellules ont été récupérées et conservées à -80°C jusqu'à analyse par qPCR.

Les résultats sont consignés dans les Figures suivantes qui représentent le taux d'expression de l'ARNm codant l'EGFR en fonction de la concentration en siRNA, pour chaque concentration de LNCs-PLL.

Comme discuté au chapitre III, les LNCs-PLL sont capables de fixer des siRNA et nous avons choisi de limiter la gamme de concentration de siRNA à des valeurs inférieures à 20nM, pour ne pas avoir des phénomènes de neutralisation électrique et d'agrégation.

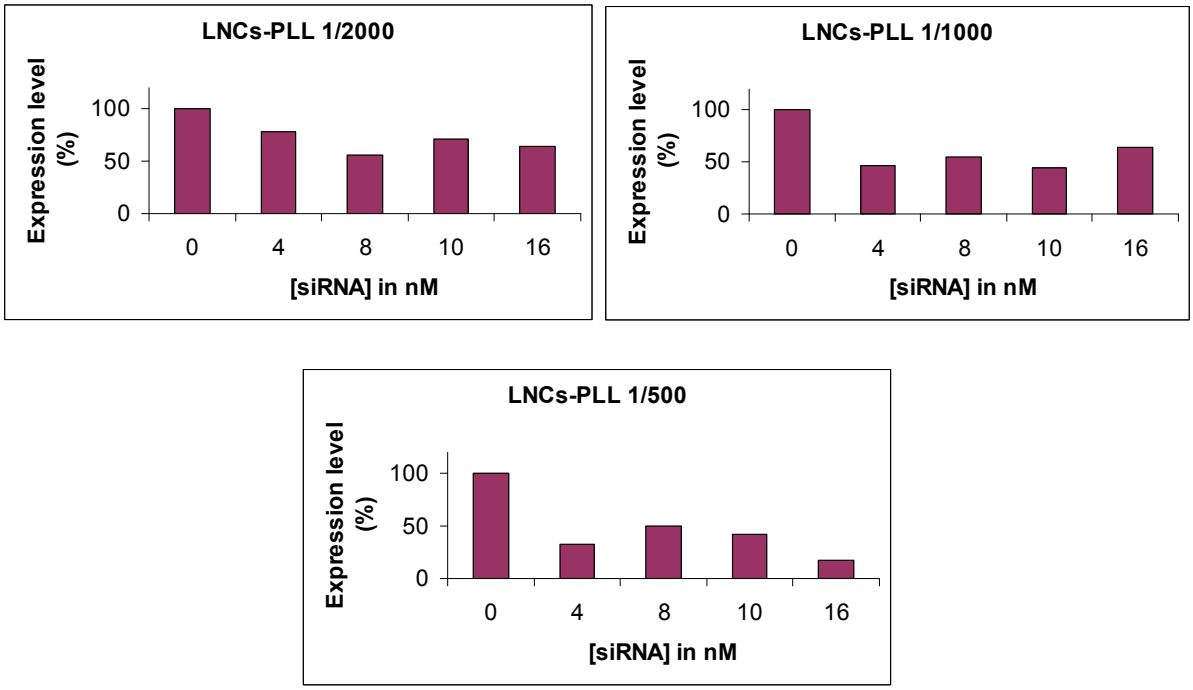

Figure IV.12 : Taux d'expression de l'ARNm de l'EGFR pour chaque condition expérimentale.

Pour des LNCs-PLL diluées au 1/2000, on observe une chute du taux d'expression dès une concentration en siRNA égale à 4nM. Le taux varie peu en fonction de la concentration en siRNA et se situe autour de 50%. Un raisonnement similaire peut être conduit pour les dilutions au 1/1000 et 1/500. On peut cependant noter le taux d'expression diminue pour toutes les concentrations de siRNA si la concentration en LNCs-PLL augmente. Plus il y a de LNCs au contact des cellules plus le siRNA semble être transféré dans les cellules. Pour illustrer cette relation entre concentrations en LNCs-PLL et concentration en siRNA, nous pouvons tracer la Figure suivante qui représente le taux d'expression moyen en fonction du facteur de dilution des LNCs-PLL.

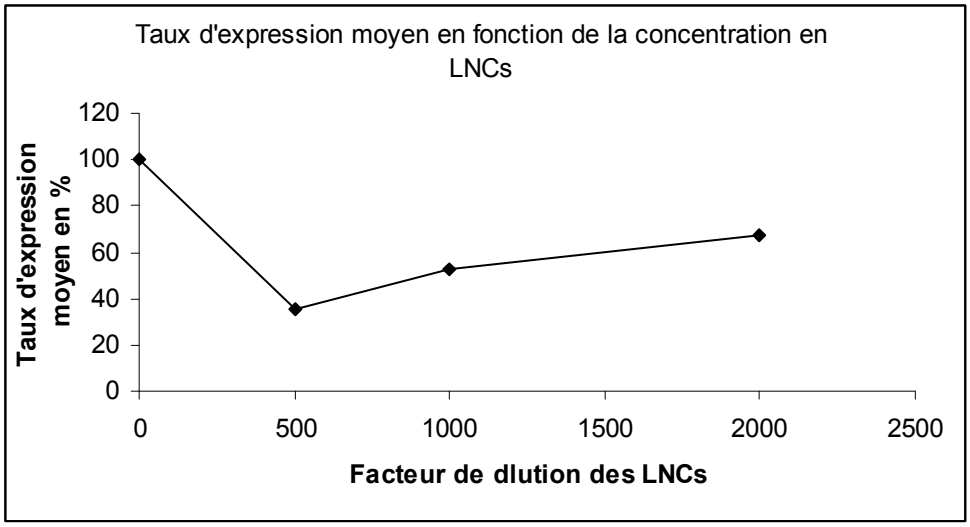

Figure IV.13 : Relation taux d'expression moyen-dilution des LNCs-PLL.

Il apparaît une relation entre le taux moyen d'expression et le facteur de dilution des LNCs-PLL. Le taux moyen d'expression est le plus faible pour la plus faible dilution des LNCs-PLL et est de l'ordre de 40%soit 60% d'inhibition. Le taux moyen d'expression remonte par la suite plus les LNCs-PLL sont diluées atteignant des valeurs de l'ordre de 67% pour les LNCs-PLL diluées au 1/2000.

De plus, pour des concentrations plus importantes en LNCs-PLL, les taux d'expression remontent et sont proches de 50%, comme illustré dans la Figure suivante :

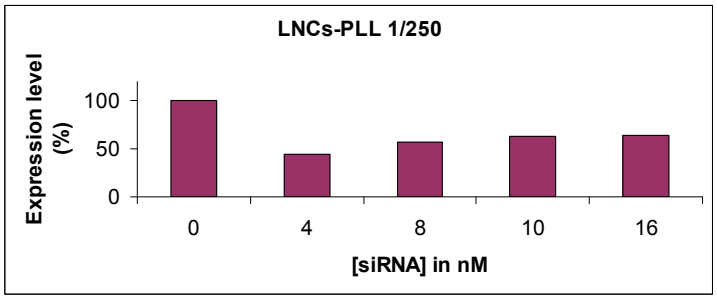

Figure IV.14 : Taux d'expression de l'ARNm de l'EGFR pour une dilution au 1/250 des LNCs-PLL.

Le fait d'incuber les cellules U87MG à des concentrations plus fortes de LNCs-PLL n'entraine pas de gain dans l'inhibition de l'expression de l'EGFR. Cet exemple constitue un cas limite car les LNCs-PLL sont sans doute toxiques à de telles concentrations.

IV) Conclusions

Nous avons démontré que LNCs post-insérées permettent d'évaluer la biodistribution des LNCs au sein d'un organe modèle, ici l'oreille interne. De plus, les LNCs post-insérées peuvent être utilisées comme une plateforme sur laquelle des molécules d'intérêt biologique sont greffées. Il faut tenir compte de la nature du lien chimique entre les LNCs et le conjugué, en fonction de l'application recherchée. Les problèmes de distribution pourraient être résolus par l'usage de gels de LNCs. D'autre part, les LNCs-PLL sont capables de transfecter des siRNA au sein de cellules cancéreuses humaines. Nous avons démontré qu'il existe une relation entre le taux d'expression de la cible et la concentration en LNCs-PLL.

Chapitre V

Discussion générale.

Conclusion générale et perspectives.

I) Discussion générale

Ce travail de thèse propose tout d'abord une étude de la structure des nanocapsules lipidiques afin de comprendre les particularités de ces nano-objets. Dans un deuxième temps, nous avons étudié la faisabilité de deux procédés de modification post-formulation, la post-insertion et le procédé de transacylation des nanocapsules lipidiques. Nous avons montré que de tels procédés pouvaient entraîner des changements importants des propriétés physico-chimiques de surface de ces particules sans altérer leur nature nanométrique ainsi que leur capacité à encapsuler des médicaments à tendance plutôt lipophile. Par la suite, nous exposons les travaux réalisés à partir des nanocapsules lipidiques modifiées. Dans cette discussion, nous proposons de relier la structure des LNCs aux faisabilités des procédés de modification post-formulation.

Dans un premier temps, il est important de revenir sur le procédé de formulation. En effet, les travaux précédents réalisés au laboratoire laissaient à penser que les LNCs étaient crées par la « fragmentation » d'une nano-émulsion obtenue par cyclage thermique (méthode PIT). Or, si on refroidit le système brutalement lorsqu'il est dans la zone d'inversion de phase (ZIP), de manière brutale (bain de glace), on obtient un système qui conserve l'aspect

macroscopique de la ZIP avec présence d'un effet Tyndall assez marqué, qui décroit lorsqu'on tend vers la formulation d'objets supérieur à 100nm. Cette phase « bloquée en ZIP » est particulièrement stable et se comporte comme un système réservoir de LNCs. C'est-à-dire que si on la redisperse dans un milieu aqueux, nous obtenons des LNCs identiques en tous points à celles obtenues par dilution de la ZIP. Cependant, de part le viscosité de cette phase et par le fait qu'elle est particulièrement concentrée, des mesures de tailles sont impossibles par diffusion de la lumière avec les appareils disponibles au laboratoire. Nous avons donc étudié ces échantillons concentrés par diffusion des neutrons aux petits angles. Les diffusogrammes obtenus sont similaires à ceux obtenus pour des suspensions diluées de LNCs. Cependant, il se produit un phénomène de multi-diffusion, dû à la forte concentration en objets diffusant ; qui induit une erreur dans l'intensité diffusée et recueillie par le détecteur de l'appareil. Ceci explique l'absence de points sur les courbes pour les LNCs non diluées pour les petites valeurs de q (Figure V.1 et V.2).

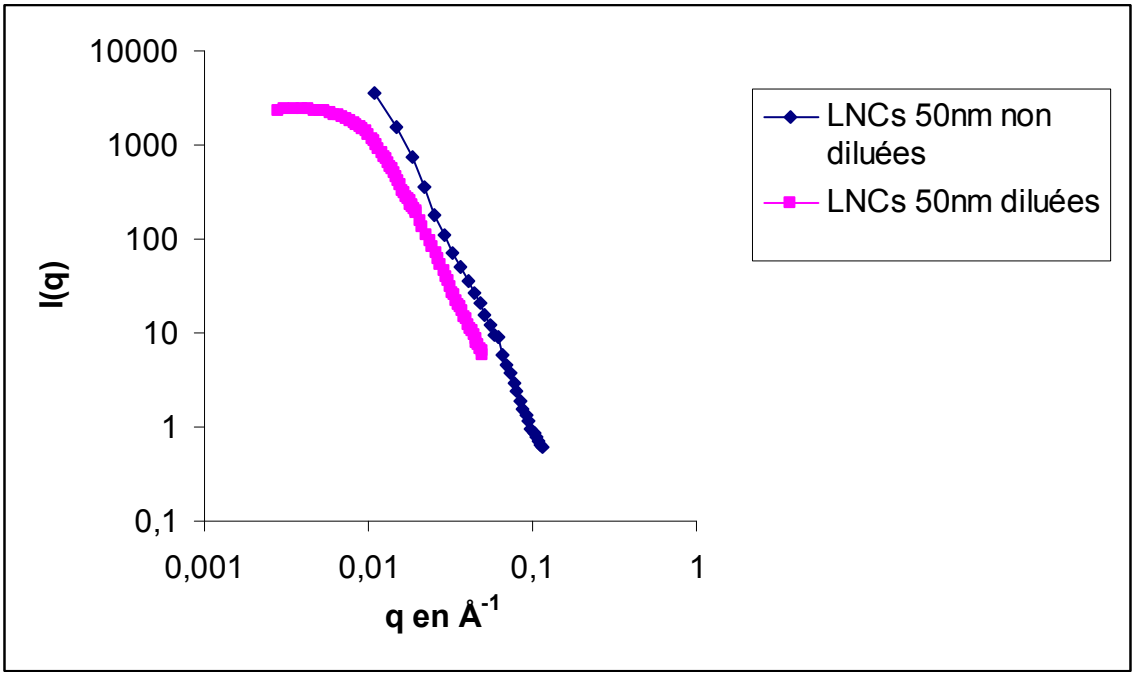

Figure V.1 : Diffusion comparée des formes concentrées et diluées pour les LNCs 50 nm.

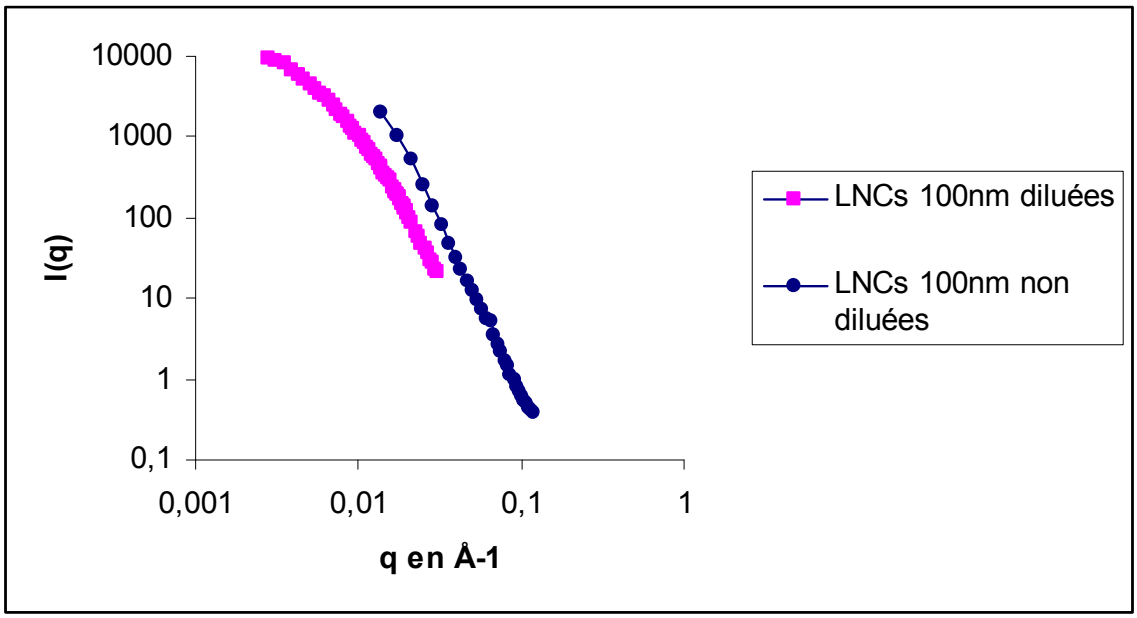

Figure V.2 : Diffusion comparée des formes concentrées et diluées pour les LNCs 100 nm.

On observe qu'il n'y a pas de différences fondamentales dans l'intensité diffusée pour les formes diluées et non diluées. Ces expériences laissent à penser que les LNCs sont déjà formées dans la ZIP et qu'une dilution par ajout d'eau froide n'est pas nécessaire pour leur génération. Des expériences sont en cours au laboratoire afin de démontrer que l'on peut s'affranchir de l'étape de dilution et que l'on peut produire des suspensions concentrées de LNCs.

Nous avons démontré dans le chapitre III que les LNCs sont des particules sphériques avec une structure cœur-couronne ; la couronne étant une monocouche mixte de tensio-actifs. Cette architecture en monocouche mixte permet d'expliquer la stabilité colloïdale des LNCs en fonction du temps et d'autres facteurs comme le pH ou la salinité. La stabilité de cette monocouche peut s'expliquer par les nombreuses interactions latérales qui existent entre les chaines hydrocarbonées des tensio-actifs. On peut supposer que, pour notre système nanoparticulaire, le rapport de Windsor R est proche de 1. Les interactions lipophiles et

hydrophiles sont égales et s'équilibrent, conférant une stabilité importante à la monocouche mixte[266].

$$R = \frac{A_{CO} - A_{OO} - A_{LL}}{A_{CW} - A_{WW} - A_{HH}}$$

Où A_{CO} : intéractions surfactant-huile

A_{CW} : intéraction surfactant-eau

A_{OO} : intéractions huile-huile

A_{WW} : intéractions eau-eau

A_{HH} : intéractions tête-tête

A_{LL} : intéractions partielipophile-partie lipophile

De plus, la densité moléculaire de cette interface, avec des molécules de tensio-actifs ayant des aires moléculaires proches des aires minimales, ralentit les phénomènes comme le murissement d'Ostwald ou la coalescence.

$$\frac{dr3}{dt} = \frac{8Dc_{\infty}\gamma M}{9\rho^2 RT}$$ (cinétique du mûrissement d'Ostwlald)

$$\frac{1}{r^2} = \frac{1}{r_0^{\,2}} - \frac{8\pi}{3\omega}t$$ (cinétique de la coalescence)

A partir de cette organisation, nous avons testé la faisabilité expérimentale de la modification de cette interface. En d'autres termes, cette monocouche mixte de tensio-actifs peut-elle subir une insertion de molécules amphiphiles (c'est le procédé de post-insertion) et peut-elle subir des réactions chimiques (c'est le procédé de transacylation) sans entraîner la destruction des LNCs?

Dans un premier temps, la post-insertion a été testée d'une manière analogue au procédé utilisé sur les liposomes. Dans la publication consacrée à la post-insertion (chapitre

[266] Cahiers FIRP : http://www.firp.ula.ve

III), nous avons démontré que le procédé était transposable aux LNCs, avec certaines limites. En effet, seulement une faible quantité d'amphiphiles peut être post-insérée, de l'ordre de 5 à 10% en mol de la quantité de tensio-actifs de la formulation (Solutol HS-15 et Lipoïd S75-3).

De plus, la nature chimique de l'amphiphile semble discriminante : deux chaînes aliphatiques sont nécessaires et à ce jour aucun amphiphile à base de cholestérol n'a pu être inséré sur les LNCs. Cependant, malgré le faible taux d'insertion, nous avons montré que la post-insertion pouvait apporter suffisamment de groupements fonctionnels et que ceux-ci pouvaient réagir avec des susbtrats. Cette approche a permis dans un premier temps de produire des LNCs fluorescentes par marquage au FITC. Ces LNCs fluorescentes ont été très utiles pour le suivi du devenir intra-cellulaire des LNCs. Cela nous a permis d'établir la biodistribution des LNCs au sein de l'oreille interne et de montrer que les LNCs sont capables de rentrer dans des cellules spécialisées, telles que les cellules ciliées. La post-insertion permet aussi d'obtenir des LNCs multifonctionnelles de façon aisée et directe : le cœur peut être chargé par une molécule hydrophobe, ensuite post-insertion et réaction ultérieure avec des molécules d'intérêts biologiques. Cette stratégie s'est avérée fructueuse pour la délivrance de siRNA, au prix de nombreux échecs. En effet, la conjugaison de siRNA, porteur d'une fonction thiol, sur des LNCs post-insérées et porteuses de groupements maleimide ; produit des LNCs qui ne possèdent peu ou pas d'activité biologique. Ces manipulations ont soulevé plusieurs questions : en effet, l'absence d'effets biologiques peut-être due à un problème de dose en principe actif, de voie d'administration, ou de changement des propriétés physico-chimiques des nanoparticules et/ou des siRNA greffés. Pour tester ces hypothèses, nous avons repris des manipulations identiques mais en changeant la nature du lien chimique : des LNCs post-insérées porteuses de groupements acides carboxyliques ont été traitées par voie chimique pour introduire des fonctions thiols. Par la suite, nous avons créé des ponts disulfures entre ces groupements thiols et les groupements thiols portés par les molécules de

siRNA. Une très bonne activité biologique a été obtenue comparable à celle d'autres systèmes de délivrance des siRNA.

	Diamètre hydrodynamique (nm)	Potentiel zeta (mV)
LNCs de départ	54,3	-9,2
LNCs 10% DSPE-PEG2000-carboxy	72,2	-20,0
LNCs 10% DSPE-PEG2000-Carboxy après couplage cystamine	77,6	11,8

Tableau V.1 : Paramètres physicochimiques des LNCs lors des étapes visant à l'incorporation de fonctions thiols.

Cet exemple illustre bien qu'un changement mineur dans l'architecture des LNCs peut-être lourd de conséquences au niveau de l'application recherchée. De plus, la post-insertion peut être réalisée avec des mélanges de tensio-actifs porteurs de fonctions chimiques différentes afin de produire en une seule étape des LNCs porteuses de différentes fonctions chimiques capables de réagir dans des conditions différentes. En effet, il est possible de réaliser des réactions successives sur les LNCs et d'introduire à chaque étape une molécule d'intérêt. Nous résumons dans le Tableau ci-dessous les caractéristiques physico-chimiques des LNCs post-insérées avec des mélanges de tensio-actifs.

Composition en tensio-actifs	Diamètre hydrodynamique (nm)	Potentiel zeta (mV)
LNCs de départ	47	-8,3
5% DSPE-PEG2000-carboxy	62,3	-26,1
10%DSPE-PEG2000-carboxy	60,7	-34,1
5%DSPE-PEG2000-methoxy	62,7	-16,1
10%DSPE-PEG2000-methoxy	62,3	-12,7
5% DSPE-PEG2000-amino	61,5	+0,4
10% DSPE-PEG2000-amino	61,8	+1,8
5%DSPE-PEG2000-maleimide	58,5	-23,8
10%DSPE-PEG2000-maleimide	61,4	-30,9
3% DSPE-PEG2000-amino 3% DSPE-PEG2000-carboxy 3%DSPE-PEG2000-maleimide	60,1	-22,1
5% DSPE-PEG2000-carboxy 5%DSPE-PEG2000-maleimide	61,8	-43,8
5% DSPE-PEG2000-amino 5%DSPE-PEG2000-maleimide	59,9	-17,1
2,5%DSPE-PEG2000-maleimide 2,5% DSPE-PEG2000-amino	62,9	-13,7

Tableau V.2 : Diamètre hydrodynamique et potentiel zeta des LNCs post-insérées avec des mélanges de tensio-actifs.

On peut pratiquer une pegylation additionnelle de la surface des LNCs : on peut conduire une réaction d'addition de PEG portant une fonction thiol sur des LNCs post-insérées avec du DSPE-PEG_{2000}-maléimide. Cette manipulation est intéressante si l'on souhaite protéger de la dégradation des susbtances préalablement greffées sur des LNCs modifiées par post-insertion.

Les caractéristiques physico-chimques des LNCs après chaque étape de la manipulation sont résumées dans le Tableau ci-dessous.

	Diamètre hydrodynamqiue (nm)	Potentiel zeta (mV)
LNCs de départ	54,3	-9,2
LNCs 10% DSPE-PEG2000-maleimide	70,4	-42,1
LNCs après réaction avec CH_3O-PEG_{20000}-SH	141,4	-64,4

Tableau V.3 : Paramètres physicochimiques des LNCs lors de l'étape de pegylation additionnelle.

Par la suite, comme nous avons montré que les ions pouvaient diffuser dans la partie externe des LNCs et que de nombreuses fonctions esters sont présentes, nous avons choisi d'adapter le procédé de transacylation aux LNCs. En employant des conditions de pH assez fortes, nous obtenons des LNCs transacylées, démontrant ainsi la faisabilité du procédé. Il apparaît de façon non ambiguë que la transacylation permet d'incorporer des substances d'intérêt biotechnologique, des polymères notamment. A partir des LNCs obtenues par transacylation et décrite dans le chapitre III, nous avons testé l'efficacité de ce système pour la délivrance de siRNA au sein de cellules humaines cancéreuses ; les siRNA étant fixés par intéractions éléctrostatiques à la surface des LNCs. Il apparaît que la quantité d'ARNm ciblé diminue en présence de LNCs transacylées avec de la poly-L-lysine, celle-ci étant capables de complexer les siRNA. Cepedant, peu de fonctions esters à la surface des LNCs sont en fait transacylées : à partir du dosage de la quantité de poly-L-lysine fixée sur les LNCs par transacylation, on peut calculer le nombre de molécules de poly-L-Lysine présentes dans l'échantillon. Connaissant le nombre de molécules de Solutol HS-15 présentes dans l'échantillon de LNCs utilisés pour l'expérience de transacylation, on peut calculer le nombre de fonction ester qui ont subi une transacylation. On constate qu'une molécule pour 54000

molécules de Solutol HS-15 a subi la transacylation, ce qui revient à dire que 30% des LNCs sont porteuses d'une molécule de poly-L-lysine. Ce taux de fonctionnalisation est très faible mais il est suffisant pour avoir des LNCs capables de transporter des siRNA et pour induire une diminution de la quantité d'ARNm ciblé in vitro. Cela peut s'expliquer par le fait que le nombre de molécules de poly-L-lysine présentes dans l'échantillon est supérieur au nombre de molécules de siRNA, ces derniers étant employés à des concentrations de l'ordre du nM.

Les LNCs obtenues par transacylation conservent ainsi les propriétées initiales des LNCs (stabilité, pénétration cellulaire) et présentent des propriétés addtionnelles, comme la capacité à fixer des molécules d'intérêt thérapeutiques comme les siRNA.

Cependant, il apparaît que l'on doit conduire des expériences de transacylation avec des quantités plus importantes de poly-L-Lysine ou que l'on doit diminuer la concentration en LNCs dans le milieu réactionnel ; cela afin d'explorer pleinement les limites et la faisabilité du procédé. Il faudra par la suite comparer la capacité de transport et de délivrance des LNCs modifiées par transacylation au taux de fonctionnalisation.

D'une manière générale, un des problèmes majeurs rencontré lors de l'administration des LNCs, que se soit par injection à travers la fenêtre ronde ou par dépôt sur celle-ci de suspension de LNCs, est le faible volume de suspension utilisé étant donné le confinement anatomique des sites d'administration. En effet, dans les deux voies d'administration utilisées, la quantité de LNCs est très faible et, de plus, nous devons employer des solutions diluées pour dimineur de phénomènes de toxicité due aux assemblages de molécules amphiphiles. Cela pose un problème de grande importance pour la délivrance d'une dose suffisante de drogues, quelque soit sa nature. Pour palier à cette difficulté, nous avons développé des formes concentrées de LNCs qui présentent des capacités réservoirs sous la forme de gels nanoparticulaires. Nous avons présenté dans le chapitre II la formulation des LNCs. Une tentative pour obtenir des formes concentrées de LNCs fut de ne pas diluer le système bloqué

en inversion de phase mais de plonger celle-ci directement dans un bain de glace, procédant ainsi à un refroidissement brutal. Par une première observation macroscopique, on peut noter les points suivants : on obtient un gel translucide fortement visqueux pour la formulation de LNCs de 20 nm, après refroidissement brutal ; le refroidissement brutal des formulations de LNCs de 50 et 100 nm ne produit pas de gels mais des suspensions liquides de faibles viscosités.

Les questions suivantes se posaient alors à nous : (i) Les solutions concentrées, gel et liquides, contiennent-elles des LNCs de la taille désirée ?(ii) Peut-on diluer le gel et obtenir des LNCs identiques à celle obtenues par le procédé standard incluant une étape de dilution ?(iii) Quelle est l'influence du pourcentage d'eau contenu dans la formulation sur la viscosité de la suspension de LNCs ? (iiii)A partir de quel pourcentage d'eau se passe la transition solution-gel ?(iiiii)Les solutions gélifiées peuvent-elles servir in vivo comme réservoir de LNCs ?

Pour répondre à ces questions, nous avons étudié la dilution des solutions concentrées et analysé les échantillons par diffusion dynamique de la lumière. Nous obtenons des LNCs identiques aux LNCs classiquement obtenues au sein du laboratoire, en termes de diamètre hydrodynamique et de potentiel zeta. Pour déterminer l'influence du pourcentage d'eau sur la transition solution-gel, nous avons réalisé une étude de viscosimétrie apparente sur des formulations de LNCs 20 nm contenant un pourcentage d'eau variable.

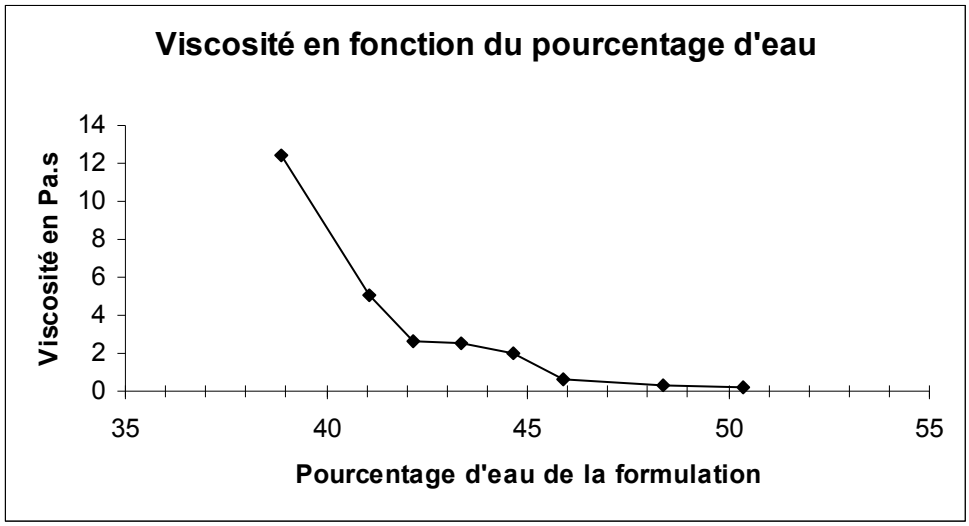

Figure V.3 : Influence du pourcentage d'eau de la formulation sur la viscosité.

Il apparaît que pour un pourcentage d'eau inférieur à 45% en masse, les suspensions de LNCs, refroidies brutalement alors qu'elles étaient en zone d'inversion de phase, présentent des viscosités supérieures à 2 Pa.s. Macroscopiquement, ces suspensions sont des gels translucides. Nous avons aussi préparés des gels contenant des LNCs avec des agents gélifiants tels que l'alginate de sodium et la gélatine. Si l'on détruit ces gels par ajout de chlorure de potassium (cas des gels d'alginate) ou par action de la trypsine (cas des gels de gélatine), on retrouve des nanoparticules par diffusion dynamique de la lumière avec des caractéristiques proches des LNCs initiales. Ces expériences démontrent que l'on peut inclure des LNCs dans des gels sans induire leur destruction. Ces manipulations sont poursuivies au sein du laboratoire. Les évaluations *in vitro/in vivo* des capacités réservoirs de ces gels vont bientôt être évaluées au sein du laboratoire.

II) Conclusion générale et perspectives

Ce travail de thèse a permis d'étudier la structure intime des nanocapsules lipidiques et de démontrer que celles-ci possédaient des atouts non négligeables surtout la facilité de

production et la stabilité colloïdale. Nous avons démontré que l'on pouvait développer le travail sur l'interface et la partie externe des nanocapsules lipidiques en apportant des propriétés nouvelles, importantes pour les utilisations à venir. La délivrance de siRNA au sein de cellules eucaryotes est un challenge extrêmement important qui présente des intérêts thérapeutiques mais aussi technologiques. L'interférence RNA permet de contrôler l'expression des gènes sans avoir à apporter du matériel génétique exogène et sans avoir à modifier le patrimoine génétique. Bien sûr, cela présente des aspects négatifs car l'interférence RNA est un phénomène temporaire, ce qui impose d'un point de vue thérapeutique de devoir apporter en continu des siRNA. Dans le cadre de l'évaluation des nanocapsules lipidiques transacylées, nous n'avons pas encore établit la relation entre la quantité de siRNA et/ou de LNCs et la durée de l'inhibition de l'expression de la protéine cible. De plus, nous n'avons pas évalué l'impact de l'administration successive de LNCs transacylées porteuses de siRNA sur le taux d'inhibition. Toutes ces questions restent en suspens.

Il apparaît très clairement que les nanocapsules lipidiques peuvent être rendues multifonctionnelles par des procédés simples et efficaces. Cependant, beaucoup de travail reste à réaliser compte tenu du nombre de variable en jeu (taille des nanocapsules lipidiques, nature de l'huile, nature des surfactants, choix des procédés de modification, caractère hydrophile/lipophile/amphiphile des agents thérapeutiques) et du fait que de nombreuses méthodologies sont disponibles pour la modification de nanoparticules. Les méthodes disponibles à ce jour permettent de réaliser des nanoparticules de plus en plus à même de satisfaire plusieurs objectifs, même si ces derniers peuvent paraître antinomiques.

Annonce de SOUTENANCE DE THESE

Laboratoire d'origine :
INSERM U646 "Ingénierie de la vectorisation particulaire" *(J.P. BENOIT)*

Doctorant : Thomas Perrier

Date et heure, lieu : Le 27 Novembre 2009 à 10 Heures. Faculté de pharmacie d'Angers

Sujet : Modifications de nanocapsules lipidiques par des procédés post-formulation. Elaboration de vecteurs multifonctionnels de médicaments.

Résumé : Ce travail de thèse a permis d'établir la carte d'identité de nanoparticules développées au laboratoire, les nanocapsules lipidiques. En effet, nous avons caractérisé les nanocapsules lipidiques par diffusion dynamique de la lumière mais aussi par diffusion des neutrons aux petits angles : ces expériences nous ont permis de démontrer que ces particules possèdent une structure cœur-couronne ; le cœur étant composé de triglycérides et la couronne d'un mélange de tensio-actifs. Nous avons aussi démontré que la couronne est une monocouche mixte de tensio-actifs à l'interface huile/eau. A partir de cette structure, nous avons développé deux méthodes de modification post-formulation des nanoparticules initiales afin d'obtenir des nanocapsules lipidiques multifonctionnelles. La première méthode est la post-insertion, initialement développée sur les liposomes ; la deuxième méthode est basée sur une réaction de transacylation entre les tensio-actifs des nanocapsules lipidiques et des substrats d'intérêt pharmaceutique et technologique. Ensuite, nous avons démontré que ces nanocapsules lipidiques multifonctionnelles possédaient de nouvelles propriétés, comme la capacité à délivrer des principes actifs hydrophiles comme des petits ARN d'interférence (siRNA).

Mots Clés :

Nanocapsules, nanoparticules, modifications post-formulation, siRNA.

1. Nanocapsules
2. Nanoparticules
3. Modifications post-formulation
4. siRNA

5.

Title : Modifications of lipidic nanocapsules by post-formulation processes. Creation of multifunctional nanoparticles evaluated as drug vectors.

Summary :

This work established the identity card of nanoparticles developped in our laboratory; these nanoparticles are called lipidic nanocapsules. Indeed, these lipidic nanocapsules were characterized by dynamic light scattering and also by small angle neutron scattering. These experiments have demonstrated the structure of the lipidic nanocapsules as core-shell systems: an oily core surrounded by a mix monolayer of surfactants. By the way, starting from these core-shell systems, we have developped two methodologies able to produce multifunctional lipidic nanocapusles. The first one is the post-insertion process, initialy developped onto liposomes; the second one is a new process based on a transacylation reaction between the surfactants of lipidic nanocapsules and an another molecule presenting a high interest towards pharmaceuticals sciences.We have demonstrated that these new nanocapsules had new properties such the ability to deliver small interfering RNA (siRNA) into mammalian cells.

Key words : Nanocapsules, nanoparticles, post-formulation modifications, siRNA.